TRANSCRIPTOMIC ANALYSIS OF CORTICAL VERSUS CANCELLOUS BONE IN RESPONSE TO MECHANICAL LOADING AND ESTROGEN SIGNALING

A Dissertation

Presented to the Faculty of the Graduate School

of Cornell University

In Partial Fulfillment of the Requirements for the Degree of

Doctor of Philosophy

by

Natalie H Kelly

January 2017

TRANSCRIPTOMIC ANALYSIS OF CORTICAL VERSUS CANCELLOUS BONE IN RESPONSE TO MECHANICAL LOADING AND ESTROGEN SIGNALING

Natalie H Kelly, Ph. D.

Cornell University 2017

Osteoporosis is a skeletal disease characterized by low bone mass that often results in fracture. Mechanical loading of the skeleton is a promising approach to maintain or recover bone mass. Mouse models of in vivo loading differentially increase bone mass in cortical and cancellous sites. The molecular mechanisms behind this anabolic response to mechanical loading need to be determined and compared between cortical and cancellous bone. This knowledge could enhance the development of drug therapies to increase bone formation in osteoporotic patients.

After developing a method to isolate high-quality RNA from marrow-free mouse cortical and cancellous bone, differences in gene transcription were determined at baseline and at two time points following mechanical loading of wild-type mice. Cortical and cancellous bone exhibited different transcriptional profiles at baseline and in response to mechanical loading. Enhanced Wnt signaling dominated the response in cortical bone at both

time points, but in cancellous bone only at the early time point. In cancellous bone at the later time point, many muscle-related genes were downregulated.

Decreased bioavailable estrogen levels are a major cause of bone loss in postmenopausal women. Estrogen signaling through estrogen receptor alpha (ERα) has been found to be particularly important in regulating bone mass and the skeletal response to mechanical loading. We recently showed that mice lacking ERα in osteoblasts and osteocytes (pOC-ERαKO) had an increased adaptive response to mechanical loading, particularly in cancellous bone. The molecular mechanisms of functional adaptation to load in the context of decreased estrogen signaling are not fully elucidated, particularly in cortical versus cancellous sites. We examined transcription in cortical versus cancellous bone of tibiae from littermate control (LC) and pOC-ERαKO mice. pOC-ERαKO mice had a blunted transcriptional response to mechanical loading in cortical bone compared to littermate controls, but had an increased response in cancellous bone. This work demonstrates the importance of examining cortical and cancellous bone separately, and that next-generation sequencing is a powerful tool for discovering the complete transcriptional mechanisms responsible for mechanical loading-related bone anabolism.

BIOGRAPHICAL SKETCH

Natalie Hillhouse Kelly was born in Wadsworth, Illinois in 1983. She graduated from Zion Benton Township High School and attended Case Western Reserve University. In 2006 she completed her Bachelor of Science degree in Biomedical Engineering with a concentration in orthopaedic biomaterials, including a one-year cooperative education experience at DePuy Orthopaedics. While at CWRU, she was captain of the Fighting Gobies ultimate frisbee team for 4 years and competed regionally. Upon graduation, Natalie published 13 peer-reviewed journal articles as a research engineer at the Hospital for Special Surgery in the Department of Biomechanics. In 2010, she entered the Biomedical Engineering PhD program at Cornell University, earning her Master of Science in 2014. While in graduate school, Natalie began running competitively, qualified for the Boston marathon twice, and completed a total of four marathons. In August 2016, she received her Doctorate of Philosophy degree in Biomedical Engineering. While at Cornell, Natalie received a prestigious three-year NSF Graduate Research Fellowship and the Robert and Helen Appel Fellowship in Biomedical Engineering. She was also honored with the Harold M. Frost Young Investigator award from the American Society of Bone and Mineral Research. She served on the New Investigators Mentoring Committee and the Annual Meeting Committee of the Orthopaedic Research Society.

I dedicate this work to Bome and G'ampa Kelly

ACKNOWLEDGMENTS

I am extremely grateful to all of the individuals who assisted me both professionally and personally on my PhD journey.

I want to thank my committee chair, Dr. Marjolein van der Meulen for her guidance throughout my career and her mentorship. My committee members Dr. John Schimenti and Dr. Jan Lammerding provided advice and encouragement. Furthermore, Dr. Schimenti graciously allowed me to conduct most of my research in his laboratory. Dr. F. Patrick Ross was practically my fourth committee member and was instrumental to the design and interpretation of this work.

Many fellow scientists and colleagues provided technical advice and personal support. I would like to thank my undergraduate mentor Dr. Clare Rimnac for encouraging me to apply to the Hospital for Special Surgery, and to Dr. Timothy Wright for hiring me and inspiring me to pursue a PhD. I would also like to thank all of the members of the van der Meulen lab, past and present. In particular, Drs. Maureen Lynch, Katie Melville and Frank Ko taught me many technical skills and provided advice in the early years of graduate school. Thank you to Funmi Adebayo for being my main sounding board and allowing me to vent on our near weekly coffee dates. Dr. Adrian McNairn taught me molecular biology, and fed me cookies along the way. Many thanks to Judy Thoroughman, Marcia Sawyer, and Belinda Floyd for all of their administrative support. I am grateful for my classmates and friends who always offered a supportive ear, especially the POB crew: Drs. Liz Wayne, Sara Che, Young Hye Song, Karin Wang, and Stephanie Lindsey, and John Foo and Fredrik Thege.

Several core facilities at Cornell University provided extensive assistance in my experiments. The Biotechnology Resource Center provided technical expertise, sequencing, and computational resources. Dr. Peter Schweitzer, and Jennifer Mosher assisted in experimental design, taught me technical skills, and performed sequencing. Dr. Jen Grenier of the RNA sequencing core provided invaluable technical expertise on RNA isolation. Dr. Qi Sun assisted me with bioinformatics techniques to analyze my data. I would like to thank the dedicated staff of the Cornell Center for Animal Resources and Education who make our animal work possible.

My time in Ithaca would not have been the same without my running and polo communities. I appreciate the many miles covered with my Wednesday morning ladies, particularly Melissa Weiner, Lesley Middleton, Katie Stettler, and Ellie Pell. I am grateful to Cornell University polo for teaching me the sport of kings, and to the entire Wednesday night polo group.

My family and loved ones shared in my triumphs and setbacks equally and were unwavering in their support. My sister, Dr. Felice Kelly, is not only my best friend and confidant, she is also an incredible scientist who contributed to my research. Finally, I owe everything to my parents Jack and Kathleen Kelly. They raised me with a curiosity of the world around me and the belief that anything is achievable if you're willing to work for it.

Funding for this work was provided by the National Institutes of Health grants R01-AG028664 and R21-AR064034. I was honored to receive a three-year Graduate Research Fellowship from the National Science Foundation, and the Robert and Helen Appel Fellowship in Biomedical Engineering from the Hospital for Special Surgery and Cornell University.

TABLE OF CONTENTS

Biographical Sketch v
Dedication vi
Acknowledgments vii
Table of Contents ix
List of Figures xii
List of Tables xiv
Chapter 1: Introduction 1
1.1 Cortical and Cancellous Bone 1
1.2 Osteoporosis 4
1.3 Bone Mechanosensitivity 7
1.4 Signaling in Bone Response to Mechanical Loading 9
1.5 Differential Gene Expression Following in vivo Mechanical Loading 21
1.6 Aims 25
1.7 References 29
Chapter 2: A Method For Isolating High Quality RNA From Mouse Cortical and Cancellous Bone 41
2.1 Introduction 41
2.2 Materials and Methods 43
2.2.1 Animals 43
2.2.2 Histology 44
2.2.3 RNA isolation from bone 45
2.2.4 RNA isolation from marrow 46
2.2.5 Gene expression 47
2.2.6 Statistics 48
2.3 Results 48
2.3.1 Histology 48
2.3.2 RNA quantity/quality 49
2.3.3 Gene expression 50
2.4 Discussion 52
2.4.1 Conclusions 54
2.5 References 56
Chapter 3: Transcriptional Profiling of Cortical Versus Cancellous Bone From Mechanically-loaded Murine Tibiae Reveals Differential Gene Expression 58
3.1 Introduction 58
3.2 Materials and Methods 60

3.2.1 Animals 60
3.2.2 RNA isolation 61
3.2.3 RNA-seq library preparation and analysis 62
3.2.4 Gene expression verification with qPCR 65
3.3 Results 66
3.3.1 Control cortical and cancellous bone exhibit different transcriptional profiles 66
3.3.2 The mechanical loading response at 3h is driven by Wnt signaling in cortical and cancellous bone 69
3.3.3 The mechanical loading response at 24h includes changes in Wnt signaling in cortical bone and muscle-related genes in cancellous bone 70
3.3.4 Temporal comparison of differentially expressed genes with mechanical loading 72
3.3.5 RNA-seq verification with qPCR 74
3.4 Discussion 75
3.4.1 Conclusions 83
3.5 References 85
Chapter 4: Female Mice Lacking Estrogen Receptor Alpha in Mature Osteoblasts Have an Increased Transcriptional Response to Mechanical Loading in Cancellous but not Cortical Bone 92
4.1 Introduction 92
4.2 Materials and Methods 96
4.2.1 Animals 96
4.2.2 RNA isolation 97
4.2.3 RNA-seq library preparation and analysis 98
4.2.4 Gene expression verification with qPCR 100
4.3 Results 101
4.3.1 Absence of ERα in mature osteoblasts resulted in markedly decreased differential gene expression in cortical bone following a single loading session 101
4.3.2 Absence of ERα in mature osteoblasts resulted in markedly increased differential gene expression in cancellous bone following a single loading session 108
4.3.3 More Wnt signaling pathway genes were differentially regulated in LC versus pOC-ERαKO mice 114
4.3.4 Cortical and cancellous bone exhibited different transcriptional profiles 116
4.3.5 Loading had systemic effects at the transcriptional level .. 118

4.3.6 RNA-seq verification with qPCR 121
4.4 Discussion 122
4.4.1 Conclusions 128
4.5 References 129
Chapter 5: Conclusions and Discussion 135
5.1 Summary 135
5.2 Strengths 141
5.3 Limitations 143
5.4 Future Work 145
5.5 Conclusions 152
5.6 References 153
Appendix A: Chapter 3 Supplementary Figures and Data 159
Appendix B: Chapter 4 Supplementary Figures and Data 202

LIST OF FIGURES

Figure 1.1 The bones of the human appendicular skeleton, such as the femur, consist of porous cancellous bone in the metaphysis at the distal and proximal ends (circled), dense cortical bone forming a shell (boxed) and a large diaphyseal space containing bone marrow. 2
Figure 1.2 Osteoporosis decreases bone mass and increases the risk of fracture 5
Figure 1.3 In vivo mechanical loading of the mouse tibia is anabolic....8
Figure 1.4 Schematic of the major signaling pathways thought to mediate bone's response to mechanical loading....11
Figure 2.1 Schematic of cortical and cancellous bone sample preparation ..45
Figure 2.2 Centrifugation removes marrow more efficiently than flushing in cortical and cancellous bone....49
Figure 2.3 Centrifugation resulted in higher expression of bone-related genes and lower expression of a gene in bone marrow....50
Figure 3.1 Control cortical and cancellous bone exhibit distinctly different transcriptional profiles....68
Figure 3.2 Differential expression of Wnt signaling genes 3h following a single loading session in cortical and cancellous bone 70
Figure 3.3 Wnt signaling changes in cortical bone and muscle-related changes in cancellous bone 24h following a single loading session 72
Figure 3.4 More genes were differentially expressed in cortical bone and at 24h 74
Figure 3.5 qPCR validated 12 differentially expressed genes 75
Figure 4.1 Littermate control and ERα knockout animals respond differently to loading in cortical and cancellous bone 102
Figure 4.2 More genes were differentially expressed in cortical bone of LC than pOC-ERαKO following mechanical loading 104
Figure 4.3 More genes were differentially expressed in cancellous bone of pOC-ERαKO than LC following mechanical loading with a higher fold change.... 110
Figure 4.4 More Wnt signaling pathway genes were differentially expressed in LC than pOC-ERαKO mice 116
Figure 4.5 Cortical and cancellous bone are transcriptionally distinct and loading has systemic effects that differ by genotype.... 120

Figure 4.6 qPCR validated 8 differentially expressed genes 3h following a single loading session 121

LIST OF TABLES

Table 1.1 Bone mass changes in female bone-specific ERα knockouts 19

Table 1.2 Response to mechanical loading in female bone-specific ERα knockouts compared to littermate controls.....20

Table 4.1 Signaling pathways and biological processes significantly changed in cortical bone 3- and 24-hours following a single loading session in LC and pOC-ERαKO mice 107

Table 4.2 Signaling pathways and biological processes significantly changed in cancellous bone 3- and 24-hours following a single loading session in LC and pOC-ERαKO mice 113

CHAPTER 1
INTRODUCTION

1.1 Cortical and Cancellous Bone

Bones are composite structures consisting of an exterior cortical shell and an inner cancellous network. This structure is essential for the demands placed on the skeleton, providing a form that meets the function of maintaining structure and resisting fracture. Cancellous (spongy) bone is a porous network of individual rods and plates called trabeculae and is found in the metaphysis of long bones. Cancellous bone has a large surface area with trabeculae surrounded by bone marrow, contributing to high metabolic activity. Cortical (compact) bone is a dense structure consisting of basic units known as osteons that are roughly cylindrical and have a central Haversian canal containing blood vessels and nerves surrounded by concentrically arranged lamellae of bone matrix (**Figure 1.1**). Long bones have a large diaphyseal cavity containing bone marrow.

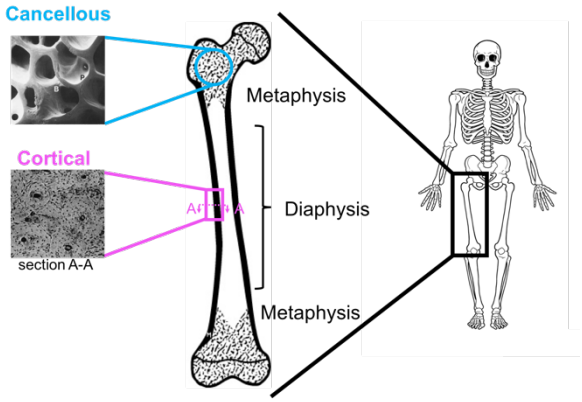

Figure 1.1 The bones of the human appendicular skeleton, such as the femur, consist of porous cancellous bone in the metaphysis at the distal and proximal ends (circled), dense cortical bone forming a shell (boxed) and a large diaphyseal space containing bone marrow. Cancellous low-power scanning electron microscope image adapted from [1], cortical image from [2].

In addition to the differences in structure and metabolic activity, cortical and cancellous bone differ in their initial development (modeling), attainment, and gain/loss of bone mass (remodeling). Cortical bone initiates from the bone collar and expands through coordinated periosteal apposition and endosteal resorption. Conversely, cancellous bone arises from cartilage precursors at the growth plate. But it has recently been shown that both tissues can arise from hypertrophic chondrocytes that can become osteoblasts and osteocytes that contribute to cancellous bone, the endosteum, and mature bone [3, 4]. Cortical and cancellous bone mass increase during growth, but cortical bone mass stabilizes at skeletal maturity and decreases during aging [5], while cancellous bone decreases immediately after reaching peak bone mass without a stabilization phase [6]. Alteration of

bone size and shape are mediated by three different cell types located on the bone surface and within the mineralized matrix.

Osteoblasts and osteoclasts are located on the bone surface and perform the physical work of adding and removing bone, respectively. Osteoblasts derive from the mesenchymal cell lineage and can be identified by their cuboidal morphology and alkaline phosphatase (ALP) activity. Osteoclasts derive from hematopoietic stem cells, are multinucleated and are often identified by their expression of tartrate-resistant acid phosphatase (TRAP).

Osteocytes are terminally differentiated osteoblasts that have been embedded in the mineralized bone matrix and compose over 90% of all bone cells. They have a stellate cell shape; their cell bodies are located in lacunae, and long dendritic processes reside in channels in the bone matrix known as canaliculi. This lacuno-canalicular network connects osteocytes to one another and to the bone surface. Osteocytes are, therefore, thought to be important in cell-to-cell signaling and orchestrating the activity of osteoblasts and osteoclasts.

Normal bone homeostasis is characterized by a constant self-renewal known as remodeling, which continually removes old bone and replaces it with new bone. As the skeleton ages, the amount of bone formed during each remodeling cycle decreases due to decreased osteoblastogenesis [7].

Additionally, women experience a distinctive change in skeletal homeostasis at the onset of menopause, when estrogen declines. Changes in bone homeostasis that cause an overall decline in bone mass result in a disease known as osteoporosis.

1.2 Osteoporosis

Osteoporosis is one of the most common musculoskeletal disorders. It is characterized by decreased bone mass as the skeleton ages, which is correlated with a reduction in estrogen production in females at menopause. This decrease in bone mass produces weaker skeletal structures that are sometimes unable to bear everyday loads, which can result in fracture at corticocancellous sites including the spine, proximal femur, and distal radius (**Figure 1.2**) [8]. One in three women and one in five men over the age of 50 will experience an osteoporosis-related fracture. The cost of treating these fractures in an increasingly aged population is predicted to reach $25 billion by 2025 [9]. Furthermore, patients who suffer an osteoporosis-related non-vertebral fracture are at higher risk of subsequent fracture within one year, and treatments for patients who incur subsequent fractures are significantly more costly [10]. Even more importantly, women who experience a hip fracture have two-fold increased mortality in the year following the fracture

[11]. Osteoporotic fractures decrease quality of life, increase mortality, and create significant treatment-related costs.

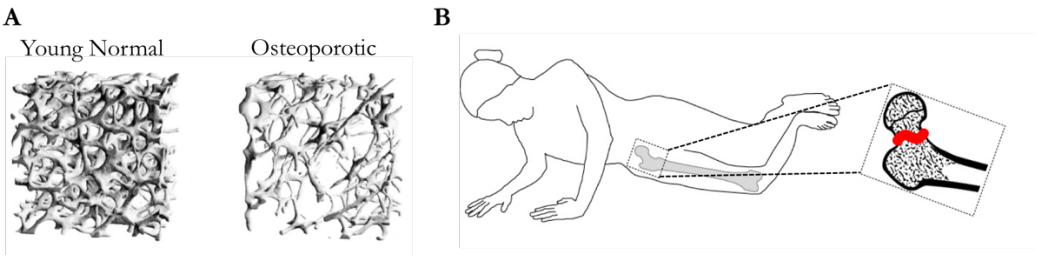

Figure 1.2 Osteoporosis decreases bone mass and increases the risk of fracture A) Representative micro-CT reconstructions of lumbar spine samples from a young normal (left) and a postmenopausal osteoporotic (right) woman (reproduced from [12]). B) In osteoporotic patients a fall from standing height can cause fracture. These fractures often occur at corticocancellous sites, such as the proximal femur (adapted from [13]).

Osteoporosis particularly affects post-menopausal women. At menopause, bioavailable estrogen declines significantly, as does bone mass, placing women at a high risk for fracture [14]. Declines in sex hormones with age in males are more gradual but produce similar effects [15, 16]. Estrogen deficiency increases bone turnover (the rate at which remodeling occurs), increases resorption by reducing osteoclast apoptosis [17], and increases osteoblast apoptosis and thus decreases formation [18]. The mechanisms of action of estrogen on bone will be introduced further in section **1.4 Signaling in bone response to mechanical loading**.

Current osteoporosis treatments are largely anti-resorptive, meaning that they block bone resorption by acting on the osteoclast. Anti-resorptive

drugs include bisphosphonates and selective estrogen receptor modulators (SERMs). Bisphosphonates are a commonly used drug therapy for osteoporosis. These agents bind to bone surfaces and block bone loss by causing osteoclast apoptosis upon resorption. Bisphosphonates increase bone mass and reduce vertebral fracture rates by 70% and non-vertebral fracture rates by 40% [19]. Following chronic use, they have been implicated in rare fractures in patients [20, 21]. Selective estrogen receptor modulators (SERMs) were developed as estrogen-like compounds that lack the steroid structure of estrogens, but possess a tertiary structure that allows them to act as either estrogen receptor agonists or antagonists. Thus, SERMs would ideally have the positive effects of estrogen on bone, without increased risk of breast and endometrial cancers.

Ultimately, therapies to increase bone mass instead of blocking bone loss could be more beneficial to patients. The only FDA-approved anabolic drug is parathyroid hormone (PTH), or teriparatide. When administered intermittently, PTH is strongly osteogenic [22] and decreases vertebral and nonvertebral fracture in postmenopausal women at high risk for fracture [23]. Other anabolic drugs are currently in clinical trials, including anti-sclerostin antibody. Sclerostin is an antagonist of Wnt signaling, and blocking this antagonism with an antibody increases bone mineral density by

17.7% at the spine and 6.2% at the hip [24]. Sclerostin's mechanism of action and the Wnt signaling pathway will be introduced further in section **1.4 Signaling in bone response to mechanical loading**. While a few anabolic drugs are in the pipeline, a promising method for the discovery of new targets for bone anabolism arises from the fact that bone is mechanosensitive.

1.3 Bone Mechanosensitivity

Bone responds robustly to biophysical cues. Physical forces are important in skeletal development [25-27] and in remodeling of the adult skeleton [28]. In adults, increased loads cause bone hypertrophy [29] and the absence of mechanical forces due to immobilization [30] or space flight [31] decreases bone mass. Clinically, mechanical loading enhances cancellous bone mineral acquisition during growth [32, 33] and is a promising treatment to prevent bone loss in older individuals [34-37]. In vivo animal models were developed to further characterize the anabolic response of bone to mechanical loading.

Mouse models of in vivo mechanical loading including tibial bending [38, 39] and ulnar [40] and tibial compression [41, 42] have been developed to examine mechanical loading in bone. Tibial compression has distinct advantages due to the ability to examine both cortical and cancellous

responses (unlike the ulna) and the fact that loads are applied along the physiologic loading axis (unlike bending). A mechanical loading waveform consisting of 4 cycles per second, for 1200 cycles per day for two weeks at a load level engendering 1200 με at the tibial midshaft has consistently increased bone mass at cortical and cancellous sites [41, 43-46]. Loading increased bone volume fraction (BV/TV) at the tibial metaphysis in a cancellous site by 60%, while the cortical area at the tibial midshaft was increased by 30%, indicating that cancellous bone may respond more than cortical to mechanical stimuli in growing mice (**Figure 1.3**) [45].

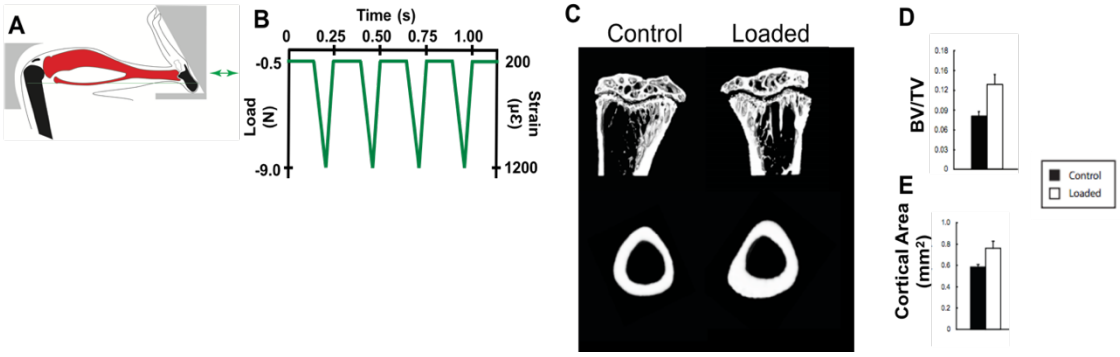

Figure 1.3 In vivo mechanical loading of the mouse tibia is anabolic. A) Schematic of the in vivo tibial loading device. The tibia is in red with cyclic loading initiating from an electromagnetic actuator at the foot while a load cell at the rigidly held knee provides force feedback control. B) The applied waveform consists of a 4 cycles per second triangular impulse to cause mid diaphyseal strains of 1200 microstrain (right axis), typically a peak load of 9N (left axis). C) Representative microCT images depict increases in metaphyseal cancellous and diaphyseal cortical bone following two weeks of tibial loading, which is quantified as a 60% increase in D) bone volume fraction (BV/TV) at the metaphysis and a 30% increase in E) cortical area at the diaphysis [45].

While tissue-level responses have been well-documented, a greater understanding of the molecular mechanisms has the potential to uncover new targets for the pharmacologic treatment of osteoporosis. Furthermore, more focus has been given to cortical bone response to load in the past, so a more in-depth examination of cancellous bone may prove useful in developing drugs to target the corticocancellous sites more frequently affected by osteoporosis. Previously, studies have demonstrated the importance of several signaling pathways in mechanotransduction including Wnt/β-catenin, parathyroid hormone (PTH), IGF, integrins, BMP/SMAD, and estrogen signaling.

1.4 Signaling in Bone Response to Mechanical Loading

The response of bone to mechanical loading does not appear to occur through a single mechanically sensitive pathway. Rather, in vitro and in vivo experiments have highlighted the importance of several independent pathways and crosstalk between these pathways. Important pathways include Wnt/β-catenin, PTH, IGF and integrins, and BMP/SMAD (**Figure 1.4**). Furthermore, combined studies of the role of estrogen signaling in osteoporosis and the anabolic effects of mechanical loading on bone have provided evidence that estrogen receptors are involved in loading-related

osteogenesis and that significant crosstalk exists between estrogen signaling and other mechanosensing pathways [47-49]. Studies have relied on reverse genetics approaches; a known pathway or signaling molecule has been assayed in vitro or genetically modified in vivo to study its effects on mechanotransduction.

1.4.1 Wnt/β-catenin signaling

One of the most important signaling pathways in bone development, homeostasis, and response to mechanical loading is the Wnt/β-catenin (or "canonical Wnt") pathway. The role of this pathway in bone health was indicated clinically by the discovery of genetic mutations responsible for two opposing bone phenotypes. Children with the autosomal recessive disorder osteoporosis-pseudoglioma syndrome (OPPG) have very low bone mass and are prone to developing fractures and deformation [50]. In contrast, kindred were identified with extremely high bone density, wide and deep mandibles, and bony palates [51]. Genetic studies found both bone disorders were caused by mutations in low-density lipoprotein receptor-related protein 5 (*LRP5*). *LRP5* is a co-receptor for Wnt, and these findings suggested a link between Wnt signaling through *LRP5* and bone density. The canonical Wnt pathway affects bone by regulating β-catenin stabilization and subcellular

location. Under basal conditions Wnt signaling is not active and β-catenin is degraded in the cytoplasm, partially due to the action of glycogen synthase kinase 3 beta (*GSK3β*).

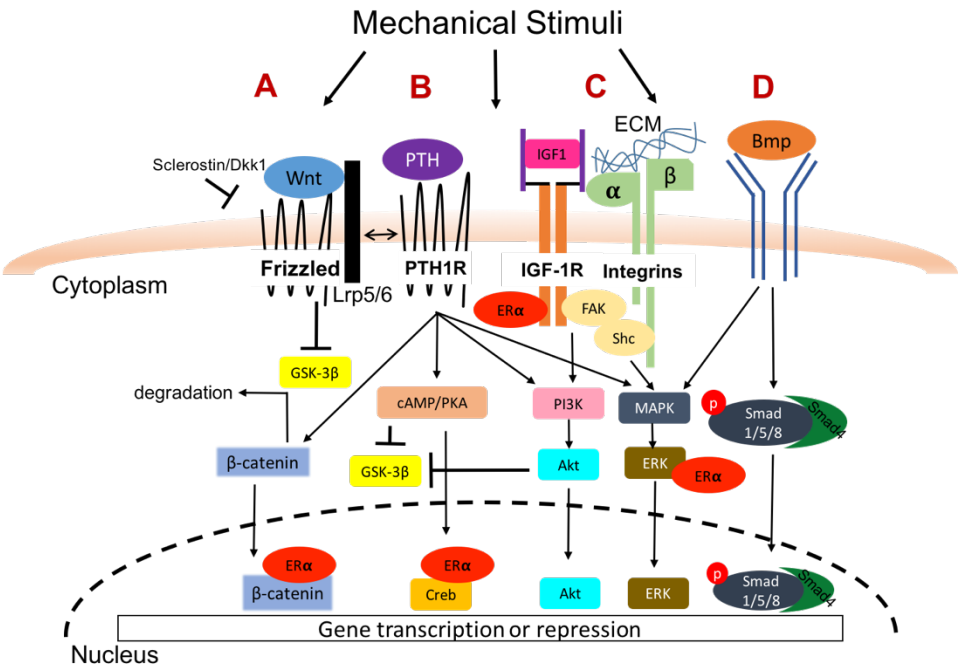

Figure 1.4. Schematic of the major signaling pathways thought to mediate bone's response to mechanical loading. When a mechanical stimulus is sensed by a bone cell, signal transduction can occur through several individual pathways that also have significant overlap in downstream effectors. A) Wnt/β-catenin signaling causes β-catenin stabilization and translocation to the nucleus and drives pro-osteogenic gene expression. Important antagonists of Wnt/β-catenin signaling are Sclerostin and Dkk1. B) PTH signaling has several downstream effectors including β-catenin, cAMP/PKA leading to Creb translocation, PI3K/Akt and MAPK. C) IGF1 and Integrins interact and mediate similar downstream events such as PI3K/Akt and MAPK/Erk, which can also be initiated by D) BMP signaling. Phosphorylation of Smad 1/5/8 is another important downstream signal caused by BMP. Several of these pathways are modulated by ERα.

Wnts bind to the co-receptors *LRP5* (or 6) and Frizzled (*FZD*) and block the degradation of β-catenin causing accumulation in the cytoplasm, translocation to the nucleus and recruitment of transcriptional co-activators to stimulate expression of osteogenic genes. Wnt antagonists such as sclerostin (*SOST*) and dickkopf-1 (*DKK1*) block *LRP5/6* and β-catenin is degraded in the cytoplasm (**Figure 1.4.A**) [52, 53].

To examine the role of the canonical Wnt pathway in bone's adaptive response to load, mice with gain- or loss-of-function mutations in *Lrp5* were developed. Mice expressing the mutated form of *Lrp5* that increases bone mass in humans had a similar phenotype with high bone mass and increased strength [54] and an increased osteogenic response to in vivo mechanical loading [55, 56]. Loss-of-function mutations in *Lrp5* caused a low bone mass phenotype [57, 58] and a decreased responsiveness to mechanical loading [59]. These studies showed that Wnt signaling played an important role in skeletal mechanotransduction. Similarly, transgenic mice with high levels of the inhibitor sclerostin failed to activate the Wnt pathway and did not display an anabolic response to mechanical stimulation, indicating that *Sost* downregulation is necessary for mechanotransduction [60]. However, mice lacking sclerostin had increased cortical bone volume and greater mineral apposition rate (MAR) and bone formation rate (BFR) than control mice

following cyclic loading, indicating that there is a sclerostin- (and thus Wnt-) independent mechanism of bone anabolism in response to mechanical loading [61].

1.4.3 PTH signaling

Parathyroid hormone was initially recognized as a major regulator of removal of calcium from the skeleton by stimulating bone resorption. However, it was discovered that intermittent doses of PTH are strongly osteogenic which, as previously mentioned, has led to PTH being the only approved drug for the anabolic treatment of osteoporosis. PTH acts by binding to a seven-transmembrane receptor (PTH1R) and activating phosphatidyl-inositol-3 kinase (PI3K) and the Akt pathway and the mitogen-activated protein kinase (MAPK) cascade. PTH appears to interact with Wnt signaling, as PTH treatment increased mRNA levels of *Lrp6*, Frizzled and β-catenin, while decreasing levels of *Dkk1* in rat distal metaphyseal bone in vivo [62]. Furthermore, PTH1R physically interacts with *Lrp6* and facilitates its recruitment of intracellular Wnt pathway components (**Figure 1.4.B**) [63].

PTH and mechanical loading seem to have synergistic anabolic effects on bone. In vivo, mechanical loading enhanced the anabolic effects of intermittent PTH (iPTH) on trabecular and cortical bone in mice [64]. In a

model of periprosthetic cancellous bone adaptation, mechanical loading and iPTH had a small additive effect on bone volume compared to iPTH alone [65].

1.4.4 IGF signaling and integrins

IGF-1 and integrin signaling share common downstream effectors such as MAPK and Akt, and it is thought that mechanical stimulation results in activation of both pathways and ultimately results in amplification of pro-survival (Akt) and proliferation (MAPK) signals (**Figure 1.4.C**) [66]. Insulin-like growth factor (IGF) signaling initiates with IGF1 binding to the IGF-1 receptor. Integrins are membrane-bound single pass receptors that form heterodimers that consist of an α and β subunit and interact with the extracellular matrix (ECM). Downstream signaling of both IGF-1 and integrins proceeds along two main pathways. The mitogen-activated protein kinase (MAPK) pathway results in the nuclear translocation of Erk1/2 and subsequent activation of transcription factors such as Elk1 and C-jun and increased Cyclin D1, a cell cycle regulator that increases proliferation. In addition, phosphatidyl-inositol-3 kinase (PI3K) activates protein kinase B (PKB, also known as Akt) which blocks apoptosis and increases cyclin D1 following nuclear translocation [66].

Studies have revealed a role for IGF-1 and integrin signaling in mediating the skeletal response to mechanical load. In vitro observations indicated that IGF-1 production is increased in osteocytes and osteoblasts following mechanical loading [67, 68]. Primary mouse osteoblasts subjected to a single period of dynamic strain activated IGF-1 receptor, PI3K phosphorylation of Akt, inhibition of GSK-3β, and increased activation of β-catenin [69]. Transgenic mice that overexpress IGF-1 in osteoblasts have increased periosteal bone formation in response to mechanical loading [38] while osteoblast-specific IGF-1 conditional knockout mice failed to respond to biomechanical stimuli in the periosteum or trabecular bone [70]. Integrin-mediated signaling pathways have been implicated in mechanotransduction in bone. Mechanical stimulation by stretching activates ERK in an integrin-dependent manner in MLO-Y4 osteocytic cells [71]. In vivo deletion of β1 integrins from cortical osteocytes reduces load-induced bone formation [72] and while control mice showed decreased Sost expression due to mechanical loading, mice deficient in integrins in osteoblast lineage cells did not [73]. Hindlimb unloading of adult mice, intended to cause bone loss, actually increased cross-sectional area and moments of inertia in mice lacking β1 integrins indicating that integrins mediate mechanotransduction sensing in vivo [74].

1.4.5 BMP/SMAD signaling

The BMP/SMAD pathway is another key component in the response to mechanical loading. SMADs are a family of transcription factors that are regulated by the members of the transforming growth factor-β (TGF-β) family of molecules, TGF-β and bone morphogenetic proteins (BMPs). BMPs signal through a multimeric cell surface complex consisting of two type I receptors and two type II receptors. After ligand binding, type II receptors phosphorylate the type I receptors. Activated type I receptors recruit and phosphorylate *Smads* 1/5/8, which form trimers with *Smad4* and translocate to the nucleus (**Figure 1.4.D**) [75]. The importance of the TGF-β superfamily in skeletal development is demonstrated by genetic disorders such as activating mutations in a type I BMP receptor (Alk2) which leads to fibrodysplasia ossificans progressiva, a disorder characterized by ectopic bone formation in soft tissues [76].

In the context of mechanotransduction, osteoblasts subjected to dynamic compressive forces or fluid flow strain had increased SMAD 1/5/8 phosphorylation, a sign of increased BMP signaling [77, 78]. The administration of BMP7 in conjunction with in vivo mechanical loading enhanced bone formation [79] and BMPs are upregulated in mice following

mechanical loading [80, 81]. However, decreased BMP signaling through conditional knockout of BMP receptor 1a (BMPR1a) enhanced trabecular bone volume in response to treadmill exercise due to decreased levels of osteoclasts [82]. Furthermore, *Bmp2* conditional knockout in osteoblasts did not impair bone formation following mechanical loading [83].

1.4.6 Estrogen signaling

Estrogen signaling proceeds through two different estrogen receptors, ERα and ERβ, which are localized to the cytoplasm. In classical signaling, estrogen binds either receptor, the receptor dimerizes and autp-phosphorylates, and then this complex can either directly bind to DNA estrogen response elements found in the control regions of genes or it can affect other intracellular signaling pathways. In 1994 a male patient presented with unfused growth plates and osteoporosis due to an inactivating point mutation in *ESR1*, the gene encoding ERα [84]. This finding caused an increased interest in the mechanisms of ERα signaling. Human polymorphisms in *ESR1* have since been linked with bone mineral density, fracture risk, and response to exercise [85-89].

Animal models have been developed to examine the effects of estrogen on the skeleton. Ovariectomy (OVX) of rodents recapitulated the

bone loss seen in humans at menopause [90, 91]. However, the removal of circulating estrogen has pleiotropic systemic effects, which does not allow the examination of effects on bone specifically. Estrogen regulates bone maintenance through two different receptors: estrogen receptor-alpha (ERα) and -beta (ERβ). Initially, whole body knockout (KO) methods were used to remove estrogen receptors in all cells. Global ERα KO had more pronounced effects on bone than ERβ deficiency, indicating that ERα may be more crucial for estrogen's effects on bone [92]. But confounding effects such as increased body and uterine mass, increased circulating estrogen, and decreased IGF-1 were observed in global KO mice [93]. Body mass, estrogen, and IGF-1 can have independent effects on bone mass, which complicates the interpretation of bone changes and led to the development of bone-specific estrogen receptor KO mice.

Conditional estrogen receptor-alpha KO mice have been created to remove the receptor from osteoclasts [94, 95], osteoblast precursors [96], mature osteoblasts [96-98], and osteocytes [99, 100]. These studies demonstrate the complexity of estrogen signaling in cancellous and cortical bone of female mice (**Table 1.1**). Our lab has used an osteocalcin-cre (OC-Cre) mouse to knock out ERα in osteoblasts [98]. Female pOC-ERαKO mice had 35% decreased cancellous bone mass and decreased osteoblast

activity in the proximal tibia. Cortical bone mass was also decreased at the tibial midshaft by 8%, indicating that the effects of estrogen signaling deficiency may be more pronounced in cancellous than cortical bone of females.

Table 1.1 Bone mass changes in female bone-specific ERα knockouts

Cell-specific	Promoter	Cancellous	Cortical
Osteoblast progenitor	*Prx1* [96]	No change	Decreased
Osteoblast precursor	*Osx1* [96]	No change	Decreased
Mature Osteoblasts	*OC* [97, 98]	Decreased	Decreased
	Col1a1 [96]	No change	No change
Osteocytes	*Dmp1* [100]	Decreased	No change
Osteoclasts	*Ctsk* [95]	Decreased	No change
	LysM [94]	Decreased	No change

ERα plays a role in loading-induced osteogenesis either directly or through crosstalk with other mechanosensing pathways. In vivo, skeletally mature female mice lacking ERα (ERα$^{-/-}$) globally had three-fold lower response to mechanical loading of the ulna [101]. ERα$^{-/-}$ mice also had severely reduced osteogenic response to axial tibial loading with significantly lower increases in cortical area than in wild-type mice [102].

Estrogen receptor's effects in mechanotransduction are complicated, however, as data from conditional knockout studies in different bone cell

lineages are conflicting (**Table 1.2**). In osteoblast progenitors (*Prx1*-cre) and precursors (*Osx1*-cre), removal of ERα decreased the response to mechanical loading in cortical bone [103]. When ERα was removed from osteocytes (*Dmp1*-cre), the cortical response to tibial loading was similar to littermate controls [99]. For these studies, cancellous bone changes were not reported. Our lab, using the previously mentioned ERα conditional knockout in mature osteoblasts (OC-cre, pOC-ERαKO), showed that mechanical loading increased cortical and cancellous bone mass to a greater extent in female pOC-ERαKO mice than their littermate controls [46].

Table 1.2 Response to mechanical loading in female bone-specific ERα knockouts compared to littermate controls

Cell-specific	Promoter	Cancellous	Cortical
Osteoblast progenitors	*Prx1* [103]	Not examined	Decreased
Osteoblast precursor	*Osx1*[103]	Not examined	Decreased
Mature Osteoblasts	*OC* [46]	Increased	Increased
Osteocytes	*Dmp1* [99]	Not examined	Similar

Evidence of ERα crosstalk with other signaling pathways has been determined using primary osteoblasts exposed to strain. A single short period of dynamic mechanical strain increased nuclear accumulation of β-catenin, and this effect was blocked by an estrogen receptor inhibitor and

was absent in osteoblasts from mice lacking ERα [104]. ERα physically associated with IGF1R and was necessary for the strain-related IGF1R activation of AKT [69]. Estrogen and shear stress independently induced ERK and MAPK signaling and increased Cox-2 expression. When combined, estrogen and shear stress augmented these responses. When cells were treated with an estrogen receptor inhibitor or when β1 integrins were blocked, the responses to estrogen and shear stress were inhibited, indicating that estrogen augments shear stress responsiveness via estrogen receptor-mediated increases in β1 integrins [105]. Many of these suggested crosstalk events are highlighted in **Figure 1.4**.

1.5 Differential gene expression following in vivo mechanical loading

Unbiased forward genetics techniques may allow the discovery of new pathways that influence mechanosensing. Forward genetics approaches identify genes responsible for a particular phenotype or mechanistic response to a perturbation. One approach to further characterize the skeletal response to mechanical loading and discover new targets and pathways is to examine the changes in gene expression following in vivo mechanical loading.

Differential gene expression in response to in vivo mechanical loading has been examined with quantitative polymerase chain reaction (qPCR) [56, 60, 106-110] or microarray [81, 104]. qPCR is limited due to the relatively small number of candidate genes that can be examined. Microarray panels contain thousands of genes but still rely on probes for known genes and are semi-quantitative. Despite their limitations, qPCR and microarray studies have contributed to our knowledge of mechanotransduction in bone.

The importance of the Wnt/β-catenin pathway for the adaptive response to in vivo mechanical loading has been verified with qPCR and microarray. Genes involved in the Wnt/β-catenin pathway such as *Wnt10b*, *Wnt2b*, *Fzd2*, *Crebbp*, *Sfrp1*, *Wisp2*, and Cyclin D1 were differentially expressed in loaded versus control tibiae following mechanical loading [56, 104]. Axial compression of bone was found to reduce osteocyte expression of sclerostin (*Sost*) [60, 106, 108]. Mice lacking the matricellular protein periostin did not exhibit increased bone mass following loading and *Sost* expression was not inhibited, indicating that *Sost* downregulation is required for the adaptive response to mechanical loading and is regulated by periostin [106]. Hindlimb suspension, which causes mechanical unloading of the bone, increased *Sost* expression in cortical bone from whole tibiae [108], while unloading via botox injection decreased *Sost* in metaphyseal cortical and

cancellous bone but increased *Sost* in diaphyseal cortical bone [111], indicating that there may be site-specific differences in the response to mechanical stimuli.

Determinations of gene expression changes following mechanical loading using microarray have demonstrated the importance of estrogen signaling in mechanotransduction. The transcriptional response of mouse bones to loading was markedly reduced and delayed in ERα global knockout mice compared with wild-type littermates [81]. In contrast to the 642 genes differentially expressed three hours after tibial loading in wild-type mice, only 26 genes were differentially expressed in the tibiae of ERα mice. Three hours following tibial compression wild-type mice had differential expression of six genes involved in Wnt signaling but only one gene was differentially expressed in mice lacking ERα [104].

The limited in vivo gene expression studies are from cortical or whole bone samples and usually do not account for marrow contamination. Several in vivo loading studies performed loading of the ulna, which is a purely cortical site with a small marrow cavity [60, 80, 107, 108, 110, 112]. Tibial loading studies extracted RNA from whole bone without marrow removal [109], after marrow flushing [56, 106], or after marrow centrifugation [81, 104]. Marrow is highly cellular and is likely to significantly affect gene

expression determination. One exception is a study that examined cancellous response to mechanical loading in the mouse vertebra using microarray [113]. However, this study did not compare the cancellous response to cortical bone and used collagenase digestion to remove marrow, which has been shown to affect the expression of bone transcripts [114]. The examination of differential gene expression with qPCR or microarray from cancellous bone of the mouse tibia is challenging due to small tissue quantity at that site, but next-generation sequencing techniques are promising for this application.

RNA sequencing (RNA-seq) is a next-generation sequencing technique that allows the quantitative determination of differential gene expression across the entire transcriptome in very small tissue samples. RNA-seq is superior to microarray in detecting low-abundance transcripts, differentiating biologically critical isoforms, and identifying genetic variants. Furthermore, RNA-seq has a broader dynamic range than microarray, allowing for the determination of more differentially expressed genes with higher fold-change [115].

RNA-seq is widely used in many scientific fields and is beginning to gain traction in the musculoskeletal field. The Warman group has pioneered RNA-seq in bone to examine the phenotype of *Lrp5* mutations and

treatments [114, 116, 117]. Other studies have used RNA-seq to examine the developmental effects of *Dlx5* deletion [118] and mechanosensitive genes during skeletal development [119]. RNA-seq has not yet been used to discover differentially expressed genes following in vivo loading but it has been used to examine osteocyte response to fluid flow in vitro [120]. RNA-seq could be used to examine marrow-free cancellous and cortical bone of mice in the context of estrogen signaling to provide a wealth of knowledge of transcription in response to in vivo mechanical loading. Data on the transcriptional response of cancellous bone to mechanical loading is lacking and could identify new targets for the treatment of osteoporosis in corticocancellous sites.

1.6 Aims

Osteoporotic fractures are a significant public health risk that can decrease quality of life and increase mortality. Osteoporosis is at least partly caused by decreased estrogen signaling, which has been recapitulated in mouse models. Mechanical forces can increase cortical and cancellous bone mass at the tissue level, but the signaling events underlying this increase remain largely unknown, particularly in cancellous bone. If the molecular mechanisms behind bone anabolism in response to mechanical loading and in the context of decreased estrogen signaling were more completely

understood, bone-restoring therapeutics could be developed to treat bone loss due to osteoporosis. This thesis aims to better elucidate the transcriptional response behind mechanical loading-induced bone anabolism in cortical and cancellous bone separately when estrogen signaling is intact and when it is decreased.

Aim 1

Our first aim was to develop a method to measure gene expression in marrow-free cortical and cancellous bone. The high incidence of fragility fractures in corticocancellous bone locations, plus the fact that individual skeletal sites exhibit different responsiveness to load and disease, emphasizes the need to document separately gene expression in cortical and cancellous bone. A further confounding factor is marrow contamination since its high cellularity may effect gene expression measurements. We isolated RNA from cortical and cancellous bone of intact mouse tibiae, and also after marrow removal by flushing or centrifugation. We performed histology to determine if centrifugation was more effective than flushing in removing marrow. Bone- and marrow-related gene expression in cortical and cancellous bone and bone marrow further demonstrated the effectiveness of marrow removal techniques.

Aim 2

Our second aim was to determine the transcriptional response to mechanical loading in cortical and cancellous bone separately. Mechanical loading is an anabolic stimulus that increases bone mass, and thus a promising method to counteract osteoporosis-related bone loss. The mechanism of this anabolism remains unclear, and needs to be established for both cortical and cancellous envelopes individually. We hypothesized that cortical and cancellous bone display different gene expression profiles at baseline and in response to mechanical loading. To test this hypothesis, the left tibiae of 10-week-old female C57Bl/6 mice were subjected to one session of axial tibial compression and euthanized 3 and 24 hours following loading. The right limb served as the contralateral control. We performed RNA-seq on marrow-free metaphyseal samples from the cortical shell and the cancellous core to determine differential gene expression at baseline (control limb) and in response to load. Differential expression was verified with qPCR.

Aim 3

Our third aim was to elucidate differences in the transcriptional response to mechanical loading in cortical versus cancellous bone with

deficient estrogen signaling. Decreased estrogen at the onset of menopause coincides with a precipitous decline in bone mass. Estrogen may also play a role in mechanotransduction. At the tissue level, mice lacking estrogen receptor alpha have decreased bone mass but increased capacity for adaptation in response to external mechanical loads when compared to littermate controls, particularly in cancellous bone. The molecular mechanism behind this increased anabolism is not well understood. We hypothesized that cortical and cancellous bone display different gene expression profiles at baseline and in response to mechanical loading and that mice lacking estrogen receptor alpha in bone cells have an increased response compared to littermate controls. To test this hypothesis, the left tibiae of 10-week-old female pOC-ERαKO and littermate control mice were subjected to one session of axial tibial compression and euthanized 3 and 24 hours following loading. The right limb served as the contralateral control. To examine the possible systemic effects of loading, a third group of naïve (never loaded) littermate control animals were examined. We performed RNA-seq on marrow-free metaphyseal samples from the cortical shell and the cancellous core to determine differential gene expression in response to load (versus contralateral control) and differential gene expression in naïve cortical and cancellous bone. Differential expression was verified with qPCR.

1.7 References

[1] Dempster DW, Shane E, Horbert W, Lindsay R. A simple method for correlative light and scanning electron microscopy of human iliac crest bone biopsies: qualitative observations in normal and osteoporotic subjects. J Bone Miner Res 1986;1: 15-21.

[2] Newton CD, Nunamaker DM. Textbook of small animal orthopaedics. Philadelphia: Lippincott; 1985.

[3] Yang L, Tsang KY, Tang HC, Chan D, Cheah KS. Hypertrophic chondrocytes can become osteoblasts and osteocytes in endochondral bone formation. Proc Natl Acad Sci U S A 2014;111: 12097-102.

[4] Zhou X, von der Mark K, Henry S, Norton W, Adams H, de Crombrugghe B. Chondrocytes transdifferentiate into osteoblasts in endochondral bone during development, postnatal growth and fracture healing in mice. PLoS Genet 2014;10: e1004820.

[5] Brodt MD, Ellis CB, Silva MJ. Growing C57Bl/6 mice increase whole bone mechanical properties by increasing geometric and material properties. J Bone Miner Res 1999;14: 2159-66.

[6] Glatt V, Canalis E, Stadmeyer L, Bouxsein ML. Age-related changes in trabecular architecture differ in female and male C57BL/6J mice. J Bone Miner Res 2007;22: 1197-207.

[7] D'Ippolito G, Schiller PC, Ricordi C, Roos BA, Howard GA. Age-related osteogenic potential of mesenchymal stromal stem cells from human vertebral bone marrow. J Bone Miner Res 1999;14: 1115-22.

[8] Bone Health and Osteoporosis: A Report of the Surgeon General. In. Rockville (MD): U.S. Department of Health and Human Services, Office of the Surgeon General; 2004.

[9] Burge R, Dawson-Hughes B, Solomon DH, Wong JB, King A, Tosteson A. Incidence and economic burden of osteoporosis-related fractures in the United States, 2005-2025. J Bone Miner Res 2007;22: 465-75.

[10] Pike CT, Birnbaum HG, Schiller M, Swallow E, Burge RT, Edgell ET. Prevalence and costs of osteoporotic patients with subsequent non-vertebral fractures in the US. Osteoporos Int 2011;22: 2611-21.

[11] LeBlanc ES, Hillier TA, Pedula KL, Rizzo JH, Cawthon PM, Fink HA, Cauley JA, Bauer DC, Black DM, Cummings SR, Browner WS. Hip fracture and increased short-term but not long-term mortality in healthy older women. Arch Intern Med 2011;171: 1831-7.

[12] Riggs BL, Khosla S, Melton LJ, 3rd. Sex steroids and the construction and conservation of the adult skeleton. Endocr Rev 2002;23: 279-302.

[13] Cole JH, van der Meulen MCH. Biomechanics of Bone. In: Adler RA, editor. Osteoporosis: Pathophysiology and Clinical Management. 2 ed: Humana Press; 2010, p. 157-180.
[14] Lee KC, Lanyon LE. Mechanical loading influences bone mass through estrogen receptor alpha. Exerc Sport Sci Rev 2004;32: 64-8.
[15] Callewaert F, Boonen S, Vanderschueren D. Sex steroids and the male skeleton: a tale of two hormones. Trends Endocrinol Metab 2010;21: 89-95.
[16] Falahati-Nini A, Riggs BL, Atkinson EJ, O'Fallon WM, Eastell R, Khosla S. Relative contributions of testosterone and estrogen in regulating bone resorption and formation in normal elderly men. J Clin Invest 2000;106: 1553-60.
[17] Hughes DE, Dai A, Tiffee JC, Li HH, Mundy GR, Boyce BF. Estrogen promotes apoptosis of murine osteoclasts mediated by TGF-beta. Nat Med 1996;2: 1132-6.
[18] Cooper LF, Tiffee JC, Griffin JP, Hamano H, Guo Z. Estrogen-induced resistance to osteoblast apoptosis is associated with increased hsp27 expression. J Cell Physiol 2000;185: 401-7.
[19] Black DM, Delmas PD, Eastell R, Reid IR, Boonen S, Cauley JA, Cosman F, Lakatos P, Leung PC, Man Z, Mautalen C, Mesenbrink P, Hu H, Caminis J, Tong K, Rosario-Jansen T, Krasnow J, Hue TF, Sellmeyer D, Eriksen EF, Cummings SR, Trial HPF. Once-yearly zoledronic acid for treatment of postmenopausal osteoporosis. N Engl J Med 2007;356: 1809-22.
[20] Odvina CV, Zerwekh JE, Rao DS, Maalouf N, Gottschalk FA, Pak CY. Severely suppressed bone turnover: a potential complication of alendronate therapy. J Clin Endocrinol Metab 2005;90: 1294-301.
[21] Shane E, Burr D, Abrahamsen B, Adler RA, Brown TD, Cheung AM, Cosman F, Curtis JR, Dell R, Dempster DW, Ebeling PR, Einhorn TA, Genant HK, Geusens P, Klaushofer K, Lane JM, McKiernan F, McKinney R, Ng A, Nieves J, O'Keefe R, Papapoulos S, Howe TS, van der Meulen MC, Weinstein RS, Whyte MP. Atypical subtrochanteric and diaphyseal femoral fractures: second report of a task force of the American Society for Bone and Mineral Research. J Bone Miner Res 2014;29: 1-23.
[22] Tam CS, Heersche JN, Murray TM, Parsons JA. Parathyroid hormone stimulates the bone apposition rate independently of its resorptive action: differential effects of intermittent and continuous administration. Endocrinology 1982;110: 506-12.

[23] Neer RM, Arnaud CD, Zanchetta JR, Prince R, Gaich GA, Reginster JY, Hodsman AB, Eriksen EF, Ish-Shalom S, Genant HK, Wang O, Mitlak BH. Effect of parathyroid hormone (1-34) on fractures and bone mineral density in postmenopausal women with osteoporosis. N Engl J Med 2001;344: 1434-41.

[24] Recker RR, Benson CT, Matsumoto T, Bolognese MA, Robins DA, Alam J, Chiang AY, Hu L, Krege JH, Sowa H, Mitlak BH, Myers SL. A randomized, double-blind phase 2 clinical trial of blosozumab, a sclerostin antibody, in postmenopausal women with low bone mineral density. J Bone Miner Res 2015;30: 216-24.

[25] LeVeau BF, Bernhardt DB. Developmental biomechanics. Effect of forces on the growth, development, and maintenance of the human body. Phys Ther 1984;64: 1874-82.

[26] Carter DR. Mechanical loading history and skeletal biology. J Biomech 1987;20: 1095-109.

[27] Stokes IA. Mechanical effects on skeletal growth. J Musculoskelet Neuronal Interact 2002;2: 277-80.

[28] Carter DR. Mechanical loading histories and cortical bone remodeling. Calcif Tissue Int 1984;36 Suppl 1: S19-24.

[29] Jones HH, Priest JD, Hayes WC, Tichenor CC, Nagel DA. Humeral hypertrophy in response to exercise. J Bone Joint Surg Am 1977;59: 204-8.

[30] Jaworski ZF, Liskova-Kiar M, Uhthoff HK. Effect of long-term immobilisation on the pattern of bone loss in older dogs. J Bone Joint Surg Br 1980;62-B: 104-10.

[31] Schneider V, Oganov V, LeBlanc A, Rakmonov A, Taggart L, Bakulin A, Huntoon C, Grigoriev A, Varonin L. Bone and body mass changes during space flight. Acta Astronaut 1995;36: 463-6.

[32] Fuchs RK, Bauer JJ, Snow CM. Jumping improves hip and lumbar spine bone mass in prepubescent children: a randomized controlled trial. J Bone Miner Res 2001;16: 148-56.

[33] Fuchs RK, Snow CM. Gains in hip bone mass from high-impact training are maintained: a randomized controlled trial in children. J Pediatr 2002;141: 357-62.

[34] Bassey EJ, Rothwell MC, Littlewood JJ, Pye DW. Pre- and postmenopausal women have different bone mineral density responses to the same high-impact exercise. J Bone Miner Res 1998;13: 1805-13.

[35] Kerr D, Ackland T, Maslen B, Morton A, Prince R. Resistance training over 2 years increases bone mass in calcium-replete postmenopausal women. J Bone Miner Res 2001;16: 175-81.
[36] Marcus R. Exercise: moving in the right direction. J Bone Miner Res 1998;13: 1793-6.
[37] Uusi-Rasi K, Beck TJ, Sievanen H, Heinonen A, Vuori I. Associations of hormone replacement therapy with bone structure and physical performance among postmenopausal women. Bone 2003;32: 704-10.
[38] Gross TS, Srinivasan S, Liu CC, Clemens TL, Bain SD. Noninvasive loading of the murine tibia: an in vivo model for the study of mechanotransduction. J Bone Miner Res 2002;17: 493-501.
[39] Turner CH, Akhter MP, Raab DM, Kimmel DB, Recker RR. A noninvasive, in vivo model for studying strain adaptive bone modeling. Bone 1991;12: 73-9.
[40] Lee KC, Maxwell A, Lanyon LE. Validation of a technique for studying functional adaptation of the mouse ulna in response to mechanical loading. Bone 2002;31: 407-12.
[41] Fritton JC, Myers ER, Wright TM, van der Meulen MC. Loading induces site-specific increases in mineral content assessed by microcomputed tomography of the mouse tibia. Bone 2005;36: 1030-8.
[42] De Souza RL, Matsuura M, Eckstein F, Rawlinson SC, Lanyon LE, Pitsillides AA. Non-invasive axial loading of mouse tibiae increases cortical bone formation and modifies trabecular organization: a new model to study cortical and cancellous compartments in a single loaded element. Bone 2005;37: 810-8.
[43] Lynch ME, Main RP, Xu Q, Schmicker TL, Schaffler MB, Wright TM, van der Meulen MC. Tibial compression is anabolic in the adult mouse skeleton despite reduced responsiveness with aging. Bone 2011;49: 439-46.
[44] Lynch ME, Main RP, Xu Q, Walsh DJ, Schaffler MB, Wright TM, van der Meulen MC. Cancellous bone adaptation to tibial compression is not sex dependent in growing mice. J Appl Physiol (1985) 2010;109: 685-91.
[45] Main RP, Lynch ME, van der Meulen MC. Load-induced changes in bone stiffness and cancellous and cortical bone mass following tibial compression diminish with age in female mice. J Exp Biol 2014.
[46] Melville KM, Kelly NH, Surita G, Buchalter DB, Schimenti JC, Main RP, Ross FP, van der Meulen MC. Effects of Deletion of ER-Alpha in Osteoblast-Lineage Cells on Bone Mass and Adaptation to

Mechanical Loading Differs in Female and Male Mice. J Bone Miner Res 2015.
[47] Klein-Nulend J, van Oers RF, Bakker AD, Bacabac RG. Bone cell mechanosensitivity, estrogen deficiency, and osteoporosis. J Biomech 2015;48: 855-65.
[48] Sapir-Koren R, Livshits G. Is interaction between age-dependent decline in mechanical stimulation and osteocyte-estrogen receptor levels the culprit for postmenopausal-impaired bone formation? Osteoporos Int 2013;24: 1771-89.
[49] Liedert A, Wagner L, Seefried L, Ebert R, Jakob F, Ignatius A. Estrogen receptor and Wnt signaling interact to regulate early gene expression in response to mechanical strain in osteoblastic cells. Biochem Biophys Res Commun 2010;394: 755-9.
[50] Gong Y, Vikkula M, Boon L, Liu J, Beighton P, Ramesar R, Peltonen L, Somer H, Hirose T, Dallapiccola B, De Paepe A, Swoboda W, Zabel B, Superti-Furga A, Steinmann B, Brunner HG, Jans A, Boles RG, Adkins W, van den Boogaard MJ, Olsen BR, Warman ML. Osteoporosis-pseudoglioma syndrome, a disorder affecting skeletal strength and vision, is assigned to chromosome region 11q12-13. Am J Hum Genet 1996;59: 146-51.
[51] Boyden LM, Mao J, Belsky J, Mitzner L, Farhi A, Mitnick MA, Wu D, Insogna K, Lifton RP. High bone density due to a mutation in LDL-receptor-related protein 5. N Engl J Med 2002;346: 1513-21.
[52] Westendorf JJ, Kahler RA, Schroeder TM. Wnt signaling in osteoblasts and bone diseases. Gene 2004;341: 19-39.
[53] Li X, Zhang Y, Kang H, Liu W, Liu P, Zhang J, Harris SE, Wu D. Sclerostin binds to LRP5/6 and antagonizes canonical Wnt signaling. J Biol Chem 2005;280: 19883-7.
[54] Babij P, Zhao W, Small C, Kharode Y, Yaworsky PJ, Bouxsein ML, Reddy PS, Bodine PV, Robinson JA, Bhat B, Marzolf J, Moran RA, Bex F. High bone mass in mice expressing a mutant LRP5 gene. J Bone Miner Res 2003;18: 960-74.
[55] Niziolek PJ, Warman ML, Robling AG. Mechanotransduction in bone tissue: The A214V and G171V mutations in Lrp5 enhance load-induced osteogenesis in a surface-selective manner. Bone 2012;51: 459-65.
[56] Robinson JA, Chatterjee-Kishore M, Yaworsky PJ, Cullen DM, Zhao W, Li C, Kharode Y, Sauter L, Babij P, Brown EL, Hill AA, Akhter MP, Johnson ML, Recker RR, Komm BS, Bex FJ. Wnt/beta-catenin

signaling is a normal physiological response to mechanical loading in bone. J Biol Chem 2006;281: 31720-8.
[57] Holmen SL, Giambernardi TA, Zylstra CR, Buckner-Berghuis BD, Resau JH, Hess JF, Glatt V, Bouxsein ML, Ai M, Warman ML, Williams BO. Decreased BMD and limb deformities in mice carrying mutations in both Lrp5 and Lrp6. J Bone Miner Res 2004;19: 2033-40.
[58] Kato M, Patel MS, Levasseur R, Lobov I, Chang BH, Glass DA, 2nd, Hartmann C, Li L, Hwang TH, Brayton CF, Lang RA, Karsenty G, Chan L. Cbfa1-independent decrease in osteoblast proliferation, osteopenia, and persistent embryonic eye vascularization in mice deficient in Lrp5, a Wnt coreceptor. J Cell Biol 2002;157: 303-14.
[59] Sawakami K, Robling AG, Ai M, Pitner ND, Liu D, Warden SJ, Li J, Maye P, Rowe DW, Duncan RL, Warman ML, Turner CH. The Wnt co-receptor LRP5 is essential for skeletal mechanotransduction but not for the anabolic bone response to parathyroid hormone treatment. J Biol Chem 2006;281: 23698-711.
[60] Tu X, Rhee Y, Condon KW, Bivi N, Allen MR, Dwyer D, Stolina M, Turner CH, Robling AG, Plotkin LI, Bellido T. Sost downregulation and local Wnt signaling are required for the osteogenic response to mechanical loading. Bone 2012;50: 209-17.
[61] Morse A, McDonald MM, Kelly NH, Melville KM, Schindeler A, Kramer I, Kneissel M, van der Meulen MC, Little DG. Mechanical load increases in bone formation via a sclerostin-independent pathway. J Bone Miner Res 2014;29: 2456-67.
[62] Kulkarni NH, Halladay DL, Miles RR, Gilbert LM, Frolik CA, Galvin RJ, Martin TJ, Gillespie MT, Onyia JE. Effects of parathyroid hormone on Wnt signaling pathway in bone. J Cell Biochem 2005;95: 1178-90.
[63] Wan M, Yang C, Li J, Wu X, Yuan H, Ma H, He X, Nie S, Chang C, Cao X. Parathyroid hormone signaling through low-density lipoprotein-related protein 6. Genes Dev 2008;22: 2968-79.
[64] Sugiyama T, Saxon LK, Zaman G, Moustafa A, Sunters A, Price JS, Lanyon LE. Mechanical loading enhances the anabolic effects of intermittent parathyroid hormone (1-34) on trabecular and cortical bone in mice. Bone 2008;43: 238-48.
[65] Grosso MJ, Courtland HW, Yang X, Sutherland JP, Stoner K, Nguyen J, Fahlgren A, Ross FP, van der Meulen MC, Bostrom MP. Intermittent PTH administration and mechanical loading are anabolic for periprosthetic cancellous bone. J Orthop Res 2015;33: 163-73.

[66] Tahimic CG, Wang Y, Bikle DD. Anabolic effects of IGF-1 signaling on the skeleton. Front Endocrinol (Lausanne) 2013;4: 6.
[67] Lean JM, Jagger CJ, Chambers TJ, Chow JW. Increased insulin-like growth factor I mRNA expression in rat osteocytes in response to mechanical stimulation. Am J Physiol 1995;268: E318-27.
[68] Reijnders CM, Bravenboer N, Holzmann PJ, Bhoelan F, Blankenstein MA, Lips P. In vivo mechanical loading modulates insulin-like growth factor binding protein-2 gene expression in rat osteocytes. Calcif Tissue Int 2007;80: 137-43.
[69] Sunters A, Armstrong VJ, Zaman G, Kypta RM, Kawano Y, Lanyon LE, Price JS. Mechano-transduction in osteoblastic cells involves strain-regulated estrogen receptor alpha-mediated control of insulin-like growth factor (IGF) I receptor sensitivity to Ambient IGF, leading to phosphatidylinositol 3-kinase/AKT-dependent Wnt/LRP5 receptor-independent activation of beta-catenin signaling. J Biol Chem 2010;285: 8743-58.
[70] Kesavan C, Wergedal JE, Lau KH, Mohan S. Conditional disruption of IGF-I gene in type 1alpha collagen-expressing cells shows an essential role of IGF-I in skeletal anabolic response to loading. Am J Physiol Endocrinol Metab 2011;301: E1191-7.
[71] Plotkin LI, Mathov I, Aguirre JI, Parfitt AM, Manolagas SC, Bellido T. Mechanical stimulation prevents osteocyte apoptosis: requirement of integrins, Src kinases, and ERKs. Am J Physiol Cell Physiol 2005;289: C633-43.
[72] Litzenberger JB, Tang WJ, Castillo AB, Jacobs CR. Deletion of beta 1 Integrins from Cortical Osteocytes Reduces Load-Induced Bone Formation. Cellular and Molecular Bioengineering 2009;2: 416-424.
[73] Kaneko K, Ito M, Naoe Y, Lacy-Hulbert A, Ikeda K. Integrin alphav in the mechanical response of osteoblast lineage cells. Biochem Biophys Res Commun 2014;447: 352-7.
[74] Phillips JA, Almeida EA, Hill EL, Aguirre JI, Rivera MF, Nachbandi I, Wronski TJ, van der Meulen MC, Globus RK. Role for beta1 integrins in cortical osteocytes during acute musculoskeletal disuse. Matrix Biol 2008;27: 609-18.
[75] Salazar VS, Gamer LW, Rosen V. BMP signalling in skeletal development, disease and repair. Nat Rev Endocrinol 2016;12: 203-21.
[76] Shore EM, Xu M, Feldman GJ, Fenstermacher DA, Cho TJ, Choi IH, Connor JM, Delai P, Glaser DL, LeMerrer M, Morhart R, Rogers JG, Smith R, Triffitt JT, Urtizberea JA, Zasloff M, Brown MA, Kaplan

FS. A recurrent mutation in the BMP type I receptor ACVR1 causes inherited and sporadic fibrodysplasia ossificans progressiva. Nat Genet 2006;38: 525-7.

[77] Kopf J, Petersen A, Duda GN, Knaus P. BMP2 and mechanical loading cooperatively regulate immediate early signalling events in the BMP pathway. BMC Biol 2012;10: 37.

[78] Rath B, Nam J, Deschner J, Schaumburger J, Tingart M, Grassel S, Grifka J, Agarwal S. Biomechanical forces exert anabolic effects on osteoblasts by activation of SMAD 1/5/8 through type 1 BMP receptor. Biorheology 2011;48: 37-48.

[79] Cheline AJ, Reddi AH, Martin RB. Bone morphogenetic protein-7 selectively enhances mechanically induced bone formation. Bone 2002;31: 570-4.

[80] McKenzie JA, Bixby EC, Silva MJ. Differential gene expression from microarray analysis distinguishes woven and lamellar bone formation in the rat ulna following mechanical loading. PLoS One 2011;6: e29328.

[81] Zaman G, Saxon LK, Sunters A, Hilton H, Underhill P, Williams D, Price JS, Lanyon LE. Loading-related regulation of gene expression in bone in the contexts of estrogen deficiency, lack of estrogen receptor alpha and disuse. Bone 2010;46: 628-42.

[82] Iura A, McNerny EG, Zhang Y, Kamiya N, Tantillo M, Lynch M, Kohn DH, Mishina Y. Mechanical Loading Synergistically Increases Trabecular Bone Volume and Improves Mechanical Properties in the Mouse when BMP Signaling Is Specifically Ablated in Osteoblasts. PLoS One 2015;10: e0141345.

[83] McBride-Gagyi SH, McKenzie JA, Buettmann EG, Gardner MJ, Silva MJ. Bmp2 conditional knockout in osteoblasts and endothelial cells does not impair bone formation after injury or mechanical loading in adult mice. Bone 2015;81: 533-43.

[84] Smith EP, Boyd J, Frank GR, Takahashi H, Cohen RM, Specker B, Williams TC, Lubahn DB, Korach KS. Estrogen resistance caused by a mutation in the estrogen-receptor gene in a man. N Engl J Med 1994;331: 1056-61.

[85] Gennari L, Merlotti D, De Paola V, Calabro A, Becherini L, Martini G, Nuti R. Estrogen receptor gene polymorphisms and the genetics of osteoporosis: a HuGE review. Am J Epidemiol 2005;161: 307-20.

[86] Remes T, Vaisanen SB, Mahonen A, Huuskonen J, Kroger H, Jurvelin JS, Penttila IM, Rauramaa R. Aerobic exercise and bone mineral density in middle-aged finnish men: a controlled randomized trial with

reference to androgen receptor, aromatase, and estrogen receptor alpha gene polymorphisms. Bone 2003;32: 412-20.
[87] Sonoda T, Takada J, Iba K, Asakura S, Yamashita T, Mori M. Interaction between ESRalpha polymorphisms and environmental factors in osteoporosis. J Orthop Res 2012;30: 1529-34.
[88] Suuriniemi M, Mahonen A, Kovanen V, Alen M, Lyytikainen A, Wang Q, Kroger H, Cheng S. Association between exercise and pubertal BMD is modulated by estrogen receptor alpha genotype. J Bone Miner Res 2004;19: 1758-65.
[89] Suuriniemi M, Suominen H, Mahonen A, Alen M, Cheng S. Estrogen receptor alpha polymorphism modifies the association between childhood exercise and bone mass: follow-up study. Pediatr Exerc Sci 2007;19: 444-58.
[90] Jee WS, Yao W. Overview: animal models of osteopenia and osteoporosis. J Musculoskelet Neuronal Interact 2001;1: 193-207.
[91] Thompson DD, Simmons HA, Pirie CM, Ke HZ. FDA Guidelines and animal models for osteoporosis. Bone 1995;17: 125S-133S.
[92] Windahl SH, Andersson G, Gustafsson JA. Elucidation of estrogen receptor function in bone with the use of mouse models. Trends Endocrinol Metab 2002;13: 195-200.
[93] Lindberg MK, Alatalo SL, Halleen JM, Mohan S, Gustafsson JA, Ohlsson C. Estrogen receptor specificity in the regulation of the skeleton in female mice. J Endocrinol 2001;171: 229-36.
[94] Martin-Millan M, Almeida M, Ambrogini E, Han L, Zhao H, Weinstein RS, Jilka RL, O'Brien CA, Manolagas SC. The estrogen receptor-alpha in osteoclasts mediates the protective effects of estrogens on cancellous but not cortical bone. Mol Endocrinol 2010;24: 323-34.
[95] Nakamura T, Imai Y, Matsumoto T, Sato S, Takeuchi K, Igarashi K, Harada Y, Azuma Y, Krust A, Yamamoto Y, Nishina H, Takeda S, Takayanagi H, Metzger D, Kanno J, Takaoka K, Martin TJ, Chambon P, Kato S. Estrogen prevents bone loss via estrogen receptor alpha and induction of Fas ligand in osteoclasts. Cell 2007;130: 811-23.
[96] Almeida M, Iyer S, Martin-Millan M, Bartell SM, Han L, Ambrogini E, Onal M, Xiong J, Weinstein RS, Jilka RL, O'Brien CA, Manolagas SC. Estrogen receptor-alpha signaling in osteoblast progenitors stimulates cortical bone accrual. J Clin Invest 2013;123: 394-404.
[97] Maatta JA, Buki KG, Gu G, Alanne MH, Vaaraniemi J, Liljenback H, Poutanen M, Harkonen P, Vaananen K. Inactivation of estrogen

receptor alpha in bone-forming cells induces bone loss in female mice. FASEB J 2013;27: 478-88.
[98] Melville KM, Kelly NH, Khan SA, Schimenti JC, Ross FP, Main RP, van der Meulen MC. Female mice lacking estrogen receptor-alpha in osteoblasts have compromised bone mass and strength. J Bone Miner Res 2014;29: 370-9.
[99] Windahl SH, Borjesson AE, Farman HH, Engdahl C, Moverare-Skrtic S, Sjogren K, Lagerquist MK, Kindblom JM, Koskela A, Tuukkanen J, Divieti Pajevic P, Feng JQ, Dahlman-Wright K, Antonson P, Gustafsson JA, Ohlsson C. Estrogen receptor-alpha in osteocytes is important for trabecular bone formation in male mice. Proc Natl Acad Sci U S A 2013;110: 2294-9.
[100] Kondoh S, Inoue K, Igarashi K, Sugizaki H, Shirode-Fukuda Y, Inoue E, Yu T, Takeuchi JK, Kanno J, Bonewald LF, Imai Y. Estrogen receptor alpha in osteocytes regulates trabecular bone formation in female mice. Bone 2014;60: 68-77.
[101] Lee K, Jessop H, Suswillo R, Zaman G, Lanyon L. Endocrinology: bone adaptation requires oestrogen receptor-alpha. Nature 2003;424: 389.
[102] Windahl SH, Saxon L, Borjesson AE, Lagerquist MK, Frenkel B, Henning P, Lerner UH, Galea GL, Meakin LB, Engdahl C, Sjogren K, Antal MC, Krust A, Chambon P, Lanyon LE, Price JS, Ohlsson C. Estrogen receptor-alpha is required for the osteogenic response to mechanical loading in a ligand-independent manner involving its activation function 1 but not 2. J Bone Miner Res 2013;28: 291-301.
[103] Iyer S KH, Ucer S, Bartell S, Warren A, Crawford J, Skinner R, Dallas M, Johnson M, Weinstein RS, Jilka RL, O'Brien CA, Almeida M, Manolagas SC. ER-alpha signaling in osterix1and prx1 expressing cells, respectively, mediates the anabolic effect of mechanical loading in the murine periosteum and the protective effects of estrogens on endocortical resorption J Bone Miner Res 2013;28: S1.
[104] Armstrong VJ, Muzylak M, Sunters A, Zaman G, Saxon LK, Price JS, Lanyon LE. Wnt/beta-catenin signaling is a component of osteoblastic bone cell early responses to load-bearing and requires estrogen receptor alpha. J Biol Chem 2007;282: 20715-27.
[105] Yeh CR, Chiu JJ, Lee CI, Lee PL, Shih YT, Sun JS, Chien S, Cheng CK. Estrogen augments shear stress-induced signaling and gene expression in osteoblast-like cells via estrogen receptor-mediated expression of beta1-integrin. J Bone Miner Res 2010;25: 627-39.

[106] Bonnet N, Standley KN, Bianchi EN, Stadelmann V, Foti M, Conway SJ, Ferrari SL. The matricellular protein periostin is required for sost inhibition and the anabolic response to mechanical loading and physical activity. J Biol Chem 2009;284: 35939-50.
[107] Li Y, Ge C, Long JP, Begun DL, Rodriguez JA, Goldstein SA, Franceschi RT. Biomechanical stimulation of osteoblast gene expression requires phosphorylation of the RUNX2 transcription factor. J Bone Miner Res 2012;27: 1263-74.
[108] Robling AG, Niziolek PJ, Baldridge LA, Condon KW, Allen MR, Alam I, Mantila SM, Gluhak-Heinrich J, Bellido TM, Harris SE, Turner CH. Mechanical stimulation of bone in vivo reduces osteocyte expression of Sost/sclerostin. J Biol Chem 2008;283: 5866-75.
[109] Silva MJ, Brodt MD, Lynch MA, Stephens AL, Wood DJ, Civitelli R. Tibial loading increases osteogenic gene expression and cortical bone volume in mature and middle-aged mice. PLoS One 2012;7: e34980.
[110] Xiao Z, Dallas M, Qiu N, Nicolella D, Cao L, Johnson M, Bonewald L, Quarles LD. Conditional deletion of Pkd1 in osteocytes disrupts skeletal mechanosensing in mice. FASEB J 2011;25: 2418-32.
[111] Macias BR, Aspenberg P, Agholme F. Paradoxical Sost gene expression response to mechanical unloading in metaphyseal bone. Bone 2013;53: 515-9.
[112] Mantila Roosa SM, Liu Y, Turner CH. Gene expression patterns in bone following mechanical loading. J Bone Miner Res 2011;26: 100-12.
[113] Wasserman E, Webster D, Kuhn G, Attar-Namdar M, Muller R, Bab I. Differential load-regulated global gene expression in mouse trabecular osteocytes. Bone 2013;53: 14-23.
[114] Ayturk UM, Jacobsen CM, Christodoulou DC, Gorham J, Seidman JG, Seidman CE, Robling AG, Warman ML. An RNA-seq protocol to identify mRNA expression changes in mouse diaphyseal bone: applications in mice with bone property altering Lrp5 mutations. J Bone Miner Res 2013;28: 2081-93.
[115] Zhao S, Fung-Leung WP, Bittner A, Ngo K, Liu X. Comparison of RNA-Seq and microarray in transcriptome profiling of activated T cells. PLoS One 2014;9: e78644.
[116] Jacobsen CM, Barber LA, Ayturk UM, Roberts HJ, Deal LE, Schwartz MA, Weis M, Eyre D, Zurakowski D, Robling AG, Warman ML. Targeting the LRP5 Pathway Improves Bone Properties in a Mouse Model of Osteogenesis Imperfecta. J Bone Miner Res 2014.

[117] Kedlaya R, Veera S, Horan DJ, Moss RE, Ayturk UM, Jacobsen CM, Bowen ME, Paszty C, Warman ML, Robling AG. Sclerostin inhibition reverses skeletal fragility in an Lrp5-deficient mouse model of OPPG syndrome. Sci Transl Med 2013;5: 211ra158.
[118] Isaac J, Erthal J, Gordon J, Duverger O, Sun HW, Lichtler AC, Stein GS, Lian JB, Morasso MI. DLX3 regulates bone mass by targeting genes supporting osteoblast differentiation and mineral homeostasis in vivo. Cell Death Differ 2014;21: 1365-76.
[119] Rolfe RA, Nowlan NC, Kenny EM, Cormican P, Morris DW, Prendergast PJ, Kelly D, Murphy P. Identification of mechanosensitive genes during skeletal development: alteration of genes associated with cytoskeletal rearrangement and cell signalling pathways. BMC Genomics 2014;15: 48.
[120] Govey PM, Kawasawa YI, Donahue HJ. Mapping the osteocytic cell response to fluid flow using RNA-Seq. J Biomech 2015;48: 4327-32.

CHAPTER 2[1]
A METHOD FOR ISOLATING HIGH QUALITY RNA FROM MOUSE CORTICAL AND CANCELLOUS BONE

2.1 Introduction

Osteoporosis is a skeletal disease characterized by low bone mass that often results in fracture. A majority of osteoporotic fractures occur at cortico-cancellous sites such as the proximal femur, distal forearm, and vertebra [1, 2]. At these sites bone is a composite tissue consisting of an outer cortical shell surrounding and inner cancellous network. Mouse models have been developed to understand the etiology of osteoporosis and to identify possible treatments for osteoporosis-related bone decline. Biophysical stimuli, including mechanical loading, are a promising approach to maintain and recover bone mass. In vivo loading often elicits a greater response in cancellous than cortical bone sites, increasing metaphyseal cancellous bone volume fraction by 49-73% and diaphyseal cortical area by 41% in the mouse tibia [3, 4]. But different loading protocols can alter cancellous and cortical bone responses selectively; some stimulate cancellous

[1]Kelly NH, Schimenti JC, Ross FP, van der Meulen MCH. A method for isolating high quality RNA from mouse cortical and cancellous bone. Bone. 2014;68:1-5.

bone to a greater extent, while others mainly affect cortical bone [5], indicating that differences in mechanoresponsiveness may exist in cortical and cancellous bone.

To identify the nature and degree of change in these two bone tissues requires definitive data on which genes are altered at cortical and cancellous sites following manipulation of test animals. To date this information is largely unknown, as most studies have used approaches that are derived from homogenized bone tissues.

The cellular and molecular mechanisms driving load-induced anabolism at the tissue level have been examined using both quantitative real-time polymerase chain reaction (qPCR) and microarray [6-9]. These studies have examined tissues from whole bones, homogenizing cortical and cancellous bone. In contrast, only a single study examined the loading response in cancellous bone from the mouse vertebrae, but did not compare the response to cortical bone [10]. Furthermore, marrow cells have been left in place [8], removed by flushing [7], centrifugation [6, 9], or sequential collagenase digestion [10, 11]. Collagenase digestion has been shown to affect expression of bone-related genes [12], but this effect may depend on the type of collagenase used; endotoxin-free collagenase had a less detrimental effect on RNA quality [13]. However, failure to remove the

highly cellular marrow component may result in extensive contamination of RNA isolated from unfractionated bone. The relative efficacy of flushing to centrifugation has not been studied, nor has the degree of bone marrow presence on gene expression. More importantly, gene expression has not been reported in minimally contaminated cortical versus cancellous bone, a challenging endeavor in murine models.

We describe a method to isolate high quality RNA from cortical and, separately, cancellous bone with almost no contamination from marrow cells. Both the quantity and quality of the RNA are suitable for transcriptome studies, providing the ability to compare cancellous and cortical tissues to elucidate differences in cellular and molecular mechanisms at these two sites.

2.2 Materials and methods

2.2.1 Animals

Fifteen 11-week-old male C57Bl/6 mice were euthanized and their tibiae rapidly dissected for histology (left leg) or RNA isolation and analysis (right leg). The epiphysis, all soft tissues, periosteum, fibula, and the very distal end were removed. In five mice, bone marrow of the tibia was not

removed (no marrow removal, NMR group). In another five mice, marrow was flushed with 1 mL of phosphate buffered saline (PBS) by inserting a 26-gauge needle into the distal tibia. The tibiae in the third group were centrifuged for 20 *s* at 16,100 *g* at room temperature in nested microcentrifuge tubes, where the inner tube (0.2 mL) had holes created with a 26-gauge needle to allow marrow to travel into the outer tube (0.65 mL). Tibiae were cut approximately 5 mm distal to the growth plate to isolate the metaphysis. The metaphysis was held with forceps so the proximal end was perpendicular to a 1 mm biopsy punch with plunger (33-31AA-P Miltex, Integra LifeSciences Corp., Plainsboro, NJ, USA), which was used to mechanically separate a cancellous core from the cortical shell (**Figure 2.1**). The IACUC of Cornell University approved all animal procedures.

2.2.2 Histology

Cancellous and cortical samples were placed in 10% formalin for 24 h for fixation, and decalcified in 45% formic acid for 4 days with daily exchange of the solution. Samples were processed and embedded in paraffin and sectioned longitudinally (6 μm sections, Leica RM2255, Buffalo Grove, IL, USA). Sectioned samples were stained with hematoxylin and eosin (H&E).

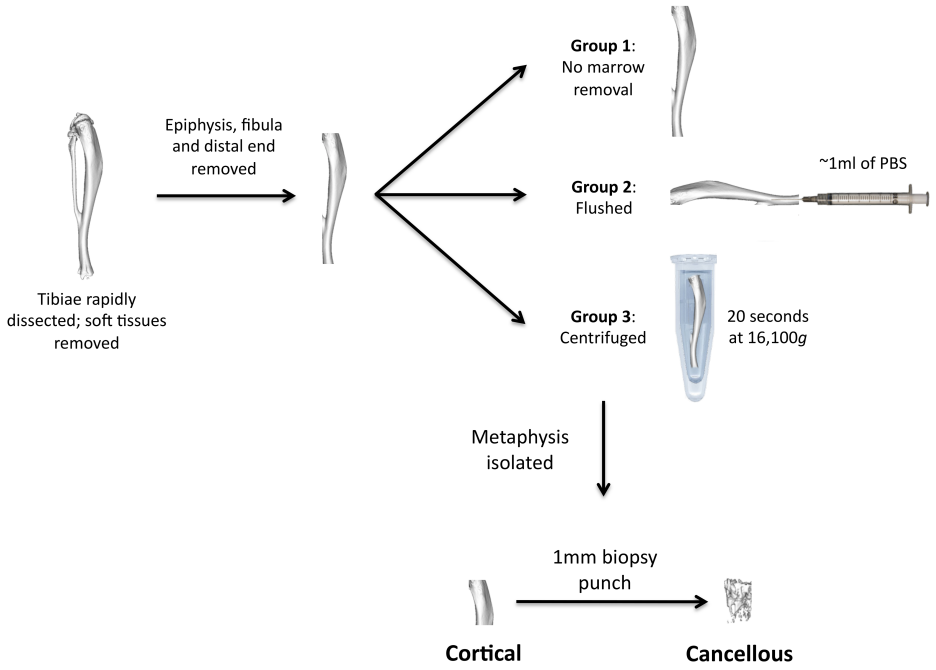

Figure 2.1 Schematic of cortical and cancellous bone sample preparation. Tibiae were rapidly dissected and soft tissues, periosteum, epiphysis, fibula, and distal end were removed. Marrow was left intact (group 1), flushed with 1 mL of PBS using a 26 g needle inserted distally (group 2), or centrifuged in nested microcentrifuge tubes for 20 *s* at 16,100 *g* (group 3). Tibiae were cut approximately 5 mm distal to the proximal end to isolate the metaphysis, and a 1 mm biopsy punch mechanically separated a cancellous core from the cortical shell.

2.2.3 RNA isolation from bone

RNA isolation was performed using Trizol (Life Technologies, Carlsbad, CA, USA) and RNeasy Mini kit (Qiagen, Germantown, MD, USA) as described previously [8]. Briefly, cancellous and cortical samples (n=30) were pulverized in liquid nitrogen-cooled flasks (Mikro-dismembrator S, Sartorius Stedim Biotech, Bohemia, NY, USA). Following pulverization,

Trizol (Life Technologies) was added to the flasks and the powdered bone/Trizol mix was incubated at room temperature for 45 min. 300 μL of chloroform was added to the samples, vortexed for 15 s, and decanted into phase lock gel tubes (PLG, heavy, 5 Prime, Gaithersburg, MD, USA). Samples were centrifuged for 15 min at 4°C and 11,500 rpm, to separate the nucleic acid phase (~600 μL), which was removed and added to an equal volume of 70% ethanol. This mixture was applied to purification columns (RNeasy Mini kit, Qiagen) following the manufacturer's instructions, including a DNase digestion (RNase free DNase kit, Qiagen). A final volume of 30 μL of RNA was eluted, and purity and quantity were tested using a spectrophotometer (NanoDrop 1000, Thermo Scientific, Wilmington, DE, USA) and RNA Quality Number (RQN) using a fragment analyzer (Advanced Analytical Technologies, Inc., Ames, IA, USA).

2.2.4 RNA isolation from marrow

Marrow from centrifuged bones (n=3) was placed in RNAlater (Qiagen) at 4°C until RNA isolation. Samples were centrifuged for 5 min, RNAlater was removed, and 600 μL of lysis buffer with β-mercaptoethanol (Buffer RLT, Qiagen) was added (as described in RNeasy Mini instructions).

Samples were homogenized by passing through an 18-gauge needle, and the supernatant (~600 μL) was added to ethanol and applied to columns for RNA purification as described above.

2.2.5 Gene expression

RNA was reverse transcribed to cDNA following the manufacturer's instructions (High Capacity cDNA Reverse Transcription kit, Life Technologies) and brought to 5 ng/μL with RNase-free water. A final volume of 20 μL containing 2X SYBR Green (Perfecta SYBR Green Fastmix, with ROX, Quanta Biosciences, Gaithersburg, MD) was assayed by triplicate qPCR using 40 cycles of denaturing (95°C, 15 s) and annealing/elongation (60°C, 60 s) (7300 Real-Time PCR System, Life Technologies). Primers for genes that are highly expressed in bone (Collagen type 1 alpha 1, *Col1a1*, and bone gamma-carboxyglutamic acid-containing protein, *Bglap*) and marrow (intracellular adhesion molecule 4, *Icam4*) were designed (available upon request). Cycles to threshold (C_T) was determined for each gene and compared to the reference gene *Gapdh*. NMR, flushed, and centrifuged groups and marrow samples are presented as relative

expression compared to *Gapdh* ($2^{-\Delta C_T}$). Fold-change to cortical and cancellous NMR groups was calculated by the $2^{-\Delta\Delta C_T}$ method [14].

2.2.6 Statistics

To test differences in relative gene expression between cancellous and cortical bone sites, and fold-change compared to NMR, a two-factor ANOVA (main effects: marrow removal and site) with interaction (marrow removal * site) was used with a Tukey's HSD post-hoc (JMP Pro 10, SAS, Cary, NC, USA). To test for differences in gene expression between marrow and cancellous and cortical bone with marrow, a one-way ANOVA was used with Tukey's HSD post-hoc. Significance was set at $p<0.05$.

2.3 Results

2.3.1 Histology

To determine if centrifugation was more effective than flushing, we performed histology with H&E of longitudinal sections of cancellous and cortical bone (**Figure 2.2**). Cortical (top panels) and cancellous bone (bottom panels) contained significant marrow that was removed incompletely by flushing. In marked contrast, marrow was barely detectable in centrifuged samples.

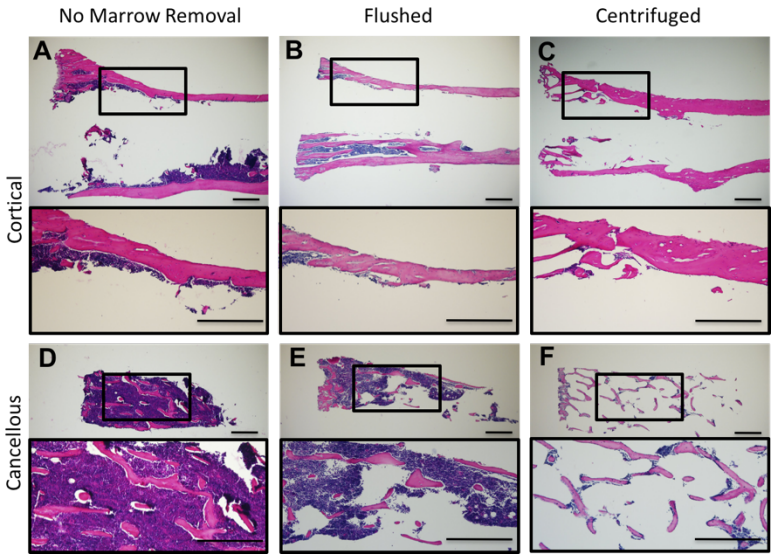

Figure 2.2 Centrifugation removes marrow more effectively than flushing in cortical and cancellous bone. Representative longitudinal 6 μm sections of (A-C) cortical and (D-F) cancellous bone stained with H&E of (A,D) bones with no marrow removal, (B,E) bones where bone marrow has been flushed, and (C,F) bones that have been centrifuged to remove marrow. Top row within each bone site is lower magnification and black rectangle outlines region of higher magnification shown on bottom row. Scale bar = 400 μm.

2.3.2 RNA quantity/quality

We also determined if sufficient, high quality RNA could be extracted from cortical and cancellous bone separately and the effect of marrow contamination on RNA quantity. Intact bone had more RNA than flushed or centrifuged bone. The mean (±SD) concentration of cortical samples was 447 (±70), 279 (±13) and 45 (±37) ng/μL for NMR, flushed, and centrifuged bone, respectively, while those for analogous cancellous samples was 186

(±54), 132 (±33) and 28 (±7) ng/μL. The average concentration for marrow samples was 191 (±130) ng/μL. The 260/280 ratio was within an acceptable range (1.8-2.1) for all samples. Cancellous samples were of higher quality than their cortical counterparts with a mean (±SD) RQN of 6.3 (±0.7) and 4.4 (±0.4), respectively.

2.3.3 Gene expression

We examined bone- and marrow-related gene expression in cortical and cancellous bone as well as bone marrow and the effect of bone marrow contamination. Centrifuged cortical bone had 12- and 13-fold higher expression of *Col1a1* and *Bglap* than bone with marrow, while the analogous data for centrifuged cancellous bone were 30- and 31-fold higher, respectively (Figure 2.3). Flushing also increased bone-related gene expression when compared to no marrow removal, but this effect was not significant (2-fold and 3-fold, *Col1a1* and *Bglap* in cortical and cancellous bone, respectively). The absolute expression of *Col1a1* and *Bglap* was lower in cancellous compared to cortical bone. Finally, marrow samples had extremely low expression of bone-related genes, ranging from 71-fold to 930-fold less than bone with marrow.

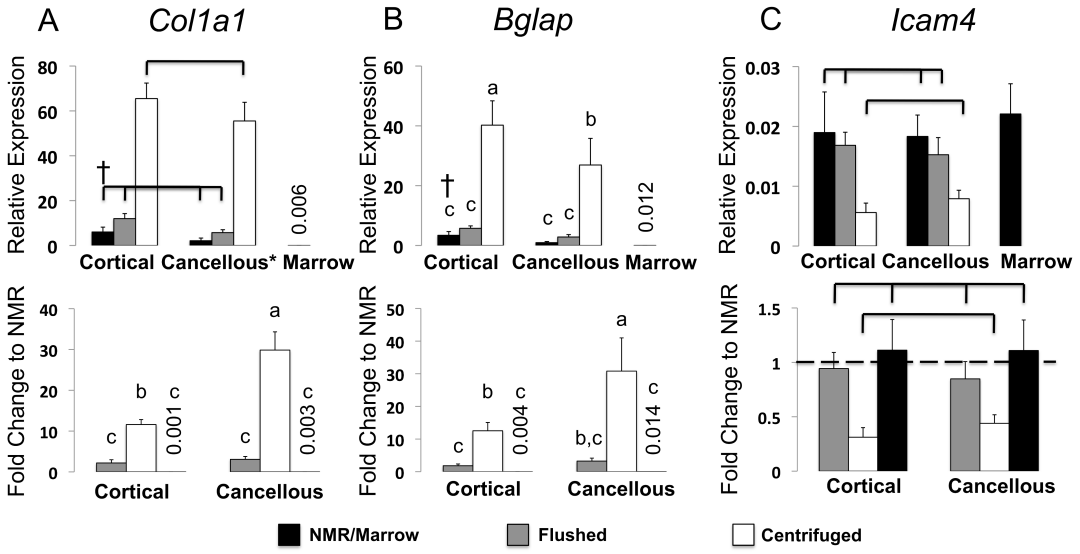

Figure 2.3 Centrifugation resulted in higher expression of bone related genes and lower expression of a gene in bone marrow. Top panels show relative expression to *Gapdh* (2−ΔCT) and bottom panels are fold-change to NMR group (2−ΔΔCT). (A) *Col1a1* was 12- and 30-fold more highly expressed in centrifuged cortical and cancellous bone, respectively, when compared to NMR. *Col1a1* expression in flushed bone was not significantly different than bone with marrow. Marrow had very low relative expression of *Col1a1* that was 932- and 307- fold lower than cortical and cancellous bone with marrow, respectively (values above bar). (B) *Bglap* was 13- and 31-fold more highly expressed in centrifuged cortical and cancellous bone, respectively, when compared to NMR. *Bglap* expression was not significantly changed in flushed bone compared to bone with marrow. Marrow had very low relative expression of *Bglap* that was 261- and 71-fold lower than cortical and cancellous bone with marrow, respectively (values above bar). (C) *Icam4* expression was decreased in centrifuged cortical and cancellous bone when compared to NMR. *Icam4* expression was similar in NMR, flushed bone, and marrow as indicated by dashed line at a fold-change value of one. Marrow had similar *Icam4* expression to bone with marrow. Data are mean±SD, n=3-5 per group. *Main effect of site: cancellous different from cortical. Brackets indicate main effect of marrow removal: no marrow removal or marrow and flushed different from centrifuged. [a-c]Groups with different letters are significantly different by Tukey HSD post-hoc. [†]Cortical NMR different from cancellous NMR and marrow groups by one-way ANOVA.

Centrifugation, but not flushing, decreased the expression of a gene that is highly expressed in bone marrow (**Figure 2.3**). *Icam4* expression in centrifuged cortical and cancellous bone was 3- and 2- fold lower, respectively, than intact bone and similar in both tissues. Flushing did not alter *Icam4* expression. Marrow samples and cortical and cancellous bone with marrow had similar expression of *Icam4*.

2.4 Discussion

We initiated these experiments based on our desire to perform more detailed analysis beyond our well-established tissue-level detailing of changes in cortical and cancellous bone following in vivo loading. Moreover, our recent report on the sexually-dimorphic and tissue-specific responses following loading of mice lacking estrogen receptor-alpha provided further impetus to pursue cellular- and molecular-based studies [15]. Finally, a review of the literature revealed no publications documenting the goals and techniques described here.

We show that RNA can be successfully isolated from centrifuged cortical and cancellous tissues of the mouse tibia separately and used for gene expression analysis. The ability to measure gene expression separately in cortical and cancellous bone is an important achievement. For example,

we discovered that the expression of two highly-expressed bone genes varies between the two tissue types. While both methods decreased marrow contamination, centrifugation removed marrow more completely than flushing in both cortical and cancellous sites when compared to intact bone. Quantitatively, this removal of contaminating marrow cells allowed bone transcripts to be more easily detected by qPCR. Bone genes were as much as 31-fold more highly expressed in centrifuged bone, while the expression of a marrow gene was decreased as much as 3-fold.

The ability to examine transcriptional activity in cortical and cancellous bone separately from a mouse is a significant achievement that has the potential to impact osteoporosis and mechanotransduction research. Cancellous bone, the major modulator of osteoporosis-associated fragility fractures, may respond differently to mechanical loading than the adjacent cortical compartment; this subject remains completely unexplored. While several studies in rodents have examined gene expression in cancellous bone [10, 16, 17], none have compared expression to the cortical bone at the same location in the mouse. Importantly, here cancellous bone from unmanipulated wild-type mice had lower expression levels of bone-related genes than cortical bone, demonstrating the importance of examining these sites separately. Moreover, these site-specific differences are likely to vary

with age, sex, genetic background or exposure to a wide range of environmental, lifestyle, or drug treatment-related simuli.

Although we have shown that centrifugation is an efficient method of marrow removal, heterogeneous cells are likely to still exist in the bone samples: for example, adherent hematopoetic and endothelial cells and a mixture of osteoblasts and osteocytes. Further work should determine the exact cellular makeup of our bone samples, including a marker of endothelial cells, such as CD31. The amount of RNA obtained from these bone sites after centrifugation was relatively small, limiting the number of genes that can be examined with qPCR. However, the RNA was of high quality and is appropriate for gene expression profiling with RNA sequencing, which requires much less input material.

2.4.1 Conclusions

Cancellous and cortical bone can be isolated separately from the mouse tibia for RNA isolation and used for gene expression studies. In all future studies examining bone gene expression centrifugation should be adopted for removing bone marrow from bone tissue since it is more efficient than flushing. The separate examination of cancellous and cortical bone has the potential to elucidate the differential response to mechanical

loading as well as genetic manipulations resulting in different bone phenotypes in these sites.

2.5 References

[1] Bone Health and Osteoporosis: A Report of the Surgeon General. In. Rockville (MD): U.S. Department of Health and Human Services, Office of the Surgeon General; 2004.

[2] Cummings SR, Melton LJ. Epidemiology and outcomes of osteoporotic fractures. Lancet 2002;359: 1761-7.

[3] Lynch ME, Main RP, Xu Q, Schmicker TL, Schaffler MB, Wright TM, van der Meulen MC. Tibial compression is anabolic in the adult mouse skeleton despite reduced responsiveness with aging. Bone 2011;49: 439-46.

[4] Lynch ME, Main RP, Xu Q, Walsh DJ, Schaffler MB, Wright TM, van der Meulen MC. Cancellous bone adaptation to tibial compression is not sex dependent in growing mice. J Appl Physiol (1985) 2010;109: 685-91.

[5] Holguin N, Brodt MD, Sanchez ME, Kotiya AA, Silva MJ. Adaptation of tibial structure and strength to axial compression depends on loading history in both C57BL/6 and BALB/c mice. Calcif Tissue Int 2013;93: 211-21.

[6] Armstrong VJ, Muzylak M, Sunters A, Zaman G, Saxon LK, Price JS, Lanyon LE. Wnt/beta-catenin signaling is a component of osteoblastic bone cell early responses to load-bearing and requires estrogen receptor alpha. J Biol Chem 2007;282: 20715-27.

[7] Bonnet N, Standley KN, Bianchi EN, Stadelmann V, Foti M, Conway SJ, Ferrari SL. The matricellular protein periostin is required for sost inhibition and the anabolic response to mechanical loading and physical activity. J Biol Chem 2009;284: 35939-50.

[8] Silva MJ, Brodt MD, Lynch MA, Stephens AL, Wood DJ, Civitelli R. Tibial loading increases osteogenic gene expression and cortical bone volume in mature and middle-aged mice. PLoS One 2012;7: e34980.

[9] Zaman G, Saxon LK, Sunters A, Hilton H, Underhill P, Williams D, Price JS, Lanyon LE. Loading-related regulation of gene expression in bone in the contexts of estrogen deficiency, lack of estrogen receptor alpha and disuse. Bone 2010;46: 628-42.

[10] Wasserman E, Webster D, Kuhn G, Attar-Namdar M, Muller R, Bab I. Differential load-regulated global gene expression in mouse trabecular osteocytes. Bone 2013;53: 14-23.

[11] Xiong J, Onal M, Jilka RL, Weinstein RS, Manolagas SC, O'Brien CA. Matrix-embedded cells control osteoclast formation. Nat Med 2011;17: 1235-41.
[12] Ayturk UM, Jacobsen CM, Christodoulou DC, Gorham J, Seidman JG, Seidman CE, Robling AG, Warman ML. An RNA-seq protocol to identify mRNA expression changes in mouse diaphyseal bone: applications in mice with bone property altering Lrp5 mutations. J Bone Miner Res 2013;28: 2081-93.
[13] Fujita K, Roforth MM, Atkinson EJ, Peterson JM, Drake MT, McCready LK, Farr JN, Monroe DG, Khosla S. Isolation and characterization of human osteoblasts from needle biopsies without in vitro culture. Osteoporos Int 2014;25: 887-95.
[14] Livak KJ, Schmittgen TD. Analysis of relative gene expression data using real-time quantitative PCR and the 2(-Delta Delta C(T)) Method. Methods 2001;25: 402-8.
[15] Melville KM, Kelly NH, Khan SA, Schimenti JC, Ross FP, Main RP, van der Meulen MC. Female mice lacking estrogen receptor-alpha in osteoblasts have compromised bone mass and strength. J Bone Miner Res 2014;29: 370-9.
[16] Macias BR, Aspenberg P, Agholme F. Paradoxical Sost gene expression response to mechanical unloading in metaphyseal bone. Bone 2013;53: 515-9.
[17] Zheng D, Peng S, Yang SH, Shao ZW, Yang C, Feng Y, Wu W, Zhen WX. The beneficial effect of Icariin on bone is diminished in osteoprotegerin-deficient mice. Bone 2012;51: 85-92.

CHAPTER 3[1]
TRANSCRIPTIONAL PROFILING OF CORTICAL VERSUS CANCELLOUS BONE FROM MECHANICALLY-LOADED MURINE TIBIAE REVEALS DIFFERENTIAL GENE EXPRESSION

3.1 Introduction

Osteoporosis is characterized by bone loss that often leads to fracture of corticocancellous sites such as the hip, spine, and wrist [1, 2]. The majority of current drug treatments are anti-catabolic and decrease the resorption of bone by osteoclasts. In contrast, parathyroid hormone (PTH) is the only FDA-approved anabolic drug proven to increase bone formation [3]. A promising route to discover other anabolic drug targets arises from the fact that bone is mechanosensitive.

Mechanical loading of the skeleton by exercise in humans increases bone mineral density [4-7]. In mouse models in vivo compression of the tibia allows for the application of controlled loads and differentially increases bone mass in cortical (Ct) and cancellous (Cn) sites [8-10]. The molecular

[1]Kelly NH, Schimenti JC, Ross FP, van der Meulen MCH. Transcriptional profiling of cortical versus cancellous bone from mechanically-loaded murine tibiae reveals differential gene expression. Bone. 2016;86:22-29.

mechanisms behind this anabolic response to mechanical loading need to be determined and compared between cancellous and cortical bone. This knowledge may enhance the development of drug therapies to increase bone formation in osteoporotic patients.

Gene expression following in vivo tibial compression in mice has been examined with qPCR and microarray of cortical or homogenized cortical and cancellous bone [11-14]. Wnt/β catenin signaling [11, 12] and estrogen receptor alpha signaling [11, 14] are involved in the anabolic loading response. Limitations of previous work include the combined examination of cortical and cancellous bone and the biased determination of pathways and genes of interest. Moreover, the presence of large numbers of contaminating bone marrow cells is likely to skew further any findings. RNA sequencing has become the standard method to examine total gene transcription at any point in time. Unlike qPCR or microarray techniques RNA sequencing is unbiased and does not examine a predetermined set of genes. Furthermore, RNA-seq requires a relatively small amount of input material (>10-100ng), and thus is ideal for examining small tissue samples such as fractionated murine bone.

We recently published a method to examine gene expression in cortical and cancellous bone and demonstrated with qPCR that

centrifugation removed marrow more efficiently and increased the expression of bone-related genes [15]. Expanding on this method, we now ask how transcriptional profiles differ in cortical and cancellous bone at baseline and in response to mechanical loading. To date, use of RNA-seq to study murine bone has been limited and only focused on the cortical diaphysis, homogenized metaphysis or whole bones [16-20]. Transcriptional profiling with RNA-seq provides an opportunity to determine gene expression in cortical and cancellous tissues separately and to examine the molecular mechanisms responsible for mechanical loading-related anabolism. We hypothesized that basal gene expression would differ in cortical and cancellous bone and that the transcriptional response to mechanical loading would differ between the two tissues. To test this hypothesis, we applied compressive loading to the mouse tibia and performed RNA-seq in cortical and cancellous bone separately at two time points.

3.2 Materials and methods

3.2.1 Animals

Fourteen 10-week-old female C57Bl/6 mice were subjected to a single session of in vivo mechanical loading of the left tibia (9N max load, 1200

cycles, 4Hz, triangle waveform) with the right tibia as contralateral control [9, 10, 21]. Three and twenty-four hours after a single loading session mice were euthanized (n=7/group), and their tibiae rapidly dissected for RNA isolation. The epiphysis, all soft tissues, periosteum, fibula, and the distal end were removed. Tibiae were centrifuged for 20s at 16,100*g* at room temperature in microcentrifuge tubes, as previously described [15] and then cut approximately 5 mm distal to the growth plate to isolate the metaphysis. The cancellous core of the metaphysis was separated from the cortical shell with a 1mm biopsy punch (Miltex, Integra LifeSciences Corp, Plainsboro, NJ). The IACUC of Cornell University approved all animal procedures.

3.2.2 RNA isolation

RNA isolation was performed using Trizol (Life Technologies, Carlsbad, CA) and RNeasy Mini kit (Qiagen, Germantown, MD) as described previously [13]. Briefly, individual cancellous and cortical samples were pulverized in liquid nitrogen-cooled flasks (Mikro-dismembrator S, Sartorius Stedim Biotech, Bohemia, NY, USA). Following pulverization, Trizol was added to the flasks and the powdered bone/Trizol mix was incubated at room temperature for 45 minutes. 300μL of chloroform was added to samples, vortexed for 15s, and decanted into phase lock gel tubes

(PLG, heavy, 5 Prime, Gaithersburg, MD). Samples were centrifuged for 15 minutes at 4C and 11,500 rpm, to separate the nucleic acid phase (~600μL), which was removed and added to an equal volume of 70% ethanol. This mixture was applied to purification columns (RNeasy Mini kit, Qiagen) following the manufacturer's instructions, including a DNase digestion (RNase free DNase kit, Qiagen). A final volume of 30μL of RNA was eluted.

RNA purity and quantity were tested using a spectrophotometer (Nanodrop 1000, Thermo Scientific, Wilmington, DE) and RNA Quality Number (RQN) using a fragment analyzer (Advanced Analytical Technologies, Inc, Ames, IA). The mean (±SD) concentration of cortical samples was 92 (±40) ng/μL, and for cancellous samples was 30 (±17) ng/μL. The 260/280 ratio was within an acceptable range (1.8-2.1) for all samples. Cancellous samples were of higher quality than their cortical counterparts with a mean (±SD) RQN of 7.4 (± 0.9) and 5.3 (± 0.8), respectively.

3.2.3 RNA-seq library preparation and analysis

Total RNA from 8 animals (n=32 samples; 4 samples/animal from cortical and cancellous tissue of two tibiae) was processed to create RNA-

seq libraries (Illumina TruSeq RNA Sample Preparation Kit v2, San Diego, CA) following the manufacturer's instructions. mRNA was purified with polyA+ magnetic beads, chemically fragmented (120-200bp fragments), reverse transcribed using random hexamers, and ligated to bar-coded adapters. The resulting cDNA fragments were amplified to provide sufficient material for subsequent analysis. Finally, primer-dimers were removed by washing with AMPure XP beads (Agencourt AMPure XP, Beckman Coulter, Brea, CA). Final libraries were tested using a fragment analyzer to determine the distribution of fragment sizes. The thirty-two individually bar-coded libraries were normalized, pooled (maximum of 12 libraries/lane), and sequenced (100-bp single-end reads, Illumina HiSeq 2000).

Sequences were aligned to the mouse genome (mm10) using TopHat followed by transcript assembly and gene counts with Cuffdiff [22]. On average, 77% of the 18 million reads/library were mapped to the mouse genome, 95% uniquely. Differential expression was determined with a paired design in edgeR [23]. The paired design consisted of an additive linear model with blocking for which the blocking factor was "tissue" when baseline cortical and cancellous tissue from the same bone were compared, and the blocking factor was "animal" when the loaded limb was compared to the

control contralateral limb in the same animal. Genes with low expression were filtered from each library by removing genes with counts per million less than one in at least four samples. Finally, differentially expressed genes were determined by fitting gene-wise generalized linear models and performing likelihood ratio tests. Genes were differentially expressed based on fold-change (FC) cut-off and 5% false discovery rate (FDR) cut-off. A more stringent fold change cut-off was applied for normal developmental changes (Ct to Cn baseline, >2-fold) than loading induced changes (>1.5-fold).

For the basal samples only, we identified contaminants from our RNA-seq data based on genes determined to be highly expressed in muscle, bone marrow, or blood compared to tibial bone by Ayturk et al. [16]. For the loaded samples all gene changes are reported including genes considered contaminants in the basal analysis.

Lists of differentially expressed genes were imported into the Database for Annotation, Visualization and Integrated Discovery (DAVID, from the National Institute of Allergy and Infectious Diseases (NIAID), NIH - http://david.abcc.ncifcrf.gov/). Gene ontology (GO) for biological processes and enriched Kyoto Encyclopedia of Genes and Genomes

(KEGG) pathways were determined for each group using the functional annotation tool ($p<0.05$) [24, 25].

3.2.4 Gene expression verification with qPCR

Using qPCR, we verified differential gene expression obtained from RNAseq for 12 genes that were different between the two tissues or with loading: *Gpr50*, *Grem1*, *Ostn*, *Ptgs2*, *Ptn*, *Sost*, *Timp1*, *Tnfrsf11b*, *Wnt1*, *Wnt10b*, *Wnt16*, and *Wnt7b* (primer sequences in **Table A.1**). RNA from the remaining animals (n=3/per group) was reverse transcribed to cDNA following the manufacturer's instructions (High Capacity cDNA Reverse Transcription kit, Life Technologies) and brought to 5ng/μL with RNase-free water. A final volume of 20μL containing 2X SYBR Green (Perfecta SYBR Green Fastmix, with ROX, Quanta Biosciences, Gaithersburg, MD) was assayed by triplicate qPCR using 39 cycles of denaturing (95C, 5s) and annealing/elongation (60C, 30s) (CFX96 Real-Time PCR System, BioRad, Hercules, CA). Quantification cycle (Cq) was determined for each gene and compared to the reference gene *Gapdh*. All groups are presented as fold change with loading or tissue type ($2^{-\Delta\Delta Cq}$). The $\log_2$ fold-change of RNA-seq versus qPCR was graphed to determine quality of correlation; a slope of one

would define perfect agreement. The strength of the relationship was quantified by Pearson correlation.

3.3 Results

3.3.1 Control cortical and cancellous bone exhibit different transcriptional profiles

We first compared the transcription profiles of cortical and cancellous bone from control limbs (>2-fold). Cortical and cancellous bone samples from the contralateral control (non-loaded) limbs were analyzed 3 hours and 24 hours after a single loading dose. A total of 178 genes were differentially expressed three hours after a single loading dose, with 110 genes more highly expressed in control cortical bone and 68 genes more highly expressed in control cancellous bone (**Figure 3.1A, Table A.2**). Genes known to be expressed in mesenchymal-derived bone cells included *ostn* (osteocrin; 29-fold, Ct>Cn), *wnt16* (wingless-related MMTV integration site 16; 12-fold, Ct>Cn), *wnt7b* (wingless-related MMTV integration site 7b; 7-fold, Ct>Cn), and *sost* (sclerostin; 4-fold, Ct>Cn).

Three hundred and twenty six genes were differentially expressed 24 hours after a single loading dose, with 287 genes more highly expressed in cortical bone and 39 genes more highly expressed in cancellous bone (**Figure 3.1A, Table A.3**). Ninety-three differentially expressed genes were shared at the two time points (77 Ct>Cn, 16 Cn>Ct) and included *ostn* (52-

fold, 24h), *wnt16* (43-fold, 24h), *wnt7b* (4-fold, 24h), and *sost* (4-fold, 24h) (**Figure 3.1B**).

When cortical vs cancellous gene expression was examined in control tissue, five differentially-expressed genes from the 3-hour group and 84 differentially-expressed genes from the 24-hour group were previously shown to be more highly expressed in skeletal muscle than bone and thus designated as "contaminants" by Ayturk et al. [16]. When we examined these genes in our data, all "contaminating" genes that were more highly expressed in cortical bone (n=83) were genes previously associated with muscle. Of those Ayturk-designated contaminant genes that were more highly expressed in cancellous bone in our data (n=4), one was from marrow, two from blood, and only one from muscle. Because the previously-identified contaminant genes in cortical bone were all from muscle and the cancellous genes from marrow and blood, we excluded these genes from the pathway analysis of the control tissue.

Gene ontology (GO) was determined separately for genes that were more highly expressed in cancellous and cortical bone. All genes from both time points were included, with the exception of the contaminating genes identified by Ayturk et al. The extracellular matrix-receptor interaction pathway was enriched in both cancellous and cortical bone, while

melanogenesis was enriched in cortical bone only and complement and coagulation cascades were enriched in cancellous bone only (**Figure 3.1C**). In cancellous bone, the top biological processes were regulation of body fluid levels, coagulation, and blood coagulation while in cortical bone cell adhesion, biological adhesion, and skeletal system development were the identified processes (**Figure 3.1D**).

A

B

Gene	Fold Change (Cortical v Cancellous)	
	3h	24h
Ostn	29.49	51.79
Itgbl1	12.27	57.04
Wnt16	11.76	42.82
Tnn	7.78	11.19
Angptl7	7.77	29.70
Col3a1	7.11	10.46
Aspn	7.08	14.62
Igfbp6	6.82	56.47
Wnt7b	6.62	3.71
Col8a2	6.50	14.20

C

Signaling Pathway	Cortical Genes	Cancellous Genes
ECM-receptor interaction	Tnxb, Col3a1, Tnn, Thbs2, Thbs4	Vwf, Gp5, Gp6, Gp1ba, Itga2b
Melanogenesis	Wnt7b, Wnt16, Wnt10b, Edn1, Wnt9a	N.S.
Complement and Coagulation Cascades	N.S.	Kng1, Vwf, Kng2, C4b

D

Cortical	Cancellous
Biological Processes	Biological Processes
Cell adhesion	Regulation of body fluid levels
Biological adhesion	Coagulation
Skeletal system development	Blood coagulation

Figure 3.1 Control cortical and cancellous bone exhibit distinctly different transcriptional profiles. (A) Venn diagram showing the number of differentially expressed genes between control cortical and cancellous bone at 3 (left) and 24 (right) hours (FDR<5%, FC>2). Arrows (%) indicate proportion of genes that were more highly expressed in cortical (green) or cancellous (red) bone. A majority of genes were more highly expressed in cortical bone. (B) Top 10 genes (by 3h FC) out of 93 total differentially expressed in cortical versus cancellous bone that were shared at both time points. All genes shown are more highly expressed in cortical bone. DAVID analysis determined C) significantly enriched pathways and D) biological processes in cortical and cancellous bone ($p<0.05$).

3.3.2 The mechanical loading response at 3h is driven by Wnt signaling in cortical and cancellous bone

Three hours after a single loading session 43 genes were differentially expressed >1.5-fold in cortical bone and 18 in cancellous bone. A majority of genes were upregulated by loading in both cortical and cancellous bone (**Figure 3.2A**). Eleven genes were shared and included *Wnt1* (wingless-related MMTV integration site 1; 6.2-fold Ct, 4.1-fold Cn), *Wnt7b* (3.2-fold Ct, 7.8-fold Cn), *Timp1* (tissue inhibitor of metalloproteinase 1; 1.6-fold Ct, 1.9-fold Cn), *Ptgs2* (prostaglandin-endoperoxide synthase 2; 4.3-fold Ct, 3.9-fold Cn), and *Tnfrsf11b* (tumor necrosis factor receptor superfamily, member 11b (osteoprotegerin); 2.2-fold Ct, 1.9-fold Cn) (Figure 3.2B). Enriched signaling pathways included Wnt signaling in both cortical and cancellous bone and hedgehog signaling in cortical bone only (Figure 3.2C). Enriched biological processes included Wnt receptor signaling in cancellous and cortical bone, biomineral formation in cortical bone, and developmental maturation in cancellous bone (**Figure 3.2D**). Complete lists of differentially expressed genes with mechanical loading can be found in **Table A.4** (cortical bone) and **Table A.5** (cancellous bone).

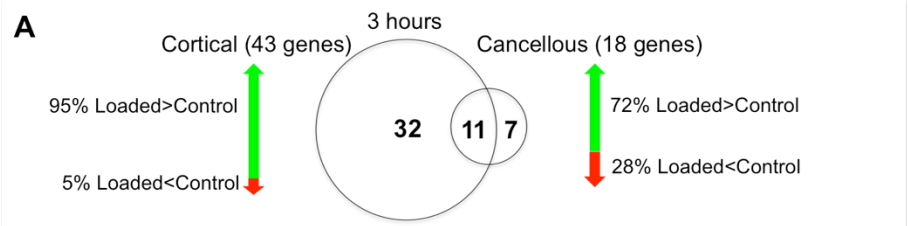

B

Gene	Fold Change (loaded vs control)	
	Cortical	Cancellous
Fam20c	1.5	1.6
Ngf	3.9	2.4
Nt5e	1.9	3.4
Ptgs2	4.3	3.9
Srxn1	1.9	1.5
Tfpi2	2.1	1.8
Timp1	1.6	1.9
Tnfrsf11b	2.2	1.9
Tnfrsf12a	2.8	3.1
Wnt1	6.2	4.1
Wnt7b	3.2	7.8

C

Signaling Pathway	Cortical Genes	Cancellous Genes
Wnt Signaling	Wnt1, Wnt7b, Wnt10b, Crebbp, Lrp5	Wnt1, Wnt7b, Dkk1
Hedgehog signaling	Wnt1, Wnt7b, Wnt10b, Bmp2	N.S.

D

Cortical		Cancellous	
Biological Processes	Genes	Biological Processes	Genes
Wnt receptor signaling	Wnt1, Wnt7b, Wnt10b	Wnt receptor signaling	Wnt1, Wnt7b, Dkk1
Biomineral Formation	Bmp2, Ptgs2, Dmp1	Developmental maturation	Wnt1, Ptgs2, Timp1

Figure 3.2 Differential expression of Wnt signaling genes 3 h following a single loading session in cortical and cancellous bone. (A) Venn diagram showing the number of genes significantly altered by mechanical loading at 3 h in cortical (left) and cancellous (right) bone (FDR<5%, FC>1.5). Arrows (%) indicate proportion of genes that were up- (green) or down- (red) regulated. A majority of genes were upregulated by loading. B) Genes differentially expressed due to mechanical loading common to both cortical and cancellous bone. DAVID analysis determined C) significantly enriched pathways and D) biological processes in cortical and cancellous bone following loading ($p<0.05$).

3.3.3 The mechanical loading response at 24h includes changes in Wnt signaling in cortical bone and muscle-related genes in cancellous bone

Twenty-four hours after a single loading session 58 genes were differentially expressed in cortical and 32 differentially expressed genes in cancellous bone (>1.5-fold). More genes were upregulated by loading in cortical bone (60%), while more genes were downregulated in cancellous

bone (66%) (**Figure 3.3A**). Both tissue types shared twelve genes, including *Ptn* (pleiotrophin; 2.7-fold Ct, 3.1-fold Cn), *Vcan* (versican; 1.8-fold Ct, 1.6-fold Cn), and *Tubb3* (tubulin beta 3; 2.5-fold Ct, 1.8-fold Cn) (Figure 3.3B). The only enriched signaling pathway in cortical bone was melanogenesis, while the only enriched pathway in cancellous bone was tight junction (**Figure 3.3C**). Biological processes included response to organic substance and response to toxin in cortical and muscle contraction and muscle system process in cancellous (**Figure 3.3D**). Notably, many highly downregulated muscle-related genes were identified in cancellous bone including *Myh4* (myosin, heavy polypeptide 4, skeletal muscle; −59.5-fold), *Tnnc2* (troponin C2, fast; −41.6-fold), *Smpx* (small muscle protein, X-linked; −32.3-fold), *Tnnt3* (troponin, T3, skeletal, fast; −36.6-fold), *Mylk2* (myosin, light polypeptide kinase 2, skeletal muscle; −22.4-fold), *Myoz1* (myozenin 1; −23.4-fold), *Myom2* (myomesin 2; −21.5-fold), *Actn3* (actinin alpha 3; −14.7-fold), *Myl1* (myosin, light polypeptide 1; −13.8-fold), *Casq1* (calsequestrin 1; −12.4-fold), *Mybpc2* (myosin binding protein C, fast-type; −12.1-fold), *Myh2* (myosin, heavy polypeptide 2, skeletal muscle, adult; −12.2-fold), *Mylpf* (myosin light chain, phosphorylatable, fast skeletal muscle; −12.9-fold), and *Tnni2* (troponin I, skeletal, fast 2; −7.7-fold). Complete lists of differentially

expressed genes can be found in **Table A.6** (cortical) and **Table A.7** (cancellous).

A

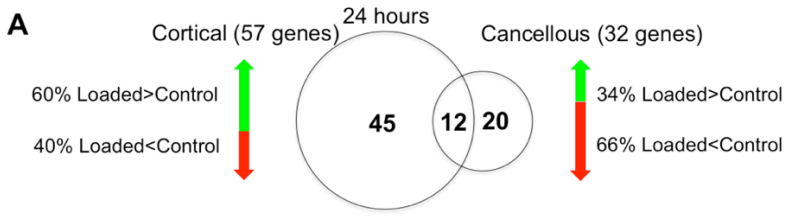

B

Gene	Fold Change (loaded vs control)	
	Cortical	Cancellous
Ampd1	-8.7	-31.2
Cthrc1	1.7	1.6
Dhrs7c	-8.3	-28.6
Fkbp11	1.6	1.6
Hapln4	1.8	1.7
Lurap1l	1.8	1.8
Nmb	-2.0	-1.9
Peg10	1.8	1.7
Ptn	2.7	3.1
Slc9b2	-1.6	-1.7
Tubb3	2.5	1.8
Vcan	1.8	1.6

C

Location	Signaling Pathway	Genes
Cortical	Melanogenesis	Wnt1, Wnt10b, Gnal1
Cancellous	Tight Junction	Myh2, Myh4, Myplf, Actn3

D

Cortical		Cancellous	
Biological Processes	Genes	Biological Processes	Genes
Response to Organic Substance	Mt2, Nr4a2, Mt1, Mt3	Muscle Contraction	Mybpc2, Myom2, Myh2, Myh4, Actn3
Response to Toxin	Mt2, Nr4a2, Mt1	Muscle System Process	

Figure 3.3 Wnt signaling changes in cortical bone and muscle-related changes in cancellous bone 24 h following a single loading session. (A) Venn diagram showing the number of genes significantly altered by mechanical loading at 24 h in cortical (left) and cancellous (right) bone (FDR<5%, FC>1.5). Arrows (%) indicate proportion of genes that were up- (green) or down- (red) regulated. A majority of genes were upregulated by loading in cortical bone, while in cancellous bone, a majority of genes were downregulated. B) Genes differentially expressed due to mechanical loading common to both cortical and cancellous bone. Negative fold change values indicate downregulation in response to loading. DAVID analysis determined C) significantly enriched pathways and D) biological processes in cortical and cancellous bone following loading ($p<0.05$).

3.3.4 Temporal comparison of differentially expressed genes with mechanical loading

The gene expression response within cortical bone was grossly different at 3 and 24 hours following a single loading dose (**Figure 3.4A**).

More genes were upregulated at 3 hours and to a greater magnitude than at 24 hours, while at 24 hours more genes were highly downregulated than at 3 hours. Four genes were differentially expressed in cortical bone at both 3 and 24 hours following a single loading session: *Wnt1*, *Wnt10b*, *Ptgs2*, and *Mt2* (metallothionein 2; upregulated at 3h, downregulated at 24h).

In cancellous bone the upregulated genes at 3 hours and 24 hours had similar magnitudes of fold-change, but more genes were downregulated with higher magnitude fold-change at 24 hours (**Figure 3.4B**). Only *Timp1* was upregulated both 3h and 24h following a single loading dose in cancellous bone (1.9-fold 3h, 1.7-fold 24h).

Finally, more genes were differentially expressed following loading at 24 hours in both cortical and cancellous bone. At both 3 and 24 hours more genes were differentially expressed in cortical than cancellous bone. The magnitude of the fold change in upregulated genes at 3h in cortical bone was larger than in cancellous bone, while at 24h the magnitude of the fold change in downregulated genes was larger in cancellous bone than in cortical bone.

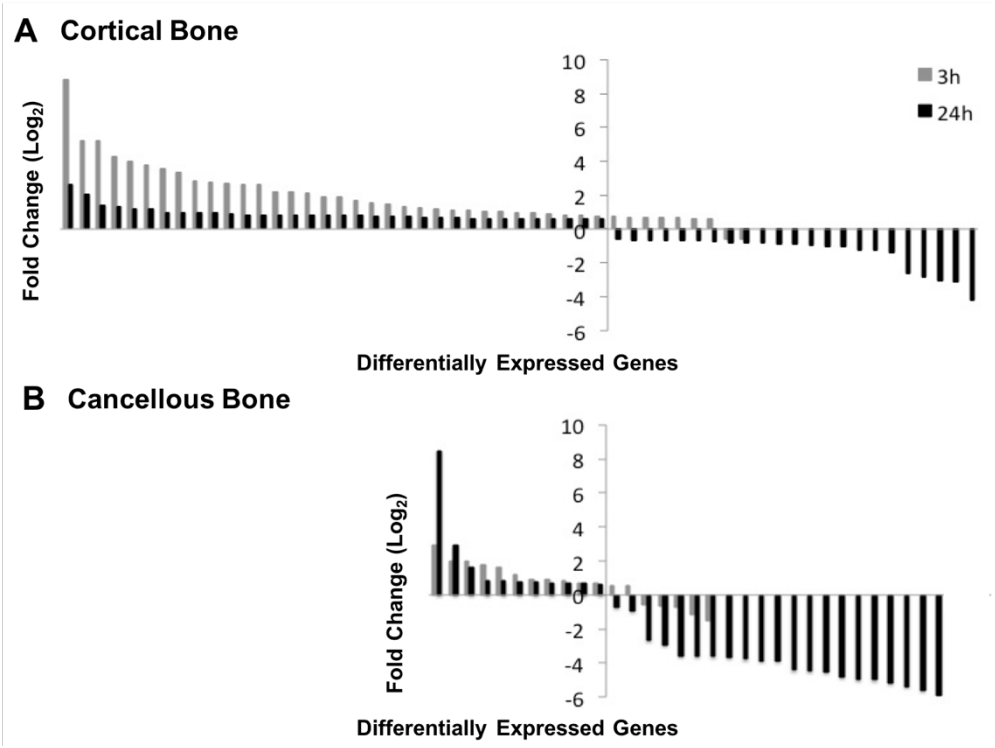

Figure 3.4 More genes were differentially expressed in cortical bone and at 24 h. Ranged $\log_2$ fold change histograms of differentially expressed genes in A) cortical and B) cancellous bone at 3 h (gray bars) and 24 h (black bars) after a single loading session. The y-axis is aligned with the inflection between up- and down-regulated genes at 24 h to assist in visualization of trends in differentially expressed genes between time points and tissue types.

3.3.5 RNA-seq verification with qPCR

We found strong agreement between qPCR and RNA-seq for the twelve genes tested. When all differentially expressed genes were included (not only significant changes), the slope of the linear fit between RNA-seq and qPCR was close to one and the Pearson correlation was 0.89 (**Figure 3.5**).

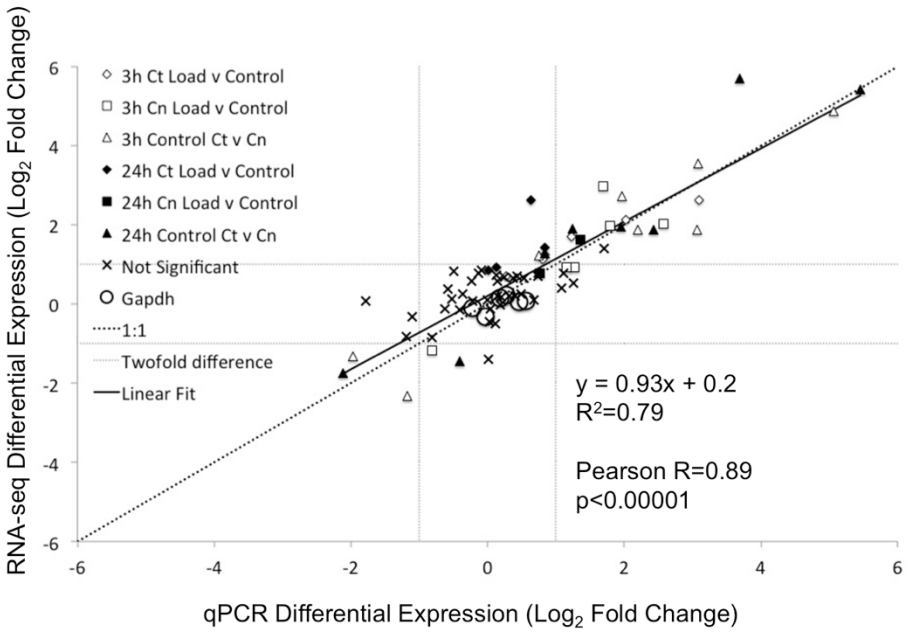

Figure 3.5 qPCR validated 12 differentially expressed genes. qPCR was performed for 12 genes identified as differentially expressed with RNA-seq. Log2 fold change from RNA-seq vs qPCR. Gray dashed lines indicate 2-fold up- and down-regulation, black dashed line is the identity line (1:1 relationship), and the solid line is the linear regression.

3.4 Discussion

We used RNA-seq to compare gene expression in cortical and cancellous bone of control and loaded limbs following a single bout of axial tibial compression in 10-week-old female mice. Cortical and cancellous bone expressed different genes basally and in response to in vivo mechanical loading at two time points. At baseline, many genes were differentially regulated between cortical and cancellous bone, the majority of which were

more highly expressed in cortical bone. Genes expressed by osteoblasts and those mediating Wnt signaling dominated the response three hours after a single loading session. Cortical expression twenty-four hours after a single loading session was still enriched for upregulated bone-related and Wnt signaling genes, while the cancellous response involved downregulation of many muscle-related genes. More genes were differentially expressed at the twenty-four hour time point in both cortical and cancellous bone than three hours after loading.

The differential gene expression in baseline cortical and cancellous bone identified here is not surprising considering differences in growth and aging in these bone sites. Cortical and cancellous bone arise through different growth processes and have different age-related bone mass accrual and subsequent loss. For both tissues, hypertrophic chondrocytes can become osteoblasts and osteocytes that contribute to cancellous bone, the endosteum and mature bone [26, 27]. Cortical bone mass increases during development, stabilizes at skeletal maturity, and decreases during aging [28, 29]. Cancellous bone mass also increases initially during growth but decreases immediately after reaching peak bone mass, without a stabilization phase [30]. These differences in development and age-related changes between cancellous and cortical bone suggest different regulatory

mechanisms driven by the differential transcription demonstrated in our study. Furthermore, we confirmed that differences in gene expression did not reflect different proportions of bone cells in cortical and cancellous bone by determining the number of osteoblasts per bone surface and the number of osteocytes per bone area. These measures were not different in cortical and cancellous samples from six animals (data not shown).

More genes were expressed differentially twenty-four hours after a single loading session in control bone, implying that mechanical loading is not a purely local response in terms of gene transcription. Dynamic loading of the tibia causes adaptation in the loaded bone only and not in adjacent, contra-lateral or remote sites when measured at the tissue level with microcomputed tomography [31]. Future studies should examine transcription in cortical and cancellous bone of naïve (not externally loaded) animals to determine if loading causes systemic changes in gene expression.

Wnt signaling is vital for skeletal development and maintenance [32]. Recently, genetic variants in *Wnt16* were linked to cortical bone thickness, bone mineral density and fracture risk in humans [33]. Mice lacking *Wnt16* have 27% thinner femoral cortices, bone strength reductions of 43%-61% and develop spontaneous fractures without changes in cancellous mass or architecture [33, 34]. *Wnt16* is osteoblast-derived and inhibits

osteoclastogenesis by decreasing osteoclast progenitors and increasing osteoblast expression of osteoprotegerin [34]. In the current study *Wnt16* was 12- to 43-fold more highly expressed in cortical bone, in agreement with the cortical bone phenotype seen in humans and mice. *Sost*, a Wnt signaling inhibitor, was also more highly expressed in cortical bone (4-fold); however, a clear cortical-only bone phenotype is not seen in humans or rodents. *Sost* gene loss-of-function in humans causes Sclerosteosis and van Buchem's diseases, characterized by drastically increased bone mass [35, 36]. Furthermore, sclerostin antibody increased bone mineral density by 3-12% at the lumbar spine, total hip and femoral neck after one year of treatment in a phase II clinical trial [37]. In addition, *Sost* deficient mice have high bone mass in both cortical and cancellous sites [38], and Sclerostin antibody increased bone formation in both cortical and cancellous bone in rats [39, 40] and cynomolgus monkeys [41].

Signaling pathways and genes regulating mechanoresponsiveness have been determined largely from studies of cortical bone, and the few studies that examine cancellous bone response have conflicting results. Osteocytes in the cancellous bone of the mouse vertebrae were examined six hours after a single loading dose. 287 genes were upregulated including *Wnt5a*, *Aspn*, and *Igf1,* while 52 genes were downregulated including *Spock2* and *Col19a1*

[42]. Notably *Sost* did not change, while we saw a 2-fold downregulation of *Sost* 3 hours following loading in cancellous bone. Furthermore, our two studies shared few genes that were differentially expressed due to mechanical stimulation. This disparity may reflect the different time points examined following loading, different bones examined, or their use of collagenase digestion, which affects gene expression [16]. Three days of hindlimb unloading in rats decreased *Sost* expression in metaphyseal cancellous bone, had no effect on metaphyseal cortical bone, and caused upregulation in the cortical diaphysis [43]. Differences in cortical and cancellous expression and the lack of studies of mechanotransduction in cancellous bone highlight the need for site-specific determination of loading-induced changes in transcription.

Canonical Wnt/β-catenin signaling is a major regulator of bone's adaptive response to mechanical loading. In vivo tibial loading increased diaphyseal expression of Wnt pathway and Wnt/β-catenin target genes including *Wnt10b*, *Sfrp1*, *Fzd2*, *Wisp2*, *Wnt2b*, and *Crebbp* [11, 44] and decreased expression of the Wnt signaling inhibitor *Sost* [14]. We found increased expression of *Wnt1*, *Wnt7b* and *Wnt10b* 3 hours after a single loading session in cortical bone, while *Crebbp* (CREB binding protein) and *Lrp5* (low density lipoprotein receptor-related protein 5) were modestly

decreased. *Wnt1* and *Wnt10b* remained upregulated at 24 hours in cortical bone. *Wnt1* and *Wnt7b* were also upregulated in cancellous bone at the earlier time point, while the Wnt inhibitors *Sost* and *Dkk1* (dickkopf homolog 1) were downregulated. Furthermore, β-catenin activation by mechanical loading requires prostaglandin [45]. We saw loading-related upregulation of *Ptgs2* (prostaglandin-endoperoxide synthase 2, aka COX-2) in cortical bone at 3 and 24 hours, and in cancellous bone at 3h only. Our data confirm the previously determined importance of Wnt signaling in the cortical response to mechanical loading and identifies the role of Wnt signaling in the early loading response in cancellous bone.

Other skeletal genes were differentially expressed following mechanical loading. Tissue inhibitor of metalloproteinase (*Timp1*) was upregulated by loading in cortical bone at 3h (1.6-fold), and in cancellous bone at 3h (1.9-fold) and 24h (1.7-fold), in agreement with findings from homogenized tibial bone subjected to mechanical loading [14, 46]. Pleiotrophin (*Ptn*) was increased by 4.3-fold twenty-four hours after four sessions of 4-point bending of the mouse tibia [46], and was also upregulated in our study at 24 hours in both cortical (2.6-fold) and cancellous bone (3.1-fold). Osteoprotegerin (*Tnfrsf11b*) is well known to inhibit osteoclast

differentiation [47] and was increased by loading at 3 hours in cortical (2.2-fold) and cancellous (1.9-fold) bone.

Muscle genes were the largest group of downregulated genes twenty-four hours following a single loading session in cancellous bone. A single loading session of the rat forearm (cortical site) also caused downregulation of muscle genes, seven of which were also identified in our study (*Ampd1*, *Smpx*, *Tnnt3*, *Mylk2*, *Actn3*, *Mylpf*, and *Tnni2*) [48]. In our experiment these gene changes are unlikely to reflect muscle contamination because muscle was carefully removed from the whole bone surface, and the cancellous core does not interface with muscle. Furthermore, calvarial-derived osteocytes express genes related to muscle function, development and differentiation, and to a greater extent than osteoblasts [49] as does young healthy articular cartilage [50]. Established expression of muscle-related genes in musculoskeletal tissues other than muscle suggests that their classification was based upon the first tissue in which they were identified or the tissue in which they are most abundant, but may not be muscle-specific. The exact cellular population in our samples has not been determined, but embedded osteocytes are a likely source; our centrifugation protocol removes marrow and non-adherent osteoblasts and osteoclasts. The role of muscle-related genes in bone biology and mechanotransduction is not well understood, and

elucidation of their functions in bone cells and the response to mechanical loading requires further study.

Despite the removal of contaminating genes determined by Ayturk et al., pathways and biological processes were identified in cancellous bone that are related to coagulation. These results may reflect the presence of blood or serum within the tibial samples.

The current study is limited in its examination of the response to loading at the transcriptional level in young mice at two time points following a single loading session. Protein levels resulting from the transcriptional changes need to be confirmed, localized to the different cells, and ideally related to the strain field, to more accurately determine spatial and temporal responses to mechanical loading. The selection of appropriate time points for these studies will be critical to the experimental design. Future work could include adult mice, earlier time points to capture changes in transcription factors, later time points to examine matrix- and mineralization-related gene expression, and multiple loading sessions. The ability to examine cortical and cancellous bone separately and compare their baseline transcription and their response to mechanical loading is unique. Many gene knockout studies have demonstrated differential phenotypes in cortical and cancellous bone; some notable examples are the

primary effect in cancellous bone of absence of estrogen receptor alpha in bone cells [51-55], the previously mentioned cortical phenotype in mice lacking Wnt16 [33, 34], and the decrease in cortical but not cancellous bone volume when BMP2 is deleted from early-stage osteoblasts [56]. With in vivo compression of the mouse tibia, cancellous bone is often more responsive to mechanical loading than cortical bone [21, 57]; however, gene knockouts can modify this responsiveness in a site-specific manner [53, 58]. Future studies utilizing our methods to determine the baseline transcription and response to loading in cortical and cancellous bone in genetically modified mice will help unravel the complex molecular mechanisms responsible for in vivo bone homeostasis and mechanotransduction.

3.4.1 Conclusions

In summary, we used RNA-seq to demonstrate differences in cortical and cancellous bone transcription separately at baseline and at two time points following a single loading session. The differences in transcription at baseline highlight the need to examine these bone tissue envelopes separately, particularly when cortical to cancellous phenotypic differences are observed. Furthermore, we discovered tissue-envelope-specific and time-dependent differences in the response to mechanical loading. In particular,

further investigation into the large downregulation of muscle-related genes in cancellous bone is necessary. Next generation sequencing is a powerful tool to study bone transcription and identify future targets for treatment of osteoporosis.

3.5 References

[1] Bone Health and Osteoporosis: A Report of the Surgeon General. In. Rockville (MD): U.S. Department of Health and Human Services, Office of the Surgeon General; 2004.

[2] Cummings SR, Melton LJ. Epidemiology and outcomes of osteoporotic fractures. Lancet 2002;359: 1761-7.

[3] Neer RM, Arnaud CD, Zanchetta JR, Prince R, Gaich GA, Reginster JY, Hodsman AB, Eriksen EF, Ish-Shalom S, Genant HK, Wang O, Mitlak BH. Effect of parathyroid hormone (1-34) on fractures and bone mineral density in postmenopausal women with osteoporosis. N Engl J Med 2001;344: 1434-41.

[4] Fuchs RK, Bauer JJ, Snow CM. Jumping improves hip and lumbar spine bone mass in prepubescent children: a randomized controlled trial. J Bone Miner Res 2001;16: 148-56.

[5] Kontulainen S, Sievanen H, Kannus P, Pasanen M, Vuori I. Effect of long-term impact-loading on mass, size, and estimated strength of humerus and radius of female racquet-sports players: a peripheral quantitative computed tomography study between young and old starters and controls. J Bone Miner Res 2003;18: 352-9.

[6] Vainionpaa A, Korpelainen R, Leppaluoto J, Jamsa T. Effects of high-impact exercise on bone mineral density: a randomized controlled trial in premenopausal women. Osteoporos Int 2005;16: 191-7.

[7] Winters-Stone KM, Snow CM. Site-specific response of bone to exercise in premenopausal women. Bone 2006;39: 1203-9.

[8] Holguin N, Brodt MD, Sanchez ME, Kotiya AA, Silva MJ. Adaptation of tibial structure and strength to axial compression depends on loading history in both C57BL/6 and BALB/c mice. Calcif Tissue Int 2013;93: 211-21.

[9] Lynch ME, Main RP, Xu Q, Schmicker TL, Schaffler MB, Wright TM, van der Meulen MC. Tibial compression is anabolic in the adult mouse skeleton despite reduced responsiveness with aging. Bone 2011;49: 439-46.

[10] Lynch ME, Main RP, Xu Q, Walsh DJ, Schaffler MB, Wright TM, van der Meulen MC. Cancellous bone adaptation to tibial compression is not sex dependent in growing mice. J Appl Physiol (1985) 2010;109: 685-91.

[11] Armstrong VJ, Muzylak M, Sunters A, Zaman G, Saxon LK, Price JS, Lanyon LE. Wnt/beta-catenin signaling is a component of osteoblastic

bone cell early responses to load-bearing and requires estrogen receptor alpha. J Biol Chem 2007;282: 20715-27.
[12] Bonnet N, Standley KN, Bianchi EN, Stadelmann V, Foti M, Conway SJ, Ferrari SL. The matricellular protein periostin is required for sost inhibition and the anabolic response to mechanical loading and physical activity. J Biol Chem 2009;284: 35939-50.
[13] Silva MJ, Brodt MD, Lynch MA, Stephens AL, Wood DJ, Civitelli R. Tibial loading increases osteogenic gene expression and cortical bone volume in mature and middle-aged mice. PLoS One 2012;7: e34980.
[14] Zaman G, Saxon LK, Sunters A, Hilton H, Underhill P, Williams D, Price JS, Lanyon LE. Loading-related regulation of gene expression in bone in the contexts of estrogen deficiency, lack of estrogen receptor alpha and disuse. Bone 2010;46: 628-42.
[15] Kelly NH, Schimenti JC, Patrick Ross F, van der Meulen MC. A method for isolating high quality RNA from mouse cortical and cancellous bones. Bone 2014.
[16] Ayturk UM, Jacobsen CM, Christodoulou DC, Gorham J, Seidman JG, Seidman CE, Robling AG, Warman ML. An RNA-seq protocol to identify mRNA expression changes in mouse diaphyseal bone: applications in mice with bone property altering Lrp5 mutations. J Bone Miner Res 2013;28: 2081-93.
[17] Isaac J, Erthal J, Gordon J, Duverger O, Sun HW, Lichtler AC, Stein GS, Lian JB, Morasso MI. DLX3 regulates bone mass by targeting genes supporting osteoblast differentiation and mineral homeostasis in vivo. Cell Death Differ 2014;21: 1365-76.
[18] Jacobsen CM, Barber LA, Ayturk UM, Roberts HJ, Deal LE, Schwartz MA, Weis M, Eyre D, Zurakowski D, Robling AG, Warman ML. Targeting the LRP5 Pathway Improves Bone Properties in a Mouse Model of Osteogenesis Imperfecta. J Bone Miner Res 2014.
[19] Kedlaya R, Veera S, Horan DJ, Moss RE, Ayturk UM, Jacobsen CM, Bowen ME, Paszty C, Warman ML, Robling AG. Sclerostin inhibition reverses skeletal fragility in an Lrp5-deficient mouse model of OPPG syndrome. Sci Transl Med 2013;5: 211ra158.
[20] Rolfe RA, Nowlan NC, Kenny EM, Cormican P, Morris DW, Prendergast PJ, Kelly D, Murphy P. Identification of mechanosensitive genes during skeletal development: alteration of genes associated with cytoskeletal rearrangement and cell signalling pathways. BMC Genomics 2014;15: 48.

[21] Fritton JC, Myers ER, Wright TM, van der Meulen MC. Loading induces site-specific increases in mineral content assessed by microcomputed tomography of the mouse tibia. Bone 2005;36: 1030-8.
[22] Trapnell C, Roberts A, Goff L, Pertea G, Kim D, Kelley DR, Pimentel H, Salzberg SL, Rinn JL, Pachter L. Differential gene and transcript expression analysis of RNA-seq experiments with TopHat and Cufflinks. Nat Protoc 2012;7: 562-78.
[23] Robinson MD, McCarthy DJ, Smyth GK. edgeR: a Bioconductor package for differential expression analysis of digital gene expression data. Bioinformatics 2010;26: 139-40.
[24] Dennis G, Jr., Sherman BT, Hosack DA, Yang J, Gao W, Lane HC, Lempicki RA. DAVID: Database for Annotation, Visualization, and Integrated Discovery. Genome Biol 2003;4: P3.
[25] Huang da W, Sherman BT, Lempicki RA. Systematic and integrative analysis of large gene lists using DAVID bioinformatics resources. Nat Protoc 2009;4: 44-57.
[26] Yang L, Tsang KY, Tang HC, Chan D, Cheah KS. Hypertrophic chondrocytes can become osteoblasts and osteocytes in endochondral bone formation. Proc Natl Acad Sci U S A 2014;111: 12097-102.
[27] Zhou X, von der Mark K, Henry S, Norton W, Adams H, de Crombrugghe B. Chondrocytes transdifferentiate into osteoblasts in endochondral bone during development, postnatal growth and fracture healing in mice. PLoS Genet 2014;10: e1004820.
[28] Main RP, Lynch ME, van der Meulen MC. In vivo tibial stiffness is maintained by whole bone morphology and cross-sectional geometry in growing female mice. J Biomech 2010;43: 2689-94.
[29] Brodt MD, Ellis CB, Silva MJ. Growing C57Bl/6 mice increase whole bone mechanical properties by increasing geometric and material properties. J Bone Miner Res 1999;14: 2159-66.
[30] Glatt V, Canalis E, Stadmeyer L, Bouxsein ML. Age-related changes in trabecular architecture differ in female and male C57BL/6J mice. J Bone Miner Res 2007;22: 1197-207.
[31] Sugiyama T, Price JS, Lanyon LE. Functional adaptation to mechanical loading in both cortical and cancellous bone is controlled locally and is confined to the loaded bones. Bone 2010;46: 314-21.
[32] Baron R, Kneissel M. WNT signaling in bone homeostasis and disease: from human mutations to treatments. Nat Med 2013;19: 179-92.
[33] Zheng HF, Tobias JH, Duncan E, Evans DM, Eriksson J, Paternoster L, Yerges-Armstrong LM, Lehtimaki T, Bergstrom U, Kahonen M, Leo PJ, Raitakari O, Laaksonen M, Nicholson GC, Viikari J, Ladouceur M,

Lyytikainen LP, Medina-Gomez C, Rivadeneira F, Prince RL, Sievanen H, Leslie WD, Mellstrom D, Eisman JA, Moverare-Skrtic S, Goltzman D, Hanley DA, Jones G, St Pourcain B, Xiao Y, Timpson NJ, Smith GD, Reid IR, Ring SM, Sambrook PN, Karlsson M, Dennison EM, Kemp JP, Danoy P, Sayers A, Wilson SG, Nethander M, McCloskey E, Vandenput L, Eastell R, Liu J, Spector T, Mitchell BD, Streeten EA, Brommage R, Pettersson-Kymmer U, Brown MA, Ohlsson C, Richards JB, Lorentzon M. WNT16 influences bone mineral density, cortical bone thickness, bone strength, and osteoporotic fracture risk. PLoS Genet 2012;8: e1002745.

[34] Moverare-Skrtic S, Henning P, Liu X, Nagano K, Saito H, Borjesson AE, Sjogren K, Windahl SH, Farman H, Kindlund B, Engdahl C, Koskela A, Zhang FP, Eriksson EE, Zaman F, Hammarstedt A, Isaksson H, Bally M, Kassem A, Lindholm C, Sandberg O, Aspenberg P, Savendahl L, Feng JQ, Tuckermann J, Tuukkanen J, Poutanen M, Baron R, Lerner UH, Gori F, Ohlsson C. Osteoblast-derived WNT16 represses osteoclastogenesis and prevents cortical bone fragility fractures. Nat Med 2014;20: 1279-88.

[35] Balemans W, Ebeling M, Patel N, Van Hul E, Olson P, Dioszegi M, Lacza C, Wuyts W, Van Den Ende J, Willems P, Paes-Alves AF, Hill S, Bueno M, Ramos FJ, Tacconi P, Dikkers FG, Stratakis C, Lindpaintner K, Vickery B, Foernzler D, Van Hul W. Increased bone density in sclerosteosis is due to the deficiency of a novel secreted protein (SOST). Hum Mol Genet 2001;10: 537-43.

[36] Balemans W, Patel N, Ebeling M, Van Hul E, Wuyts W, Lacza C, Dioszegi M, Dikkers FG, Hildering P, Willems PJ, Verheij JB, Lindpaintner K, Vickery B, Foernzler D, Van Hul W. Identification of a 52 kb deletion downstream of the SOST gene in patients with van Buchem disease. J Med Genet 2002;39: 91-7.

[37] McClung MR, Grauer A, Boonen S, Bolognese MA, Brown JP, Diez-Perez A, Langdahl BL, Reginster JY, Zanchetta JR, Wasserman SM, Katz L, Maddox J, Yang YC, Libanati C, Bone HG. Romosozumab in postmenopausal women with low bone mineral density. N Engl J Med 2014;370: 412-20.

[38] Li X, Ominsky MS, Niu QT, Sun N, Daugherty B, D'Agostin D, Kurahara C, Gao Y, Cao J, Gong J, Asuncion F, Barrero M, Warmington K, Dwyer D, Stolina M, Morony S, Sarosi I, Kostenuik PJ, Lacey DL, Simonet WS, Ke HZ, Paszty C. Targeted deletion of the sclerostin gene in mice results in increased bone formation and bone strength. J Bone Miner Res 2008;23: 860-9.

[39] Li X, Ominsky MS, Warmington KS, Morony S, Gong J, Cao J, Gao Y, Shalhoub V, Tipton B, Haldankar R, Chen Q, Winters A, Boone T, Geng Z, Niu QT, Ke HZ, Kostenuik PJ, Simonet WS, Lacey DL, Paszty C. Sclerostin antibody treatment increases bone formation, bone mass, and bone strength in a rat model of postmenopausal osteoporosis. J Bone Miner Res 2009;24: 578-88.
[40] Li X, Warmington KS, Niu QT, Asuncion FJ, Barrero M, Grisanti M, Dwyer D, Stouch B, Thway TM, Stolina M, Ominsky MS, Kostenuik PJ, Simonet WS, Paszty C, Ke HZ. Inhibition of sclerostin by monoclonal antibody increases bone formation, bone mass, and bone strength in aged male rats. J Bone Miner Res 2010;25: 2647-56.
[41] Ominsky MS, Vlasseros F, Jolette J, Smith SY, Stouch B, Doellgast G, Gong J, Gao Y, Cao J, Graham K, Tipton B, Cai J, Deshpande R, Zhou L, Hale MD, Lightwood DJ, Henry AJ, Popplewell AG, Moore AR, Robinson MK, Lacey DL, Simonet WS, Paszty C. Two doses of sclerostin antibody in cynomolgus monkeys increases bone formation, bone mineral density, and bone strength. J Bone Miner Res 2010;25: 948-59.
[42] Wasserman E, Webster D, Kuhn G, Attar-Namdar M, Muller R, Bab I. Differential load-regulated global gene expression in mouse trabecular osteocytes. Bone 2013;53: 14-23.
[43] Macias BR, Aspenberg P, Agholme F. Paradoxical Sost gene expression response to mechanical unloading in metaphyseal bone. Bone 2013;53: 515-9.
[44] Robinson JA, Chatterjee-Kishore M, Yaworsky PJ, Cullen DM, Zhao W, Li C, Kharode Y, Sauter L, Babij P, Brown EL, Hill AA, Akhter MP, Johnson ML, Recker RR, Komm BS, Bex FJ. Wnt/beta-catenin signaling is a normal physiological response to mechanical loading in bone. J Biol Chem 2006;281: 31720-8.
[45] Lara-Castillo N, Kim-Weroha NA, Kamel MA, Javaheri B, Ellies DL, Krumlauf RE, Thiagarajan G, Johnson ML. In vivo mechanical loading rapidly activates beta-catenin signaling in osteocytes through a prostaglandin mediated mechanism. Bone 2015;76: 58-66.
[46] Xing W, Baylink D, Kesavan C, Hu Y, Kapoor S, Chadwick RB, Mohan S. Global gene expression analysis in the bones reveals involvement of several novel genes and pathways in mediating an anabolic response of mechanical loading in mice. J Cell Biochem 2005;96: 1049-60.
[47] Lacey DL, Timms E, Tan HL, Kelley MJ, Dunstan CR, Burgess T, Elliott R, Colombero A, Elliott G, Scully S, Hsu H, Sullivan J, Hawkins

N, Davy E, Capparelli C, Eli A, Qian YX, Kaufman S, Sarosi I, Shalhoub V, Senaldi G, Guo J, Delaney J, Boyle WJ. Osteoprotegerin ligand is a cytokine that regulates osteoclast differentiation and activation. Cell 1998;93: 165-76.

[48] Mantila Roosa SM, Liu Y, Turner CH. Gene expression patterns in bone following mechanical loading. J Bone Miner Res 2011;26: 100-12.

[49] Paic F, Igwe JC, Nori R, Kronenberg MS, Franceschetti T, Harrington P, Kuo L, Shin DG, Rowe DW, Harris SE, Kalajzic I. Identification of differentially expressed genes between osteoblasts and osteocytes. Bone 2009;45: 682-92.

[50] Poulet B, Ulici V, Stone TC, Pead M, Gburcik V, Constantinou E, Palmer DB, Beier F, Timmons JA, Pitsillides AA. Time-series transcriptional profiling yields new perspectives on susceptibility to murine osteoarthritis. Arthritis Rheum 2012;64: 3256-66.

[51] Melville KM, Kelly NH, Khan SA, Schimenti JC, Ross FP, Main RP, van der Meulen MC. Female mice lacking estrogen receptor-alpha in osteoblasts have compromised bone mass and strength. J Bone Miner Res 2014;29: 370-9.

[52] Melville KM, Kelly NH, Surita G, Buchalter DB, Schimenti JC, Main RP, Ross FP, van der Meulen MC. Effects of Deletion of ER-Alpha in Osteoblast-Lineage Cells on Bone Mass and Adaptation to Mechanical Loading Differs in Female and Male Mice. J Bone Miner Res 2015.

[53] Kondoh S, Inoue K, Igarashi K, Sugizaki H, Shirode-Fukuda Y, Inoue E, Yu T, Takeuchi JK, Kanno J, Bonewald LF, Imai Y. Estrogen receptor alpha in osteocytes regulates trabecular bone formation in female mice. Bone 2014;60: 68-77.

[54] Martin-Millan M, Almeida M, Ambrogini E, Han L, Zhao H, Weinstein RS, Jilka RL, O'Brien CA, Manolagas SC. The estrogen receptor-alpha in osteoclasts mediates the protective effects of estrogens on cancellous but not cortical bone. Mol Endocrinol 2010;24: 323-34.

[55] Windahl SH, Borjesson AE, Farman HH, Engdahl C, Moverare-Skrtic S, Sjogren K, Lagerquist MK, Kindblom JM, Koskela A, Tuukkanen J, Divieti Pajevic P, Feng JQ, Dahlman-Wright K, Antonson P, Gustafsson JA, Ohlsson C. Estrogen receptor-alpha in osteocytes is important for trabecular bone formation in male mice. Proc Natl Acad Sci U S A 2013;110: 2294-9.

[56] McBride SH, McKenzie JA, Bedrick BS, Kuhlmann P, Pasteris JD, Rosen V, Silva MJ. Long bone structure and strength depend on BMP2 from osteoblasts and osteocytes, but not vascular endothelial cells. PLoS One 2014;9: e96862.

[57] Main RP, Lynch ME, van der Meulen MC. Load-induced changes in bone stiffness and cancellous and cortical bone mass following tibial compression diminish with age in female mice. J Exp Biol 2014.
[58] Grimston SK, Watkins MP, Brodt MD, Silva MJ, Civitelli R. Enhanced periosteal and endocortical responses to axial tibial compression loading in conditional connexin43 deficient mice. PLoS One 2012;7: e44222.

CHAPTER 4

FEMALE MICE LACKING ESTROGEN RECEPTOR ALPHA IN MATURE OSTEOBLASTS HAVE AN INCREASED TRANSCRIPTIONAL RESPONSE TO MECHANICAL LOADING IN CANCELLOUS BUT NOT CORTICAL BONE

4.1 Introduction

Postmenopausal osteoporosis is characterized by decreased bone mass and weaker skeletal structures caused in part by decreased bioavailable estrogen. Estrogen signaling in bone occurs through estrogen receptor alpha and beta (ERα and ERβ). The importance of ERα was underscored by the discovery of a mutation in the ERα gene (*ESR1*) that resulted in unfused growth plates and low bone mass [1]. Human polymorphisms in *ESR1* have since been linked to bone mineral density, fracture risk, and response to exercise [2-6]. Cancellous bone loss due to postmenopausal osteoporosis is more rapid than that occurring in cortical tissue, and fractures occur in corticocancellous sites [7, 8], suggesting that the effects of ERα may be distinct in cortical and cancellous bone tissue.

The role of estrogen in bone cells has been studied increasingly with cell-specific ERα knockout (KO) mice. ERα has been removed at different osteoblastic cell lineages, with conflicting effects on cortical and cancellous bone mass in female mice. Deletion of ERα in osteoblast progenitors and precursors (*Prx1*- and *Osx1*-cre) decreased cortical bone mass while cancellous mass was unaffected [9]. In mature osteoblasts (*OC*-cre, pOC-ERαKO), ERα deletion decreased cortical and cancellous bone in females [10, 11], while deletion of ERα in committed osteoblasts (*Col1a1*-cre) failed to affect bone mass [9]. Finally, when ERα was removed from osteocytes (*Dmp1*-cre) cancellous bone volume decreased but cortical bone was unaffected in female mice [12]. Thus, estrogen is osteoprotective, and loss of estrogen reduces bone mass. Given estrogen's pleiotropic role in regulation of bone mass and the fact that loading of bone is anabolic, estrogen may also play a role in bone mechanotransduction.

Mechanical loading increases bone mass while disuse or reduced mechanical loading decreases bone mass in adult animals. Increased bone mass due to mechanical loading can be studied with rodent models of bone cyclic compression [13-15]. The response to mechanical loading in cortical bone of mice lacking ERα in osteoblast progenitors and precursors was decreased [16], while when ERα was

deleted in osteocytes the cortical response was similar to controls [17]. In contrast, adaptation to external mechanical loads was increased in mice lacking ERα in mature osteoblasts compared to littermate controls, particularly in cancellous bone [18]. The molecular mechanisms behind this site-specific increased anabolism are not well understood.

Wnt/β-catenin signaling mediates the skeletal response to mechanical loading. Expression of Wnt agonists including *Wnt10b*, *Wnt2b*, *Fzd2* (frizzled class receptor 2), and *Wisp2* (Wnt1 inducible signaling pathway protein 2) was increased following loading in cortical bone [19, 20], while the Wnt antagonist *Sost* (sclerostin) was decreased [21-23]. Crosstalk between estrogen and Wnt/β-catenin signaling has been demonstrated. A single short period of dynamic mechanical strain increased nuclear accumulation of β-catenin, and this effect was blocked by an estrogen receptor inhibitor and was absent in osteoblasts from mice lacking ERα [19]. Three hours following tibial compression wild-type mice had differential expression of six genes involved in Wnt signaling but only retinoic acid receptor γ (RARγ) was differentially expressed in mice lacking ERα [19]. Although decreases in Wnt-related gene expression in response to mechanical loading have been demonstrated in cortical bone of mice lacking ERαKO, we saw increased tissue-

level response to loading in mice with osteoblast-specific knockout of ERα, particularly in the cancellous compartment [18]. Examination of the transcriptional differences in cortical versus cancellous bone of pOC-ERαKO mice following mechanical loading will add to our knowledge of ERα and Wnt signaling crosstalk and the transcriptome level changes in bone functional adaptation.

We hypothesized that mechanical loading causes systemic changes in bone at the transcriptional level and that mice lacking ERα in bone cells have an increased response compared to littermate controls due to altered Wnt/β-catenin signaling, particularly in cancellous bone. We previously demonstrated that gene expression in response to mechanical loading differed in cortical versus cancellous marrow-free murine bone [24, 25]. We now extend these techniques to further characterize the transcriptional response to mechanical loading in mice lacking ERα in mature osteoblasts. The left tibiae of 10-week-old female pOC-ERαKO and littermate control mice were subjected to a single session of axial tibial compression and the mice were euthanized 3 or 24 hours following loading. To determine baseline differences in cortical versus cancellous transcription and the possible systemic effects of loading, a third group of naïve (never loaded) littermate control animals was compared to contralateral control limbs of loaded animals (LC and pOC-

ERαKO). We performed RNA-seq on marrow-free metaphyseal samples from the cortical shell and the cancellous core of the metaphysis to determine differential gene expression in response to load (versus contralateral control) and differential gene expression in naïve cortical and cancellous bone.

4.2 Materials and Methods

4.2.1 Animals

Mice lacking ERα in mature osteoblasts (osteocalcin promoter, pOC-ERαKO) along with their littermate controls (LC) were bred as previously described on a C57Bl/6 background [11, 18]. Ten-week-old female mice were subjected to a single session of in vivo mechanical loading of the left tibia (9N max load, 1200 cycles, 4Hz, triangle waveform) with the right tibia as contralateral control [14, 26, 27]. Three and twenty-four hours after a single loading session mice were euthanized (n=4-7/group). Another set of LC mice (n=4) was euthanized without external load application (naïve). Following euthanasia, tibiae were rapidly dissected for RNA isolation. The epiphysis, all soft tissues, periosteum, fibula, and the distal end were removed. Tibiae were centrifuged for 20s at 16,100 *g* at room temperature in microcentrifuge tubes, as previously described [24], and then cut approximately 5 mm distal to the growth plate to isolate the metaphysis. The

cancellous core of the metaphysis was separated from the cortical shell with a 1mm biopsy punch (Miltex, Integra LifeSciences Corp, Plainsboro, NJ). The IACUC of Cornell University approved all animal procedures.

4.2.2 RNA isolation

RNA isolation was performed using Trizol (Life Technologies, Carlsbad, CA) and RNeasy Mini kit (Qiagen, Germantown, MD) as described previously with a few important changes [24]. Individual cancellous and cortical samples were pulverized for 5 minutes in liquid-nitrogen-cooled 2mL tubes containing 2.8mm ceramic beads and Trizol (Mikro-dismembrator S, Sartorius Stedim Biotech, Bohemia, NY, USA), rather than dry pulverization with subsequent Trizol addition. Following pulverization the powdered bone/Trizol mix was incubated for 30 minutes at room temperature and then stored at -80C overnight. Samples were thawed, transferred to new 1.5mL tubes, and centrifuged at 4C and 11,500 rpm for 5 minutes, and then added to phase lock gel tubes (PLG, heavy, 5 Prime, Gaithersburg, MD) containing 300μL of chloroform. Samples were centrifuged for 15 minutes at 4C and 11,500 rpm to separate the nucleic acid phase (~500μL), which was removed and added to an equal volume of 70% ethanol. This mixture was applied to purification columns (RNeasy Mini kit, Qiagen) following the

manufacturer's instructions, including a DNase digestion (RNase free DNase kit, Qiagen). A final volume of 30μL of RNA was eluted.

RNA purity and quantity were tested on all samples using a spectrophotometer (Nanodrop 1000, Thermo Scientific, Wilmington, DE). RNA Quality Number (RQN) was determined for a subset of samples (4-12/group) using a fragment analyzer (Advanced Analytical Technologies, Inc, Ames, IA). The mean (±SD) concentration of cortical samples was 108 (±29) ng/μL, and for cancellous samples was 35 (±15) ng/μL. The 260/280 ratio was within an acceptable range (1.5-2.1) for all samples. Cancellous and cortical samples were of high quality with mean (±SD) RQNs of 8.0 (± 1.0) and 8.6 (± 0.5), respectively.

4.2.3 RNA-seq library preparation and analysis

Total RNA from 20 animals (n=80 samples; 4 samples/animal from cortical and cancellous tissue of both tibiae) was processed following the manufacturer's instructions to create RNA-seq libraries (Illumina TruSeq RNA Sample Preparation Kit v2, San Diego, CA). mRNA was purified with polyA+ magnetic beads, chemically fragmented (120-200bp fragments), reverse transcribed using random hexamers, and ligated to bar-coded adapters. The resulting cDNA fragments were amplified to provide sufficient material for subsequent analysis. Finally, primer-

dimers were removed by washing with AMPure XP beads (Agencourt AMPure XP, Beckman Coulter, Brea, CA). Final libraries were tested using a fragment analyzer to determine the distribution of fragment sizes. The eighty individually bar-coded libraries were normalized, pooled (maximum of 20 libraries/lane), and sequenced (75-bp single-end reads, Illumina NextSeq 500).

Sequences were aligned to the mouse genome (mm10) using TopHat followed by transcript assembly and gene counts with Cuffdiff [28]. On average, 94% of the 27 million reads/library were mapped to the mouse genome, 95% uniquely. Differential expression was determined with a paired design in edgeR [29]. The paired design consisted of an additive linear model with blocking for which the blocking factor was "tissue" when baseline cortical and cancellous tissue from the same bone were compared, and the blocking factor was "animal" when the loaded limb was compared to the control contralateral limb in the same animal. Genes with low expression were filtered from each library by removing genes with counts per million less than one in at least four samples. Finally, differentially expressed genes were determined by fitting gene-wise generalized linear models and performing likelihood ratio tests. Differentially expressed genes were determined based on fold-change cut-off and 5% false discovery rate (FDR) cut-off. A more

stringent fold change cut-off was applied for normal developmental changes (Ct to Cn baseline, >2-fold) than for loading-induced changes (>1.5-fold).

For the naïve LC and contralateral control samples only, we identified contaminants from our RNA-seq data based on genes determined to be highly expressed in muscle, bone marrow, or blood compared to tibial bone by Ayturk et al. [30]. For the loaded samples all gene changes were reported including genes considered contaminants in the control analysis.

Lists of differentially expressed genes were imported into the Database for Annotation, Visualization and Integrated Discovery (DAVID, from the National Institute of Allergy and Infectious Diseases (NIAID), NIH - http://david.abcc.ncifcrf.gov/). Gene ontology (GO) for biological processes and enriched Kyoto Encyclopedia of Genes and Genomes (KEGG) pathways were determined for each group using the functional annotation tool ($p<0.05$) [31, 32].

4.2.4 Gene expression verification with qPCR

Using qPCR, we verified differential gene expression obtained from RNAseq for 8 genes that were different between the two tissues or with loading: Ostn, Ptgs2, Ptn, Timp1, Tnfrsf11b, Wnt1, Wnt16, and Wnt7b (primer sequences in supplementary table S1). RNA from the 3-hour time point (n=3/per group) was

reverse transcribed to cDNA following the manufacturer's instructions (High Capacity cDNA Reverse Transcription kit, Life Technologies) and brought to 5ng/μL with RNase-free water. A final volume of 20μL containing 2X SYBR Green (Perfecta SYBR Green Fastmix, with ROX, Quanta Biosciences, Gaithersburg, MD) was assayed by triplicate qPCR using 39 cycles of denaturing (95C, 5s) and annealing/elongation (60C, 30s) (CFX96 Real-Time PCR System, BioRad, Hercules, CA). Quantification cycle (Cq) was determined for each gene and compared to the reference gene Gapdh. All groups are presented as fold change with loading or tissue type ($2^{-\Delta\Delta Cq}$). The log2 fold-change of RNA-seq versus qPCR was graphed to determine quality of correlation; a slope of one would define perfect agreement. The strength of the relationship was quantified by Pearson correlation.

4.3. Results

4.3.1 Absence of ERα in mature osteoblasts resulted in markedly decreased differential gene expression in cortical bone following a single loading session

A single session of in vivo mechanical loading caused differential expression of more genes in cortical bone of LC than pOC-ERαKO mice. Cortical samples from LC animals had differential expression of 772 genes (**Table B2**) three hours

following mechanical loading, while only 32 genes were differentially expressed in cortical bone from pOC-ERαKO animals (**Table B3**). For both groups, most affected genes were upregulated. Twenty-four hours following loading LC animals had 65 differentially expressed genes, of which a majority were downregulated (**Table B4**), while pOC-ERαKO animals had only 11 differentially expressed genes in cortical bone, which were mostly upregulated (**Table B5**) (**Figure 4.1**).

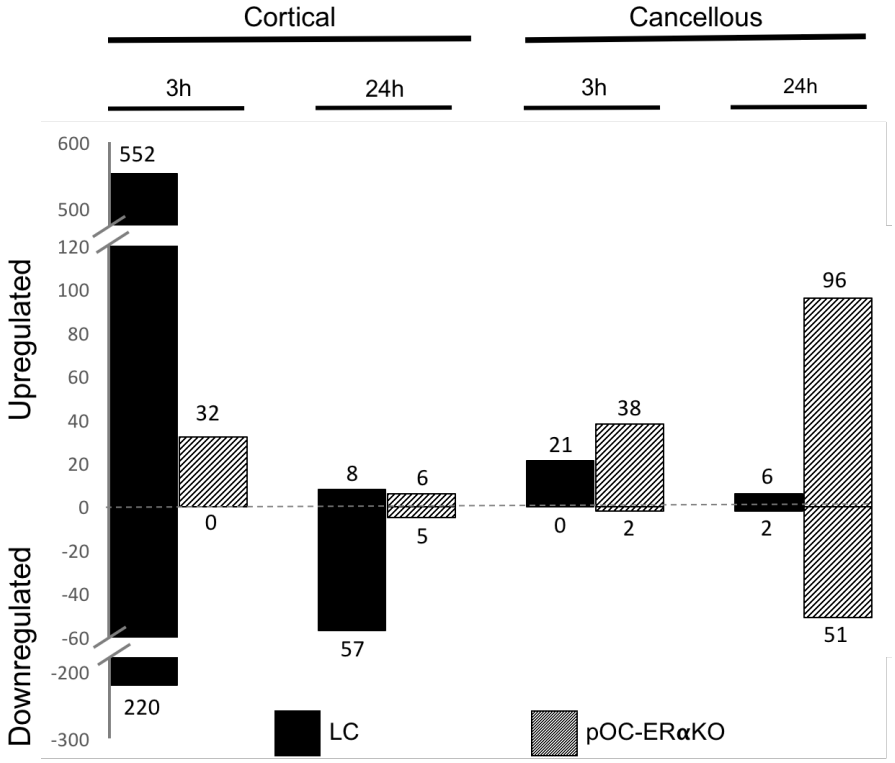

Figure 4.1. Littermate control and ERα knockout animals respond differently to loading in cortical and cancellous bone. The number of genes differentially expressed in cortical and cancellous bone 3 and 24 hours after a single session of in vivo tibial loading of littermate control (solid) and pOC-ERαKO animals (hashed) compared to their contralateral, non-loaded controls.

Thirteen genes were differentially expressed in both LC and pOC-ERαKO cortical bone three hours following a single loading session (**Figure 4.2A**). These genes included *Ptgs2* (prostaglandin-endoperoxide synthase 2), *Medag* (mesenteric estrogen-dependent adipogenesis), *Ngf* (nerve growth factor), *Lgr6* (leucine-rich repeat containing G protein-coupled receptor 6), *Tnfrsf11b* (tumor necrosis factor receptor superfamily member 11b, or osteoprotegerin), *Adamts1* (a disintegrin-like and metallopeptidase (reprolysin type) with thrombospondin type 1 motif, 1), and *Ccl7* (chemokine (C-C motif) ligand 7) (**Figure 4.2A**). *Wnt7b* was the only gene that was shared between the two time points in cortical bone, being upregulated at 3h and downregulated at 24h in LC.

Six genes were differentially expressed in both LC and pOC-ERαKO cortical bone 24 hours following a single loading session. *Gsg1l* (germ cell associated 1-like) and *Tubb3* (tubulin, beta 3 class III) were upregulated, while *Wisp2* (Wnt1 inducible signaling pathway protein 2), *Galnt6* (UDP-N-acetyl-alpha-D-galactosamine:polypeptide N-acetylgalactosaminyltransferase 6), *Ccr1* (chemokine (C-C motif) receptor 1), and *Cd83* (CD83 antigen) were downregulated (**Figure 4.2A**).

Over 700 genes in LC mice at 3 hours and 58 genes at 24 hours were differentially expressed in cortical bone in only one genotype or time point

following loading. Those genes that were over 2-fold up or downregulated are shown (**Figure 4.2B**, 24 hours only. See **Table B2** for 3-hour changes).

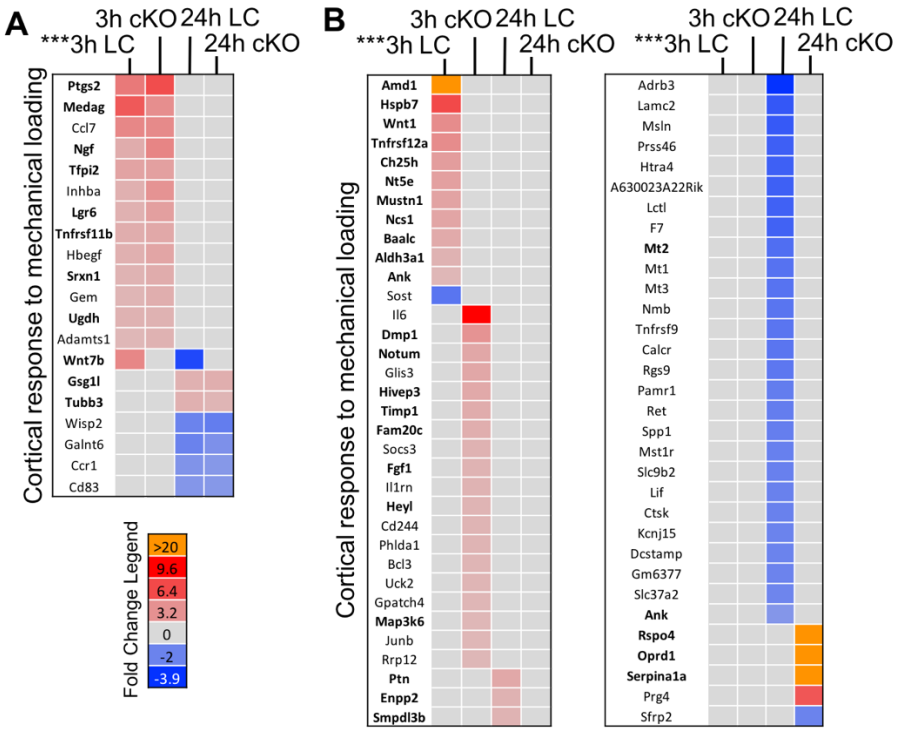

Figure 4.2: More genes were differentially expressed in cortical bone of LC than pOC-ERαKO following mechanical loading Heat maps of differentially expressed (DE) genes in loaded cortical samples compared to contralateral controls 3 and 24 hours following a single loading session in LC and pOC-ERαKO animals. Red indicates upregulation, blue downregulation, and gray no significant change. Genes in orange were highly upregulated. Gene names in bold were also DE in cancellous bone following a single loading session. A) 20 genes were DE in cortical bone of two or more groups following a single loading session. B) 65 genes were DE in cortical bone of only one group, mostly in LC cortical bone. ***LC Cortical bone at 3 hours had a total of 772 genes DE with loading, 220 which were downregulated. The full DE gene list for LC cortical bone at 3 hours can be found in **Table B2**, only those genes found in other groups are displayed in this figure. LC = littermate control, cKO = pOC-ERαKO.

Notably, *Sost* (sclerostin), an important inhibitor of Wnt signaling, was downregulated only at 3h in LC animals. *Amd1* (S-adenosylmethionine decarboxylase 1) was highly upregulated (226-fold) in cortical bone of LC animals 3 hours following loading. Other genes with known musculoskeletal functions included *Wnt1*, *Tnfrsf12a*, *Ank*. At 24 hours following loading several genes with known osteoclast function were downregulated including *Ctsk* (cathepsin K), *Dcstamp* (dentrocyte expressed seven transmembrane protein), and *Oscar* (osteoclast associated receptor; see **Table B9**).

In general, pOC-ERαKO mice had fewer genes that were differentially expressed following loading in cortical bone. However, 19 genes were differentially expressed in pOC-ERαKO cortical bone only 3 hours following loading. The most highly upregulated gene was *Il6* (interleukin 6, 9.6-fold). Known bone-related genes included *Dmp1* (dentin matrix protein 1), *Notum*, *Timp1*, and *Fam20c*. Five genes were differentially expressed only at 24 hours in pOC-ERαKO cortical bone, but 3 of the 5 genes were very highly upregulated: *Rspo4,* R-spondin 4, 138-fold; *Oprd1*, opioid receptor, delta 1, 49-fold; and *Serpina1a*, serine (or cysteine) peptidase inhibitor, clade A, member 1A, 29-fold.

Enriched signaling pathways and biological processes were determined for cortical bone from LC and pOC-ERαKO animals at 3 and 24 hours following a

single loading session. In LC cortical bone at 3 hours, signaling pathways included oxidative phosphorylation and ribosome. Enriched biological processes for LC cortical bone included muscle system process, myofibril assembly, and muscle contraction. After 24 hours of loading in LC cortical bone, enriched signaling pathways included osteoclast differentiation, glycosaminoglycan degradation, and cytokine-cytokine receptor interaction. pOC-ERαKO animals had few enriched signaling pathways and no enriched biological processes. The TNF signaling pathway and osteoclast differentiation were the only enriched pathways in pOC-ERαKO cortical bone 3 hours following loading (**Table 4.1**)

Table 4.1: Signaling pathways and biological processes significantly changed in cortical bone 3 and 24 hours following a single loading session in LC and pOC-ERαKO mice

	3 hours		24 hours	
	LC	**pOC-ERαKO**	**LC**	**pOC-ERαKO**
Signaling Pathways	Oxidative phosphorylation	TNF signaling pathway	Osteoclast differentiation	N.S.
	Ribosome	Osteoclast differentiation	Glycosaminoglycan degradation	
	Huntington's Disease		Cytokine-cytokine receptor interaction	
	Parkinson's Disease		Rheumatoid arthritis	
	Alzheimer's Disease			
Biological Processes	Generation of precursor metabolites and energy	N.S.	Osteoclast differentiation	N.S.
	Muscle system process		Cellular zinc ion homeostasis	
	Myofibril assembly		Cell adhesion	
	Muscle contraction		Positive regulation of gene expression	
	Striated muscle cell development		Immune response	

4.3.2 Absence of ERα in mature osteoblasts resulted in markedly increased differential gene expression in cancellous bone following a single loading session

A single session of in vivo mechanical loading caused differential expression of more genes in cancellous bone of pOC-ERαKO than it did in LC mice. Three hours following a single loading session cancellous samples from pOC-ERαKO animals had differential expression of 40 genes (**Table B7**), while only 21 genes were differentially expressed in LC animals (**Table B6**). Twenty-four hours following a single loading session 147 genes were differentially expressed in cancellous bone of pOC-ERαKO animals (**Table B9**), while LC animals had only 8 differentially expressed genes (**Table B8**). The majority of genes were upregulated in both genotypes and time points. (**Figure 4.3**).

Seventeen genes were differentially expressed in both pOC-ERαKO and LC cancellous bone at 3 hours, and 2 genes at 24 hours (**Figure 4.3A**). The magnitude of the fold change was generally higher in pOC-ERαKO cancellous bone for genes that were shared. For example, 16 of the 17 genes differentially expressed three hours following a single loading session in cancellous bone of both genotypes were between 1.1 and 2.2 times more highly expressed in pOC-ERαKO compared to

LC (**Figure 4.3B**). Five genes were differentially expressed at 3 and 24 hours only in pOC-ERαKO cancellous bone, including *Notum* and *Fam180a* (**Figure 4.3A**).

More genes were differentially expressed at only one time point in pOC-ERαKO than in LC cancellous bone (**Figure 4.3C**). In pOC-ERαKO cancellous bone, 18 genes were differentially expressed at 3 hours including *Amd1,* which was highly upregulated (157-fold), *Wnt7b* (8.4-fold), *Ank*, and *Fgf1*. At 24 hours in pOC-ERαKO cancellous bone, 70 genes had greater than 2-fold differential expression. Six genes were highly upregulated including *Rspo4* (537-fold), *Ear12* (292-fold), *Myoz2* (51-fold), *Oprd1* (43-fold), *Serpina1a* (24-fold), and *Pax1* (23-fold). In LC cancellous bone, 4 genes were differentially expressed in each of the 3- and 24-hour time points.

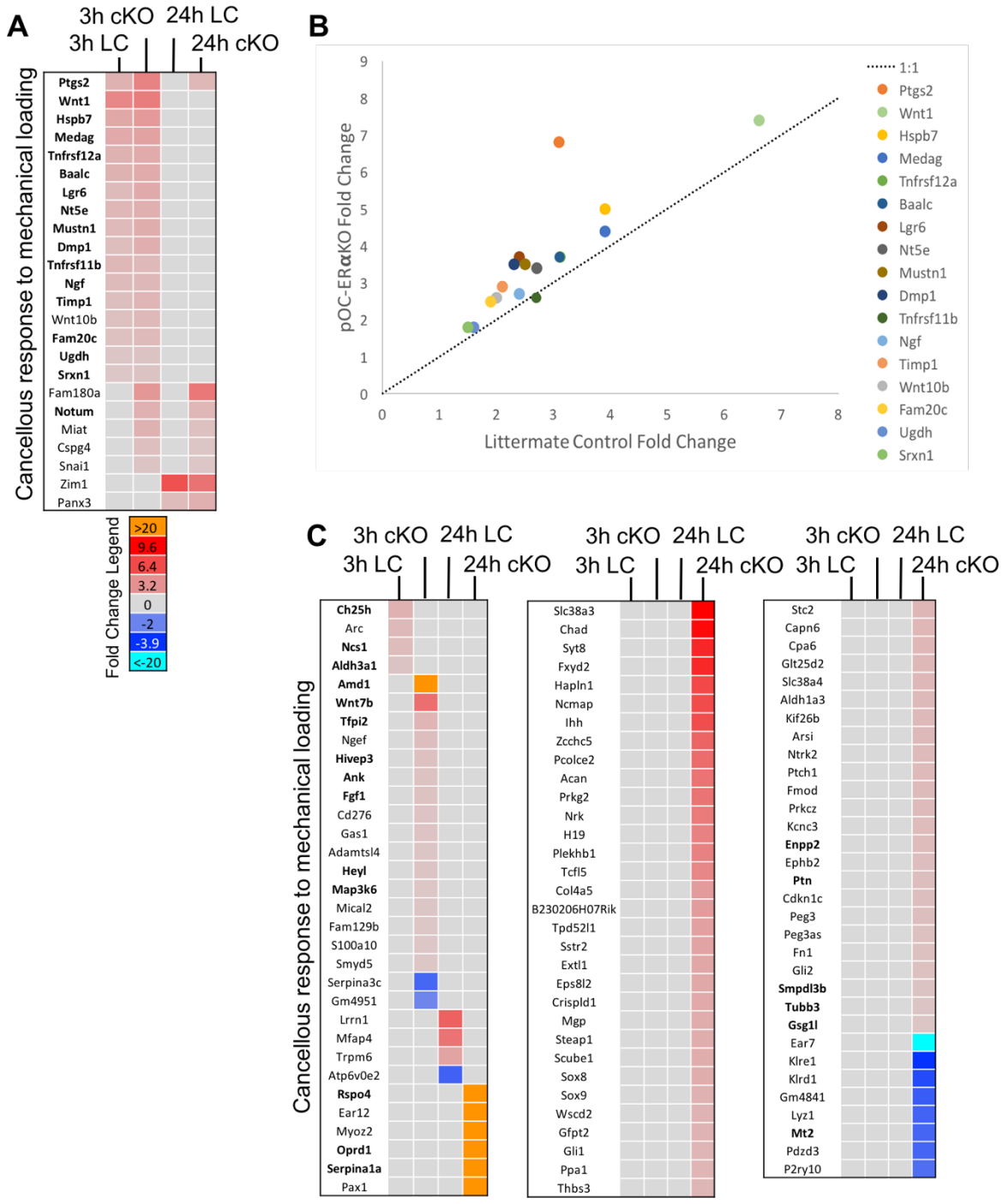

Figure 4.3: More genes are differentially expressed in cancellous bone of pOC-ERαKO than LC following mechanical loading with a higher fold change. A) Heat map of 24 differentially expressed (DE) genes in loaded

cancellous samples compared to contralateral controls that were shared by two or more groups in LC and pOC-ERαKO mice 3 and 24 hours following a single loading session. Upregulated genes in red, genes with no significant change in gray. Genes in orange and turquoise were highly up and down regulated, respectively. Gene names in bold were also DE in loaded cortical bone of at least one genotype/time point. B) 17 genes were upregulated 3 hours following a single loading session in LC and pOC-ERαKO cancellous bone and 16 of these DE genes were more highly upregulated in pOC-ERαKO mice. C) Heat maps of genes that were only differentially expressed in one genotype or time point in cancellous bone of LC and pOC-ERαKO cancellous bone (>2-fold). pOC-ERαKO cancellous bone had more DE genes in response to load, particularly at 24 hours. At 3 hours, Amd1 and Wnt7b were highly upregulated in pOC-ERαKO cancellous bone only. At 24 hours, Rspo4, Ear12, Myoz2, Oprd1, Serpina1a and Pax1 were highly upregulated while Ear7 was highly downregulated in pOC-ERαKO cancellous bone only.

In cancellous bone, the only enriched signaling pathways were found in pOC-ERαKO samples. The Hedgehog signaling pathway was enriched both 3 and 24 hours following loading. Other enriched pathways three hours following loading included hippo signaling pathway, basal cell carcinoma, pathways in cancer, and melanogenesis. Twenty-four hours following loading the enriched pathways were mineral absorption, leishmaniasis, salivary secretion, and rheumatoid arthritis. Biological processes in cancellous bone of LC animals included cell-cell signaling, oxidation-reduction process, and hematopoietic stem cell proliferation at 3 hours and ion transport and cation transport at 24

hours. pOC-ERαKO cancellous bone shared several biological processes at 3 and 24 hours including positive regulation of cell proliferation, and (positive regulation of) osteoblast differentiation. Biological processes in pOC-ERαKO cancellous bone at 3 hours included only Wnt signaling pathway and angiogenesis, while at 24 hours skeletal system development, retinal rod cell differentiation, and cellular response to interleukin-1 processes were also enriched (**Table 4.2**).

Table 4.2: Signaling pathways and biological processes significantly changed in cancellous bone 3 and 24 hours following a single loading session in LC and pOC-ERαKO mice

	3 hours		24 hours	
	LC	**pOC-ERαKO**	**LC**	**pOC-ERαKO**
Signaling Pathways	N.S.	Hedgehog signaling pathway	N.S.	Mineral absorption
		Hippo signaling pathway		Hedgehog signaling pathway
		Basal cell carcinoma		Leishmaniasis
		Pathways in cancer		Salivary secretion
		Melanogenesis		Rheumatoid arthritis
Biological Processes	Positive regulation of cell proliferation	Positive regulation of cell proliferation	Ion transport	Skeletal system development
	Cell-cell signaling	Multicellular organismal development	Cation transport	Positive regulation of cell proliferation
	Oxidation-reduction process	Positive regulation of osteoblast differentiation		Osteoblast differentiation
	Positive regulation of sequence-specific DNA binding transcription factor activity	Wnt signaling pathway		Retinal rod cell differentiation
	Hematopoietic stem cell proliferation	Angiogenesis		Cellular response to interleukin-1

4.3.3 More Wnt signaling pathway genes were differentially regulated in LC versus pOC-ERαKO mice

To specifically examine differences in Wnt signaling between LC and pOC-ERαKO mice, differentially expressed genes that were found within the gene ontology term "Wnt signaling pathway" (GO: 0016055), which contains a total of 382 genes in the mouse, were determined for all groups and time points (**Figure 4.4**). A total of 33 genes from the Wnt signaling pathway were differentially expressed in one or more groups. Differential expression of 25 of the 33 genes occurred in LC mice, while differential expression of 13 of the 33 genes occurred in pOC-ERαKO mice. Five genes were differentially expressed in both LC and pOC-ERαKO mice: *Wnt1*, *Wnt7b*, *Wnt10b*, *Wisp2*, and *Lgr6*. These 5 genes positively regulate Wnt signaling, and were generally upregulated with loading in both LC and pOC-ERαKO mice. *Wnt1* was upregulated in cortical and cancellous bone of LC animals, and, to a greater extent, in cancellous bone of pOC-ERαKO mice at 3 hours. *Lgr6* was upregulated in cortical and cancellous bone at 3 hours in both LC and pOC-ERαKO animals, but the upregulation was higher in pOC-ERαKO mice. *Wnt10b* was upregulated in cancellous bone 3 hours following loading in both

genotypes (LC: 2.0-fold, pOC-ERαKO: 2.6-fold). 24 hours following loading, *Wnt7b* was downregulated in cortical bone of LC mice, and *Wisp2* was downregulated in both genotypes. *Rspo4*, as previously mentioned, was highly upregulated in cortical and cancellous bone at 24 hours in pOC-ERαKO mice only. Twenty Wnt signaling pathway genes were differentially expressed in cortical bone at 3 hours in LC animals only. *Sost*, previously shown to be an important inhibitor of Wnt signaling, was downregulated 2.3-fold. However, several positive regulators of Wnt signaling were also downregulated, including *Lrp5* (low density lipoprotein receptor-related protein 5), *Lef1* (lymphoid enhancer binding factor 1), *Dlx5* (distal-less homeobox 5), and *Dvl3* (dishevelled segment polarity protein 3). The Wnt signaling inhibitor *Sfrp5* (secreted frizzled-related protein 5) was downregulated in cortical bone of pOC-ERαKO mice at 24 hours.

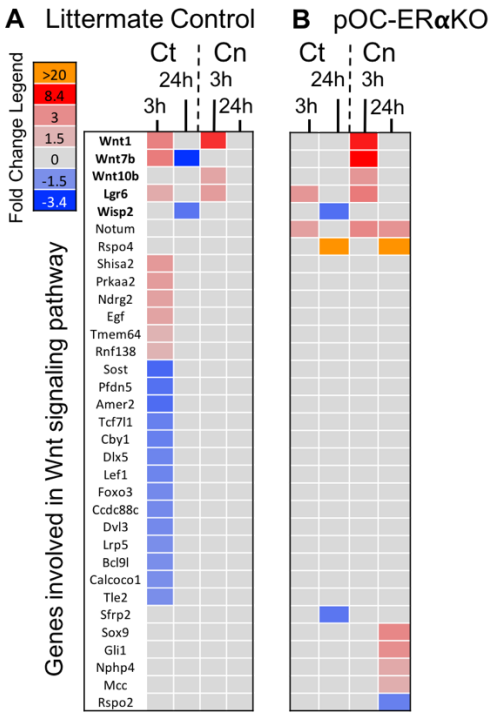

Figure 4.4. More Wnt signaling pathway genes were differentially expressed in LC than pOC-ERαKO. Heat maps of differentially expressed (DE) genes that are involved in the Wnt signaling pathway (GO:0016055, 382 genes total) in A) littermate control and B) pOC-ERαKO animals. Upregulated genes in red, downregulated in blue, and genes with no significant change in gray. Genes in orange were highly up regulated. Gene names in bold were DE in LC and pOC-ERαKO animals. A) Littermate control animals had DE of 25/33 genes, while B) pOC-ERαKO animals had DE of 13/33 genes. Ct = cortical, Cn = cancellous, 3h = 3 hours following a single loading session, 24h = 24 hours following a single loading session.

4.3.4 Cortical and cancellous bone exhibited different transcriptional profiles

To determine transcriptional differences between cortical and cancellous bone, we compared expression in the right cortical versus right cancellous samples of four naïve animals. After removal of contaminants 285 genes were differentially

expressed (2-fold cut-off), with 73% being more highly expressed in cortical bone (208 genes Ct>Cn) (**Table B10**). By comparing differentially expressed genes between cortical and cancellous bone in naïve animals to those in the right limbs (contralateral control) of loaded LC and pOC-ERαKO animals, we identified genes that were consistently different in cortical versus cancellous bone, and genes associated with systemic effects of loading. At the 3-hour time point, 261 genes were differentially expressed in cortical versus cancellous bone of LC contralateral control limbs (**Table B11**) and 279 in pOC-ERαKO animals (**Table B13**). Eighty-eight genes were shared between all three groups (Naïve, contralateral LC and contralateral pOC-ERαKO control tissues). At the 24-hour time point 294 genes were differentially expressed in cortical versus cancellous bone of LC contralateral control limbs (**Table B12**), 172 in pOC-ERαKO contralateral control limbs (**Table B14**), and 69 genes were shared by the three groups (**Figure 4.5**). The top shared genes were all more highly expressed in cortical than cancellous bone. Highly expressed genes that were shared by the three groups at both 3 and 24 hours included *Cilp* and *Cilp2*, *Wnt16* (wingless-type MMTV integration site family, member 16), *Ostn* (osteocrin), *Mfap4* (microfibrillar associated protein 4), *Itgbl1* (integrin, beta-like 1), *Igfbp6* (insulin like growth factor binding protein 6), and *Lrrn1* (leucine rich repeat neuronal 1). These genes were consistently different in cortical

versus cancellous bone, and likely represent true transcriptional differences between bone tissues.

4.3.5 Loading had systemic effects at the transcriptional level

To address whether loading was purely local at the transcriptional level, we compared right and left limbs from 10-week-old female C57Bl/6 littermate control mice that were not externally loaded (naïve LC, n=4). Right and left cortical and cancellous samples had very similar gene expression within each bone envelope with only three genes differing for cortical right/left samples and 4 genes differing for cancellous right/left samples using a 2-fold cut-off. Overall, agreement was excellent between left and right limbs (R^2=0.999 and R^2=0.998 for cortical and cancellous samples, respectively) (**Figure B1**).

Genes that were shared by contralateral control limbs of loaded animals but were not significantly different in the naïve (not loaded) animals may represent systemic changes following in vivo mechanical loading. At the 3-hour time point 26 genes were more highly expressed in cortical bone and shared between the contralateral control limbs of LC and pOC-ERαKO animals (**Figure 4.5C**), while at 24 hours 21 genes were altered (**Figure 4.5F**). Of the top 10 shared genes only one gene overlapped between 3 and 24 hours in contralateral limbs: *Sall1* (spalt-like

transcription factor 1: 8- to 9-fold). At 3 hours highly differentially expressed genes (>5-fold) included *Myoc* (myocilin), *Igfn1* (immunoglobulin-like and fibronectin type III domain containing 1), *Fgf14* and *Fgf23* (fibroblast growth factors 14 and 23), and *Bnc2* (basonuclin 2). At 24 hours highly differentially expressed genes (>5-fold) included *Tigd4* (tigger transposable element derived 4), *Jph4* (junctophilin 4), and *Ear12* (eosinophil-associated, ribonuclease A family, member 12). Although not one of the top shared genes, *Sost* was more highly expressed in cortical bone of LC and pOC-ERαKO contralateral limbs (2.2-fold)

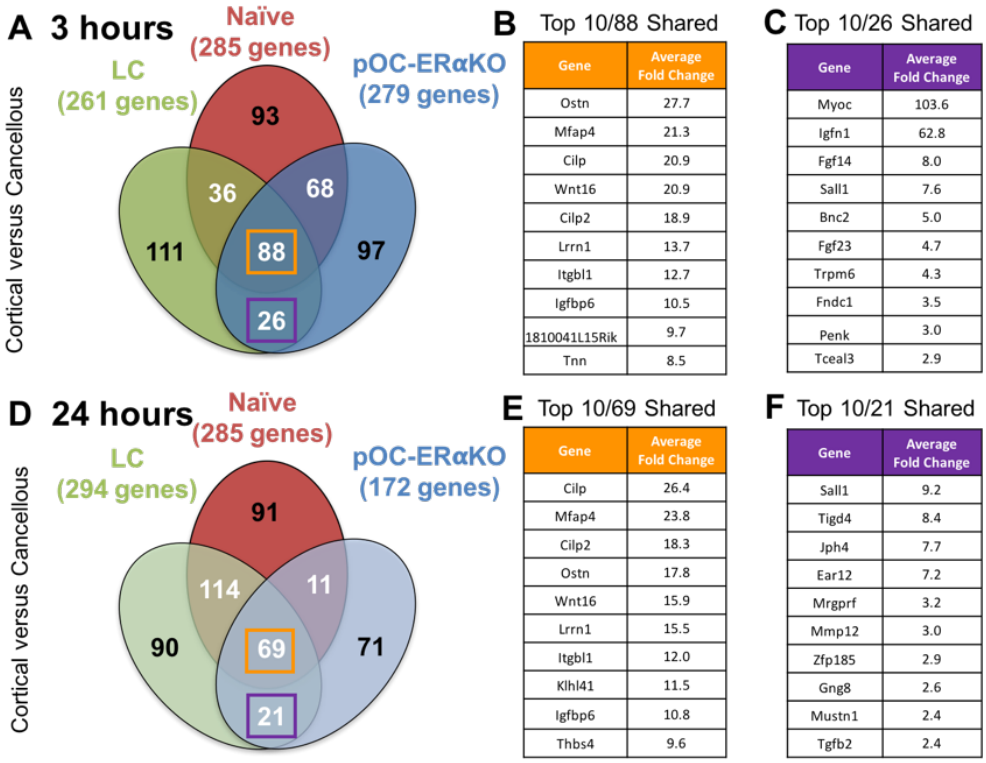

Gene	Average Fold Change
Ostn	27.7
Mfap4	21.3
Cilp	20.9
Wnt16	20.9
Cilp2	18.9
Lrrn1	13.7
Itgbl1	12.7
Igfbp6	10.5
1810041L15Rik	9.7
Tnn	8.5

Gene	Average Fold Change
Myoc	103.6
Igfn1	62.8
Fgf14	8.0
Sall1	7.6
Bnc2	5.0
Fgf23	4.7
Trpm6	4.3
Fndc1	3.5
Penk	3.0
Tceal3	2.9

Gene	Average Fold Change
Cilp	26.4
Mfap4	23.8
Cilp2	18.3
Ostn	17.8
Wnt16	15.9
Lrrn1	15.5
Itgbl1	12.0
Klhl41	11.5
Igfbp6	10.8
Thbs4	9.6

Gene	Average Fold Change
Sall1	9.2
Tigd4	8.4
Jph4	7.7
Ear12	7.2
Mrgprf	3.2
Mmp12	3.0
Zfp185	2.9
Gng8	2.6
Mustn1	2.4
Tgfb2	2.4

Figure 4.5. Cortical and cancellous bone were transcriptionally distinct and loading had systemic effects that differed by genotype. Differential expression (DE) in non-loaded cortical vs cancellous bone of naïve LC animals compared to control right limbs of LC and pOC-ERαKO animals A,B,C) 3 hours and D,E,F) 24 hours after a single loading session. A) 3 hours following a single loading session 261 to 285 genes were DE between non-loaded cortical and cancellous bone (after contaminant removal). Orange box indicates B) Top 10 of 88 DE genes between cortical and cancellous bone and shared by all groups. Purple box indicates C) Top 10 of 26 DE genes in cortical vs cancellous bone and shared in the contralateral limbs of LC and pOC-ERαKO animals. All top shared genes were more highly expressed in cortical than cancellous bone. D) 24 hours following a single loading session 172 to 294 genes were DE between cortical and cancellous bone (after contaminant removal). Orange box indicates E) Top 10 of 69 genes that were DE between cortical and cancellous bone and shared by all groups. Purple box indicates F) Top 10 of 21 genes that were differentially expressed in cortical vs cancellous bone and shared in the contralateral limbs of LC and pOC-ERαKO animals. All top shared genes were more highly expressed in cortical than cancellous bone. In A,D) black numbers indicate genes in only one group, white numbers are genes shared by two or three groups.

4.3.6 RNA-seq verification with qPCR

We found strong agreement between qPCR and RNA-seq for the eight genes tested at the 3-hour time point. When all genes were included (not only those with significant differential expression), the slope of the linear fit between RNA-seq and qPCR Log_2 fold change was close to 1.0 and the Pearson correlation was 0.80 (**Figure 4.6**).

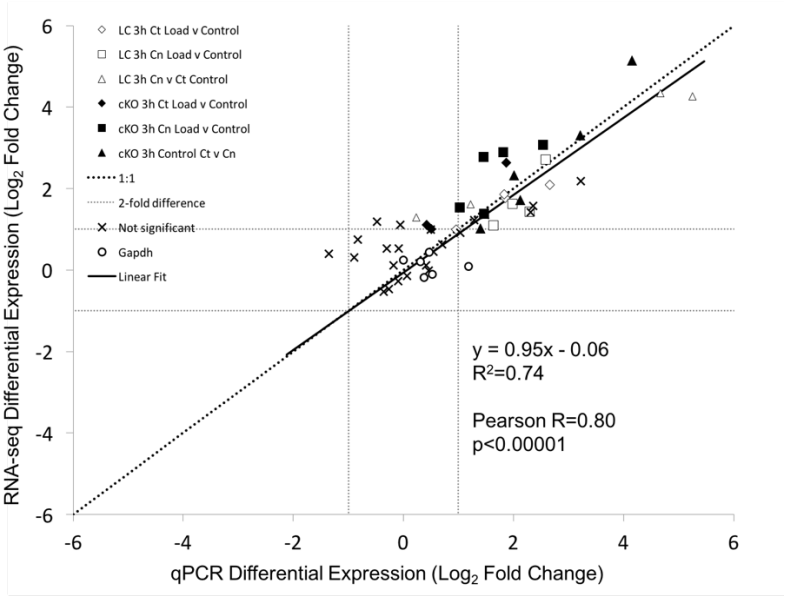

Figure 4.6: qPCR validated 8 differentially expressed genes 3-hours following a single loading session. qPCR was performed for 8 genes identified as differentially expressed with RNA-seq. Log_2 fold change from RNA-seq vs qPCR. Grey dashed lines indicate 2-fold up- and down-regulation, black dashed line is the identity line (1:1 relationship), and the solid line is the linear regression. Strong agreement was found with a Pearson correlation of 0.80.

4.4 Discussion

Differential gene expression was determined in cortical and cancellous bone of control and loaded limbs following a single bout of axial tibial compression in 10-week-old female mice lacking estrogen receptor alpha in mature osteoblasts (pOC-ERαKO) compared to their littermate controls (LC). More genes were differentially expressed in cortical bone of LC animals following a single session of mechanical loading than in cortical bone of pOC-ERαKO animals, particularly three hours following a single loading session. However, in cancellous bone, more genes were differentially expressed in pOC-ERαKO animals, particularly twenty-four hours following a single loading session. More Wnt signaling pathway genes were differentially expressed in LC animals, while Wnt signaling pathway genes were generally more upregulated in pOC-ERαKO animals. We also compared expression in cortical versus cancellous bone of naïve (not externally loaded) littermate control animals and the control limbs of LC and pOC-ERαKO animals. We determined a set of genes that were more highly expressed in cortical bone, demonstrating that cortical versus cancellous bone are transcriptionally distinct. Additionally, genes that were shared in the contralateral limbs of LC and pOC-ERαKO animals but were not differentially expressed in cortical versus cancellous

bone of naïve LC animals may represent genes that are systemically altered by loading.

The molecular mechanisms of the skeletal response to mechanical loading have largely been studied in cortical or whole bone. In agreement with another study examining gene expression in response to tibial compression, we saw 6 to 24 times fewer genes differentially regulated in cortical bone of ERα KO animals compared to littermate controls [33]. Cancellous bone response has not previously been examined at the transcriptional level in mice lacking ERα.

Our laboratory showed previously that female mice lacking ERα in mature osteoblasts have decreased bone mass and strength but respond more to mechanical loading, particularly in cancellous bone [11, 18]. The current data show that pOC-ERαKO mice had 2 to 18 times the number of differentially expressed genes in cancellous bone following mechanical loading when compared to LC mice. Three hours following a single loading session pOC-ERαKO cancellous bone had larger differential expression of sixteen shared genes compared to LC. *Wnt7b*, an important regulator of osteoblast differentiation [34], was upregulated 8.4-fold three hours following loading in pOC-ERαKO but not significantly different in LC mice. *Notum,* which suppresses Wnt signaling by deacylating Wnt

proteins [35], was upregulated 3 hours following loading in cortical and cancellous bone and 24 hours after loading in cancellous bone of pOC-ERαKO animals. Twenty-four hours following a single loading session the number of differentially expressed genes in cancellous bone was markedly decreased in pOC-ERαKO and several genes were very highly upregulated.

Genes that were highly upregulated in both cortical and cancellous bone of pOC-ERαKO, but not littermate control mice, included R-spondin 4 (*Rspo4*), opioid receptor delta 1 (*Oprd1*), and serine (or cysteine) peptidase inhibitor, clade A, member 1A (*Serpina1a*). The degree of upregulation ranged from 20- to 550-fold in cortical and cancellous bone 24 hours following mechanical loading. R-spondins interact with and enhance Wnt signaling, and R-spondin 1 (*Rspo1*) promoted vibration-induced bone formation in physiologically aged and telomere dysfunction-based mouse models of osteoporosis [36-39]. The drastic upregulation of *Rspo4* in mice lacking estrogen receptor alpha may reflect an important compensatory mechanism for altered Wnt signaling and deserves further study. *Oprd1* has been examined mostly in the context of the nervous system, but nerve growth factor (*Ngf*) induced expression of *Oprd1* through PI3K/Akt signaling [40]. PI3K/Akt signaling is an important pathway in bone mechanotransduction [41]. *Ngf* was also upregulated with mechanical loading in our studies. *Ngf* may play a

role in the skeleton to stimulate osteoblast differentiation [42] and increase bone formation and quality during fracture repair [43, 44]. Neurotrophic factors such as *Ngf* and *Oprd1* may play an important role in bone adaptation and should be further investigated. Finally, the *Serpina1a* gene encodes a protein called alpha-1 antitrypsin, which is a type of serine protease inhibitor (serpin) with anti-inflammatory properties [45]. Alpha-1 antitrypsin gene therapy was recently shown to ameliorate bone loss due to ovariectomy, possibly through inhibition of the pro-inflammatory cytokine IL-6 and RANK gene expression [46]. IL-6 was upregulated nearly 10-fold in cortical bone of pOC-ERαKO mice three hours after loading, and *Ptgs2* (Cox2) was upregulated in several groups and time points, highlighting the need to understand the role of inflammatory cytokines in bone and the response to loading.

Crosstalk between estrogen and canonical Wnt signaling has been reported but the exact mechanisms are not fully understood [19]. The hallmark of activated canonical Wnt signaling is β-catenin stabilization and translocation to the nucleus to enhance osteogenic gene transcription. The mechanisms of estrogen/Wnt crosstalk are not clear, but ERα and β-catenin physically interact [47]. Although we did not see changes in β-catenin gene transcription, we saw differential expression of 33 Wnt signaling pathway genes. More Wnt signaling pathway genes were

differentially expressed in LC mice (25/33 LC, 13/33 pOC-ERαKO), but effectors such as *Wnt1*, *Wnt7b*, and *Wisp2* were differentially expressed even in pOC-ERαKO mice. Furthermore, Rspo4 was highly upregulated in pOC-ERαKO mice. Distinguishing the exact effects of lack of ERα on Wnt signaling is difficult, but our data do not suggest that Wnt signaling was absent or deficient in pOC-ERαKO mice. To examine differences in downstream Wnt signaling in the context of decreased estrogen signaling, we performed western blot for β-catenin 24 hours following loading in LC and pOC-ERαKO mice (data not shown). Total β-catenin protein levels were not different with loading or by genotype.

Transcriptional differences in control cortical versus cancellous bone have been demonstrated previously and imply different regulatory mechanisms governing the two tissue types [25]. *Wnt16* was found to be more highly expressed in cortical bone in naïve LC and contralateral control LC and pOC-ERαKO animals. Accumulating evidence shows that *Wnt16* is an important regulator of cortical bone [48-50], and recent studies have demonstrated that overexpression of *Wnt16* increases both cortical and cancellous bone mass [51, 52]. Osteocrin (*Ostn*) was also more highly expressed in control cortical bone from all groups and is a soluble osteoblast regulator that is localized to osteoblasts and young osteocytes

[53]. Overexpression of *Ostn* in transgenic mice caused elongated bones and a marked kyphosis associated with elevated bone cGMP levels [54].

At the tissue level, evidence is conflicting regarding the systemic effects of loading, while the systemic effects on gene expression have not been examined. Tibial loading of mice was controlled locally and confined to the loaded bones [55]. Conversely, rat ulnar loading induced bone formation in distant skeletal sites that were not loaded [56, 57]. Our data indicate that loading may have systemic effects on transcription. Differential gene expression occurred in cortical versus cancellous bone in the contralateral limbs of LC and pOC-ERαKO limbs but not in naïve limbs. This finding implies that systemic gene expression changes should be taken into account when comparing loaded limb response to the contralateral control at the transcriptional level.

Strengths of the current study include the unbiased examination of gene expression in cortical and cancellous bone separately in a biologically relevant bone-specific knockout mouse model. We were limited, however, to the examination of skeletally immature female mice at two time points following a single loading session. Our examination of female mice at 10 weeks of age was based on our previous data indicating differences in the response to mechanical loading in cancellous versus cortical bone of ERα KO female, but not male, mice

[18]. We are currently examining the tissue-level loading response in adult female and male mice lacking ERα in mature osteoblasts, and a future study to determine the differential gene expression in adult mice would complement this study. Examination of other time points following a single loading session, particularly immediate (30 minutes to 1 hour) and long-term (3 days to 1 week) time points would further characterize the time course of signaling events.

4.4.1 Conclusions

We used RNA-seq to demonstrate differences in cortical and cancellous bone transcription separately at two time points following a single loading session in mice lacking ERα in mature osteoblasts and their littermate controls. pOC-ERαKO mice had markedly decreased gene expression in response to mechanical loading in cortical bone compared to littermate controls. In cancellous bone, however, pOC-ERαKO mice had increased gene expression corroborating the enhanced load-induced bone formation seen previously at the tissue level. R-spondin 4 was highly upregulated in cortical and cancellous bone of pOC-ERαKO mice following loading, indicating this pathway may be an important compensatory mechanism when estrogen signaling is reduced.

4.5 References

[1] Smith EP, Boyd J, Frank GR, Takahashi H, Cohen RM, Specker B, Williams TC, Lubahn DB, Korach KS. Estrogen resistance caused by a mutation in the estrogen-receptor gene in a man. N Engl J Med 1994;331: 1056-61.

[2] Gennari L, Merlotti D, De Paola V, Calabro A, Becherini L, Martini G, Nuti R. Estrogen receptor gene polymorphisms and the genetics of osteoporosis: a HuGE review. Am J Epidemiol 2005;161: 307-20.

[3] Remes T, Vaisanen SB, Mahonen A, Huuskonen J, Kroger H, Jurvelin JS, Penttila IM, Rauramaa R. Aerobic exercise and bone mineral density in middle-aged finnish men: a controlled randomized trial with reference to androgen receptor, aromatase, and estrogen receptor alpha gene polymorphisms. Bone 2003;32: 412-20.

[4] Sonoda T, Takada J, Iba K, Asakura S, Yamashita T, Mori M. Interaction between ESRalpha polymorphisms and environmental factors in osteoporosis. J Orthop Res 2012;30: 1529-34.

[5] Suuriniemi M, Mahonen A, Kovanen V, Alen M, Lyytikainen A, Wang Q, Kroger H, Cheng S. Association between exercise and pubertal BMD is modulated by estrogen receptor alpha genotype. J Bone Miner Res 2004;19: 1758-65.

[6] Suuriniemi M, Suominen H, Mahonen A, Alen M, Cheng S. Estrogen receptor alpha polymorphism modifies the association between childhood exercise and bone mass: follow-up study. Pediatr Exerc Sci 2007;19: 444-58.

[7] In: Bone Health and Osteoporosis: A Report of the Surgeon General. Rockville (MD); 2004.

[8] Riggs BL, Wahner HW, Seeman E, Offord KP, Dunn WL, Mazess RB, Johnson KA, Melton LJ, 3rd. Changes in bone mineral density of the proximal femur and spine with aging. Differences between the postmenopausal and senile osteoporosis syndromes. J Clin Invest 1982;70: 716-23.

[9] Almeida M, Iyer S, Martin-Millan M, Bartell SM, Han L, Ambrogini E, Onal M, Xiong J, Weinstein RS, Jilka RL, O'Brien CA, Manolagas SC. Estrogen receptor-alpha signaling in osteoblast progenitors stimulates cortical bone accrual. J Clin Invest 2013;123: 394-404.

[10] Maatta JA, Buki KG, Gu G, Alanne MH, Vaaraniemi J, Liljenback H, Poutanen M, Harkonen P, Vaananen K. Inactivation of estrogen receptor alpha in bone-forming cells induces bone loss in female mice. FASEB J 2013;27: 478-88.

[11] Melville KM, Kelly NH, Khan SA, Schimenti JC, Ross FP, Main RP, van der Meulen MC. Female mice lacking estrogen receptor-alpha in osteoblasts have compromised bone mass and strength. J Bone Miner Res 2014;29: 370-9.
[12] Kondoh S, Inoue K, Igarashi K, Sugizaki H, Shirode-Fukuda Y, Inoue E, Yu T, Takeuchi JK, Kanno J, Bonewald LF, Imai Y. Estrogen receptor alpha in osteocytes regulates trabecular bone formation in female mice. Bone 2014;60: 68-77.
[13] De Souza RL, Matsuura M, Eckstein F, Rawlinson SC, Lanyon LE, Pitsillides AA. Non-invasive axial loading of mouse tibiae increases cortical bone formation and modifies trabecular organization: a new model to study cortical and cancellous compartments in a single loaded element. Bone 2005;37: 810-8.
[14] Fritton JC, Myers ER, Wright TM, van der Meulen MC. Loading induces site-specific increases in mineral content assessed by microcomputed tomography of the mouse tibia. Bone 2005;36: 1030-8.
[15] Torrance AG, Mosley JR, Suswillo RF, Lanyon LE. Noninvasive loading of the rat ulna in vivo induces a strain-related modeling response uncomplicated by trauma or periostal pressure. Calcif Tissue Int 1994;54: 241-7.
[16] Iyer S KH, Ucer S, Bartell S, Warren A, Crawford J, Skinner R, Dallas M, Johnson M, Weinstein RS, Jilka RL, O'Brien CA, Almeida M, Manolagas SC. ER-alpha signaling in osterix1and prx1 expressing cells, respectively, mediates the anabolic effect of mechanical loading in the murine periosteum and the protective effects of estrogens on endocortical resorption J Bone Miner Res 2013;28: S1.
[17] Windahl SH, Borjesson AE, Farman HH, Engdahl C, Moverare-Skrtic S, Sjogren K, Lagerquist MK, Kindblom JM, Koskela A, Tuukkanen J, Divieti Pajevic P, Feng JQ, Dahlman-Wright K, Antonson P, Gustafsson JA, Ohlsson C. Estrogen receptor-alpha in osteocytes is important for trabecular bone formation in male mice. Proc Natl Acad Sci U S A 2013;110: 2294-9.
[18] Melville KM, Kelly NH, Surita G, Buchalter DB, Schimenti JC, Main RP, Ross FP, van der Meulen MC. Effects of Deletion of ER-Alpha in Osteoblast-Lineage Cells on Bone Mass and Adaptation to Mechanical Loading Differs in Female and Male Mice. J Bone Miner Res 2015.
[19] Armstrong VJ, Muzylak M, Sunters A, Zaman G, Saxon LK, Price JS, Lanyon LE. Wnt/beta-catenin signaling is a component of osteoblastic bone cell early responses to load-bearing and requires estrogen receptor alpha. J Biol Chem 2007;282: 20715-27.

[20] Robinson JA, Chatterjee-Kishore M, Yaworsky PJ, Cullen DM, Zhao W, Li C, Kharode Y, Sauter L, Babij P, Brown EL, Hill AA, Akhter MP, Johnson ML, Recker RR, Komm BS, Bex FJ. Wnt/beta-catenin signaling is a normal physiological response to mechanical loading in bone. J Biol Chem 2006;281: 31720-8.
[21] Bonnet N, Standley KN, Bianchi EN, Stadelmann V, Foti M, Conway SJ, Ferrari SL. The matricellular protein periostin is required for sost inhibition and the anabolic response to mechanical loading and physical activity. J Biol Chem 2009;284: 35939-50.
[22] Robling AG, Niziolek PJ, Baldridge LA, Condon KW, Allen MR, Alam I, Mantila SM, Gluhak-Heinrich J, Bellido TM, Harris SE, Turner CH. Mechanical stimulation of bone in vivo reduces osteocyte expression of Sost/sclerostin. J Biol Chem 2008;283: 5866-75.
[23] Tu X, Rhee Y, Condon KW, Bivi N, Allen MR, Dwyer D, Stolina M, Turner CH, Robling AG, Plotkin LI, Bellido T. Sost downregulation and local Wnt signaling are required for the osteogenic response to mechanical loading. Bone 2012;50: 209-17.
[24] Kelly NH, Schimenti JC, Patrick Ross F, van der Meulen MC. A method for isolating high quality RNA from mouse cortical and cancellous bones. Bone 2014.
[25] Kelly NH, Schimenti JC, Ross FP, van der Meulen MC. Transcriptional profiling of cortical versus cancellous bone from mechanically-loaded murine tibiae reveals differential gene expression. Bone 2016;86: 22-9.
[26] Lynch ME, Main RP, Xu Q, Schmicker TL, Schaffler MB, Wright TM, van der Meulen MC. Tibial compression is anabolic in the adult mouse skeleton despite reduced responsiveness with aging. Bone 2011;49: 439-46.
[27] Lynch ME, Main RP, Xu Q, Walsh DJ, Schaffler MB, Wright TM, van der Meulen MC. Cancellous bone adaptation to tibial compression is not sex dependent in growing mice. J Appl Physiol (1985) 2010;109: 685-91.
[28] Trapnell C, Roberts A, Goff L, Pertea G, Kim D, Kelley DR, Pimentel H, Salzberg SL, Rinn JL, Pachter L. Differential gene and transcript expression analysis of RNA-seq experiments with TopHat and Cufflinks. Nat Protoc 2012;7: 562-78.
[29] Robinson MD, McCarthy DJ, Smyth GK. edgeR: a Bioconductor package for differential expression analysis of digital gene expression data. Bioinformatics 2010;26: 139-40.

[30] Ayturk UM, Jacobsen CM, Christodoulou DC, Gorham J, Seidman JG, Seidman CE, Robling AG, Warman ML. An RNA-seq protocol to identify mRNA expression changes in mouse diaphyseal bone: applications in mice with bone property altering Lrp5 mutations. J Bone Miner Res 2013;28: 2081-93.
[31] Dennis G, Jr., Sherman BT, Hosack DA, Yang J, Gao W, Lane HC, Lempicki RA. DAVID: Database for Annotation, Visualization, and Integrated Discovery. Genome Biol 2003;4: P3.
[32] Huang da W, Sherman BT, Lempicki RA. Systematic and integrative analysis of large gene lists using DAVID bioinformatics resources. Nat Protoc 2009;4: 44-57.
[33] Zaman G, Saxon LK, Sunters A, Hilton H, Underhill P, Williams D, Price JS, Lanyon LE. Loading-related regulation of gene expression in bone in the contexts of estrogen deficiency, lack of estrogen receptor alpha and disuse. Bone 2010;46: 628-42.
[34] Chen J, Tu X, Esen E, Joeng KS, Lin C, Arbeit JM, Ruegg MA, Hall MN, Ma L, Long F. WNT7B promotes bone formation in part through mTORC1. PLoS Genet 2014;10: e1004145.
[35] Kakugawa S, Langton PF, Zebisch M, Howell SA, Chang TH, Liu Y, Feizi T, Bineva G, O'Reilly N, Snijders AP, Jones EY, Vincent JP. Notum deacylates Wnt proteins to suppress signalling activity. Nature 2015;519: 187-92.
[36] Carmon KS, Gong X, Lin Q, Thomas A, Liu Q. R-spondins function as ligands of the orphan receptors LGR4 and LGR5 to regulate Wnt/beta-catenin signaling. Proc Natl Acad Sci U S A 2011;108: 11452-7.
[37] Carmon KS, Lin Q, Gong X, Thomas A, Liu Q. LGR5 interacts and cointernalizes with Wnt receptors to modulate Wnt/beta-catenin signaling. Mol Cell Biol 2012;32: 2054-64.
[38] Nam JS, Turcotte TJ, Smith PF, Choi S, Yoon JK. Mouse cristin/R-spondin family proteins are novel ligands for the Frizzled 8 and LRP6 receptors and activate beta-catenin-dependent gene expression. J Biol Chem 2006;281: 13247-57.
[39] Wang H, Brennan TA, Russell E, Kim JH, Egan KP, Chen Q, Israelite C, Schultz DC, Johnson FB, Pignolo RJ. R-Spondin 1 promotes vibration-induced bone formation in mouse models of osteoporosis. J Mol Med (Berl) 2013;91: 1421-9.

[40] Sen D, Huchital M, Chen YL. Crosstalk between delta opioid receptor and nerve growth factor signaling modulates neuroprotection and differentiation in rodent cell models. Int J Mol Sci 2013;14: 21114-39.
[41] Tahimic CG, Wang Y, Bikle DD. Anabolic effects of IGF-1 signaling on the skeleton. Front Endocrinol (Lausanne) 2013;4: 6.
[42] Yada M, Yamaguchi K, Tsuji T. NGF stimulates differentiation of osteoblastic MC3T3-E1 cells. Biochem Biophys Res Commun 1994;205: 1187-93.
[43] Eppley BL, Snyders RV, Winkelmann TM, Roufa DG. Efficacy of nerve growth factor in regeneration of the mandibular nerve: a preliminary report. J Oral Maxillofac Surg 1991;49: 61-8.
[44] Grills BL, Schuijers JA, Ward AR. Topical application of nerve growth factor improves fracture healing in rats. J Orthop Res 1997;15: 235-42.
[45] Paterson T, Moore S. The expression and characterization of five recombinant murine alpha 1-protease inhibitor proteins. Biochem Biophys Res Commun 1996;219: 64-9.
[46] Akbar MA, Cao JJ, Lu Y, Nardo D, Chen MJ, Elshikha AS, Ahamed R, Brantly M, Holliday LS, Song S. Alpha-1 Antitrypsin Gene Therapy Ameliorates Bone Loss in Ovariectomy-Induced Osteoporosis Mouse Model. Hum Gene Ther 2016.
[47] Kouzmenko AP, Takeyama K, Ito S, Furutani T, Sawatsubashi S, Maki A, Suzuki E, Kawasaki Y, Akiyama T, Tabata T, Kato S. Wnt/beta-catenin and estrogen signaling converge in vivo. J Biol Chem 2004;279: 40255-8.
[48] Garcia-Ibarbia C, Perez-Nunez MI, Olmos JM, Valero C, Perez-Aguilar MD, Hernandez JL, Zarrabeitia MT, Gonzalez-Macias J, Riancho JA. Missense polymorphisms of the WNT16 gene are associated with bone mass, hip geometry and fractures. Osteoporos Int 2013;24: 2449-54.
[49] Moverare-Skrtic S, Henning P, Liu X, Nagano K, Saito H, Borjesson AE, Sjogren K, Windahl SH, Farman H, Kindlund B, Engdahl C, Koskela A, Zhang FP, Eriksson EE, Zaman F, Hammarstedt A, Isaksson H, Bally M, Kassem A, Lindholm C, Sandberg O, Aspenberg P, Savendahl L, Feng JQ, Tuckermann J, Tuukkanen J, Poutanen M, Baron R, Lerner UH, Gori F, Ohlsson C. Osteoblast-derived WNT16 represses osteoclastogenesis and prevents cortical bone fragility fractures. Nat Med 2014;20: 1279-88.
[50] Zheng HF, Tobias JH, Duncan E, Evans DM, Eriksson J, Paternoster L, Yerges-Armstrong LM, Lehtimaki T, Bergstrom U, Kahonen M, Leo PJ, Raitakari O, Laaksonen M, Nicholson GC, Viikari J, Ladouceur M, Lyytikainen LP, Medina-Gomez C, Rivadeneira F, Prince RL, Sievanen H,

Leslie WD, Mellstrom D, Eisman JA, Moverare-Skrtic S, Goltzman D, Hanley DA, Jones G, St Pourcain B, Xiao Y, Timpson NJ, Smith GD, Reid IR, Ring SM, Sambrook PN, Karlsson M, Dennison EM, Kemp JP, Danoy P, Sayers A, Wilson SG, Nethander M, McCloskey E, Vandenput L, Eastell R, Liu J, Spector T, Mitchell BD, Streeten EA, Brommage R, Pettersson-Kymmer U, Brown MA, Ohlsson C, Richards JB, Lorentzon M. WNT16 influences bone mineral density, cortical bone thickness, bone strength, and osteoporotic fracture risk. PLoS Genet 2012;8: e1002745.

[51] Alam I, Alkhouli M, Gerard-O'Riley RL, Wright WB, Acton D, Gray AK, Patel B, Reilly AM, Lim KE, Robling AG, Econs MJ. Osteoblast-Specific Overexpression of Human WNT16 Increases Both Cortical and Trabecular Bone Mass and Structure in Mice. Endocrinology 2016;157: 722-36.

[52] Moverare-Skrtic S, Wu J, Henning P, Gustafsson KL, Sjogren K, Windahl SH, Koskela A, Tuukkanen J, Borjesson AE, Lagerquist MK, Lerner UH, Zhang FP, Gustafsson JA, Poutanen M, Ohlsson C. The bone-sparing effects of estrogen and WNT16 are independent of each other. Proc Natl Acad Sci U S A 2015;112: 14972-7.

[53] Thomas G, Moffatt P, Salois P, Gaumond MH, Gingras R, Godin E, Miao D, Goltzman D, Lanctot C. Osteocrin, a novel bone-specific secreted protein that modulates the osteoblast phenotype. J Biol Chem 2003;278: 50563-71.

[54] Moffatt P, Thomas G, Sellin K, Bessette MC, Lafreniere F, Akhouayri O, St-Arnaud R, Lanctot C. Osteocrin is a specific ligand of the natriuretic Peptide clearance receptor that modulates bone growth. J Biol Chem 2007;282: 36454-62.

[55] Sugiyama T, Price JS, Lanyon LE. Functional adaptation to mechanical loading in both cortical and cancellous bone is controlled locally and is confined to the loaded bones. Bone 2010;46: 314-21.

[56] Sample SJ, Behan M, Smith L, Oldenhoff WE, Markel MD, Kalscheur VL, Hao Z, Miletic V, Muir P. Functional adaptation to loading of a single bone is neuronally regulated and involves multiple bones. J Bone Miner Res 2008;23: 1372-81.

[57] Sample SJ, Collins RJ, Wilson AP, Racette MA, Behan M, Markel MD, Kalscheur VL, Hao Z, Muir P. Systemic effects of ulna loading in male rats during functional adaptation. J Bone Miner Res 2010;25: 2016-28.

CHAPTER 5
CONCLUSIONS AND DISCUSSION

5.1 Summary

The objective of this research was to elucidate the molecular mechanisms of bone adaptation to mechanical loading in cortical versus cancellous bone in the context of estrogen signaling. Mechanical loading is a potential anabolic therapy for bone loss due to postmenopausal osteoporosis. Following menopause, bone mass and circulating estrogen decrease. Estrogen also plays a role in mechanotransduction in bone. An increased understanding of estrogen signaling in the skeletal response to mechanical loading is critical in developing potential new therapies to combat postmenopausal bone loss. However, molecular mechanisms of mechanotransduction have been studied exclusively in cortical or whole bone with a candidate gene approach. Cortical and cancellous bone respond differently to mechanical loading at the tissue level, underscoring the importance of examining cellular responses in these two tissues separately. Whole transcriptome sequencing allows for the unbiased examination of the genes affected by mechanical loading. After developing a method to isolate high quality RNA from marrow-free mouse cortical and cancellous bone, differences in gene transcription were determined at baseline and following mechanical loading of wild-type mice, and osteoblast-specific ERα knockout (pOC-ERαKO) compared to littermate control mice. Cortical and cancellous bone exhibited

different transcriptional profiles at baseline and in response to mechanical loading. The transcriptional profile in contralateral, unloaded limbs differed at both time points, indicating mechanical loading may have systemic effects at the gene level. pOC-ERαKO mice had a blunted response to mechanical loading in cortical bone compared to littermate controls, but had an increased response in cancellous bone.

Aim 1

Our first aim was to develop a method to measure gene expression in marrow-free cortical and cancellous bone. The high incidence of fragility fractures in cortico-cancellous sites, plus the fact that individual skeletal sites exhibit different responsiveness to load and disease, reveals the need to document gene expression in cortical versus cancellous bone. The cellular and molecular mechanisms driving load-induced bone anabolism have been examined using quantitative real-time polymerase chain reaction (qPCR) and microarray [1-4]. These studies have examined tissues from whole bones, homogenizing cortical and cancellous bone. Marrow cells were left in place [3], or removed by flushing [2] or centrifugation [1, 4]. However, failure to remove the highly cellular marrow component may result in contamination of RNA isolated from bone. Prior to the work presented here the relative efficacy of flushing to centrifugation had not been studied, nor had the effect of bone marrow contamination on apparent bone specific gene expression. More importantly, gene

expression had not been reported in minimally contaminated cortical versus cancellous bone, a challenging endeavor in murine models.

This work describes a method to isolate high quality RNA from cortical and, separately, cancellous bone with minimal contamination from marrow cells. Centrifugation removed contaminating cells more efficiently that flushing, as indexed by histology, and decreased detection of a highly expressed erythroid gene. Furthermore, centrifuged cortical and cancellous bone had higher apparent relative expression of bone-related genes when compared to bone for which marrow was left intact. Lastly, cortical bone had higher expression of bone-related genes than cancellous bone. RNA isolated by this novel approach can reveal site-specific changes in gene expression in cortical and cancellous bone sites.

Aim 2

Our second aim was to determine the transcriptional response to mechanical loading in cortical and cancellous bone separately. Mechanical loading is an anabolic stimulus that increases bone mass, and thus a promising method to counteract osteoporosis-related bone loss. The mechanism of this anabolism remains unclear, and needs to be established for both cortical and cancellous envelopes individually. Transcriptional profiling with RNA sequencing provides an opportunity to determine gene expression in cortical and cancellous tissues separately and to examine the molecular mechanisms responsible for mechanical loading-related anabolism. We

hypothesized that basal gene expression and the transcriptional response to mechanical loading would differ in cortical versus cancellous bone. To test this hypothesis, we applied compressive loading to the mouse tibia and performed RNA-seq in cortical versus cancellous bone at two time points.

Cortical and cancellous bone exhibited different transcriptional profiles basally and in response to mechanical loading. At baseline, more genes were expressed differentially 24 hours after a single loading session in control bone, implying that the response to mechanical loading is, at least partly, systemic. Enhanced Wnt signaling dominated the response to mechanical loading in cortical bone at 3 and 24 hours, but in cancellous bone only at 3 hours. In cancellous bone at 24 hours many muscle-related genes were downregulated. These findings reveal key differences between cortical and cancellous genetic regulation in response to mechanical loading.

Aim 3

Our third aim was to elucidate differences in the transcriptional response to mechanical loading in cortical versus cancellous bone with deficient estrogen signaling. Postmenopausal osteoporosis is characterized by reduced bone mass and estrogen signaling. Mechanical loading is an anabolic stimulus that increases bone mass. We recently showed that mice lacking ERα in osteoblasts and osteocytes (pOC-ERαKO) had an increased adaptive response to mechanical loading, particularly in

cancellous bone [5]. The molecular mechanisms of functional adaptation to load in the context of decreased estrogen signaling are not fully elucidated, particularly in cortical versus cancellous sites. We examined transcription in cortical versus cancellous bone of tibiae from littermate control (LC) and pOC-ERαKO mice. Female mice were subjected to one session of mechanical loading with the contralateral tibia as control or euthanized without application of external loads (naïve). We performed RNA-seq on cortical versus cancellous bone to determine differential gene expression at two time points following a single loading session and at baseline (naïve animals and control limbs).

Cortical bone responded more to a single session of mechanical loading in LC than pOC-ERαKO animals, particularly 3 hours following a single loading session. In cancellous bone, however, the transcriptional response to mechanical loading was greater in pOC-ERαKO than LC animals, particularly 24 hours following a single loading session. The increased gene expression in cancellous bone of pOC-ERαKO agrees with our previous tissue-level data showing enhanced response to loading.

Wnt signaling is an important pathway for mechanotransduction and may require ERα. More Wnt signaling pathway genes were differentially expressed in LC mice, but effectors such as Wnt1, Wnt7b, and Wisp2 were differentially expressed even in pOC-ERαKO mice. Furthermore, Rspo4 was highly upregulated in pOC-ERαKO mice. The exact effects of lack of ERα on Wnt signaling are difficult to

distinguish, but our data do not suggest that Wnt signaling was absent or deficient in pOC-ERαKO mice.

A set of genes was more highly expressed in cortical bone, demonstrating that cortical and cancellous bone are transcriptionally distinct. Additionally, loading may cause systemic alterations in transcription. RNA-seq analysis of the in vivo mechanical loading response in cortical versus cancellous bone provides transcriptome level data to identify estrogen's role in mechanotransduction and new targets for the treatment of osteoporosis.

Comparing across the wild-type/littermate control animals that were mechanically loaded in Aim 2 versus Aim 3, demonstrates some similarities and some differences in our results. Wnt signaling genes that were consistently affected by loading included *Wnt1*, *Wnt7b*, and *Wnt10b*. Other genes differentially expressed with loading in both experiments included *Ptgs2*, *Tnfrsf11b*, and *Timp1*. One major difference was the number of genes differentially expressed in cortical bone 3 hours following a single session of mechanical loading. In Aim 2, 43 genes were differentially expressed, while in Aim 3 772 genes were differentially expressed. Furthermore, more genes were differentially expressed 24 hours following a single loading session than at 3 hours in Aim 2, but not in Aim 3. Finally, we demonstrated a significant downregulation of muscle-related genes at 24 hours in cancellous bone in our second aim, but this response was not recapitulated in our third aim. The causes

for discrepancies in our data is not clear. Experimental differences included improved RNA isolation techniques that resulted in higher RNA quality in our third aim, particularly in cortical bone, and technical differences including different sequencing platforms, read lengths, sequencing depths, and read alignment metrics.

5.2 Strengths

We are the first to establish a method for isolating high-quality RNA from mouse cortical and cancellous bone with minimal marrow contamination. Our technique was applied to examine transcriptomic differences in response to mechanical loading in cortical versus cancellous bone. Previous work has examined cancellous bone from mechanically loaded murine vertebrae, but expression was separately determined in cortical bone [6]. Furthermore, marrow was sequentially digested, a technique that has been shown to alter the expression of bone-related genes [7]. We determined that centrifugation efficiently removed marrow and increased the detection of bone-related genes.

The tibial compression model used in this work is consistently osteogenic in both cortical and cancellous bone. Other loading models either cannot examine cancellous bone in the case of ulnar compression [8] or use a different waveform that decreases cancellous bone volume in the tibial metaphysis [9]. We have shown increased cortical and cancellous bone mass with our loading model in growing and adult male and female mice, and following gonadectomy or genetic modification [5,

10-13]. Anabolism in both cortical and cancellous bone allows for the separate quantification of the cellular mechanisms responsible for bone adaptation in these two tissues types. Cancellous bone tissue, however, is limited in the murine tibial metaphysis. Thus, gene expression measurement is challenging with standard techniques.

RNA sequencing is an emerging technique that reveals the presence and quantity of the RNA transcriptome in small biological samples. The alternative methods to determine differential gene expression include quantitative polymerase chain reaction (qPCR) and microarray. qPCR is highly quantitative and sensitive but generally best for interrogating a relatively small number of transcripts in a large set of samples. Microarrays and RNA-seq offer genome-wide surveys of the transcriptome, but microarrays can only detect sequences homologous to known probes on the array. In contrast, RNA-seq is "unbiased," and thus ideal for discovery. RNA-seq provides transcriptome level data from a very small quantity of input material, an important strength when examining the very small volumes of tissue in cancellous regions of mouse bone.

The pOC-ERαKO mouse model, in which ERα is removed from mature osteoblasts and osteocytes, is another strength of this work. Global ERα knockout causes systemic changes which confound the determination of specific skeletal effects [14]. We had previously shown that female pOC-ERαKO mice had decreased bone

mass and strength, but responded more to mechanical loading than their littermate controls, particularly in cancellous bone [5, 15]. A logical next step was to determine the differential regulation occurring in cortical versus cancellous bone of pOC-ERαKO mice following mechanical loading.

5.3 Limitations

The central dogma of molecular biology is a framework to understand the transfer of genetic information within a biological system. It defines the dominant flow of biological information as replication (DNA can be copied to DNA), transcription (DNA information can be copied into mRNA), and translation (proteins are synthesized using the information in mRNA as a template) [16]. Our studies are limited to examining transcription, without determining the effect on translation.

At a more granular level, our studies were limited to examining a single age and gender of animal, at two time points following a single loading session. We chose to focus on adolescent (10 week old) females because we had previously shown a robust response to mechanical loading in cortical and cancellous bone of these animals, as well as an interesting differential response in female estrogen receptor alpha knockout mice [5, 12, 13]. It is important to determine the transcriptional response in older mice, however, as osteoporosis affects aged individuals and the skeleton becomes less responsive to mechanical loading with age [12]. Furthermore, NIH is developing

policies to balance the use of male and female animals in preclinical studies, so our examination of only females is an important limitation that should be addressed in the future [17]. Examination of the response at two time points following a single loading session was an important first step, but could be substantially expanded to include multiple time points and more loading sessions. Our early time point, three hours following a single loading session, may not capture transcription factor changes that occur within minutes of the stimulus. Additionally, later time points may provide important information on matrix production, which occurs three days to several weeks following mechanical loading in bone [18, 19].

The magnitude of controlled loads applied during in vivo tibial loading were determined based on strain measurements at the cortical diaphysis, but the corresponding tissue-level strains in the metaphysis are difficult to characterize, particularly in cancellous bone. A physiologic strain of +1200 microstrain (με) at the mid-diaphysis has typically been used to study bone adaptation [12, 13, 20]. Bone stiffness was previously found to be similar between female pOC-ERαKO and LC mice, requiring a peak load of -9.0N to engender +1200 με [5]. Therefore, peak loads of -9.0N were applied in the current studies. However, tissue measurements demonstrated that female pOC-ERαKO mice had decreased bone volume fraction at the tibial metaphysis compared to LC yet responded more to mechanical loading [5]. It is difficult to determine if the increased response in pOC-ERαKO mice is due to

differences in genotype, and thus intrinsic signaling factors, or differences in extrinsic cancellous bone strain application.

An additional limitation is that we do not know the exact cellular makeup of our bone samples. Cortical versus cancellous samples could contain different proportions of osteoblasts and osteocytes. This limitation would only affect our examination of baseline cortical versus cancellous transcription differences. For loading-related changes we are comparing within tissue types, so cellular proportions should be similar. Embedded osteocytes are the most likely source of RNA in our samples. Osteocytes account for more than 90% of bone cells, and non-adherent osteoblasts and osteoclasts are likely removed with centrifugation. We counted osteoblasts and osteocytes per bone surface and area in cortical versus cancellous histological samples and did not find a difference in the proportions. This result is reassuring but does not rule out the possibility of differences in cellular makeup.

5.4 Future Work

The function and relative contributions of genes and pathways that were differentially expressed following mechanical loading in this work could be further elucidated. The methodology developed in this thesis can be easily extended to examine different ages, time points, and number of mechanical loading sessions. More importantly, the transcriptional differences need to be verified at the protein level, localized to different cells and ideally related to the strain field to more accurately

determine spatial and cell-specific responses to mechanical loading. Future studies could also examine changes in bone mass and transcription following targeted disruption of important mechanotransduction pathways such as Wnt signaling.

Follow up studies of genes discovered

The goal of any large scale sequencing study is to discover genes of interest as potential targets of future studies. A few of the genes to emerge from the current work are *Timp1*, *Ptgs2*, *Rspo4*, *Oprd1* and *Serpin1a1*. Tissue inhibitor of metalloproteinase (*Timp1*) and prostaglandin-endoperoxide synthase 2 (*Ptgs2*) were upregulated after loading in cortical and cancellous bone at several time points and across genotypes. *Timp1* inhibits metalloproteinases, and thus degradation of extracellular matrix, and was previously found to be upregulated in homogenized tibial bone subjected to mechanical loading [4, 21]. Furthermore, *Timp1* has been shown to be regulated by Wnt signaling [22]. *Ptgs2*, also known as Cox-2, produces prostaglandin, which is necessary for mechanical-loading induced β-catenin activation [23]. Another study demonstrated that Cox-2 activity is more important for endocortical bone adaptive response to mechanical loading than the periosteal response [24]. The molecular mechanisms responsible for such site-specific differences could be examined using our methodology.

Several genes were found to be highly upregulated in both cortical and cancellous bone of pOC-ERαKO, but not littermate control mice. R-spondin 4 (*Rspo4*), opioid receptor delta 1 (*Oprd1*), and serine (or cysteine) peptidase inhibitor, clade A, member 1A (*Serpina1a*) were upregulated 20- to 550-fold in cortical and cancellous bone 24 hours following mechanical loading. R-spondins have been shown to interact with and enhance Wnt signaling, and R-spondin 1 (*Rspo1*) promoted vibration-induced bone formation in physiologically aged and telomere-dysfunction based mouse models of osteoporosis [25-28]. The drastic upregulation of *Rspo4* in mice lacking estrogen receptor alpha may reflect an important compensatory mechanism for altered Wnt signaling and deserves further study. *Oprd1* has been examined mostly in the context of the nervous system, but nerve growth factor (*Ngf*) induced expression of *Oprd1* through PI3K/Akt signaling [29]. PI3K/Akt signaling is an important pathway in bone mechanotransduction [30]. *Ngf* also was upregulated with mechanical loading in our studies. *Ngf* may play a role in the skeleton, as it can stimulate differentiation of an osteoblastic cell line [31] and can increase bone formation and quality of fracture repair [32, 33]. Neurotrophic factors such as *Ngf* and *Oprd1* may play an important role in bone adaptation and could be further investigated. Finally, the *Serpina1a* gene encodes a protein called alpha-1 antitrypsin, which is a type of serine protease inhibitor (serpin) with anti-inflammatory properties [34]. Alpha-1 antitrypsin gene therapy was recently shown to ameliorate bone loss due

to ovariectomy, possibly through inhibition of the proinflammatory cytokine IL-6 and RANK gene expression [35]. IL-6 was upregulated nearly 10-fold in cortical bone of pOC-ERαKO mice three hours after loading, highlighting the need to understand the role of inflammatory cytokines in bone loss and the response to loading.

Based on the results from Chapter 3, the role of muscle-related genes in bone mechanotransduction may be another area of interest. Muscle genes were the largest group of downregulated genes 24 hours following a single loading session in cancellous bone of wild-type mice. A single loading session of the rat forearm (cortical site) also caused downregulation of muscle genes [36] and calvarial-derived osteocytes [37] and young healthy articular cartilage [38] express genes related to muscle function, development, and differentiation. Elucidation of the function of muscle-related genes in bone cells and the response to mechanical loading requires further study.

Effects of age, gender, time point, and number of loading sessions

Differential gene expression can be determined using these methods for adult and aged mice, males, earlier and later time points and after multiple loading sessions. We have previously shown that adult (26-week-old) female mice are not as responsive to mechanical loading as young (10-week-old) mice [12]. A study comparing the transcriptomes of young, adult and aged mice subjected to mechanical loading could

determine the molecular mechanisms behind the reduced response with age. This data would have important clinical implications, as bone's anabolic response to exercise declines with age [39] and osteoporosis mostly affects the elderly. As previously mentioned, there is a drive in the scientific community to perform preclinical studies in male and female animals, so our studies should also be performed on males. Finally, early and later time points following a single loading session as well as examining the response after multiple loading sessions would extend our knowledge of the time course of signaling events and effects of differing stimuli.

Identification of translational changes

An important and logical next step would be to verify that the transcriptional changes we identified also result in differences in protein translation. The experimental design of these studies is complicated, as the selection of time point and proteins to verify is critical. We examined transcription three and twenty-four hours following mechanical loading, but translation may occur minutes to hours following transcription, depending on the gene size and post-transcriptional modifications. Furthermore, protein quantification methods including western blot and immunohistochemistry (IHC) can be functionally performed on only a small number of proteins. Protein isolation from bone is another challenge due to the relatively small amount of tissue and cells compared to matrix. It may be possible to use

proteomics to examine the entire set of proteins produced following mechanical loading [40].

Spatial and cell-specific responses

We isolated RNA from the metaphyseal cortical shell and cancellous core of the mouse tibia, without quantification of the cellular population. Future studies could examine transcription at the tibial mid-diaphysis, where strains are typically measured. This is purely cortical, but transcriptional changes could be more directly linked to differing strain levels. Furthermore, the curvature of the mouse tibia results in regions of compression and tension on the cortical surface [41]. A recent study identified differences in teriparatide treatment on the compressive and tensile regions of the femoral neck in humans [42]. The transcriptional changes responsible for this differential effect could be determined for compressive and tensile regions of mouse cortical bone treated with teriparatide. Cell-specific responses could be determined by performing fluorescence-activated cell sorting (FACS) on bone samples from animals with GFP-labeled osteocytes [43], allowing for the specific determination of osteocyte-driven transcription in response to mechanical loading. Another approach to examine cell-specific transcription would be laser capture microdissection (LMD). This technique allows the study of individual cells or regions of cells [44]. RNA-seq can be performed on even a single cell, allowing for the quantification of the transcriptome at a very specific location [45]. Thus, performing RNA-seq on specific

regions of bone after LMD would provide a wealth of data on strain-dependent and even cell-specific transcription.

Targeted disruption of the Wnt pathway

The current studies and many others have highlighted the importance of the Wnt signaling pathway in bone mechanotransduction. Recent genome-wide association studies have identified two SNPs that are strongly associated with decreased bone mass located within an intron of the human *GPR177* gene [46, 47]. Wntless (*Wls*, also known as *Gpr177*) is required for normal secretion of Wnt ligands from cells and is highly specific [48, 49]. A recent study generated osteoblast-specific Wntless deficient mice (*OC*-Cre;*Wls*-flox) and found significantly reduced bone-mass accrual as early as 20 days of age, spontaneous fractures, and premature lethality at around 2 months of age [50]. An inducible Cre would allow for normal bone development and subsequent examination of Wnt deficiency, circumventing the drastic bone effects and premature death. A tamoxifen-inducible Cre fusion protein under the control of the type I collagen promoter (*Col1*-CreER^{TM}) exists [51] and when crossed with the Wls-floxed mouse would allow for the controlled disruption of Wnt signaling after bone mass accrual. Tissue-level response to two weeks of mechanical loading would determine if bone adaptation requires Wnt ligands, and RNA-seq studies would determine any transcriptional response to counteract the loss of Wnt. Alternatively, the Porcupine gene (PORCN) encodes a protein that is the only

enzyme known to be required for Wnt ligand palmitoylation, which is essential for Wnt secretion [52]. Pharmaceutical companies have initiated clinical trials of a Porcupine inhibitor in patients with melanoma and some types of breast cancer [53, 54]. Treatment of mice with Porcupine inhibitor would be another way to ablate Wnt signaling and examine the effects on bone mechanotransduction at the tissue and transcription level. Furthermore, crosstalk with estrogen signaling could be examined by administration of Porcupine inhibitor to pOC-ERαKO mice.

5.5 Conclusions

We developed a method of whole transcriptome analysis of cortical versus cancellous bone, an important contribution to the field that can be applied to many outstanding research questions in orthopaedics. We elucidated differences in the transcriptional response to mechanical load in cortical and cancellous bone with and without ERα. Wnt signaling is an important early response to mechanical loading that may be altered by decreased estrogen signaling. We have performed an important first step towards understanding the cellular responses to mechanical loading that ultimately result in increased bone mass on the organismal level. Developing new drugs that harness the fundamental differences in mechanotransduction in cancellous and cortical bone could revolutionize the treatment of osteoporosis-related bone loss in these sites.

5.6 References

[1] Armstrong VJ, Muzylak M, Sunters A, Zaman G, Saxon LK, Price JS, Lanyon LE. Wnt/beta-catenin signaling is a component of osteoblastic bone cell early responses to load-bearing and requires estrogen receptor alpha. J Biol Chem 2007;282: 20715-27.

[2] Bonnet N, Standley KN, Bianchi EN, Stadelmann V, Foti M, Conway SJ, Ferrari SL. The matricellular protein periostin is required for sost inhibition and the anabolic response to mechanical loading and physical activity. J Biol Chem 2009;284: 35939-50.

[3] Silva MJ, Brodt MD, Lynch MA, Stephens AL, Wood DJ, Civitelli R. Tibial loading increases osteogenic gene expression and cortical bone volume in mature and middle-aged mice. PLoS One 2012;7: e34980.

[4] Zaman G, Saxon LK, Sunters A, Hilton H, Underhill P, Williams D, Price JS, Lanyon LE. Loading-related regulation of gene expression in bone in the contexts of estrogen deficiency, lack of estrogen receptor alpha and disuse. Bone 2010;46: 628-42.

[5] Melville KM, Kelly NH, Surita G, Buchalter DB, Schimenti JC, Main RP, Ross FP, van der Meulen MC. Effects of Deletion of ER-Alpha in Osteoblast-Lineage Cells on Bone Mass and Adaptation to Mechanical Loading Differs in Female and Male Mice. J Bone Miner Res 2015.

[6] Wasserman E, Webster D, Kuhn G, Attar-Namdar M, Muller R, Bab I. Differential load-regulated global gene expression in mouse trabecular osteocytes. Bone 2013;53: 14-23.

[7] Ayturk UM, Jacobsen CM, Christodoulou DC, Gorham J, Seidman JG, Seidman CE, Robling AG, Warman ML. An RNA-seq protocol to identify mRNA expression changes in mouse diaphyseal bone: applications in mice with bone property altering Lrp5 mutations. J Bone Miner Res 2013;28: 2081-93.

[8] Torrance AG, Mosley JR, Suswillo RF, Lanyon LE. Noninvasive loading of the rat ulna in vivo induces a strain-related modeling response uncomplicated by trauma or periostal pressure. Calcif Tissue Int 1994;54: 241-7.

[9] Holguin N, Brodt MD, Sanchez ME, Kotiya AA, Silva MJ. Adaptation of tibial structure and strength to axial compression depends on loading history in both C57BL/6 and BALB/c mice. Calcif Tissue Int 2013;93: 211-21.

[10] Fritton JC, Myers ER, Wright TM, van der Meulen MC. Loading induces site-specific increases in mineral content assessed by microcomputed tomography of the mouse tibia. Bone 2005;36: 1030-8.
[11] Fritton JC, Myers ER, Wright TM, van der Meulen MC. Bone mass is preserved and cancellous architecture altered due to cyclic loading of the mouse tibia after orchidectomy. J Bone Miner Res 2008;23: 663-71.
[12] Lynch ME, Main RP, Xu Q, Schmicker TL, Schaffler MB, Wright TM, van der Meulen MC. Tibial compression is anabolic in the adult mouse skeleton despite reduced responsiveness with aging. Bone 2011;49: 439-46.
[13] Lynch ME, Main RP, Xu Q, Walsh DJ, Schaffler MB, Wright TM, van der Meulen MC. Cancellous bone adaptation to tibial compression is not sex dependent in growing mice. J Appl Physiol (1985) 2010;109: 685-91.
[14] Lindberg MK, Alatalo SL, Halleen JM, Mohan S, Gustafsson JA, Ohlsson C. Estrogen receptor specificity in the regulation of the skeleton in female mice. J Endocrinol 2001;171: 229-36.
[15] Melville KM, Kelly NH, Khan SA, Schimenti JC, Ross FP, Main RP, van der Meulen MC. Female mice lacking estrogen receptor-alpha in osteoblasts have compromised bone mass and strength. J Bone Miner Res 2014;29: 370-9.
[16] Crick F. Central dogma of molecular biology. Nature 1970;227: 561-3.
[17] Clayton JA, Collins FS. Policy: NIH to balance sex in cell and animal studies. Nature 2014;509: 282-3.
[18] Forwood MR, Owan I, Takano Y, Turner CH. Increased bone formation in rat tibiae after a single short period of dynamic loading in vivo. Am J Physiol 1996;270: E419-23.
[19] Mantila Roosa SM, Turner CH, Liu Y. Regulatory mechanisms in bone following mechanical loading. Gene Regul Syst Bio 2012;6: 43-53.
[20] Main RP, Lynch ME, van der Meulen MC. In vivo tibial stiffness is maintained by whole bone morphology and cross-sectional geometry in growing female mice. J Biomech 2010;43: 2689-94.
[21] Xing W, Baylink D, Kesavan C, Hu Y, Kapoor S, Chadwick RB, Mohan S. Global gene expression analysis in the bones reveals involvement of several novel genes and pathways in mediating an anabolic response of mechanical loading in mice. J Cell Biochem 2005;96: 1049-60.
[22] Nakashima A, Tamura M. Regulation of matrix metalloproteinase-13 and tissue inhibitor of matrix metalloproteinase-1 gene expression by WNT3A

and bone morphogenetic protein-2 in osteoblastic differentiation. Front Biosci 2006;11: 1667-78.
[23] Lara-Castillo N, Kim-Weroha NA, Kamel MA, Javaheri B, Ellies DL, Krumlauf RE, Thiagarajan G, Johnson ML. In vivo mechanical loading rapidly activates beta-catenin signaling in osteocytes through a prostaglandin mediated mechanism. Bone 2015;76: 58-66.
[24] Li J, Burr DB, Turner CH. Suppression of prostaglandin synthesis with NS-398 has different effects on endocortical and periosteal bone formation induced by mechanical loading. Calcif Tissue Int 2002;70: 320-9.
[25] Carmon KS, Gong X, Lin Q, Thomas A, Liu Q. R-spondins function as ligands of the orphan receptors LGR4 and LGR5 to regulate Wnt/beta-catenin signaling. Proc Natl Acad Sci U S A 2011;108: 11452-7.
[26] Carmon KS, Lin Q, Gong X, Thomas A, Liu Q. LGR5 interacts and cointernalizes with Wnt receptors to modulate Wnt/beta-catenin signaling. Mol Cell Biol 2012;32: 2054-64.
[27] Nam JS, Turcotte TJ, Smith PF, Choi S, Yoon JK. Mouse cristin/R-spondin family proteins are novel ligands for the Frizzled 8 and LRP6 receptors and activate beta-catenin-dependent gene expression. J Biol Chem 2006;281: 13247-57.
[28] Wang H, Brennan TA, Russell E, Kim JH, Egan KP, Chen Q, Israelite C, Schultz DC, Johnson FB, Pignolo RJ. R-Spondin 1 promotes vibration-induced bone formation in mouse models of osteoporosis. J Mol Med (Berl) 2013;91: 1421-9.
[29] Sen D, Huchital M, Chen YL. Crosstalk between delta opioid receptor and nerve growth factor signaling modulates neuroprotection and differentiation in rodent cell models. Int J Mol Sci 2013;14: 21114-39.
[30] Tahimic CG, Wang Y, Bikle DD. Anabolic effects of IGF-1 signaling on the skeleton. Front Endocrinol (Lausanne) 2013;4: 6.
[31] Yada M, Yamaguchi K, Tsuji T. NGF stimulates differentiation of osteoblastic MC3T3-E1 cells. Biochem Biophys Res Commun 1994;205: 1187-93.
[32] Eppley BL, Snyders RV, Winkelmann TM, Roufa DG. Efficacy of nerve growth factor in regeneration of the mandibular nerve: a preliminary report. J Oral Maxillofac Surg 1991;49: 61-8.
[33] Grills BL, Schuijers JA, Ward AR. Topical application of nerve growth factor improves fracture healing in rats. J Orthop Res 1997;15: 235-42.

[34] Paterson T, Moore S. The expression and characterization of five recombinant murine alpha 1-protease inhibitor proteins. Biochem Biophys Res Commun 1996;219: 64-9.
[35] Akbar MA, Cao JJ, Lu Y, Nardo D, Chen MJ, Elshikha AS, Ahamed R, Brantly M, Holliday LS, Song S. Alpha-1 Antitrypsin Gene Therapy Ameliorates Bone Loss in Ovariectomy-Induced Osteoporosis Mouse Model. Hum Gene Ther 2016.
[36] Mantila Roosa SM, Liu Y, Turner CH. Gene expression patterns in bone following mechanical loading. J Bone Miner Res 2011;26: 100-12.
[37] Paic F, Igwe JC, Nori R, Kronenberg MS, Franceschetti T, Harrington P, Kuo L, Shin DG, Rowe DW, Harris SE, Kalajzic I. Identification of differentially expressed genes between osteoblasts and osteocytes. Bone 2009;45: 682-92.
[38] Poulet B, Ulici V, Stone TC, Pead M, Gburcik V, Constantinou E, Palmer DB, Beier F, Timmons JA, Pitsillides AA. Time-series transcriptional profiling yields new perspectives on susceptibility to murine osteoarthritis. Arthritis Rheum 2012;64: 3256-66.
[39] Bassey EJ, Rothwell MC, Littlewood JJ, Pye DW. Pre- and postmenopausal women have different bone mineral density responses to the same high-impact exercise. J Bone Miner Res 1998;13: 1805-13.
[40] Desjardin C, Balliau T, Valot B, Zivy M, Wimel L, Guerin G, Cribiu E, Schibler L. A method for proteomic analysis of equine subchondral bone and epiphyseal cartilage. Proteomics 2012;12: 1870-4.
[41] Patel TK, Brodt MD, Silva MJ. Experimental and finite element analysis of strains induced by axial tibial compression in young-adult and old female C57Bl/6 mice. J Biomech 2014;47: 451-7.
[42] Rooney AMB, M.P.G.; Dempster, D.W.; Nieves, J.W.; Zhou, H.; Zion, M.; Roimisher, C.; Houle, Y.; Cosman, F. Tension increases teriparatide-induced bone formation more than compression in the human femoral neck. Trans 62nd Ortho Res Soc 2016;41: 40.
[43] Kalajzic I, Braut A, Guo D, Jiang X, Kronenberg MS, Mina M, Harris MA, Harris SE, Rowe DW. Dentin matrix protein 1 expression during osteoblastic differentiation, generation of an osteocyte GFP-transgene. Bone 2004;35: 74-82.
[44] Emmert-Buck MR, Bonner RF, Smith PD, Chuaqui RF, Zhuang Z, Goldstein SR, Weiss RA, Liotta LA. Laser capture microdissection. Science 1996;274: 998-1001.

[45] Tang F, Barbacioru C, Nordman E, Li B, Xu N, Bashkirov VI, Lao K, Surani MA. RNA-Seq analysis to capture the transcriptome landscape of a single cell. Nat Protoc 2010;5: 516-35.
[46] Rivadeneira F, Styrkarsdottir U, Estrada K, Halldorsson BV, Hsu YH, Richards JB, Zillikens MC, Kavvoura FK, Amin N, Aulchenko YS, Cupples LA, Deloukas P, Demissie S, Grundberg E, Hofman A, Kong A, Karasik D, van Meurs JB, Oostra B, Pastinen T, Pols HA, Sigurdsson G, Soranzo N, Thorleifsson G, Thorsteinsdottir U, Williams FM, Wilson SG, Zhou Y, Ralston SH, van Duijn CM, Spector T, Kiel DP, Stefansson K, Ioannidis JP, Uitterlinden AG, Genetic Factors for Osteoporosis C. Twenty bone-mineral-density loci identified by large-scale meta-analysis of genome-wide association studies. Nat Genet 2009;41: 1199-206.
[47] Styrkarsdottir U, Halldorsson BV, Gudbjartsson DF, Tang NL, Koh JM, Xiao SM, Kwok TC, Kim GS, Chan JC, Cherny S, Lee SH, Kwok A, Ho S, Gretarsdottir S, Kostic JP, Palsson ST, Sigurdsson G, Sham PC, Kim BJ, Kung AW, Kim SY, Woo J, Leung PC, Kong A, Thorsteinsdottir U, Stefansson K. European bone mineral density loci are also associated with BMD in East-Asian populations. PLoS One 2010;5: e13217.
[48] Banziger C, Soldini D, Schutt C, Zipperlen P, Hausmann G, Basler K. Wntless, a conserved membrane protein dedicated to the secretion of Wnt proteins from signaling cells. Cell 2006;125: 509-22.
[49] Fu J, Jiang M, Mirando AJ, Yu HM, Hsu W. Reciprocal regulation of Wnt and Gpr177/mouse Wntless is required for embryonic axis formation. Proc Natl Acad Sci U S A 2009;106: 18598-603.
[50] Zhong Z, Zylstra-Diegel CR, Schumacher CA, Baker JJ, Carpenter AC, Rao S, Yao W, Guan M, Helms JA, Lane NE, Lang RA, Williams BO. Wntless functions in mature osteoblasts to regulate bone mass. Proc Natl Acad Sci U S A 2012;109: E2197-204.
[51] Kamiya N, Ye L, Kobayashi T, Lucas DJ, Mochida Y, Yamauchi M, Kronenberg HM, Feng JQ, Mishina Y. Disruption of BMP signaling in osteoblasts through type IA receptor (BMPRIA) increases bone mass. J Bone Miner Res 2008;23: 2007-17.
[52] van den Heuvel M, Harryman-Samos C, Klingensmith J, Perrimon N, Nusse R. Mutations in the segment polarity genes wingless and porcupine impair secretion of the wingless protein. EMBO J 1993;12: 5293-302.
[53] Liu J, Pan S, Hsieh MH, Ng N, Sun F, Wang T, Kasibhatla S, Schuller AG, Li AG, Cheng D, Li J, Tompkins C, Pferdekamper A, Steffy A, Cheng J,

Kowal C, Phung V, Guo G, Wang Y, Graham MP, Flynn S, Brenner JC, Li C, Villarroel MC, Schultz PG, Wu X, McNamara P, Sellers WR, Petruzzelli L, Boral AL, Seidel HM, McLaughlin ME, Che J, Carey TE, Vanasse G, Harris JL. Targeting Wnt-driven cancer through the inhibition of Porcupine by LGK974. Proc Natl Acad Sci U S A 2013;110: 20224-9.

[54] Wang X, Moon J, Dodge ME, Pan X, Zhang L, Hanson JM, Tuladhar R, Ma Z, Shi H, Williams NS, Amatruda JF, Carroll TJ, Lum L, Chen C. The development of highly potent inhibitors for porcupine. J Med Chem 2013;56: 2700-4.

APPENDIX A. **CHAPTER 3 SUPPLEMENTARY FIGURES AND DATA**

TABLE OF CONTENTS

Table A.1 List of primers for genes verified with qPCR 160
Table A.2, Part I List of genes more highly expressed in control cancellous bone at 3 hours 162
Table A.2, Part II List of genes more highly expressed in control cortical bone at 3 hours 166
Table A.3, Part I: List of genes more highly expressed in control cancellous bone at 24 hours 172
Table A.3, Part II: List of genes more highly expressed in control cortical bone at 24 hours 174
Table A.4, Part I: List of genes upregulated 3 hours after a single loading session in cortical bone 190
Table A.4, Part II: List of genes downregulated 3 hours after a single loading session in cortical bone 192
Table A.5, Part I: List of genes upregulated 3 hours after a single loading session in cancellous bone .. 193
Table A.5, Part II: List of genes downregulated 3 hours after a single loading session in cancellous bone 194
Table A.6, Part I: List of genes upregulated 24 hours after a single loading session in cortical bone 195
Table A.6, Part II: List of genes downregulated 24 hours after a single loading session in cortical bone 197
Table A.7, Part I: List of genes upregulated 24 hours after a single loading session in cancellous bone 199
Table A.7, Part II: List of genes downregulated 24 hours after a single loading session in cancellous bone 200

Table A.1 List of primers for genes verified with qPCR.

Accession #	Gene Symbol	Gene Name	DE by Loading	DE in Ct vs Cn	Forward primer	Reverse Primer
NM_021279	Wnt1	wingless-type MMTV integration site family, member 1	3h Ct, 3h Cn, 24h Ct	N.S.	GATTTTGGTCGCCTCTTTGG	CGTGGCATTTGCACTCTTG
NM_011718	Wnt10b	wingless-type MMTV integration site family, member 10b	3h Ct, 24h Ct	Ct>Cn	GATCCTGCACCTGAACCG	TTAGAGCCCGACTGAACAAAG
NM_009528	Wnt7b	wingless-type MMTV integration site family, member 7b	3h Ct, 3h Cn	Ct>Cn	AATGAGGCGGGCAGAAAG	TGCGTTGTACTTCTCCTTGAG
NM_011198	Ptgs2	prostaglandin-endoperoxide synthase 2	3h Ct, 3h Cn, 24h Ct	N.S.	CTCACGAAGGAACTCAGCAC	GGATTGGAACAGCAAGGATTTG
NM_008973	Ptn	Pleiotrophin	24h Ct, 24h Cn	N.S.	AACTGTCACCATCTCCAAGC	TCTCCTGTTTCTTGCCTTCC
NM_024449	Sost	Sclerostin	3h Cn, 3h Ct	Ct>Cn	GAGAGAGCGTTTGTAACAGAAG	GGCTTTCAGTCTTTGTGGATG
NM_008764	Tnfrsf11b	tumor necrosis factor receptor superfamily member 11B	3h Ct, 3h Cn, 24h Ct	N.S.	GAGAGGATAAAACGGAGACACAG	CTGCTTTCACAGAGGTCAATG
NM_011593	Timp1	Tissue inhibitor of metalloproteinase 1	3h Ct, 3h Cn, 24h Cn	N.S.	CTCAAAGACCTATAGTGCTGGC	CAAAGTGACGGCTCTGGTAG
NM_053116	Wnt16	wingless-type MMTV integration site family, member 16	N.S.	Ct>Cn	CGAGAGGTGGAACTGTATGG	TGAATGCTGTCTCCTTGGTG
NM_010340	Gpr50	G-protein-coupled receptor 50	N.S.	Cn>Ct	GGAACTCCATGGTCATTTTGG	CATACAGCATCAAAGGGTAGGG
NM_011824	Grem1	Gremlin 1	N.S.	Cn>Ct	GCTCTCCTTCGTCTTCCTC	AGTGTATGCGGTGCGATTC
NM_198112	Ostn	Osteocrin	N.S.	Ct>Cn	GGACTGGAGATTGGCAAGTAC	CTTCTCTGGCTGTGGGTG

Gene accession numbers (column A), gene symbols (column B), gene names (column C), time points and tissue if gene was differentially expressed with loading (column D) or at baseline (column E), forward primer (column F) and reverse primer (column G). N.S.: not significant, Ct: cortical, Cn: cancellous.

Table A.2: A complete list of genes that were differentially expressed at 3 hours in cortical vs cancellous bone at baseline in order of decreasing fold change that were: I. more highly expressed in cancellous bone and II. More highly expressed in cortical bone. Number of genes (column A), gene symbols (column B), gene names (column C), fold change (column D), control cortical (Ct) fragments per kilobase per million reads (FPKM) (column E), control cancellous (Cn) FPKM (column F), false discovery rate (FDR) (column G). * indicates contamination as determined by Ayturk et al.

Table A.2, part I. List of genes more highly expressed in control Cancellous bone at 3 hours

	Gene Symbol	Gene	Fold Change	Control.Ct. fpkm	Control.Cn. fpkm	FDR
1	Gpr50	G-protein-coupled receptor 50	5.02	0.26	1.31	0.0001
2	Dclk3	doublecortin-like kinase 3	4.69	0.10	0.54	0.0009
3	Cyp2f2	cytochrome P450, family 2, subfamily f, polypeptide 2	3.80	0.53	3.03	0.0028
4	Havcr1	hepatitis A virus cellular receptor 1	3.52	0.22	0.84	0.0199
5	Cyp2b10	cytochrome P450, family 2, subfamily b, polypeptide 10	3.34	0.16	0.63	0.0306
6	Nlrp6	NLR family, pyrin domain containing 6	3.33	0.19	0.71	0.0016
7	Lypd6	LY6/PLAUR domain containing 6	3.03	0.19	0.68	0.0224
8	Fmo2	flavin containing monooxygenase 2	2.99	4.99	16.21	4.2E-10
9	Hhip	Hedgehog-interacting protein	2.91	0.70	2.02	0.0182
10	Gm1968	predicted gene 1968	2.83	0.85	2.65	0.0224
11	Efemp1	EGL nine homolog 3 (C. elegans)	2.62	2.11	6.02	4.4E-05
12	Tubb1	tubulin, beta 1	2.57	33.59	90.13	2.0E-12
13	Serpina3c	serine (or cysteine) peptidase inhibitor, clade A, member 3C	2.55	1.50	4.07	0.0017
14	Ccdc150	coiled-coil domain containing 150	2.49	0.35	0.96	0.0126
15	Grem1	gremlin 1	2.49	4.26	12.18	0.0007

Table A.2, Part I. Continued

	Gene Symbol	Gene	Fold Change	Control.Ct. fpkm	Control.Cn. fpkm	FDR
16	Cd226*	CD226 antigen	2.37	5.78	14.41	2.3E-06
17	Hal	histidine ammonia lyase	2.37	0.32	0.80	0.0147
18	Tesc	tescalcin; similar to Tescalcin	2.34	5.38	13.32	0.0027
19	Ppbp	pro-platelet basic protein	2.34	484.60	1169.65	1.9E-08
20	Ly6g6f	lymphocyte antigen 6 complex, locus G6F	2.32	8.11	20.73	3.3E-05
21	Gcsam	germinal center associated, signaling and motility	2.31	3.72	8.91	1.7E-09
22	Clec1b	C-type lectin domain family 1, member b	2.29	25.18	60.24	5.1E-07
23	F2rl2	coagulation factor II (thrombin) receptor-like 2	2.28	13.04	30.52	4.3E-11
24	Gp6	glycoprotein 6 (platelet)	2.27	9.09	21.90	2.3E-07
25	Adcyap1r1	adenylate cyclase activating polypeptide 1 receptor 1	2.27	0.26	0.70	0.0229
26	Treml1	triggering receptor expressed on myeloid cells-like 1	2.26	24.78	58.56	1.7E-06
27	Esm1	ets variant gene 4 (E1A enhancer binding protein, E1AF)	2.26	20.04	48.19	3.2E-06
28	Pf4	platelet factor 4	2.26	265.90	632.00	5.8E-09
29	Gp5	glycoprotein 5 (platelet)	2.25	18.45	44.06	1.5E-09
30	Clec4b2	C-type lectin domain family 4, member b2	2.24	1.49	3.33	0.0478
31	Slc24a5	solute carrier family 24, member 5	2.24	2.96	7.48	0.0010
32	Serpinb2	serine (or cysteine) peptidase inhibitor, clade B, member 2	2.23	3.16	7.29	6.0E-05
33	Itga2b	integrin alpha 2b	2.22	32.63	76.59	5.5E-09
34	Mmrn1	multimerin 1	2.20	9.31	21.20	1.7E-09
35	AU023871	expressed sequence AU023871	2.20	10.24	23.55	3.3E-10
36	Alox12	arachidonate 12-lipoxygenase	2.20	25.26	57.84	6.9E-09

Table A.2, Part I. Continued

	Gene Symbol	Gene	Fold Change	Control.Ct. fpkm	Control.Cn. fpkm	FDR
37	Gpm6a	glycoprotein m6a	2.20	4.67	10.06	1.9E-08
38	Cd5l	CD5 antigen-like	2.19	7.25	16.53	1.5E-06
39	Slamf1	signaling lymphocytic activation molecule family member 1	2.19	3.94	9.03	8.7E-06
40	Fcna	ficolin A	2.19	33.63	79.88	1.4E-07
41	Gp1ba	glycoprotein 1b, alpha polypeptide; hypothetical protein LOC100048807	2.17	13.10	29.30	2.8E-09
42	Kcnj5	potassium inwardly-rectifying channel, subfamily J, member 5	2.17	2.67	6.09	3.9E-07
43	Vwf	Von Willebrand factor homolog	2.16	8.79	20.07	1.9E-08
44	Cass4	Cas scaffolding protein family member 4	2.16	1.83	4.21	1.9E-05
45	Gp9*	glycoprotein 9 (platelet)	2.16	32.87	74.68	9.0E-05
46	Slc6a4	solute carrier family 6 (neurotransmitter transporter, serotonin), member 4	2.15	8.94	20.05	1.5E-07
47	Mpl	myeloproliferative leukemia virus oncogene	2.15	8.13	18.09	3.8E-08
48	Ttll11	tubulin tyrosine ligase-like family, member 11	2.15	1.39	3.07	0.0005
49	Kcna2	potassium voltage-gated channel, shaker-related subfamily, member 2	2.15	0.54	1.20	0.0003
50	Ptger3	prostaglandin E receptor 3 (subtype EP3)	2.15	1.22	2.62	0.0098
51	Tmem151b	transmembrane protein 151B	2.14	0.41	0.87	0.0288
52	Adipoq	adiponectin, C1Q and collagen domain containing	2.13	67.20	152.58	5.9E-08
53	Il1a	interleukin 1 alpha	2.13	2.47	5.33	0.0038

Table A.2, Part I. Continued

	Gene Symbol	Gene	Fold Change	Control.Ct. fpkm	Control.Cn. fpkm	FDR
54	2410076I21Rik	RIKEN cDNA 2410076I21 gene	2.12	2.97	6.42	0.0106
55	P2rx1	purinergic receptor P2X, ligand-gated ion channel, 1	2.12	8.49	18.78	1.8E-08
56	Prkcq*	protein kinase C, theta	2.11	4.95	10.73	2.1E-08
57	Sele	selectin, endothelial cell	2.11	3.23	6.90	1.5E-08
58	C4b	complement component 4B (Childo blood group)	2.10	9.10	20.03	1.3E-06
59	Serpina3b	serine (or cysteine) peptidase inhibitor, clade A, member 3B	2.09	1.98	4.40	0.0074
60	Mrvi1	MRV integration site 1	2.08	7.64	16.49	6.4E-11
61	Ubd	ubiquitin D	2.07	4.64	9.77	0.0178
62	Clca1	chloride channel calcium activated 1	2.06	6.52	13.55	1.2E-07
63	BC147527	cDNA sequence BC147527	2.05	2.27	4.73	0.0049
64	Plek	pleckstrin	2.05	59.47	124.43	6.3E-08
65	Sntb1	syntrophin, basic 1	2.04	1.72	3.82	0.0207
66	Kng2	kininogen 2	2.04	10.49	22.07	1.2E-07
67	Ubash3a	ubiquitin associated and SH3 domain containing, A	2.00	2.36	4.84	6.2E-06
68	Hpse	heparanase	2.00	5.69	11.67	7.7E-07

Table A.2, Part II. List of genes more highly expressed in control Cortical bone at 3 hours

	Gene Symbol	Gene	Fold Change	Control.Ct. fpkm	Control.Cn. fpkm	FDR
1	Ostn	osteocrin	29.49	9.82	0.37	3.3E-16
2	Myh4*	myosin, heavy polypeptide 4, skeletal muscle	16.15	4.55	0.27	0.0120
3	Itgbl1	integrin, beta-like 1	12.27	6.10	0.69	3.3E-05
4	Wnt16	wingless-related MMTV integration site 16	11.76	2.55	0.27	0.0001
5	Tnn	tenascin N	7.78	30.23	5.39	1.1E-05
6	Angptl7	angiopoietin-like 7	7.77	3.11	0.36	0.0098
7	Col3a1	collagen, type III, alpha 1	7.11	355.74	65.55	6.3E-06
8	Aspn	asporin	7.08	56.72	9.28	1.4E-07
9	Igfbp6	insulin-like growth factor binding protein 6	6.82	4.40	0.76	0.0002
10	Wnt7b	wingless-related MMTV integration site 7B	6.62	0.89	0.16	8.7E-06
11	Col8a2	collagen, type VIII, alpha 2	6.50	5.00	1.06	0.0014
12	Cilp2	cartilage intermediate layer protein 2	6.29	1.38	0.25	0.0023
13	Krt75	keratin 75	6.10	0.28	0.04	0.0120
14	Prrx2	paired related homeobox 2	5.84	3.09	0.65	0.0003
15	Tbx4	T-box 4	5.82	0.57	0.10	0.0002
16	Meox2	mesenchyme homeobox 2	5.81	0.98	0.16	0.0001
17	Cdh6	cadherin 6	5.60	0.34	0.06	0.0087
18	Dpysl4	dihydropyrimidinase-like 4	5.39	0.48	0.07	0.0010
19	Lrrc15	leucine rich repeat containing 15	5.21	5.51	1.21	1.1E-07
20	Olfr78	olfactory receptor 78	5.10	0.39	0.09	0.0029
21	Lrrn1	leucine rich repeat protein 1, neuronal	4.94	0.68	0.15	0.0003
22	Mfap4	microfibrillar-associated protein 4	4.47	1.23	0.33	0.0109

Table A.2, Part II. Continued

	Gene Symbol	Gene	Fold Change	Control.Ct. fpkm	Control.Cn. fpkm	FDR
23	Spock1	sparc/osteonectin, cwcv and kazal-like domains proteoglycan 1	4.26	1.07	0.25	0.0082
24	Foxp2	forkhead box P2	4.17	0.88	0.22	2.4E-05
25	Rgs11	regulator of G-protein signaling 11	4.17	0.66	0.14	0.0440
26	Nov	nephroblastoma overexpressed gene	3.77	0.91	0.24	0.0102
27	Slc6a17	solute carrier family 6 (neurotransmitter transporter), member 17	3.66	0.22	0.06	0.0150
28	Sost	sclerostin	3.65	351.06	101.32	1.3E-09
29	Ptn	pleiotrophin	3.65	8.73	2.93	0.0003
30	1810041L15 Rik	RIKEN cDNA 1810041L15 gene	3.54	0.39	0.14	0.0197
31	A330021E22 Rik	RIKEN cDNA A330021E22 gene	3.50	0.41	0.12	0.0237
32	Plekhg4	pleckstrin homology domain containing, family G (with RhoGef domain) member 4	3.26	2.42	0.73	1.2E-06
33	Epha3	Eph receptor B3	3.23	3.93	1.21	5.9E-12
34	Asic3	acid-sensing (proton-gated) ion channel 3	3.20	5.68	1.86	1.2E-06
35	Chst8	carbohydrate (N-acetylgalactosamine 4-0) sulfotransferase 8	3.18	0.61	0.20	0.0358
36	Adamtsl5	ADAMTS-like 5	3.16	2.18	0.62	4.8E-05
37	Gcnt4	glucosaminyl (N-acetyl) transferase 4, core 2 (beta-1,6-N-acetylglucosaminyltransferase)	3.15	0.61	0.20	0.0005
38	Postn	periostin, osteoblast specific factor	3.11	364.74	124.58	3.1E-08
39	Col16a1	collagen, type XVI, alpha 1	2.92	38.12	13.22	1.0E-11
40	Dpt	dermatopontin	2.90	1.64	0.56	0.0159
41	Galr2	galanin receptor 2	2.88	3.30	1.17	8.7E-06

Table A.2, Part II. Continued

	Gene Symbol	Gene	Fold Change	Control.Ct. fpkm	Control.Cn. fpkm	FDR
42	P4ha3	procollagen-proline, 2-oxoglutarate 4-dioxygenase (proline 4-hydroxylase), alpha polypeptide III	2.86	5.21	1.88	0.0001
43	Slc17a8	solute carrier family 17 (sodium-dependent inorganic phosphate cotransporter), member 8	2.82	0.27	0.10	0.0499
44	Htra4	HtrA serine peptidase 4	2.82	2.75	1.05	0.0002
45	Gm10635	predicted gene 10635	2.81	0.44	0.16	0.0235
46	Akr1c18	aldo-keto reductase family 1, member C18	2.81	1.30	0.48	0.0452
47	Piwil2	piwi-like homolog 2 (Drosophila)	2.81	0.53	0.18	0.0117
48	Lrrc8e	leucine rich repeat containing 8 family, member E	2.80	0.36	0.13	0.0237
49	Car11	carbonic anhydrase 11	2.71	2.57	1.00	0.0326
50	Fmod	fibromodulin	2.68	92.51	48.37	0.0190
51	Meox1	mesenchyme homeobox 1	2.63	2.26	0.86	0.0022
52	Apln	apelin	2.52	3.07	1.25	4.1E-06
53	Ccdc3	coiled-coil domain containing 3	2.51	19.49	8.08	7.3E-09
54	Mmp12	matrix metallopeptidase 12	2.51	0.44	0.19	0.0454
55	Kcnab1	potassium voltage-gated channel, shaker-related subfamily, beta member 1	2.50	1.23	0.50	0.0051
56	Tenm3	teneurin transmembrane protein 3	2.50	1.43	0.58	0.0227
57	Adamtsl1	ADAMTS-like 1	2.50	0.70	0.28	0.0001
58	Plat	plasminogen activator, tissue	2.46	5.67	2.91	0.0026
59	Prtg	protogenin homolog (Gallus gallus)	2.45	0.47	0.18	0.0161

Table A.2, Part II. Continued

	Gene Symbol	Gene	Fold Change	Control.Ct. fpkm	Control.Cn. fpkm	FDR
60	Grip2	glutamate receptor interacting protein 2	2.44	1.98	0.83	0.0309
61	F3	coagulation factor III	2.43	4.96	2.09	0.0005
62	Megf6	multiple EGF-like-domains 6	2.43	0.80	0.34	0.0013
63	Tgfb2	transforming growth factor, beta 2	2.42	8.04	3.62	8.3E-06
64	Adamtsl2	ADAMTS-like 2	2.39	6.69	3.25	0.0038
65	Ebf4	enoyl Coenzyme A hydratase domain containing 2	2.36	1.40	0.58	0.0159
66	Thbs2	thrombospondin 2	2.34	38.95	17.37	5.8E-08
67	Aebp1	AE binding protein 1	2.33	26.29	11.63	9.9E-09
68	Wnt10b	wingless related MMTV integration site 10b	2.33	8.27	3.51	0.0030
69	Col12a1	collagen, type XII, alpha 1	2.29	87.73	39.98	4.5E-05
70	C1qtnf5	C1q and tumor necrosis factor related protein 5; membrane-type frizzled-related protein	2.28	19.35	8.66	8.5E-07
71	Spock2	sparc/osteonectin, cwcv and kazal-like domains proteoglycan 2	2.28	2.51	1.13	0.0006
72	Tnmd	tenomodulin	2.26	2.40	1.11	0.0330
73	Egr3	elastase 2, neutrophil	2.26	9.41	4.15	0.0005
74	Fcrls	Fc receptor-like S, scavenger receptor	2.26	6.12	2.89	0.0027
75	Epcam	Eph receptor A3	2.25	7.63	3.63	0.0002
76	Glt8d2	glycosyltransferase 8 domain containing 2	2.24	2.08	0.90	0.0325
77	Tppp3	tubulin polymerization-promoting protein family member 3	2.23	5.98	2.76	0.0076
78	Fam69c	RIKEN cDNA B230399E16 gene	2.23	1.58	0.69	0.0430
79	Scn2b	sodium channel, voltage-gated, type II, beta	2.23	0.52	0.22	0.0419
80	Mustn1	musculoskeletal, embryonic nuclear protein 1	2.21	9.81	4.64	0.0074

Table A.2, Part II. Continued

	Gene Symbol	Gene	Fold Change	Control.Ct. fpkm	Control.Cn. fpkm	FDR
81	Etv4	ets variant 4	2.20	1.38	0.61	0.0106
82	Nmnat2	nicotinamide nucleotide adenylyltransferase 2	2.20	2.29	1.16	0.0181
83	AU015836	expressed sequence AU015836	2.18	1.64	0.76	0.0230
84	Arc	activity regulated cytoskeletal-associated protein	2.18	2.48	1.20	0.0065
85	Tg	thyroglobulin	2.15	6.20	3.05	0.0001
86	Shroom1	shroom family member 1	2.15	0.85	0.41	0.0335
87	Cpeb1	cytoplasmic polyadenylation element binding protein 1	2.14	4.59	2.18	0.0252
88	Asap3	ArfGAP with SH3 domain, ankyrin repeat and PH domain 3	2.12	1.52	0.74	0.0076
89	Cys1	cystin 1	2.12	2.88	1.39	0.0412
90	Wfdc1*	WAP four-disulfide core domain 1	2.11	5.95	2.97	0.0082
91	Ccdc68	coiled-coil domain containing 68	2.11	5.10	2.52	0.0007
92	Gpc3	glypican 3	2.10	1.73	0.86	0.0337
93	Pcdhga12	protocadherin gamma subfamily A, 12	2.10	0.87	0.39	0.0468
94	Lum	lumican	2.09	748.03	381.13	0.0010
95	Celf5	bruno-like 5, RNA binding protein (Drosophila)	2.09	1.27	0.62	0.0174
96	Itm2a	integral membrane protein 2A	2.08	36.55	18.11	0.0002
97	Anxa8	annexin A8	2.08	31.39	17.50	0.0048
98	Gabra3	gamma-aminobutyric acid (GABA) A receptor, subunit alpha 3	2.07	0.75	0.36	0.0288
99	Lrrc17	leucine rich repeat containing 17	2.06	9.09	4.47	8.5E-07
100	Prss23	protease, serine, 23	2.06	13.10	6.43	9.8E-07

Table A.2, Part II. Continued

	Gene Symbol	Gene	Fold Change	Control.Ct. fpkm	Control.Cn. fpkm	FDR
101	Edn1	epidermal growth factor-containing fibulin-like extracellular matrix protein 1	2.04	1.25	0.63	0.0479
102	Angptl2	angiopoietin-like 2	2.03	28.30	14.86	0.0005
103	Echdc2	endothelin 1	2.02	6.53	3.32	0.0282
104	Tnfaip6	similar to TNF-stimulated gene 6 protein; tumor necrosis factor alpha induced protein 6	2.01	5.23	2.61	0.0019
105	Dkk3	dickkopf homolog 3 (Xenopus laevis)	2.01	18.28	9.33	0.0001
106	Sybu	syntabulin (syntaxin-interacting)	2.01	4.98	2.59	0.0062
107	Miat	myocardial infarction associated transcript (non-protein coding)	2.00	1.07	0.56	0.0120
108	Nbl1	neuroblastoma, suppression of tumorigenicity 1	2.00	85.84	46.25	0.0019
109	Mepe	matrix extracellular phosphoglycoprotein with ASARM motif (bone)	2.00	587.96	296.94	3.8E-09
110	Serpine1	serine (or cysteine) peptidase inhibitor, clade E, member 1	2.00	12.70	7.11	0.0009

total	178
*indicates contaminant	5
total without contaminants	173

Table A.3: A complete list of genes that were differentially expressed at 24 hours in cortical vs cancellous bone at baseline in order of decreasing fold change that were: I. more highly expressed in cancellous bone and II. More highly expressed in cortical bone. Number of genes (column A), gene symbols (column B), gene names (column C), fold change (column D), control cortical (Ct) fragments per kilobase per million reads (FPKM) (column E), control cancellous (Cn) FPKM (column F), false discovery rate (FDR) (column G). * indicates contamination as determined by Ayturk et al.

Table A.3, Part I. List of genes more highly expressed in control cancellous bone at 24 hours

	Gene Symbol	Gene	Fold Change	Control.Ct. fpkm	Control.Cn. fpkm	FDR
1	Apoo-ps	apolipoprotein O, pseudogene	42.97	1.53E-04	1.20	0.0020
2	Epha8	Eph receptor A8	3.72	0.08	0.32	0.0230
3	Gpr50	G-protein-coupled receptor 50	3.35	0.23	0.82	0.0467
4	Cbln1	cerebellin 1 precursor protein; similar to precerebellin-1	3.29	0.17	0.64	0.0459
5	H2-L	histocompatibility 2, D region; histocompatibility 2, D region locus 1	3.29	4.79	15.61	6.2E-06
6	Ltb4r2	leukotriene B4 receptor 2	3.02	0.35	1.03	0.0094
7	Grem1	gremlin 1	2.74	3.66	10.29	4.2E-08
8	Klrc1	killer cell lectin-like receptor subfamily C, member 1	2.68	0.65	2.07	0.0370
9	Abcc2	ATP-binding cassette, sub-family C (CFTR/MRP), member 2	2.55	0.11	0.32	0.0184
10	Xylt1	xylosyltransferase 1	2.53	2.92	7.51	0.0334
11	Akap5	A kinase (PRKA) anchor protein 5	2.48	0.49	1.22	0.0007
12	Klk1	kallikrein 1	2.48	1.49	3.87	0.0181
13	Htr2a	5-hydroxytryptamine (serotonin) receptor 2A	2.45	0.53	1.37	0.0009

Table A.3, Part I. Continued

	Gene Symbol	Gene	Fold Change	Control.Ct. fpkm	Control.Cn. fpkm	FDR
14	Sele	selectin, endothelial cell	2.40	2.55	6.46	0.0011
15	Pkd1l3	polycystic kidney disease 1 like 3	2.37	0.81	1.96	0.0034
16	Plin1	perilipin	2.36	1.24	2.76	0.0057
17	Esm1	endothelial cell-specific molecule 1	2.33	21.71	51.71	3.5E-05
18	Gpm6a	glycoprotein m6a	2.32	4.08	9.72	0.0004
19	Nlrp6	NLR family, pyrin domain containing 6	2.27	0.36	0.84	0.0174
20	Lipg	lipase, endothelial	2.26	1.69	3.85	2.7E-05
21	Cd226*	CD226 antigen	2.22	6.46	14.25	0.0020
22	Gpr128	G protein-coupled receptor 128	2.22	0.41	0.95	0.0136
23	Kcna2	potassium voltage-gated channel, shaker-related subfamily, member 2	2.21	0.49	1.14	0.0007
24	Chl1	cell adhesion molecule with homology to L1CAM	2.21	0.50	1.12	4.3E-05
25	Pde3a	phosphodiesterase 3A, cGMP inhibited	2.20	2.23	5.01	0.0006
26	Kcnj5	potassium inwardly-rectifying channel, subfamily J, member 5	2.19	2.81	6.22	0.0011
27	Gm13139	predicted gene 13139	2.16	1.02	2.35	0.0010
28	Gp6	glycoprotein 6 (platelet)	2.13	10.81	23.03	0.0013
29	Mmrn1	multimerin 1	2.11	10.36	21.90	0.0004
30	Tubb1	tubulin, beta 1	2.10	43.36	91.24	0.0016
31	Kng1	kininogen 1	2.10	8.76	19.12	0.0002
32	Ptch1	patched homolog 1	2.09	7.47	15.40	0.0439
33	Plin4*	plasma membrane associated protein, S3-12	2.09	1.23	2.99	0.0336
34	Cass4	Cas scaffolding protein family member 4	2.07	2.27	4.77	0.0046
35	Pls1	plastin 1 (I-isoform)	2.06	3.69	7.53	0.0026

Table A.3, Part I. Continued

	Gene Symbol	Gene	Fold Change	Control.Ct. fpkm	Control.Cn. fpkm	FDR
36	C4b	complement component 4B (Chido blood group)	2.04	11.80	24.26	3.9E-07
37	Ccr9	chemokine (C-C motif) receptor 9	2.04	0.63	1.41	0.0145
38	Slc24a5	solute carrier family 24, member 5	2.02	3.33	6.83	0.0005
39	Mpl	myeloproliferative leukemia virus oncogene	2.00	9.51	18.97	0.0021
36	C4b	complement component 4B (Chido blood group)	2.04	11.80	24.26	3.9E-07
37	Ccr9	chemokine (C-C motif) receptor 9	2.04	0.63	1.41	0.0145
38	Slc24a5	solute carrier family 24, member 5	2.02	3.33	6.83	0.0005
39	Mpl	myeloproliferative leukemia virus oncogene	2.00	9.51	18.97	0.0021

Table A.3, Part II. List of genes more highly expressed in control Cortical bone at 24 hours

	Gene Symbol	Gene	Fold Change	Control.Ct. fpkm	Control.Cn. fpkm	FDR
1	ChkbCpt1b	Chkb-Cpt1b readthrough transcript (NMD candidate)	618.04	1.23	9.64E-05	7.0E-19
2	Ccl21a	chemokine (C-C motif) ligand 21A; predicted gene 1987	198.86	2.18	0.00	0.0002
3	Myoc	myocilin	134.79	5.56	0.05	2.5E-06
4	Cilp	cartilage intermediate layer protein, nucleotide pyrophosphohydrolase	72.50	8.23	0.13	1.6E-09
5	Mfap4	microfibrillar-associated protein 4	64.72	3.89	0.06	7.5E-09
6	Itgbl1	integrin, beta-like 1	57.04	9.66	0.17	3.7E-09
7	Igfbp6	insulin-like growth factor binding protein 6	56.47	16.46	0.25	2.9E-11

Table A.3, Part II. Continued

	Gene Symbol	Gene	Fold Change	Control.Ct. fpkm	Control.Cn. fpkm	FDR
8	Ostn	osteocrin	51.79	13.52	0.29	7.0E-19
9	Wnt16	wingless-related MMTV integration site 16	42.82	3.18	0.09	8.4E-07
10	Chodl	chondrolectin	40.32	0.58	0.01	2.9E-05
11	Mybpc1*	myosin binding protein C, slow-type	37.16	8.85	0.30	3.9E-05
12	Myh2*	myosin, heavy polypeptide 2, skeletal muscle, adult	31.68	5.29	0.17	1.8E-14
13	Mb*	myoglobin	31.11	95.69	3.54	6.7E-05
14	Angptl7	angiopoietin-like 7	29.70	10.19	0.28	7.4E-09
15	Myh1*	myosin, heavy polypeptide 1, skeletal muscle, adult	28.67	18.67	0.84	0.0066
16	Meox2	mesenchyme homeobox 2	25.81	1.51	0.06	1.0E-11
17	Thbs4	thrombospondin 4	22.40	24.21	1.02	1.0E-10
18	Tnxb	tenascin XB	19.83	0.95	0.04	1.5E-07
19	Cilp2	cartilage intermediate layer protein 2	18.88	5.89	0.50	1.5E-05
20	Smtnl1*	smoothelin-like 1	17.26	1.83	0.11	0.0020
21	Tpsb2	tryptase beta 2	17.05	1.01	0.05	2.0E-05
22	Actn2*	actinin alpha 2	14.86	3.52	0.24	6.2E-06
23	Aspn	asporin	14.62	62.09	4.03	1.7E-12
24	Col8a2	collagen, type VIII, alpha 2	14.20	10.48	0.80	6.2E-06
25	Slc17a8	solute carrier family 17 (sodium-dependent inorganic phosphate cotransporter), member 8	13.86	0.23	0.01	2.0E-05
26	Mylk2*	myosin, light polypeptide kinase 2, skeletal muscle	13.53	7.51	1.35	0.0090

Table A.3, Part II. Continued

	Gene Symbol	Gene	Fold Change	Control.Ct. fpkm	Control.Cn. fpkm	FDR
27	Lrrn1	leucine rich repeat protein 1, neuronal	12.50	0.74	0.06	0.0001
28	Ckmt2*	creatine kinase, mitochondrial 2	11.84	8.25	1.22	0.0021
29	Smpx*	small muscle protein, X-linked	11.78	8.54	1.41	0.0054
30	Tnn	tenascin N	11.19	19.25	1.75	1.5E-40
31	Tbx4	T-box 4	11.15	0.61	0.05	1.7E-08
32	Lmod2*	leiomodin 2 (cardiac)	11.08	2.01	0.16	3.3E-06
33	Apobec2*	apolipoprotein B mRNA editing enzyme, catalytic polypeptide 2	10.59	14.37	1.93	0.0023
34	Col3a1	collagen, type III, alpha 1	10.46	316.67	29.37	1.8E-13
35	Pgm5	phosphoglucomutase 5	10.31	0.47	0.05	3.4E-08
36	Prg4	proteoglycan 4 (megakaryocyte stimulating factor, articular superficial zone protein)	10.17	8.78	1.14	7.5E-05
37	Ankrd1	ankyrin repeat domain 1 (cardiac muscle)	9.68	1.03	0.13	0.0001
38	Asb15*	ankyrin repeat and SOCS box-containing 15	9.66	0.35	0.03	0.0019
39	Hhatl*	hedgehog acyltransferase-like	9.49	1.35	0.23	0.0101
40	Fitm1*	fat storage-inducing transmembrane protein 1	9.38	5.39	0.76	0.0038
41	Rgs11	regulator of G-protein signaling 11	9.32	1.14	0.10	3.6E-07
42	Tigd4	tigger transposable element derived 4	9.04	0.80	0.08	0.0005
43	Myl2*	myosin, light polypeptide 2, regulatory, cardiac, slow	8.71	5.07	0.59	1.1E-06
44	C1qtnf9	C1q and tumor necrosis factor related protein 9	8.61	1.38	0.15	1.3E-08
45	Nov	nephroblastoma overexpressed gene	8.57	2.05	0.26	6.0E-07
46	Duoxa1	dual oxidase maturation factor 1	8.50	1.03	0.11	5.6E-06

Table A.3, Part II. Continued

	Gene Symbol	Gene	Fold Change	Control.Ct. fpkm	Control.Cn. fpkm	FDR
47	Prrx2	paired related homeobox 2	7.94	6.12	0.84	7.2E-05
48	Trim54*	tripartite motif-containing 54	7.81	4.19	0.78	0.0500
49	Eef1a2*	eukaryotic translation elongation factor 1 alpha 2	7.73	8.44	1.94	0.0425
50	Kcnc4*	potassium voltage gated channel, Shaw-related subfamily, member 4	7.64	1.17	0.24	0.0309
51	1810041L15Rik	RIKEN cDNA 1810041L15 gene	7.52	0.70	0.09	0.0090
52	Chst8	carbohydrate (N-acetylgalactosamine 4-0) sulfotransferase 8	7.47	0.95	0.12	1.6E-07
53	Nrap*	nebulin-related anchoring protein	7.21	4.23	0.96	0.0019
54	Sypl2*	synaptophysin-like 2	7.20	2.03	0.62	0.0324
55	Ano5*	anoctamin 5	7.07	0.69	0.20	0.0301
56	Sgcg*	sarcoglycan, gamma (dystrophin-associated glycoprotein)	6.91	1.39	0.27	0.0129
57	Csrp3	cysteine and glycine-rich protein 3	6.54	3.41	0.49	0.0007
58	Myoz2*	myozenin 2	6.50	2.88	0.40	0.0020
59	Des*	desmin	6.46	35.50	7.93	0.0042
60	Rpl3l*	ribosomal protein L3-like	6.40	8.78	1.56	0.0022
61	Dhrs7c*	dehydrogenase/reductase (SDR family) member 7C	6.22	3.79	0.98	0.0143
62	Myoz3*	myozenin 3	6.20	1.08	0.28	0.0312
63	Cox8b*	cytochrome c oxidase, subunit VIIIb	6.13	61.42	10.40	0.0079
64	Snhg11	small nucleolar RNA host gene 11 (non-protein coding)	6.11	0.58	0.10	0.0001
65	Ampd1*	adenosine monophosphate deaminase 1 (isoform M)	6.11	4.97	2.17	0.0269

Table A.3, Part II. Continued

	Gene Symbol	Gene	Fold Change	Control.Ct. fpkm	Control.Cn. fpkm	FDR
66	C1qtnf2	C1q and tumor necrosis factor related protein 2	6.10	2.07	0.31	5.7E-06
67	Ugt1a6b	UDP glucuronosyltransferase 1 family, polypeptide A6B	6.04	3.02	0.68	0.0236
68	Murc*	muscle-related coiled-coil protein	6.02	2.00	0.40	0.0106
69	Kcna7*	potassium voltage-gated channel, shaker-related subfamily, member 7	5.89	1.02	0.22	0.0083
70	Cox7a1*	cytochrome c oxidase, subunit VIIa 1	5.88	58.14	9.46	0.0002
71	Ldb3*	LIM domain binding 3	5.81	17.15	4.57	0.0269
72	Adamts8	a disintegrin-like and metallopeptidase (reprolysin type) with thrombospondin type 1 motif, 8	5.72	0.19	0.03	0.0155
73	Cacna1s*	calcium channel, voltage-dependent, L type, alpha 1S subunit	5.59	2.93	0.79	0.0108
74	Neb*	nebulin	5.52	3.33	1.02	0.0305
75	Me3	malic enzyme 3, NADP(+)-dependent, mitochondrial	5.45	0.74	0.13	3.9E-06
76	Xirp1*	xin actin-binding repeat containing 1	5.42	0.41	0.08	0.0087
77	Jsrp1*	junctional sarcoplasmic reticulum protein 1	5.40	6.87	1.73	0.0411
78	Htra4	HtrA serine peptidase 4	5.39	4.25	0.80	1.3E-10
79	Dusp26	dual specificity phosphatase 26 (putative)	5.32	1.19	0.20	0.0077
80	Scn4b*	sodium channel, type IV, beta	5.32	2.04	0.46	0.0098
81	Klhl41	kelch-like 41	5.30	5.70	1.41	0.0111
82	Cacng1*	calcium channel, voltage-dependent, gamma subunit 1	5.20	5.70	1.44	0.0163
83	Sel1l3*	RIKEN cDNA 2310045A20 gene	5.14	0.60	0.14	0.0118
84	Lrrc15	leucine rich repeat containing 15	5.01	4.69	0.90	1.5E-13

Table A.3, Part II. Continued

	Gene Symbol	Gene	Fold Change	Control.Ct. fpkm	Control.Cn. fpkm	FDR
85	Spock1	sparc/osteonectin, cwcv and kazal-like domains proteoglycan 1	4.99	0.61	0.12	0.0010
86	Chrna10	cholinergic receptor, nicotinic, alpha polypeptide 10	4.84	0.70	0.15	0.0006
87	Dpt	dermatopontin	4.77	2.94	0.60	0.0001
88	Clcn1*	chloride channel 1	4.68	0.52	0.14	0.0411
89	Mfap5	microfibrillar associated protein 5	4.64	0.99	0.21	0.0198
90	Dpysl4	dihydropyrimidinase-like 4	4.61	0.51	0.10	0.0055
91	Meg3	maternally expressed 3	4.58	3.70	0.78	3.5E-05
92	2310002L09Rik*	RIKEN cDNA 2310002L09 gene	4.53	1.82	0.51	0.0394
93	Tnmd	tenomodulin	4.52	3.45	0.74	1.4E-05
94	H19*	H19 fetal liver mRNA	4.50	9.36	3.07	0.0157
95	Hspb8*	heat shock protein 8	4.44	6.96	1.64	0.0007
96	Trim72*	tripartite motif-containing 72	4.38	2.18	0.50	0.0013
97	Pgam2*	phosphoglycerate mutase 2	4.35	39.56	13.10	0.0275
98	Kcnj11	potassium inwardly rectifying channel, subfamily J, member 11	4.35	1.41	0.34	0.0064
99	Hspb7*	heat shock protein family, member 7 (cardiovascular)	4.34	5.63	1.27	9.1E-06
100	Foxp2	forkhead box P2	4.33	0.70	0.17	3.6E-06
101	Ttn*	titin	4.32	1.56	0.56	0.0249
102	Bnc2	basonuclin 2	4.28	0.21	0.05	0.0251
103	Megf6	multiple EGF-like-domains 6	4.26	1.53	0.35	2.7E-06

Table A.3, Part II. Continued

	Gene Symbol	Gene	Fold Change	Control.Ct. fpkm	Control.Cn. fpkm	FDR
104	3425401B19Rik*	RIKEN cDNA 3425401B19 gene	4.18	1.42	0.43	0.0080
105	Plekhg4	pleckstrin homology domain containing, family G (with RhoGef domain) member 4	4.17	3.17	0.73	4.6E-15
106	Tppp3	tubulin polymerization-promoting protein family member 3	4.17	13.35	3.04	1.1E-06
107	Apod	apolipoprotein D	4.15	4.35	1.07	0.0020
108	Pdlim3*	PDZ and LIM domain 3	4.09	6.71	2.44	0.0283
109	Coch	coagulation factor C homolog (Limulus polyphemus)	4.09	0.44	0.09	0.0114
110	Obscn*	obscurin, cytoskeletal calmodulin and titin-interacting RhoGEF	4.06	1.12	0.31	0.0062
111	Rnf207	ring finger protein 207	3.93	0.47	0.11	0.0047
112	Ephx3	epoxide hydrolase 3	3.88	0.43	0.11	0.0048
113	Sost	sclerostin	3.85	376.71	99.15	1.3E-16
114	Trnp1	TMF1-regulated nuclear protein 1	3.74	3.17	0.80	1.7E-06
115	Mustn1	musculoskeletal, embryonic nuclear protein 1	3.73	16.43	4.38	2.9E-13
116	Higd1b	HIG1 domain family, member 1B	3.71	3.37	0.79	0.0105
117	Wnt7b	wingless-related MMTV integration site 7B	3.71	0.54	0.14	0.0012
118	2900041M22Rik	RIKEN cDNA 2900041M22 gene	3.67	0.99	0.26	0.0036
119	Fndc5*	fibronectin type III domain containing 5	3.66	0.86	0.24	0.0396
120	Txlnb*	taxilin beta	3.66	2.61	0.82	0.0034
121	Ptn	pleiotrophin	3.66	6.05	1.66	2.4E-07
122	Rtn2*	reticulon 2 (Z-band associated protein)	3.63	21.81	6.52	0.0056
123	Ryr1*	ryanodine receptor 1, skeletal muscle	3.63	2.68	0.87	0.0400

Table A.3, Part II. Continued

	Gene Symbol	Gene	Fold Change	Control.Ct. fpkm	Control.Cn. fpkm	FDR
124	Olfr78	olfactory receptor 78	3.61	0.49	0.14	0.0326
125	Ankrd23*	ankyrin repeat domain 23	3.61	28.51	9.06	0.0276
126	Sh3bgr*	SH3-binding domain glutamic acid-rich protein	3.60	9.91	3.32	0.0482
127	Adamtsl5	ADAMTS-like 5	3.59	2.60	0.74	3.7E-06
128	Rps27	ribosomal protein S27	3.59	37.74	3.34	0.0309
129	Epcam	epithelial cell adhesion molecule	3.55	10.24	2.90	9.1E-10
130	Prss23	protease, serine, 23	3.54	14.98	4.14	4.0E-16
131	Alpk3*	alpha-kinase 3	3.50	0.93	0.25	0.0004
132	9130019P16Rik	RIKEN cDNA 9130019P16 gene	3.45	1.53	0.44	2.6E-09
133	Pkia*	protein kinase inhibitor, alpha	3.43	3.79	1.51	0.0220
134	Asic3	acid-sensing (proton-gated) ion channel 3	3.43	5.70	1.60	3.7E-09
135	Atp1a2*	ATPase, Na+/K+ transporting, alpha 2 polypeptide	3.39	5.46	1.62	0.0177
136	Wnt9a	wingless-type MMTV integration site 9A	3.36	0.66	0.20	0.0008
137	C130021I20Rik	Riken cDNA C130021I20 gene	3.36	0.49	0.15	0.0023
138	Wnk2	WNK lysine deficient protein kinase 2	3.34	0.46	0.15	0.0047
139	Trpm6	transient receptor potential cation channel, subfamily M, member 6	3.34	0.24	0.07	0.0089
140	Rab15	RAB15, member RAS oncogene family	3.30	0.89	0.25	0.0004
141	Jph2*	junctophilin 2	3.30	4.43	1.55	0.0073
142	Cox6a2*	cytochrome c oxidase, subunit VI a, polypeptide 2	3.29	39.66	12.60	0.0034
143	Ablim3	actin binding LIM protein family, member 3	3.29	0.62	0.20	0.0007

Table A.3, Part II. Continued

	Gene Symbol	Gene	Fold Change	Control.Ct. fpkm	Control.Cn. fpkm	FDR
144	Gpr115	G protein-coupled receptor 115	3.27	0.41	0.12	0.0141
145	Ky*	kyphoscoliosis peptidase	3.26	0.76	0.22	0.0116
146	F3	coagulation factor III	3.24	3.51	1.10	4.2E-08
147	P4ha3	procollagen-proline, 2-oxoglutarate 4-dioxygenase (proline 4-hydroxylase), alpha polypeptide III	3.22	5.98	1.84	7.2E-09
148	Tekt2	tektin 2	3.22	1.51	0.47	0.0019
149	Medag	mesenteric estrogen dependent adipogenesis	3.20	1.18	0.35	0.0067
150	Tmem255b	transmembrane protein 255B	3.20	1.57	0.49	0.0091
151	A330021E22Rik	RIKEN cDNA A330021E22 gene	3.19	0.45	0.13	0.0104
152	Mss51	MSS51 mitochondrial translational activator	3.16	4.33	1.31	0.0001
153	Sh3rf2	SH3 domain containing ring finger 2	3.15	0.42	0.13	0.0144
154	Lrrc38	leucine rich repeat containing 38	3.14	1.04	0.33	0.0286
155	Itm2a	integral membrane protein 2A	3.12	55.11	18.14	6.5E-10
156	Thpo	thrombopoietin	3.12	0.64	0.20	0.0237
157	Tmem38a*	transmembrane protein 38A	3.12	14.20	4.43	0.0028
158	Rian	RNA imprinted and accumulated in nucleus	3.10	2.19	0.77	0.0010
159	Grip2	glutamate receptor interacting protein 2	3.08	1.67	0.55	0.0006
160	Rbp7	retinol binding protein 7, cellular	3.07	4.95	1.50	0.0093
161	Hspb6*	heat shock protein, alpha-crystallin-related, B6	3.05	19.76	6.56	0.0015
162	Mrgprf	MAS-related GPR, member F	3.03	1.11	0.35	0.0186
163	Art1*	ADP-ribosyltransferase 1	3.01	10.77	3.61	4.8E-05

Table A.3, Part II. Continued

	Gene Symbol	Gene	Fold Change	Control.Ct. fpkm	Control.Cn. fpkm	FDR
164	Rbm24*	RNA binding motif protein 24	3.00	1.40	0.44	0.0147
165	Eno3*	enolase 3, beta muscle	3.00	78.99	30.91	0.0091
166	Mapt	microtubule-associated protein tau	3.00	0.77	0.28	0.0074
167	Tlx1	T-cell leukemia, homeobox 1	2.99	0.66	0.21	0.0164
168	Car11	carbonic anhydrase 11	2.98	1.99	0.63	0.0056
169	Fam131c	family with sequence similarity 131, member C	2.97	1.31	0.42	0.0036
170	Stac3*	SH3 and cysteine rich domain 3	2.96	3.52	1.16	0.0065
171	Mpp3	membrane protein, palmitoylated 3 (MAGUK p55 subfamily member 3)	2.89	0.52	0.18	0.0313
172	Bai2	brain-specific angiogenesis inhibitor 2	2.88	0.41	0.14	0.0025
173	Fam19a5	family with sequence similarity 19, member A5	2.86	1.21	0.44	0.0003
174	Postn	periostin, osteoblast specific factor	2.85	340.06	115.06	6.2E-08
175	Plat	plasminogen activator, tissue	2.78	7.30	2.67	1.5E-13
176	Pcdhga2	protocadherin gamma subfamily A, 2	2.78	0.60	0.22	0.0165
177	Tpm2*	tropomyosin 2, beta	2.77	65.32	23.06	0.0002
178	Sncg	synuclein, gamma	2.76	5.89	2.08	0.0016
179	Lrrn4cl	LRRN4 C-terminal like	2.76	1.74	0.61	5.3E-05
180	Fcrls	Fc receptor-like S, scavenger receptor	2.75	7.56	2.59	1.5E-07
181	Ccdc3	coiled-coil domain containing 3	2.74	17.98	6.40	1.8E-14
182	Tagln	transgelin	2.74	18.78	6.79	1.9E-07
183	Sowahb	trans-acting transcription factor 6	2.73	1.54	0.55	0.0001
184	Prtg	protogenin homolog (Gallus gallus)	2.70	0.59	0.22	0.0001
185	Hbb-b2	hemoglobin, beta adult minor chain	2.69	81.01	27.88	0.0269

Table A.3, Part II. Continued

	Gene Symbol	Gene	Fold Change	Control.Ct. fpkm	Control.Cn. fpkm	FDR
186	Adamtsl2	ADAMTS-like 2	2.69	7.15	2.42	0.0013
187	Zfp185	zinc finger protein 185	2.67	0.31	0.11	0.0363
188	Tfap2a	transcription factor AP-2, alpha	2.67	0.84	0.30	0.0017
189	Cyp46a1	cytochrome P450, family 46, subfamily a, polypeptide 1	2.66	1.01	0.37	0.0091
190	Gpnmb	glycoprotein (transmembrane) nmb	2.64	1.68	0.59	0.0048
191	Hs3st5	heparan sulfate (glucosamine) 3-O-sulfotransferase 5	2.64	0.45	0.17	0.0364
192	Ppp1r1a*	protein phosphatase 1, regulatory (inhibitor) subunit 1A	2.63	1.90	0.69	0.0175
193	Thbs2	thrombospondin 2	2.62	32.11	12.01	1.3E-11
194	Pianp	PILR alpha associated neural protein	2.61	2.25	0.87	0.0002
195	Dkk3	dickkopf homolog 3 (Xenopus laevis)	2.61	19.52	7.44	1.9E-19
196	Cpxm2	carboxypeptidase X 2 (M14 family)	2.60	5.51	2.11	0.0064
197	Ndufa4l2	NADH dehydrogenase (ubiquinone) 1 alpha subcomplex, 4-like 2	2.60	17.98	6.91	2.1E-08
198	Lrrc8e	leucine rich repeat containing 8 family, member E	2.55	0.46	0.17	0.0208
199	Mepe	matrix extracellular phosphoglycoprotein with ASARM motif (bone)	2.54	460.56	184.38	1.6E-10
200	Art5*	ADP-ribosyltransferase 5	2.54	4.18	1.63	6.0E-05
201	Gm996	predicted gene 996	2.53	0.61	0.24	0.0005
202	Cys1	cystin 1	2.52	3.18	1.22	5.1E-05
203	Ebf4	early B-cell factor 4	2.51	1.57	0.62	0.0003
204	Pygm*	muscle glycogen phosphorylase	2.51	32.38	14.74	0.0306
205	Nbl1	neuroblastoma, suppression of tumorigenicity 1	2.51	81.12	32.02	4.9E-09

Table A.3, Part II. Continued

	Gene Symbol	Gene	Fold Change	Control.Ct. fpkm	Control.Cn. fpkm	FDR
206	Sparcl1	SPARC-like 1	2.51	20.52	8.26	1.0E-11
207	Hspb2*	heat shock protein 2	2.50	25.97	10.47	0.0012
208	Kcnc1	potassium voltage gated channel, Shaw-related subfamily, member 1	2.50	1.37	0.57	2.8E-06
209	Nox4	NADPH oxidase 4	2.49	0.66	0.25	0.0189
210	Hspa1a	heat shock protein 1B; heat shock protein 1A; heat shock protein 1-like	2.48	0.59	0.23	0.0176
211	Glrb	glycine receptor, beta subunit	2.48	0.51	0.21	0.0375
212	Cacng7	calcium channel, voltage-dependent, gamma subunit 7	2.48	2.40	1.00	0.0319
213	Tg	thyroglobulin	2.47	6.73	2.68	9.7E-10
214	Galr2	galanin receptor 2	2.47	3.13	1.27	0.0010
215	Etv4	ets variant gene 4 (E1A enhancer binding protein, E1AF)	2.47	1.41	0.55	0.0064
216	Piwil2	piwi-like homolog 2 (Drosophila)	2.47	0.70	0.29	0.0014
217	Lcat	lecithin cholesterol acyltransferase	2.46	7.06	2.83	0.0002
218	Arhgap22	Rho GTPase activating protein 22	2.45	1.24	0.50	0.0108
219	Lrp2bp	Lrp2 binding protein	2.44	0.37	0.15	0.0235
220	Olfr1372-ps1	olfactory receptor 1372, pseudogene 1	2.44	0.84	0.37	0.0249
221	Cabp1	calcium binding protein 1	2.42	1.27	0.51	0.0262
222	Cacna1a	calcium channel, voltage-dependent, P/Q type, alpha 1A subunit	2.41	0.61	0.26	0.0015
223	Gja3	gap junction protein, alpha 3	2.40	0.67	0.28	0.0281
224	Tcea3*	transcription elongation factor A (SII), 3	2.40	11.83	4.89	2.0E-05

Table A.3, Part II. Continued

	Gene Symbol	Gene	Fold Change	Control.Ct. fpkm	Control.Cn. fpkm	FDR
225	Tnni3	troponin I, cardiac 3	2.40	3.04	1.20	0.0361
226	Wnt10b	wingless related MMTV integration site 10b	2.40	9.81	4.03	1.6E-07
227	Adamtsl1	ADAMTS-like 1	2.38	0.70	0.29	0.0018
228	Fndc1	fibronectin type III domain containing 1	2.36	5.50	2.13	5.5E-05
229	Col16a1	collagen, type XVI, alpha 1	2.36	35.79	15.02	1.9E-05
230	Gabra3	gamma-aminobutyric acid (GABA) A receptor, subunit alpha 3	2.36	0.87	0.36	0.0320
231	Gcnt4	glucosaminyl (N-acetyl) transferase 4, core 2 (beta-1,6-N-acetylglucosaminyltransferase)	2.34	0.40	0.17	0.0129
232	Aknad1	RIKEN cDNA 4921525H12 gene	2.34	0.66	0.28	0.0301
233	Dmd	dystrophin, muscular dystrophy	2.33	0.52	0.23	0.0032
234	Acta2	actin, alpha 2, smooth muscle, aorta	2.33	15.20	6.39	0.0002
235	Mamstr	MEF2 activating motif and SAP domain containing transcriptional regulator	2.33	0.94	0.39	0.0139
236	Slc6a7	solute carrier family 6 (neurotransmitter transporter, L-proline), member 7	2.30	1.77	0.76	0.0002
237	Tmod2	tropomodulin 2	2.30	0.35	0.15	0.0018
238	Lor	loricrin	2.29	0.77	0.32	0.0417
239	Nmnat2	nicotinamide nucleotide adenylyltransferase 2	2.29	2.01	0.90	3.1E-05
240	Wfdc1*	WAP four-disulfide core domain 1	2.28	9.15	3.91	0.0011
241	Coro6*	coronin 6	2.28	3.46	1.52	0.0016
242	Lrrc51	leucine rich repeat containing 51	2.27	3.94	1.63	0.0092
243	Plekha4	pleckstrin homology domain containing, family A (phosphoinositide binding specific) member 4	2.25	1.26	0.53	0.0065

Table A.3, Part II. Continued

	Gene Symbol	Gene	Fold Change	Control.Ct. fpkm	Control.Cn. fpkm	FDR
244	Mn1	meningioma 1	2.25	0.94	0.42	0.0066
245	Rem1	rad and gem related GTP binding protein 1	2.24	1.19	0.52	0.0305
246	Adam33	a disintegrin and metallopeptidase domain 33	2.22	1.47	0.68	0.0032
247	A930006K02Rik	RIKEN cDNA A930006K02 gene	2.21	4.10	1.80	0.0129
248	Meox1	mesenchyme homeobox 1	2.21	2.65	1.18	0.0045
249	Adam23	a disintegrin and metallopeptidase domain 23; similar to ADAM23	2.21	0.45	0.19	0.0123
250	Cpeb1	cytoplasmic polyadenylation element binding protein 1	2.21	4.70	2.06	1.4E-07
251	Trib3	tribbles homolog 3 (Drosophila)	2.20	1.12	0.48	0.0202
252	Aox1	aldehyde oxidase 1	2.20	2.13	0.97	6.7E-05
253	Slc47a1	solute carrier family 47, member 1	2.20	1.43	0.63	0.0356
254	P2rx6	purinergic receptor P2X, ligand-gated ion channel, 6	2.20	1.27	0.56	0.0101
255	C1qtnf5	C1q and tumor necrosis factor related protein 5	2.19	20.02	9.05	4.2E-05
256	Bglap3	bone gamma-carboxyglutamate protein 3	2.19	9.46	4.21	0.0222
257	Ssc5d	scavenger receptor cysteine rich family, 5 domains	2.18	2.31	1.06	0.0005
258	Egflam	EGF-like, fibronectin type III and laminin G domains	2.18	0.39	0.17	0.0254
259	Casq2	calsequestrin 2	2.17	1.63	0.72	0.0018
260	Lum	lumican	2.16	636.92	293.03	5.7E-06
261	Tbx3	T-box 3	2.15	0.96	0.43	0.0052
262	Aebp1	AE binding protein 1	2.14	25.21	11.75	3.3E-07

Table A.3, Part II. Continued

	Gene Symbol	Gene	Fold Change	Control.Ct. fpkm	Control.Cn. fpkm	FDR
263	Best1	bestrophin 1; hypothetical protein LOC100046789	2.12	1.27	0.59	0.0163
264	3000002C10Rik	RIKEN cDNA 3000002C10 gene; predicted gene 7251	2.12	5.09	2.36	0.0005
265	Prr15	proline rich 15	2.11	14.45	6.83	4.2E-05
266	Pdlim4	PDZ and LIM domain 4	2.10	12.97	6.05	5.1E-06
267	Shroom1	shroom family member 1	2.10	0.92	0.43	0.0182
268	Myom3	myomesin family, member 3	2.08	0.81	0.39	0.0071
269	4933436C20Rik	RIKEN cDNA 4933436C20 gene	2.08	16.65	7.99	8.4E-06
270	Tmeff1	transmembrane protein with EGF-like and two follistatin-like domains 1	2.07	1.27	0.60	0.0252
271	Irx6	Iroquois related homeobox 6 (Drosophila)	2.07	3.54	1.66	0.0144
272	Fgf9	fibroblast growth factor 9	2.06	0.75	0.36	0.0081
273	Srl*	sarcalumenin	2.06	7.56	3.77	0.0176
274	Atp6v0e2*	ATPase, H+ transporting, lysosomal V0 subunit E2	2.05	3.46	1.65	0.0056
275	Cav3	caveolin 3	2.05	3.53	1.59	0.0333
276	Stmn2	stathmin-like 2	2.05	2.09	1.05	0.0084
277	Flnc*	filamin C, gamma	2.05	2.06	1.00	0.0249
278	Trim7	tripartite motif-containing 7	2.04	2.62	1.26	0.0053
279	ORF63	open reading frame 63	2.03	2.19	0.99	0.0343
280	Kcnab1	potassium voltage-gated channel, shaker-related subfamily, beta member 1	2.02	0.93	0.47	0.0196
281	Ablim2	actin-binding LIM protein 2	2.02	2.05	0.99	0.0038
282	Hr	hairless	2.02	2.68	1.31	0.0006

Table A.3, Part II. Continued

	Gene Symbol	Gene	Fold Change	Control.Ct. fpkm	Control.Cn. fpkm	FDR
283	Eno2	enolase 2, gamma neuronal	2.01	1.40	0.70	0.0393
284	Dok5	docking protein 5	2.00	4.56	2.25	0.0017
285	Tgfb2	transforming growth factor, beta 2	2.00	7.81	4.21	0.0017
286	Slc25a27	solute carrier family 25, member 27	2.00	1.85	0.93	0.0014
287	Pacsin3*	protein kinase C and casein kinase substrate in neurons 3	2.00	8.15	4.09	0.0032

total	326
*indicates contaminant	84
total without contaminants	242

Table A.4: A complete list of genes that were differentially expressed 3 hours following a single loading session in cortical bone in order of decreasing fold change that were: I. upregulated by mechanical loading and II. downregulated by mechanical loading. Number of genes (column A), gene symbols (column B), gene names (column C), fold change (column D), control cortical (Ct) fragments per kilobase per million reads (FPKM) (column E), loaded cortical (Ct) FPKM (column F), false discovery rate (FDR) (column G).

Table A.4, Part I. List of genes upregulated 3 hours after a single loading session in cortical bone

	Gene Symbol	Gene	Fold Change	Control.Ct. fpkm	Loaded.Ct. fpkm	FDR
1	Gm5512	required for meiotic nuclear division 1 homolog (S. cerevisiae); predicted gene 5512	459.83	0.32	8.66	0.0088
2	Mb	myoglobin	38.31	9.04	76.12	0.0334
3	Csrp3	cysteine and glycine-rich protein 3	36.66	0.29	9.21	0.0342
4	Klhl41	kelch-like 41	19.31	0.37	3.75	0.0064
5	Acta1	actin, alpha 1, skeletal muscle	15.99	24.86	147.42	0.0387
6	Rgs17	regulator of G-protein signaling 17	13.97	0.02	0.20	0.0253
7	Rpl3l	ribosomal protein L3-like	11.62	0.92	6.33	0.0230
8	Mylpf	myosin light chain, phosphorylatable, fast skeletal muscle	10.17	27.37	184.46	0.0387
9	Murc	muscle-related coiled-coil protein	7.04	0.28	1.93	0.0286
10	Hspb7	heat shock protein family, member 7 (cardiovascular)	6.99	1.41	9.70	9.3E-06
11	Ch25h	cholesterol 25-hydroxylase	6.55	0.29	2.29	0.0030
12	Mfap5	microfibrillar associated protein 5	6.34	0.22	1.49	0.0342
13	Wnt1	wingless-related MMTV integration site 1	6.18	0.80	4.59	6.1E-13
14	Gem	GTP binding protein (gene overexpressed in skeletal muscle)	4.67	1.86	8.60	6.5E-16

Table A.4, Part I. Continued

	Gene Symbol	Gene	Fold Change	Control.Ct. fpkm	Loaded.Ct. fpkm	FDR
15	Medag	mesenteric estrogen dependent adipogenesis	4.66	0.81	3.90	3.5E-07
16	Ptgs2	prostaglandin-endoperoxide synthase 2	4.32	1.19	5.22	5.8E-09
17	Ngf	nerve growth factor	3.85	3.06	11.61	6.7E-07
18	Ccl7	chemokine (C-C motif) ligand 7	3.76	1.37	4.85	0.0008
19	Wnt7b	wingless-related MMTV integration site 7B	3.22	0.89	3.01	0.0251
20	Ccl12	chemokine (C-C motif) ligand 12; similar to monocyte chemoattractant protein-5	2.93	5.51	16.62	0.0064
21	Tnfrsf12a	tumor necrosis factor receptor superfamily, member 12a	2.82	10.22	29.78	2.4E-11
22	Mustn1	musculoskeletal, embryonic nuclear protein 1	2.51	9.81	27.38	0.0088
23	Wnt10b	wingless related MMTV integration site 10b	2.39	8.27	20.11	0.0131
24	Lmcd1	LIM and cysteine-rich domains 1	2.27	9.34	21.29	1.0E-07
25	Tnfrsf11b	tumor necrosis factor receptor superfamily, member 11b (osteoprotegerin)	2.17	18.91	41.62	3.5E-07
26	Tfpi2	tissue factor pathway inhibitor 2	2.13	6.50	14.26	0.0002
27	Epcam	epithelial cell adhesion molecule	2.07	7.63	16.52	0.0064
28	Hbegf	heparin-binding EGF-like growth factor	2.06	2.44	5.20	0.0175
29	Bmp2	bone morphogenetic protein 2	1.93	13.90	28.45	0.0029
30	Srxn1	sulfiredoxin 1 homolog (S. cerevisiae)	1.91	12.97	25.15	1.2E-07
31	Nt5e	5' nucleotidase, ecto	1.89	13.38	24.99	0.0230
32	Mt2	metallothionein 2	1.77	353.79	647.46	0.0011
33	Dmp1	dentin matrix protein 1	1.74	734.28	1283.10	0.0088
34	Ugdh	UDP-glucose dehydrogenase	1.68	39.39	66.19	5.4E-10

Table A.4, Part I. Continued

	Gene Symbol	Gene	Fold Change	Control.Ct. fpkm	Loaded.Ct. fpkm	FDR
35	Phlda1	pleckstrin homology-like domain, family A, member 1	1.66	11.45	18.99	0.0002
36	Glrx3	predicted gene 12669; glutaredoxin 3	1.64	21.98	35.44	0.0230
37	Timp1	tissue inhibitor of metalloproteinase 1	1.63	197.17	330.52	0.0003
38	S100a10	S100 calcium binding protein A10 (calpactin)	1.59	232.79	379.16	0.0006
39	Rgcc	regulator of cell cycle	1.57	44.65	69.46	0.0029
40	Trib1	tribbles homolog 1 (Drosophila)	1.56	3.50	5.55	0.0029
41	Fam20c	family with sequence similarity 20, member C	1.52	48.29	72.66	0.0002

Table A.4, Part II. List of genes downregulated 3 hours after a single loading session in cortical bone

	Gene Symbol	Gene	Fold Change	Control.Ct. fpkm	Loaded.Ct. fpkm	FDR
1	Crebbp	CREB binding protein	-1.51	5.78	3.85	0.0230
2	Lrp5	low density lipoprotein receptor-related protein 5	-1.50	28.68	19.12	0.0251

Table A.5: A complete list of genes that were differentially expressed 3 hours following a single loading session in cancellous bone in order of decreasing fold change that were: I. upregulated by mechanical loading and II. downregulated by mechanical loading. Number of genes (column A), gene symbols (column B), gene names (column C), fold change (column D), control cancellous (Cn) fragments per kilobase per million reads (FPKM) (column E), loaded cancellous (Cn) FPKM (column F), false discovery rate (FDR) (column G).

Table A.5, Part I. List of genes upregulated 3 hours after a single loading session in cancellous bone

	Gene Symbol	Gene	Fold Change	Control.Cn. fpkm	Loaded.Cn. fpkm	FDR
1	Wnt7b	wingless-related MMTV integration site 7B	7.78	0.16	1.24	4.1E-06
2	Wnt1	wingless-related MMTV integration site 1	4.08	0.45	1.85	2.8E-06
3	Ptgs2	prostaglandin-endoperoxide synthase 2	3.90	0.81	3.01	4.1E-07
4	Nt5e	5' nucleotidase, ecto	3.41	10.47	33.00	5.2E-10
5	Tnfrsf12a	tumor necrosis factor receptor superfamily, member 12a	3.10	7.19	21.84	6.8E-13
6	Ngf	nerve growth factor	2.36	2.89	6.80	0.0405
7	Timp1	tissue inhibitor of metalloproteinase 1	1.90	112.05	211.16	1.6E-07
8	Tnfrsf11b	tumor necrosis factor receptor superfamily, member 11b (osteoprotegerin)	1.89	12.45	23.24	0.0003
9	Tfpi2	tissue factor pathway inhibitor 2	1.83	6.77	12.67	0.0135
10	Col6a3	collagen, type VI, alpha 3	1.65	32.00	51.05	0.0438
11	Fam20c	family with sequence similarity 20, member C	1.63	35.89	56.86	2.8E-06
12	Srxn1	sulfiredoxin 1 homolog (S. cerevisiae)	1.51	13.19	19.92	0.0222
13	Cspg4	chondroitin sulfate proteoglycan 4	1.50	11.35	16.49	0.0135

Table A.5, Part II. List of genes downregulated 3 hours after a single loading session in cancellous bone

	Gene Symbol	Gene	Fold Change	Control.Cn. fpkm	Loaded.Cn. fpkm	FDR
1	9130019 P16Rik	RIKEN cDNA 9130019P16 gene	-2.93	0.86	0.26	0.0406
2	Sost	sclerostin	-2.27	101.32	42.60	0.0048
3	Mepe	matrix extracellular phosphoglycoprotein with ASARM motif (bone)	-1.65	296.94	178.20	0.0008
4	Dkk1	dickkopf homolog 1 (Xenopus laevis)	-1.59	44.40	27.43	0.0011
5	Fbln2	fibulin 2	-1.54	6.37	4.13	0.0243

Table A.6: A complete list of genes that were differentially expressed 24 hours following a single loading session in cortical bone in order of decreasing fold change that were: I. upregulated by mechanical loading and II. downregulated by mechanical loading. Number of genes (column A), gene symbols (column B), gene names (column C), fold change (column D), control cortical (Ct) fragments per kilobase per million reads (FPKM) (column E), loaded cortical (Ct) FPKM (column F), false discovery rate (FDR) (column G).

Table A.6, Part I. List of genes upregulated 24 hours after a single loading session in cortical bone

	Gene Symbol	Gene	Fold Change	Control.Ct. fpkm	Loaded.Ct. fpkm	FDR
1	Wnt1	wingless-related MMTV integration site 1	6.11	0.41	2.36	7.0E-07
2	Adamts8	a disintegrin-like and metallopeptidase (reprolysin type) with thrombospondin type 1 motif, 8	4.19	0.19	0.66	0.0082
3	Ptn	pleiotrophin	2.68	6.05	15.51	0.0006
4	Tubb3	tubulin, beta 3; tubulin, beta 3, pseudogene 1	2.48	4.97	11.73	7.0E-07
5	Zfp365	zinc finger protein 365	2.32	0.50	1.14	0.0030
6	Bcan	brevican	2.24	2.98	6.08	0.0002
7	Gabrb2	gamma-aminobutyric acid (GABA) A receptor, subunit beta 2	2.01	0.31	0.65	0.0135
8	Gsg1l	GSG1-like	1.96	1.73	3.40	0.0025
9	Nr4a2	nuclear receptor subfamily 4, group A, member 2	1.96	5.30	10.29	0.0008
10	Qpct	glutaminyl-peptide cyclotransferase (glutaminyl cyclase)	1.93	5.25	9.89	0.0010
11	Ptgs2	prostaglandin-endoperoxide synthase 2	1.88	0.90	1.66	0.0111
12	Wnt10b	wingless related MMTV integration site 10b	1.81	9.81	17.33	0.0045

Table A.6, Part I. Continued

	Gene Symbol	Gene	Fold Change	Control.Ct. fpkm	Loaded.Ct. fpkm	FDR
13	Peg10	paternally expressed 10	1.80	1.48	2.70	0.0054
14	Dclk1	doublecortin-like kinase 1	1.80	2.62	4.66	0.0002
15	Lurap1l	leucine rich adaptor protein 1-like	1.79	10.70	18.61	0.0006
16	Brsk1	BR serine/threonine kinase 1	1.79	2.34	3.82	0.0242
17	Hapln4	hyaluronan and proteoglycan link protein 4	1.78	4.19	7.28	0.0063
18	Pi15	peptidase inhibitor 15	1.77	4.65	7.75	0.0121
19	Apcdd1	adenomatosis polyposis coli down-regulated 1	1.75	12.16	20.45	0.0010
20	Cthrc1	collagen triple helix repeat containing 1	1.68	158.90	255.67	0.0031
21	Vcan	versican	1.68	10.63	18.69	9.1E-05
22	Cdo1	cysteine dioxygenase 1, cytosolic	1.67	105.10	173.08	0.0019
23	Dusp14	dual specificity phosphatase 14	1.62	7.34	12.04	0.0499
24	Fkbp11	FK506 binding protein 11	1.62	50.85	78.72	0.0045
25	Aldh1l2	aldehyde dehydrogenase 1 family, member L2	1.61	12.49	19.68	0.0031
26	Slc2a13	solute carrier family 2 (facilitated glucose transporter), member 13	1.56	4.57	7.02	0.0202
27	Pdzrn3	PDZ domain containing RING finger 3	1.55	5.51	8.46	0.0082
28	Psd3	pleckstrin and Sec7 domain containing 3	1.53	8.17	12.61	0.0328
29	Mamdc2	MAM domain containing 2	1.53	16.00	24.10	0.0180
30	Gnai1	guanine nucleotide binding protein (G protein), alpha inhibiting 1	1.53	26.75	40.45	0.0082
31	Dcbld1	discoidin, CUB and LCCL domain containing 1	1.52	4.42	6.49	0.0425

Table A.6, Part I. Continued

	Gene Symbol	Gene	Fold Change	Control.Ct. fpkm	Loaded.Ct. fpkm	FDR
32	Sema3b	sema domain, immunoglobulin domain (Ig), short basic domain, secreted, (semaphorin) 3B	1.51	15.76	23.05	0.0092
33	P4ha1	procollagen-proline, 2-oxoglutarate 4-dioxygenase (proline 4-hydroxylase), alpha 1 polypeptide	1.51	39.99	59.81	0.0095
34	1700066 M21Rik	RIKEN cDNA 1700066M21 gene	1.50	16.12	24.29	0.0082

Table A.6, Part II. List of genes downregulated 24 hours after a single loading session in cortical bone

	Gene Symbol	Gene	Fold Change	Control.Ct. fpkm	Loaded.Ct. fpkm	FDR
1	Actc1	actin, alpha, cardiac muscle 1;	-18.55	3.44	0.58	0.0380
2	Ampd1	adenosine monophosphate deaminase 1 (isoform M)	-8.74	4.97	0.78	0.0215
3	Dhrs7c	dehydrogenase/reductase (SDR family) member 7C	-8.34	3.79	0.54	0.0151
4	Tnxb	tenascin XB	-7.03	0.95	0.11	0.0056
5	Angptl7	angiopoietin-like 7	-6.10	10.19	1.39	0.0164
6	F7	coagulation factor VII	-2.66	1.08	0.40	0.0328
7	Htra4	HtrA serine peptidase 4	-2.44	4.25	1.68	0.0082
8	Tppp3	tubulin polymerization-promoting protein family member 3	-2.39	13.35	5.13	0.0278
9	Mt3	metallothionein 3	-2.07	191.75	95.64	0.0082
10	Nmb	neuromedin B	-2.02	70.58	36.33	0.0031

Table A.6, Part II. Continued

	Gene Symbol	Gene	Fold Change	Control.Ct. fpkm	Loaded.Ct. fpkm	FDR
11	Mt1	metallothionein 1	-1.93	323.04	176.08	0.0045
12	Cxcr5	chemochine (C-X-C motif) receptor 5	-1.84	1.42	0.78	0.0270
13	Mt2	metallothionein 2	-1.83	133.91	76.98	0.0111
14	Wisp2	WNT1 inducible signaling pathway protein 2	-1.81	42.71	23.77	0.0003
15	Bdh2	3-hydroxybutyrate dehydrogenase, type 2	-1.77	9.21	5.14	0.0155
16	Chchd10	coiled-coil-helix-coiled-coil-helix domain containing 10	-1.76	36.81	20.42	0.0054
17	Mst1r	macrophage stimulating 1 receptor (c-met-related tyrosine kinase)	-1.66	16.83	10.02	0.0054
18	Lif	leukemia inhibitory factor	-1.65	3.66	2.24	0.0351
19	Smim5	small integral membrane protein 5	-1.64	22.22	12.80	0.0468
20	Galnt6	UDP-N-acetyl-alpha-D-galactosamine:polypeptide N-acetylgalactosaminyltransferase 6	-1.63	7.96	4.79	0.0006
21	Slc9b2	solute carrier family 9, subfamily B (NHA2, cation proton antiporter 2), member 2	-1.60	74.27	46.61	0.0186
22	Sgsm3	small G protein signaling modulator 3	-1.59	10.25	6.44	0.0103
23	Adssl1	adenylosuccinate synthetase like 1	-1.51	38.10	24.61	0.0145

Table A.7: A complete list of genes that were differentially expressed 24 hours following a single loading session in cancellous bone in order of decreasing fold change that were: I. upregulated by mechanical loading and II. downregulated by mechanical loading. Number of genes (column A), gene symbols (column B), gene names (column C), fold change (column D), control cancellous (Cn) fragments per kilobase per million reads (FPKM) (column E), loaded cancellous (Cn) FPKM (column F), false discovery rate (FDR) (column G).

Table A.7, Part I. List of genes upregulated 24 hours after a single loading session in cancellous bone

	Gene Symbol	Gene	Fold Change	Control.Cn. fpkm	Loaded.Cn. fpkm	FDR
1	ChkbCpt1b	Chkb-Cpt1b readthrough transcript (NMD candidate)	362.52	9.64E-05	0.66	8.5E-14
2	Apoo-ps	apolipoprotein O, pseudogene	7.59	1.20	5.41	0.0186
3	Ptn	pleiotrophin	3.08	1.66	5.47	0.0006
4	Tubb3	tubulin, beta 3; tubulin, beta 3, pseudogene 1	1.80	4.30	7.92	0.0205
5	Lurap1l	leucine rich adaptor protein 1-like	1.76	7.78	13.69	0.0035
6	Timp1	tissue inhibitor of metalloproteinase 1	1.71	93.30	163.44	0.0082
7	Peg10	paternally expressed 10	1.68	2.20	3.67	0.0365
8	Hapln4	hyaluronan and proteoglycan link protein 4	1.67	3.81	6.28	0.0442
9	Vcan	versican	1.63	5.99	9.80	0.0007
10	Cthrc1	collagen triple helix repeat containing 1	1.62	124.37	197.56	0.0186
11	Fkbp11	FK506 binding protein 11	1.56	47.11	73.82	0.0199

Table A.7, Part II. List of genes downregulated 24 hours after a single loading session in cancellous bone

	Gene Symbol	Gene	Fold Change	Control.Cn. fpkm	Loaded.Cn. fpkm	FDR
1	Myh4	myosin, heavy polypeptide 4, skeletal muscle	-59.48	32.30	0.51	0.0243
2	Sypl2	synaptophysin-like 2	-49.05	0.62	4.06E-03	0.0031
3	Tnnc2	troponin C2, fast	-41.61	134.42	2.41	0.0434
4	Ampd1	adenosine monophosphate deaminase 1 (isoform M)	-31.88	2.17	0.03	0.0007
5	Dhrs7c	dehydrogenase/reductase (SDR family) member 7C	-28.60	0.98	0.01	0.0074
6	Smpx	small muscle protein, X-linked	-32.29	1.41	0.01	0.0160
7	Tnnt3	troponin T3, skeletal, fast	-36.62	150.70	2.74	0.0186
8	Mylk2	myosin, light polypeptide kinase 2, skeletal muscle	-22.40	1.35	0.02	0.0432
9	Myoz1	myozenin 1	-23.38	11.13	0.26	0.0421
10	Myom2	myomesin 2	-21.54	1.35	0.03	0.0137
11	2310002 L09Rik	RIKEN cDNA 2310002L09 gene	-14.99	0.51	0.01	0.0432
12	Actn3	actinin alpha 3	-14.74	18.20	0.68	0.0063
13	Myl1	myosin, light polypeptide 1	-13.81	108.90	3.66	0.0186
14	Casq1	calsequestrin 1	-12.36	9.45	0.38	0.0434
15	Mybpc2	myosin binding protein C, fast-type	-12.09	6.85	0.34	0.0242
16	Myh2	myosin, heavy polypeptide 2, skeletal muscle, adult	-12.17	0.17	0.01	0.0019
17	Mylpf	myosin light chain, phosphorylatable, fast skeletal muscle	-12.85	122.42	5.10	0.0184
18	Tnni2	troponin I, skeletal, fast 2	-7.69	116.33	11.62	0.0442

Table A.7, Part II. Continued

	Gene Symbol	Gene	Fold Change	Control.Cn. fpkm	Loaded.Cn. fpkm	FDR
19	Sh3bgr	similar to putative SH3BGR protein; SH3-binding domain glutamic acid-rich protein	-6.42	3.32	0.38	0.0492
20	Nmb	neuromedin B	-1.94	69.75	36.90	0.0137
21	Slc9b2	solute carrier family 9, subfamily B (NHA2, cation proton antiporter 2), member 2	-1.66	72.66	44.47	0.0186

APPENDIX B. **CHAPTER 4 SUPPLEMENTARY FIGURES AND DATA**

TABLE OF CONTENTS

Figure B.1 Right and Left limbs of naïve animals have similar transcriptional profiles..... 204
Table B.1 List of primers for genes verified with qPCR.....205
Table B.2, Part I: List of genes upregulated 3 hours after a single loading session in cortical bone of littermate control animals.....206
Table B.2, Part II: List of genes downregulated 3 hours after a single loading session in cortical bone of littermate control animals 228
Table B.3, Part I: List of genes upregulated 3 hours after a single loading session in cortical bone of pOC-ERαKO animals.....238
Table B.4, Part I: List of genes upregulated 24 hours after a single loading session in cortical bone of littermate control animals.....240
Table B.4, Part II: List of genes downregulated 24 hours after a single loading session in cortical bone of littermate control animals.240
Table B.5, Part I: List of genes upregulated 24 hours after a single loading session in cortical bone of pOC-ERαKO animals.....243
Table B.5, Part II: List of genes downregulated 24 hours after a single loading session in cortical bone of pOC-ERaKO animals.....243
Table B.6, Part I: List of genes upregulated 3 hours after a single loading session in cancellous bone of littermate control animals.....244
Table B.7, Part I: List of genes upregulated 3 hours after a single loading session in cancellous bone of pOC-ERαKO animals 246
Table B.7, Part II: List of genes downregulated 3 hours after a single loading session in cancellous bone of pOC-ERαKO animals 247
Table B.8, Part I: List of genes upregulated 24 hours after a single loading session in cancellous bone of littermate control animals.....248
Table B.8, Part II: List of genes downregulated 24 hours after a single loading session in cancellous bone of littermate control animals 248
Table B.9, Part I: List of genes upregulated 24 hours after a single loading session in cancellous bone of pOC-ERαKO animals 249
Table B.9, Part II: List of genes downregulated 24 hours after a single loading session in cancellous bone of pOC-ERαKO animals 253
Table B.10, Part I: List of genes more highly expressed in naïve control cortical bone 256

Table B.10, Part II: List of genes more highly expressed in naïve control cancellous bone 267
Table B.11, Part I: List of genes more highly expressed in control cortical bone of littermate control animals at 3 hours 271
Table B.11, Part II: List of genes more highly expressed in control cancellous bone of littermate control animals at 3 hours 281
Table B.12, Part I: List of genes more highly expressed in control cortical bone of littermate control animals at 24 hours 285
Table B.12, Part II: List of genes more highly expressed in control cancellous bone of littermate control animals at 24 hours 296
Table B.13, Part I: List of genes more highly expressed in control cortical bone of pOC-ERαKO animals at 3 hours 301
Table B.13, Part II: List of genes more highly expressed in control cancellous bone of pOC-ERαKO animals at 3 hours 312
Table B.14, Part I: List of genes more highly expressed in control cortical bone of pOC-ERαKO animals at 24 hours 318
Table B.14, Part II: List of genes more highly expressed in control cancellous bone of pOC-ERαKO animals at 24 hours 328

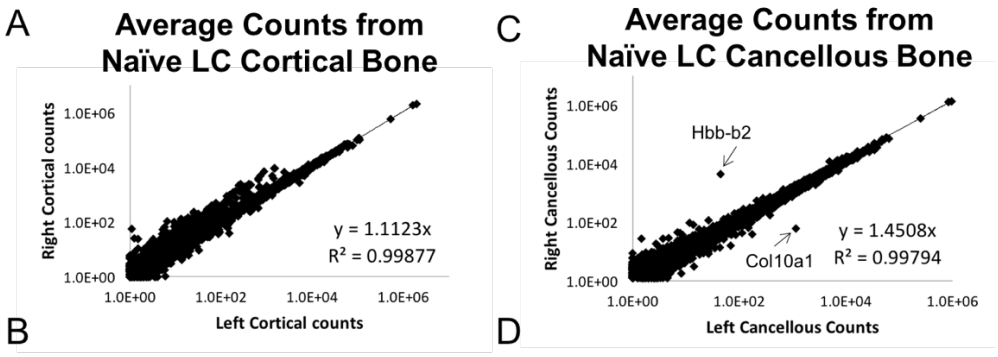

Gene	Fold Change (Right v Left)
Ndufs5	1.8
0610039K10Rik	2.7
1700007J10Rik	4.8

Gene	Fold Change (Right v Left)
Hbb-b2	112.4
Cilp2	5.4
Col10a1	-13.5
0610039K10Rik	-2.2

Figure B.1 Right and Left limbs of naïve animals have similar transcriptional profiles. A) Scatter plot of gene counts between right and left cortical bone were very similar with B) only three genes that were differentially expressed. Right versus left cancellous samples were also very similar in their C) scatter plot of gene counts and D) only four differentially expressed genes. Hbb-b2 (hemoglobin, beta adult minor chain) was 112-fold higher in right cancellous samples, but this is likely due to contamination as it is a major component of blood. Cilp2 (cartilage intermediate layer protein-2) was 5-fold higher in right cancellous bone and Col10a1 (collagen type X alpha 1) was 13-fold higher in left cancellous samples, but both of these may be due to slight variations in preparation and amount of the hypertrophic chondrocytes and cartilage that were removed proximally from the sample.

Table B.1 List of primers for genes verified with qPCR.

Accession #	Gene Symbol	Gene Name	Forward primer	Reverse Primer
NM_021279	Wnt1	wingless-type MMTV integration site family, member 1	GATTTTGGTCGCCTCTTTGG	CGTGGCATTTGCACTCTTG
NM_009528	Wnt7b	wingless-type MMTV integration site family, member 7b	AATGAGGCGGGCAGAAAG	TGCGTTGTACTTCTCCTTGAG
NM_011198	Ptgs2	prostaglandin-endoperoxide synthase 2	CTCACGAAGGAACTCAGCAC	GGATTGGAACAGCAAGGATTTG
NM_008973	Ptn	Pleiotrophin	AACTGTCACCATCTCCAAGC	TCTCCTGTTTCTTGCCTTCC
NM_008764	Tnfrsf11b	tumor necrosis factor receptor superfamily member 11B	GAGAGGATAAAACGGAGACACAG	CTGCTTTCACAGAGGTCAATG
NM_011593	Timp1	Tissue inhibitor of metalloproteinase 1	CTCAAAGACCTATAGTGCTGGC	CAAAGTGACGGCTCTGGTAG
NM_053116	Wnt16	wingless-type MMTV integration site family, member 16	CGAGAGGTGGAACTGTATGG	TGAATGCTGTCTCCTTGGTG
NM_198112	Ostn	Osteocrin	GGACTGGAGATTGGCAAGTAC	CTTCTCTGGCTGTGGGTG

Gene accession numbers (column A), gene symbols (column B), gene names (column C), forward primer (column D) and reverse primer (column D).

Table B.2: A complete list of genes that were differentially expressed 3 hours following a single loading session in littermate control cortical bone in order of decreasing fold change that were: I. upregulated by mechanical loading and II. downregulated by mechanical loading. Number of genes (column A), gene symbols (column B), gene names (column C), fold change (column D), false discovery rate (FDR) (column E).

Table B.2, Part I. Upregulated 3 hours after a single loading session in cortical bone of littermate control animals

	Gene Symbol	Gene	Fold Change	FDR
1	Amd1	S-adenosylmethionine decarboxylase 1	225.88	2.2E-04
2	Gm20594	predicted gene, 20594	22.12	1.6E-02
3	Sypl2	synaptophysin-like 2	16.71	8.8E-04
4	Sgcg	sarcoglycan, gamma (dystrophin-associated glycoprotein)	16.00	2.1E-03
5	Smpx	small muscle protein, X-linked	15.88	2.9E-03
6	Hfe2	hemochromatosis type 2 (juvenile) (human homolog)	15.30	1.8E-02
7	Trim63	tripartite motif-containing 63	15.24	1.2E-03
8	Xirp1	xin actin-binding repeat containing 1	15.10	1.8E-03
9	Myot	myotilin	14.48	1.7E-02
10	Mylk4	myosin light chain kinase family, member 4	14.17	2.6E-04
11	Murc	muscle-related coiled-coil protein	13.75	8.0E-05
12	Myom2	myomesin 2	13.66	8.8E-03
13	Actn2	actinin alpha 2	11.99	3.4E-04
14	Cilp	cartilage intermediate layer protein, nucleotide pyrophosphohydrolase	11.98	8.1E-03
15	Mylk2	myosin, light polypeptide kinase 2, skeletal muscle	11.25	1.2E-02
16	Atp2a1	ATPase, Ca++ transporting, cardiac muscle, fast twitch 1	11.23	2.3E-03
17	Klhl41	kelch-like 41	11.07	8.0E-05
18	Eef1a2	eukaryotic translation elongation factor 1 alpha 2	11.07	7.4E-03
19	Myl1	myosin, light polypeptide 1	11.04	1.2E-03

Table B.2, Part I. Continued

	Gene Symbol	Gene	Fold Change	FDR
20	Mybpc1	myosin binding protein C, slow-type	10.94	8.1E-03
21	Neb	nebulin	10.72	5.9E-04
22	Lmod2	leiomodin 2 (cardiac)	10.66	8.8E-03
23	A930016O22Rik	RIKEN cDNA A930016O22 gene	10.23	1.7E-03
24	Ucp3	uncoupling protein 3 (mitochondrial, proton carrier)	10.17	4.3E-05
25	Ckmt2	creatine kinase, mitochondrial 2	9.93	7.4E-03
26	Myoz1	myozenin 1	9.90	3.3E-02
27	Apobec2	apolipoprotein B mRNA editing enzyme, catalytic polypeptide 2	9.82	4.3E-04
28	Smyd1	SET and MYND domain containing 1	9.77	1.4E-02
29	Mylpf	myosin light chain, phosphorylatable, fast skeletal muscle	9.65	1.2E-03
30	Acta1	actin, alpha 1, skeletal muscle	9.20	3.0E-02
31	Casq1	calsequestrin 1	9.16	8.0E-03
32	Nrap	nebulin-related anchoring protein	9.07	9.4E-04
33	Ttn	titin	9.03	7.9E-04
34	Ryr1	ryanodine receptor 1, skeletal muscle	8.98	2.2E-04
35	Myoz3	myozenin 3	8.98	2.6E-02
36	Mypn	myopalladin	8.92	1.1E-02
37	Mb	myoglobin	8.85	1.5E-02
38	Mybpc2	myosin binding protein C, fast-type	8.57	2.7E-03
39	Myh1	myosin, heavy polypeptide 1, skeletal muscle, adult	8.56	3.3E-02
40	Gm12505	predicted gene 12505	8.50	1.9E-05
41	Actc1	actin, alpha, cardiac muscle 1	8.47	2.3E-02
42	Ldb3	LIM domain binding 3	8.37	5.7E-04
43	Tnnt3	troponin T3, skeletal, fast	8.23	2.2E-02
44	Trim54	tripartite motif-containing 54	8.11	1.5E-02

Table B.2, Part I. Continued

	Gene Symbol	Gene	Fold Change	FDR
45	Rsc1a1	regulatory solute carrier protein, family 1, member 1	8.02	3.8E-02
46	Tnni2	troponin I, skeletal, fast 2	7.81	7.2E-03
47	Cacna1s	calcium channel, voltage-dependent, L type, alpha 1S subunit	7.77	2.7E-03
48	Sh3bgr	SH3-binding domain glutamic acid-rich protein	7.73	2.4E-03
49	Tnnc2	troponin C2, fast	7.72	1.6E-02
50	Scn4b	sodium channel, type IV, beta	7.32	3.4E-04
51	Prg4	proteoglycan 4 (megakaryocyte stimulating factor, articular superficial zone protein)	7.18	1.4E-07
52	Trim72	tripartite motif-containing 72	7.00	1.3E-04
53	Atp1a2	ATPase, Na+/K+ transporting, alpha 2 polypeptide	6.97	8.7E-05
54	Tmod4	tropomodulin 4	6.95	6.4E-04
55	Angptl7	angiopoietin-like 7	6.90	1.2E-03
56	Actn3	actinin alpha 3	6.83	2.8E-03
57	Myoz2	myozenin 2	6.81	1.3E-03
58	Mir703	microRNA 703	6.80	3.0E-02
59	Trdn	triadin	6.73	3.3E-02
60	Rpl3l	ribosomal protein L3-like	6.56	3.1E-03
61	Cpt1b	carnitine palmitoyltransferase 1b, muscle	6.49	3.2E-03
62	Obscn	obscurin, cytoskeletal calmodulin and titin-interacting RhoGEF	6.48	1.6E-04
63	Des	desmin	6.41	3.9E-04
64	Hspb7	heat shock protein family, member 7 (cardiovascular)	6.38	3.6E-05
65	Pgam2	phosphoglycerate mutase 2	6.15	3.5E-04
66	Pkia	protein kinase inhibitor, alpha	5.99	1.0E-03
67	Tcap	titin-cap	5.95	3.8E-02
68	Medag	mesenteric estrogen dependent adipogenesis	5.65	2.2E-08
69	Mlf1	myeloid leukemia factor 1	5.39	1.5E-04

Table B.2, Part I. Continued

	Gene Symbol	Gene	Fold Change	FDR
70	Txlnb	taxilin beta	5.37	2.7E-03
71	Hspb8	heat shock protein 8	5.25	4.5E-05
72	Phkg1	phosphorylase kinase gamma 1	5.21	1.9E-04
73	Eno3	enolase 3, beta muscle	5.01	8.0E-05
74	Synpo2l	synaptopodin 2-like	4.86	1.0E-02
75	Myo18b	myosin XVIIIb	4.78	2.4E-03
76	Ccdc175	coiled-coil domain containing 175	4.72	4.0E-02
77	Cox7a1	cytochrome c oxidase, subunit VIIa 1	4.45	2.0E-03
78	Itgb1bp2	integrin beta 1 binding protein 2	4.38	5.5E-03
79	Serpina3n	serine (or cysteine) peptidase inhibitor, clade A, member 3N	4.31	4.0E-05
80	Myl2	myosin, light polypeptide 2, regulatory, cardiac, slow	4.29	2.9E-02
81	Srl	sarcalumenin	4.27	3.5E-04
82	Ptgs2	prostaglandin-endoperoxide synthase 2	4.24	1.2E-08
83	Ankrd23	ankyrin repeat domain 23	4.23	8.2E-04
84	Flnc	filamin C, gamma	4.18	5.2E-04
85	Jsrp1	junctional sarcoplasmic reticulum protein 1	4.17	4.3E-02
86	Lrrc2	leucine rich repeat containing 2	4.16	6.4E-04
87	Pygm	muscle glycogen phosphorylase	4.12	4.3E-04
88	Tmem38a	transmembrane protein 38A	4.01	3.0E-04
89	Pdlim3	PDZ and LIM domain 3	3.99	5.1E-03
90	Thbs4	thrombospondin 4	3.86	1.6E-03
91	Scn4a	sodium channel, voltage-gated, type IV, alpha	3.82	1.3E-03
92	Ccl2	chemokine (C-C motif) ligand 2	3.75	1.2E-05
93	Glrx3	predicted gene 12669; glutaredoxin 3	3.68	1.1E-04
94	Cox6a2	cytochrome c oxidase, subunit VI a, polypeptide 2	3.67	4.9E-03

Table B.2, Part I. Continued

	Gene Symbol	Gene	Fold Change	FDR
95	Ccl7	chemokine (C-C motif) ligand 7	3.65	3.0E-05
96	Wnt7b	wingless-related MMTV integration site 7B	3.63	1.8E-02
97	Alpk3	alpha-kinase 3	3.59	2.8E-03
98	Tnxb	tenascin XB	3.56	8.9E-04
99	Rpl22l1	ribosomal protein L22 like 1	3.52	2.7E-03
100	Ppp1r3c	protein phosphatase 1, regulatory (inhibitor) subunit 3C	3.50	5.2E-03
101	Wnt1	wingless-related MMTV integration site 1	3.42	1.3E-05
102	Tnfrsf12a	tumor necrosis factor receptor superfamily, member 12a	3.41	2.2E-08
103	Olfr1033	olfactory receptor 1033	3.36	4.2E-04
104	Pm20d2	peptidase M20 domain containing 2	3.32	6.3E-03
105	Tmsb15l	thymosin beta 15b like	3.31	1.4E-02
106	Rbm20	RNA binding motif protein 20	3.28	2.3E-03
107	Asb2	ankyrin repeat and SOCS box-containing 2	3.26	1.2E-03
108	Ndufc1	NADH dehydrogenase (ubiquinone) 1, subcomplex unknown, 1	3.25	4.7E-04
109	Rtn2	reticulon 2 (Z-band associated protein)	3.21	4.9E-03
110	1700063D05Rik	RIKEN cDNA 1700063D05 gene	3.20	1.9E-02
111	Gm6402	predicted pseudogene 6402	3.14	2.6E-02
112	Smtnl2	smoothelin-like 2	3.13	3.3E-03
113	1700007J10Rik	RIKEN cDNA 1700007J10 gene	2.98	2.7E-03
114	Jph2	junctophilin 2	2.94	4.8E-03
115	2310040G24Rik	RIKEN cDNA 2310040G24 gene	2.92	6.0E-03
116	Rpl39	ribosomal protein L39	2.90	4.8E-03
117	Myadml2	myeloid-associated differentiation marker-like 2	2.90	2.4E-02
118	Fsd2	fibronectin type III and SPRY domain containing 2	2.89	1.2E-02
119	Plin4	perilipin 4	2.88	1.8E-03

Table B.2, Part I. Continued

	Gene Symbol	Gene	Fold Change	FDR
120	Gm561	predicted gene 561	2.87	7.2E-03
121	Snrpe	small nuclear ribonucleoprotein E; predicted gene 6487	2.87	1.8E-03
122	Mt2	metallothionein 2	2.86	1.1E-04
123	Nkx6-2	NK6 homeobox 2	2.83	2.2E-02
124	Cmya5	cardiomyopathy associated 5	2.82	2.6E-03
125	Hspb6	heat shock protein, alpha-crystallin-related, B6	2.78	3.5E-02
126	Il20ra	interleukin 20 receptor, alpha	2.76	7.3E-03
127	Rragd	Ras-related GTP binding D	2.75	3.1E-04
128	Pgm5	phosphoglucomutase 5	2.74	4.6E-03
129	Dpt	dermatopontin	2.72	5.2E-04
130	Acyp2	acylphosphatase 2, muscle type	2.72	4.0E-04
131	Ch25h	cholesterol 25-hydroxylase	2.65	5.8E-03
132	Mlxipl	MLX interacting protein-like	2.57	1.0E-02
133	Snrpg	predicted gene 8186; small nuclear ribonucleoprotein polypeptide G	2.56	5.9E-04
134	Gm6634	predicted gene 6634	2.55	4.6E-03
135	LOC100038947	signal-regulatory protein beta 1	2.54	2.7E-03
136	2010107E04Rik	RIKEN cDNA 2010107E04 gene	2.54	2.2E-04
137	Shisa2	shisa homolog 2 (Xenopus laevis)	2.53	1.5E-02
138	Nt5e	5' nucleotidase, ecto	2.53	1.9E-04
139	Nov	nephroblastoma overexpressed gene	2.52	2.8E-02
140	Gm4980	predicted gene 4980	2.52	3.4E-04
141	Cap2	CAP, adenylate cyclase-associated protein, 2 (yeast)	2.49	1.1E-02
142	Zdhhc2	zinc finger, DHHC domain containing 2	2.46	1.4E-02
143	Prkaa2	protein kinase, AMP-activated, alpha 2 catalytic subunit	2.45	2.7E-03
144	Gt(ROSA)26Sor	gene trap ROSA 26, Philippe Soriano	2.44	1.1E-02

Table B.2, Part I. Continued

	Gene Symbol	Gene	Fold Change	FDR
145	0610009L18Rik	RIKEN cDNA 0610009L18 gene	2.44	7.3E-03
146	Nup62-il4i1	predicted gene, 21948	2.42	3.2E-04
147	Snhg6	small nucleolar RNA host gene (non-protein coding) 6	2.40	8.5E-04
148	Rian	RNA imprinted and accumulated in nucleus	2.40	1.6E-03
149	Mrps14	mitochondrial ribosomal protein S14	2.40	1.7E-03
150	Tfpi2	tissue factor pathway inhibitor 2	2.40	1.1E-07
151	Mustn1	musculoskeletal, embryonic nuclear protein 1	2.39	1.7E-03
152	Cyp2r1	cytochrome P450, family 2, subfamily r, polypeptide 1	2.39	3.4E-02
153	Ankrd2	ankyrin repeat domain 2 (stretch responsive muscle)	2.38	2.3E-02
154	Steap1	six transmembrane epithelial antigen of the prostate 1	2.37	3.5E-02
155	3425401B19Rik	RIKEN cDNA 3425401B19 gene	2.37	2.0E-02
156	Gm20939	predicted gene, 20939	2.37	4.3E-02
157	Dmd	dystrophin, muscular dystrophy	2.36	1.2E-02
158	Gprc5a	G protein-coupled receptor, family C, group 5, member A	2.36	1.3E-02
159	Hist2h3c2	histone cluster 2, H3c2	2.35	4.5E-02
160	2310010M20Rik	RIKEN cDNA 2310010M20 gene	2.32	1.1E-02
161	Ncs1	neuronal calcium sensor 1	2.32	1.1E-04
162	5730408K05Rik	RIKEN cDNA 5730408K05 gene	2.31	4.1E-03
163	Sema3c	sema domain, immunoglobulin domain (Ig), short basic domain, secreted, (semaphorin) 3C	2.30	3.1E-03
164	Fhl1	four and a half LIM domains 1	2.30	1.6E-03
165	Nxpe5	neurexophilin and PC-esterase domain family, member 5	2.30	7.2E-04
166	0610039K10Rik	RIKEN cDNA 0610039K10 gene	2.29	2.2E-03
167	Ociad2	OCIA domain containing 2	2.29	1.5E-02
168	Fam69c	family with sequence similarity 69, member C	2.27	1.4E-02
169	Pfkm	phosphofructokinase, muscle	2.26	4.0E-03

Table B.2, Part I. Continued

	Gene Symbol	Gene	Fold Change	FDR
170	Pp2d1	protein phosphatase 2C-like domain containing 1	2.26	1.9E-02
171	Mapt	microtubule-associated protein tau	2.24	4.0E-02
172	H2afz	H2A histone family, member Z; predicted gene 6722; predicted gene 8203	2.24	3.0E-03
173	Igfbp6	insulin-like growth factor binding protein 6	2.24	3.4E-02
174	Cox5a	cytochrome c oxidase, subunit Va	2.23	3.6E-05
175	Hint3	histidine triad nucleotide binding protein 3	2.23	1.5E-02
176	Stard3nl	STARD3 N-terminal like	2.22	5.3E-03
177	AU041133	expressed sequence AU041133	2.22	2.4E-02
178	Cib2	calcium and integrin binding family member 2	2.22	1.2E-04
179	0610010B08Rik	RIKEN cDNA 0610010B08 gene	2.21	1.5E-02
180	Ndrg2	N-myc downstream regulated gene 2	2.20	3.2E-03
181	Cd53	CD53 antigen	2.19	2.1E-03
182	Stac3	SH3 and cysteine rich domain 3	2.18	1.6E-02
183	Lyz1	lysozyme 1	2.17	1.1E-02
184	Ccl12	chemokine (C-C motif) ligand 12	2.16	1.2E-03
185	Rpl39l	ribosomal protein L39-like	2.16	1.4E-02
186	Tpm2	tropomyosin 2, beta	2.14	3.7E-02
187	Slirp	SRA stem-loop interacting RNA binding protein	2.14	6.4E-04
188	1110058L19Rik	RIKEN cDNA 1110058L19 gene	2.14	1.1E-02
189	Tacc2	transforming, acidic coiled-coil containing protein 2	2.14	8.3E-04
190	Tm4sf1	transmembrane 4 superfamily member 1	2.13	5.9E-04
191	Pvt1	plasmacytoma variant translocation 1	2.13	1.4E-03
192	Eda2r	ectodysplasin A2 isoform receptor	2.11	2.4E-02
193	Rfc4	replication factor C (activator 1) 4	2.11	2.0E-03
194	Ddn	dendrin	2.10	4.6E-02

Table B.2, Part I. Continued

	Gene Symbol	Gene	Fold Change	FDR
195	2010003O02Rik	RIKEN cDNA 2010003O02 gene	2.10	6.8E-03
196	Scn7a	sodium channel, voltage-gated, type VII, alpha	2.10	1.8E-02
197	Slc4a4	solute carrier family 4 (anion exchanger), member 4	2.09	1.7E-03
198	Ms4a6d	membrane-spanning 4-domains, subfamily A, member 6D	2.08	3.7E-07
199	Baalc	brain and acute leukemia, cytoplasmic	2.08	3.6E-02
200	Churc1	churchill domain containing 1	2.08	1.2E-03
201	Ptp4a1	protein tyrosine phosphatase 4a1	2.07	1.6E-03
202	Egf	epidermal growth factor	2.07	2.2E-02
203	Ly6a	lymphocyte antigen 6 complex, locus A	2.07	8.0E-05
204	Timm9	translocase of inner mitochondrial membrane 9 homolog (yeast)	2.06	5.9E-04
205	Sar1b	SAR1 gene homolog B (S. cerevisiae)	2.06	3.0E-04
206	Pigp	phosphatidylinositol glycan anchor biosynthesis, class P	2.05	9.8E-03
207	Rps27rt	ribosomal protein S27, retrogene	2.04	4.0E-03
208	Cfl2	cofilin 2, muscle	2.04	4.0E-04
209	Pdzd9	PDZ domain containing 9	2.04	3.7E-02
210	Ndufb6	NADH dehydrogenase (ubiquinone) 1 beta subcomplex, 6	2.03	3.8E-04
211	Zxdb	zinc finger, X-linked, duplicated B	2.03	2.4E-02
212	Uqcc2	ubiquinol-cytochrome c reductase complex assembly factor 2	2.02	1.6E-04
213	Cav2	caveolin 2	2.02	2.4E-03
214	Cisd1	CDGSH iron sulfur domain 1	2.02	8.0E-05
215	Zfp938	zinc finger protein 938	2.02	2.0E-02
216	Ppap2c	phosphatidic acid phosphatase type 2C	2.02	1.6E-03
217	Lars2	leucyl-tRNA synthetase, mitochondrial	2.01	7.3E-04
218	Ngf	nerve growth factor	2.01	1.7E-03
219	Slc25a33	solute carrier family 25, member 33	2.00	5.2E-03

Table B.2, Part I. Continued

	Gene Symbol	Gene	Fold Change	FDR
220	Clec4b1	C-type lectin domain family 4, member b1	2.00	3.8E-02
221	Fdx1	ferredoxin 1	2.00	1.9E-03
222	Gm16596	predicted gene, 16596	1.98	2.5E-02
223	Ccl8	chemokine (C-C motif) ligand 8	1.98	4.3E-02
224	Tnfrsf11b	tumor necrosis factor receptor superfamily, member 11b (osteoprotegerin)	1.98	2.6E-04
225	Lmcd1	LIM and cysteine-rich domains 1	1.97	2.0E-03
226	B3gat2	beta-1,3-glucuronyltransferase 2 (glucuronosyltransferase S)	1.97	1.2E-02
227	Acn9	ACN9 homolog (S. cerevisiae)	1.96	2.1E-02
228	Mir22hg	Mir22 host gene (non-protein coding)	1.95	1.2E-03
229	Rps27a	ribosomal protein S27A	1.95	4.6E-03
230	Art1	ADP-ribosyltransferase 1	1.95	3.3E-02
231	Dmkn	dermokine	1.94	1.1E-02
232	Gng10	guanine nucleotide binding protein (G protein), gamma 10	1.94	2.0E-03
233	5830428M24Rik	RIKEN cDNA 5830428M24 gene	1.93	4.8E-02
234	Mrps18c	mitochondrial ribosomal protein S18C	1.93	1.8E-03
235	Kbtbd3	kelch repeat and BTB (POZ) domain containing 3	1.93	4.8E-02
236	Ndufs4	NADH dehydrogenase (ubiquinone) Fe-S protein 4	1.92	4.8E-04
237	Cntf	ciliary neurotrophic factor	1.92	4.3E-02
238	Kcne4	potassium voltage-gated channel, Isk-related subfamily, gene 4	1.92	2.5E-02
239	Myom3	myomesin family, member 3	1.92	2.6E-02
240	A730017L22Rik	RIKEN cDNA A730017L22 gene	1.92	9.9E-03
241	Smim4	small integral membrane protein 4	1.92	2.8E-02
242	Mss51	MSS51 mitochondrial translational activator	1.92	3.2E-02
243	Popdc2	popeye domain containing 2	1.92	4.1E-02
244	3110007F17Rik	RIKEN cDNA 3110007F17 gene	1.91	2.3E-02

Table B.2, Part I. Continued

	Gene Symbol	Gene	Fold Change	FDR
245	Unc45b	unc-45 homolog B (C. elegans)	1.90	1.2E-03
246	Cenpw	centromere protein W	1.89	2.9E-02
247	Eif1	eukaryotic translation initiation factor 1	1.89	1.8E-03
248	Zfp825	zinc finger protein 825	1.89	1.4E-02
249	Rpl10	ribosomal protein L10	1.89	9.6E-03
250	Tatdn1	TatD DNase domain containing 1	1.88	6.4E-03
251	1110001J03Rik	RIKEN cDNA 1110001J03 gene	1.88	4.3E-03
252	Vbp1	von Hippel-Lindau binding protein 1	1.88	4.0E-03
253	Tmem128	transmembrane protein 128	1.88	5.9E-03
254	Usp13	ubiquitin specific peptidase 13 (isopeptidase T-3)	1.88	2.4E-02
255	Rps14	ribosomal protein S14	1.87	6.4E-03
256	Rps19	ribosomal protein S19	1.87	4.0E-03
257	Rgs16	regulator of G-protein signaling 16	1.87	1.4E-02
258	1110046J04Rik	RIKEN cDNA 1110046J04 gene	1.87	4.5E-02
259	1810032O08Rik	RIKEN cDNA 1810032O08 gene	1.87	2.7E-03
260	Plat	plasminogen activator, tissue	1.86	2.8E-02
261	Mcts1	malignant T cell amplified sequence 1	1.86	9.2E-03
262	Vmp1	vacuole membrane protein 1	1.86	2.2E-04
263	Glmn	glomulin, FKBP associated protein	1.86	2.1E-02
264	Rpl34	ribosomal protein L34	1.86	4.1E-02
265	Eef1e1	eukaryotic translation elongation factor 1 epsilon 1	1.86	1.1E-03
266	1500015O10Rik	RIKEN cDNA 1500015O10 gene	1.86	1.4E-02
267	Klhl30	kelch-like 30 (Drosophila)	1.85	1.0E-02
268	Art3	ADP-ribosyltransferase 3	1.85	4.0E-02
269	Gpd1	glycerol-3-phosphate dehydrogenase 1 (soluble)	1.85	4.5E-03

Table B.2, Part I. Continued

	Gene Symbol	Gene	Fold Change	FDR
270	Tceanc	transcription elongation factor A (SII) N-terminal and central domain containing	1.85	1.4E-02
271	Fam108b	family with sequence similarity 108, member B	1.84	1.1E-02
272	Cox16	cytochrome c oxidase assembly protein 16	1.84	7.6E-03
273	Inhba	inhibin beta-A	1.84	6.2E-03
274	Myeov2	myeloma overexpressed 2	1.83	2.4E-03
275	Ndufb2	NADH dehydrogenase (ubiquinone) 1 beta subcomplex, 2	1.83	8.4E-03
276	2410076I21Rik	RIKEN cDNA 2410076I21 gene	1.83	4.7E-02
277	Ak4	adenylate kinase 4	1.83	1.8E-03
278	Tbca	tubulin cofactor A	1.83	1.2E-02
279	Tspan4	tetraspanin 4	1.82	1.2E-03
280	Hbegf	heparin-binding EGF-like growth factor	1.82	1.3E-03
281	Mettl23	methyltransferase like 23	1.82	2.0E-02
282	Pole4	polymerase (DNA-directed), epsilon 4 (p12 subunit)	1.82	2.4E-03
283	Zfp593	zinc finger protein 593	1.81	9.5E-04
284	Zfp930	zinc finger protein 930	1.81	8.9E-03
285	Pcgf6	polycomb group ring finger 6	1.81	7.4E-03
286	Gls	glutaminase	1.80	3.0E-03
287	B630005N14Rik	RIKEN cDNA B630005N14 gene	1.80	8.8E-03
288	Hgh1	HGH1 homolog	1.80	5.0E-03
289	Zfp932	zinc finger protein 932	1.80	4.1E-03
290	Atf3	activating transcription factor 3	1.80	4.3E-02
291	Slpi	secretory leukocyte peptidase inhibitor	1.80	7.5E-03
292	Synm	synemin, intermediate filament protein	1.80	3.0E-04
293	Lgr6	leucine-rich repeat-containing G protein-coupled receptor 6	1.79	4.1E-02
294	Zfp119a	zinc finger protein 119a	1.79	1.1E-02

Table B.2, Part I. Continued

	Gene Symbol	Gene	Fold Change	FDR
295	Cox11	COX11 homolog, cytochrome c oxidase assembly protein (yeast)	1.79	9.7E-04
296	Hspb1	heat shock protein 1	1.79	4.3E-03
297	Fam96a	family with sequence similarity 96, member A	1.78	2.0E-03
298	Slc2a4	solute carrier family 2 (facilitated glucose transporter), member 4	1.78	2.4E-02
299	2310001H17Rik	RIKEN cDNA 2310001H17 gene	1.78	3.4E-02
300	Sdcbp	syndecan binding protein	1.78	1.2E-03
301	2010315B03Rik	RIKEN cDNA 2010315B03 gene	1.78	7.0E-03
302	Ndufab1	NADH dehydrogenase (ubiquinone) 1, alpha/beta subcomplex, 1	1.78	2.7E-03
303	Ap4s1	adaptor-related protein complex AP-4, sigma 1	1.78	3.7E-03
304	Got1	glutamate oxaloacetate transaminase 1, soluble	1.78	6.4E-04
305	Stbd1	starch binding domain 1	1.78	1.9E-02
306	1700113A16Rik	RIKEN cDNA 1700113A16 gene	1.77	1.7E-02
307	Tmed5	transmembrane emp24 protein transport domain containing 5	1.77	2.8E-03
308	Chac2	ChaC, cation transport regulator homolog 2 (E. coli)	1.77	1.6E-02
309	Crip1	cysteine-rich protein 1 (intestinal)	1.76	8.7E-04
310	Pfkfb1	6-phosphofructo-2-kinase/fructose-2,6-biphosphatase 1	1.76	2.6E-02
311	Tmsb4x	thymosin, beta 4, X chromosome	1.76	7.5E-03
312	0610009B22Rik	RIKEN cDNA 0610009B22 gene	1.76	2.6E-02
313	2210013O21Rik	RIKEN cDNA 2210013O21 gene	1.76	9.1E-03
314	Snhg3	small nucleolar RNA host gene (non-protein coding) 3	1.76	2.0E-03
315	Ms4a7	membrane-spanning 4-domains, subfamily A, member 7	1.75	9.7E-05
316	Tmem256	transmembrane protein 256	1.75	2.1E-03
317	Ugdh	UDP-glucose dehydrogenase	1.75	8.0E-05
318	Car14	carbonic anhydrase 14	1.75	2.1E-02
319	Mdh1	malate dehydrogenase 1, NAD (soluble)	1.74	9.9E-04

Table B.2, Part I. Continued

	Gene Symbol	Gene	Fold Change	FDR
320	Chchd2	coiled-coil-helix-coiled-coil-helix domain containing 2	1.74	3.8E-04
321	Gstp1	glutathione S-transferase, pi 1	1.74	4.1E-03
322	Dancr	differentiation antagonizing non-protein coding RNA	1.74	9.1E-03
323	Slc35a1	solute carrier family 35 (CMP-sialic acid transporter), member 1	1.74	3.8E-03
324	Ndufaf5	NADH dehydrogenase (ubiquinone) complex I, assembly factor 5	1.74	9.8E-03
325	Aldh3a1	aldehyde dehydrogenase family 3, subfamily A1	1.74	4.9E-04
326	Clec4a2	C-type lectin domain family 4, member a2	1.73	4.9E-03
327	Atp5g3	ATP synthase, H+ transporting, mitochondrial F0 complex, subunit c (subunit 9), isoform 3	1.73	9.9E-04
328	Il1b	interleukin 1 beta	1.73	1.7E-03
329	Ndufa4	NADH dehydrogenase (ubiquinone) 1 alpha subcomplex, 4	1.73	5.9E-04
330	Cept1	choline/ethanolaminephosphotransferase 1	1.72	3.8E-03
331	Gabarapl2	gamma-aminobutyric acid (GABA) A receptor-associated protein-like 2	1.72	4.6E-03
332	Smim7	small integral membrane protein 7	1.72	4.6E-03
333	Tmem60	transmembrane protein 60	1.72	3.7E-02
334	Coq10b	coenzyme Q10 homolog B (S. cerevisiae)	1.71	5.2E-03
335	Cklf	chemokine-like factor	1.71	1.5E-02
336	Actr6	ARP6 actin-related protein 6 homolog (yeast)	1.71	1.9E-02
337	Lipt2	lipoyl(octanoyl) transferase 2 (putative)	1.71	1.4E-02
338	Pdrg1	p53 and DNA damage regulated 1	1.71	8.0E-05
339	Cox14	cytochrome c oxidase assembly protein 14	1.71	9.2E-03
340	Fsd1l	fibronectin type III and SPRY domain containing 1-like	1.70	3.1E-02
341	Srxn1	sulfiredoxin 1 homolog (S. cerevisiae)	1.70	8.0E-05
342	Hist1h4i	histone cluster 1, H4i	1.70	2.2E-02
343	1810043H04Rik	RIKEN cDNA 1810043H04 gene	1.70	1.1E-02
344	Cript	cysteine-rich PDZ-binding protein	1.69	5.1E-03

Table B.2, Part I. Continued

	Gene Symbol	Gene	Fold Change	FDR
345	Stard7	START domain containing 7	1.69	1.7E-03
346	C1d	C1D nuclear receptor co-repressor	1.69	1.3E-02
347	Usp2	ubiquitin specific peptidase 2	1.69	9.8E-03
348	Tmod1	tropomodulin 1	1.69	2.1E-02
349	Atp5e	ATP synthase, H+ transporting, mitochondrial F1 complex, epsilon subunit	1.69	3.5E-04
350	Kbtbd8	kelch repeat and BTB (POZ) domain containing 8	1.69	3.3E-02
351	Wdr92	WD repeat domain 92	1.69	2.6E-04
352	Igj	immunoglobulin joining chain	1.69	1.2E-02
353	Clec2d	C-type lectin domain family 2, member d	1.68	2.0E-03
354	Cnbp	cellular nucleic acid binding protein	1.68	8.0E-04
355	Tmem126a	transmembrane protein 126A	1.68	3.2E-03
356	Mettl5	methyltransferase like 5	1.68	1.2E-02
357	Cops5	COP9 (constitutive photomorphogenic) homolog, subunit 5 (Arabidopsis thaliana)	1.68	2.6E-03
358	Amn1	antagonist of mitotic exit network 1 homolog (S. cerevisiae)	1.68	3.4E-02
359	Tcp11l2	t-complex 11 (mouse) like 2	1.68	6.2E-03
360	Psma3	proteasome (prosome, macropain) subunit, alpha type 3; predicted gene 5406	1.68	1.1E-03
361	Nipa2	non imprinted in Prader-Willi/Angelman syndrome 2 homolog (human)	1.68	6.5E-03
362	Fam213b	family with sequence similarity 213, member B	1.67	9.5E-04
363	Pgk1	phosphoglycerate kinase 1	1.67	1.0E-04
364	Tnfsf11	tumor necrosis factor (ligand) superfamily, member 11	1.67	3.1E-03
365	Qrsl1	glutaminyl-tRNA synthase (glutamine-hydrolyzing)-like 1	1.67	2.4E-02
366	Pdp1	protein phosphatase 2C, magnesium dependent, catalytic subunit	1.67	4.2E-03
367	Pde4b	phosphodiesterase 4B, cAMP specific	1.67	5.5E-04
368	Gyk	glycerol kinase	1.67	4.0E-03

Table B.2, Part I. Continued

	Gene Symbol	Gene	Fold Change	FDR
369	Gp49a	glycoprotein 49 A; leukocyte immunoglobulin-like receptor, subfamily B, member 4	1.67	4.8E-04
370	Tefm	transcription elongation factor, mitochondrial	1.66	1.3E-02
371	Ndufa3	NADH dehydrogenase (ubiquinone) 1 alpha subcomplex, 3	1.66	2.3E-03
372	1600020E01Rik	RIKEN cDNA 1600020E01 gene	1.66	2.4E-02
373	Fundc2	FUN14 domain containing 2	1.66	7.2E-03
374	S100a9	S100 calcium binding protein A9 (calgranulin B)	1.66	1.9E-02
375	Scn1b	sodium channel, voltage-gated, type I, beta	1.65	5.6E-04
376	Hnrnpa1	heterogeneous nuclear ribonucleoprotein A1	1.65	2.1E-03
377	Gcsh	glycine cleavage system protein H (aminomethyl carrier)	1.65	6.9E-04
378	Slc25a3	solute carrier family 25 (mitochondrial carrier, phosphate carrier), member 3	1.65	2.7E-03
379	Bbs12	Bardet-Biedl syndrome 12 (human)	1.65	2.8E-02
380	Styx	serine/threonine/tyrosine interaction protein	1.65	1.4E-02
381	Acacb	acetyl-Coenzyme A carboxylase beta	1.65	4.9E-02
382	Eny2	enhancer of yellow 2 homolog (Drosophila); predicted gene 16373	1.64	5.2E-03
383	Ildr2	immunoglobulin-like domain containing receptor 2	1.64	1.9E-02
384	Zfp711	zinc finger protein 711	1.64	3.4E-02
385	Tspan8	tetraspanin 8	1.64	1.6E-02
386	Gnl3	guanine nucleotide binding protein-like 3 (nucleolar)	1.64	1.2E-04
387	Rchy1	ring finger and CHY zinc finger domain containing 1	1.64	7.2E-04
388	Chchd4	coiled-coil-helix-coiled-coil-helix domain containing 4	1.64	1.8E-03
389	Aldoa	aldolase A, fructose-bisphosphate	1.63	1.1E-02
390	Tm2d1	TM2 domain containing 1	1.63	2.1E-02
391	Ctps	cytidine 5'-triphosphate synthase	1.63	8.4E-06
392	Soat2	sterol O-acyltransferase 2	1.63	3.7E-02

Table B.2, Part I. Continued

	Gene Symbol	Gene	Fold Change	FDR
393	Chi3l3	chitinase 3-like 3	1.63	2.2E-02
394	Fyttd1	forty-two-three domain containing 1	1.63	4.6E-03
395	S100a6	S100 calcium binding protein A6 (calcyclin)	1.62	8.3E-04
396	Chuk	conserved helix-loop-helix ubiquitous kinase	1.62	1.1E-02
397	L2hgdh	L-2-hydroxyglutarate dehydrogenase	1.62	1.0E-02
398	Prdx3	peroxiredoxin 3	1.62	7.4E-03
399	Hdgfrp3	hepatoma-derived growth factor, related protein 3	1.62	2.5E-02
400	Bcap29	B-cell receptor-associated protein 29	1.62	1.4E-02
401	Zfp472	zinc finger protein 472	1.62	1.4E-02
402	Idh3a	isocitrate dehydrogenase 3 (NAD+) alpha	1.62	1.7E-03
403	Polr2l	polymerase (RNA) II (DNA directed) polypeptide L	1.61	8.6E-04
404	2900076A07Rik	RIKEN cDNA 2900076A07 gene	1.61	3.7E-02
405	Capza2	capping protein (actin filament) muscle Z-line, alpha 2	1.61	7.1E-03
406	Mrpl13	mitochondrial ribosomal protein L13	1.61	8.0E-05
407	Slc35b3	solute carrier family 35, member B3	1.61	2.5E-02
408	Cd320	CD320 antigen	1.61	3.4E-02
409	Pla2g16	phospholipase A2, group XVI	1.61	4.3E-03
410	Eif3m	eukaryotic translation initiation factor 3, subunit M	1.61	9.2E-04
411	Zfp52	zinc finger protein 52	1.61	3.8E-03
412	Paip2b	poly(A) binding protein interacting protein 2B	1.61	2.8E-03
413	Gem	GTP binding protein (gene overexpressed in skeletal muscle)	1.61	3.3E-02
414	Bvht	braveheart long non-coding RNA	1.61	1.6E-02
415	Ccnb1	cyclin B1	1.61	1.9E-02
416	Acat3	acetyl-Coenzyme A acetyltransferase 3	1.60	1.7E-02
417	2610001J05Rik	RIKEN cDNA 2610001J05 gene	1.60	2.8E-03

Table B.2, Part I. Continued

	Gene Symbol	Gene	Fold Change	FDR
418	Ccr3	chemokine (C-C motif) receptor 3	1.60	3.1E-02
419	Prdx4	peroxiredoxin 4	1.60	5.1E-03
420	Tmem70	transmembrane protein 70	1.60	4.8E-03
421	Fam26e	family with sequence similarity 26, member E	1.60	4.7E-02
422	Pnp	purine-nucleoside phosphorylase	1.60	3.7E-03
423	BC017612	cDNA sequence BC017612	1.60	1.7E-02
424	Wdr12	WD repeat domain 12	1.60	3.4E-04
425	Psmg4	proteasome (prosome, macropain) assembly chaperone 4	1.60	5.0E-02
426	Calcrl	calcitonin receptor-like	1.60	9.9E-03
427	Cyb561	cytochrome b-561	1.59	2.3E-02
428	Polr3k	polymerase (RNA) III (DNA directed) polypeptide K	1.59	5.1E-03
429	Mtcp1	mature T-cell proliferation 1	1.59	8.8E-03
430	Gm17066	predicted gene 17066	1.59	2.1E-02
431	Gnb4	guanine nucleotide binding protein (G protein), beta 4	1.59	3.8E-03
432	Rps21	ribosomal protein S21	1.59	9.2E-03
433	Zfand5	zinc finger, AN1-type domain 5	1.59	7.2E-03
434	Rps15a	ribosomal protein S15A	1.59	3.3E-03
435	Ube2e3	ubiquitin-conjugating enzyme E2E 3, UBC4/5 homolog (yeast)	1.59	1.3E-02
436	Apold1	apolipoprotein L domain containing 1	1.59	4.4E-03
437	Ran	RAN, member RAS oncogene family	1.58	1.1E-03
438	Msr1	macrophage scavenger receptor 1	1.58	3.5E-04
439	Cnep1r1	CTD nuclear envelope phosphatase 1 regulatory subunit 1	1.58	1.1E-02
440	Timm8a1	translocase of inner mitochondrial membrane 8 homolog a1 (yeast)	1.58	7.9E-04
441	Ccr5	chemokine (C-C motif) receptor 5	1.58	4.0E-03
442	Mir17hg	Mir17 host gene (non-protein coding)	1.58	1.2E-02

Table B.2, Part I. Continued

	Gene Symbol	Gene	Fold Change	FDR
443	2700097O09Rik	RIKEN cDNA 2700097O09 gene	1.58	4.4E-02
444	Tceb1	transcription elongation factor B (SIII), polypeptide 1	1.58	9.6E-03
445	Phka1	phosphorylase kinase alpha 1	1.58	8.9E-03
446	Uqcr10	RIKEN cDNA 1110020P15 gene; predicted gene 6293	1.58	8.3E-04
447	Tmem126b	transmembrane protein 126B	1.58	3.6E-02
448	Cmc1	COX assembly mitochondrial protein homolog (S. cerevisiae)	1.58	4.1E-02
449	Tex30	testis expressed 30	1.58	3.9E-02
450	Ifi47	interferon gamma inducible protein 47	1.58	9.8E-03
451	Psmd6	proteasome (prosome, macropain) 26S subunit, non-ATPase, 6	1.58	7.4E-03
452	1110038B12Rik	RIKEN cDNA 1110038B12 gene	1.57	1.3E-02
453	Itga7	integrin alpha 7	1.57	9.6E-03
454	Mmadhc	methylmalonic aciduria (cobalamin deficiency) cblD type, with homocystinuria	1.57	5.2E-03
455	Suz12	suppressor of zeste 12 homolog (Drosophila)	1.57	1.2E-02
456	Rab28	RAB28, member RAS oncogene family	1.57	1.7E-02
457	Mbip	MAP3K12 binding inhibitory protein 1	1.57	2.6E-02
458	Tomm20	translocase of outer mitochondrial membrane 20 homolog (yeast)	1.57	2.5E-03
459	Qtrtd1	queuine tRNA-ribosyltransferase domain containing 1	1.57	9.3E-04
460	Orc4	origin recognition complex, subunit 4	1.56	1.3E-02
461	Hspa1l	heat shock protein 1B; heat shock protein 1A; heat shock protein 1-like	1.56	3.6E-02
462	Vmn1r58	vomeronasal 1 receptor 58	1.56	3.4E-02
463	Drg1	developmentally regulated GTP binding protein 1	1.56	5.1E-03
464	Trim59	tripartite motif-containing 59	1.56	2.2E-02
465	Timm8b	translocase of inner mitochondrial membrane 8 homolog b (yeast)	1.56	2.7E-03
466	Sft2d1	SFT2 domain containing 1	1.56	7.4E-03
467	Uqcrfs1	ubiquinol-cytochrome c reductase, Rieske iron-sulfur polypeptide 1	1.56	1.4E-03

Table B.2, Part I. Continued

	Gene Symbol	Gene	Fold Change	FDR
468	Wdyhv1	WDYHV motif containing 1	1.56	1.7E-02
469	Rangrf	RAN guanine nucleotide release factor	1.56	1.5E-02
470	Unc50	unc-50 homolog (C. elegans)	1.56	1.2E-02
471	Eif1a	eukaryotic translation initiation factor 1A	1.56	3.8E-04
472	Wfdc17	WAP four-disulfide core domain 17	1.56	1.0E-02
473	Hilpda	hypoxia inducible lipid droplet associated	1.56	2.7E-02
474	Atp5j2	ATP synthase, H+ transporting, mitochondrial F0 complex, subunit F2	1.56	6.9E-04
475	Pcmt1	protein-L-isoaspartate (D-aspartate) O-methyltransferase 1	1.55	5.2E-03
476	Atp6v0e	ATPase, H+ transporting, lysosomal V0 subunit E	1.55	1.3E-02
477	Ufc1	ubiquitin-fold modifier conjugating enzyme 1	1.55	2.8E-02
478	Egln3	EGL nine homolog 3 (C. elegans)	1.55	4.0E-02
479	Mkks	McKusick-Kaufman syndrome protein	1.55	1.2E-02
480	Rbbp4	retinoblastoma binding protein 4	1.55	7.8E-03
481	Ube2v2	ubiquitin-conjugating enzyme E2 variant 2	1.55	1.4E-02
482	Mff	mitochondrial fission factor; hypothetical protein LOC637796	1.55	1.1E-02
483	Emp1	epithelial membrane protein 1	1.55	2.3E-03
484	Cd209a	CD209a antigen	1.55	1.3E-02
485	Tmem147	transmembrane protein 147	1.55	4.3E-03
486	Cops8	COP9 (constitutive photomorphogenic) homolog, subunit 8 (Arabidopsis thaliana)	1.55	8.3E-04
487	Tmem167	transmembrane protein 167	1.55	2.4E-02
488	Epdr1	ependymin related protein 1 (zebrafish)	1.55	4.4E-03
489	Aasdhppt	aminoadipate-semialdehyde dehydrogenase-phosphopantetheinyl transferase; hypothetical protein LOC100044211	1.55	1.4E-02
490	Mrps17	mitochondrial ribosomal protein S17	1.55	2.9E-03
491	Skp1a	S-phase kinase-associated protein 1A	1.55	5.2E-03

Table B.2, Part I. Continued

	Gene Symbol	Gene	Fold Change	FDR
492	Tmem59	transmembrane protein 59	1.54	3.4E-02
493	Jtb	jumping translocation breakpoint	1.54	9.2E-03
494	Cd36	CD36 antigen	1.54	9.2E-03
495	Ank	progressive ankylosis	1.54	1.6E-02
496	Ndufa2	NADH dehydrogenase (ubiquinone) 1 alpha subcomplex, 2	1.54	1.8E-03
497	Fgl2	fibrinogen-like protein 2	1.54	1.2E-03
498	Adamts1	a disintegrin-like and metallopeptidase (reprolysin type) with thrombospondin type 1 motif, 1	1.54	1.4E-03
499	Tmem62	transmembrane protein 62	1.54	9.2E-03
500	Med6	mediator of RNA polymerase II transcription, subunit 6 homolog (yeast)	1.54	1.4E-02
501	Fdxacb1	ferredoxin-fold anticodon binding domain containing 1	1.54	2.2E-02
502	Sgk1	serum/glucocorticoid regulated kinase 1	1.54	1.2E-04
503	Pex2	peroxisomal biogenesis factor 2	1.54	7.4E-03
504	Nudt16	nudix (nucleoside diphosphate linked moiety X)-type motif 16	1.54	2.9E-02
505	2700094K13Rik	RIKEN cDNA 2700094K13 gene	1.54	3.1E-02
506	Ldha	lactate dehydrogenase A	1.53	3.0E-04
507	Mmp19	matrix metallopeptidase 19	1.53	2.7E-03
508	Heatr1	HEAT repeat containing 1	1.53	1.3E-03
509	Etfa	electron transferring flavoprotein, alpha polypeptide	1.53	5.2E-03
510	Rps18	ribosomal protein S18	1.53	1.5E-02
511	Cldn25	predicted gene 16492	1.53	9.7E-03
512	Zfx	zinc finger protein X-linked	1.53	2.4E-02
513	Nrep	neuronal regeneration related protein	1.53	1.1E-02
514	Gpr171	G protein-coupled receptor 171	1.53	4.6E-02
515	Slc4a7	solute carrier family 4, sodium bicarbonate cotransporter, member 7	1.53	1.6E-02
516	Anxa1	annexin A1	1.53	8.0E-03

Table B.2, Part I. Continued

	Gene Symbol	Gene	Fold Change	FDR
517	Slc22a5	solute carrier family 22 (organic cation transporter), member 5	1.53	1.4E-02
518	Atp5l	ATP synthase, H+ transporting, mitochondrial F0 complex, subunit G	1.53	4.9E-04
519	Cox17	cytochrome c oxidase assembly protein 17	1.53	1.3E-02
520	Reep1	receptor accessory protein 1	1.53	2.0E-02
521	Fau	Finkel-Biskis-Reilly murine sarcoma virus (FBR-MuSV) ubiquitously expressed (fox derived)	1.52	3.5E-02
522	Tmem64	transmembrane protein 64	1.52	2.9E-02
523	1810026B05Rik	RIKEN cDNA 1810026B05 gene	1.52	1.5E-02
524	Arrdc3	arrestin domain containing 3	1.52	6.4E-04
525	Naa50	N(alpha)-acetyltransferase 50, NatE catalytic subunit	1.52	4.6E-03
526	Mrps6	mitochondrial ribosomal protein S6	1.52	1.1E-02
527	Ddit4l	DNA-damage-inducible transcript 4-like	1.52	2.8E-03
528	Rtn4	reticulon 4	1.52	1.7E-03
529	Fam126b	family with sequence similarity 126, member B	1.52	2.6E-02
530	Prdx1	peroxiredoxin 1	1.52	3.1E-03
531	Srsf7	serine/arginine-rich splicing factor 7	1.52	6.6E-03
532	Aif1	allograft inflammatory factor 1	1.51	2.0E-02
533	Gyg	glycogenin	1.51	1.2E-02
534	Zfp383	zinc finger protein 383	1.51	4.1E-02
535	Rnf138	ring finger protein 138	1.51	3.0E-02
536	Fastkd3	FAST kinase domains 3	1.51	1.6E-02
537	Slc30a4	solute carrier family 30 (zinc transporter), member 4	1.51	2.0E-02
538	Immp1l	IMP1 inner mitochondrial membrane peptidase-like (S. cerevisiae)	1.51	3.1E-02
539	Tubgcp5	tubulin, gamma complex associated protein 5	1.51	1.6E-02
540	Mpp7	membrane protein, palmitoylated 7 (MAGUK p55 subfamily member 7)	1.51	1.2E-02
541	Gm11974	predicted gene 11974	1.51	4.7E-02

Table B.2, Part I. Continued

	Gene Symbol	Gene	Fold Change	FDR
542	Desi2	desumoylating isopeptidase 2	1.51	1.4E-02
543	Echs1	enoyl Coenzyme A hydratase, short chain, 1, mitochondrial	1.51	7.4E-03
544	Vamp3	vesicle-associated membrane protein 3	1.51	1.0E-02
545	Mat2a	methionine adenosyltransferase II, alpha	1.51	9.2E-03
546	Olfr613	olfactory receptor 613	1.51	4.1E-02
547	Actr2	ARP2 actin-related protein 2 homolog (yeast); predicted gene 6828	1.50	1.2E-02
548	Hemk1	HemK methyltransferase family member 1	1.50	3.1E-02
549	2410015M20Rik	RIKEN cDNA 2410015M20 gene	1.50	4.1E-03
550	Ndufb8	NADH dehydrogenase (ubiquinone) 1 beta subcomplex 8	1.50	1.0E-03
551	Smcr7	Smith-Magenis syndrome chromosome region, candidate 7 homolog (human)	1.50	3.9E-03
552	Dynll2	dynein light chain LC8-type 2	1.50	5.5E-03

Table B.2, Part II. List of genes downregulated 3 hours after a single loading session in cortical bone of littermate control animals

	Gene Symbol	Gene	Fold Change	FDR
1	Gm5512	required for meiotic nuclear division 1 homolog (S. cerevisiae); predicted gene 5512	-239.27	4.0E-03
2	Ear12	eosinophil-associated, ribonuclease A family, member 12	-78.20	2.3E-02
3	Ppp1r1b	protein phosphatase 1, regulatory (inhibitor) subunit 1B	-7.23	2.3E-02
4	Ihh	Indian hedgehog	-3.55	1.9E-02
5	2810055G20Rik	RIKEN cDNA 2810055G20 gene	-3.16	3.4E-04
6	Oaz1	ornithine decarboxylase antizyme 1	-3.07	1.9E-03
7	Tgoln2	trans-golgi network protein 2; trans-golgi network protein	-2.67	4.3E-04
8	Map3k19	mitogen-activated protein kinase kinase kinase 19	-2.59	1.8E-02

Table B.2, Part II. Continued

	Gene Symbol	Gene	Fold Change	FDR
9	Cyp2e1	cytochrome P450, family 2, subfamily e, polypeptide 1	-2.58	2.9E-02
10	Muc5b	mucin 5, subtype B, tracheobronchial	-2.51	3.6E-02
11	Il4i1	interleukin 4 induced 1	-2.34	9.1E-03
12	Sost	sclerostin	-2.33	2.2E-08
13	Aox4	aldehyde oxidase 4	-2.30	1.5E-02
14	Amer2	APC membrane recruitment 2	-2.23	3.1E-02
15	Pfdn5	prefoldin 5	-2.11	3.9E-03
16	Reep6	receptor accessory protein 6	-2.06	3.4E-02
17	Fam71b	family with sequence similarity 71, member B	-2.05	2.0E-02
18	Ccdc170	coiled-coil domain containing 170	-2.05	2.2E-03
19	Stc2	stanniocalcin 2	-2.04	8.6E-03
20	Eomes	eomesodermin homolog (Xenopus laevis)	-2.03	1.5E-02
21	A730008H23Rik	RIKEN cDNA A730008H23 gene	-2.02	1.8E-03
22	4930526I15Rik	RIKEN cDNA 4930526I15 gene	-2.01	1.5E-02
23	Gm10532	predicted gene 10532	-1.99	5.4E-03
24	Crebbp	CREB binding protein	-1.97	5.9E-04
25	Ciz1	CDKN1A interacting zinc finger protein 1	-1.91	8.2E-04
26	Ccdc15	coiled-coil domain containing 15	-1.90	2.7E-02
27	Nabp2	nucleic acid binding protein 2	-1.89	2.0E-03
28	Adarb2	adenosine deaminase, RNA-specific, B2	-1.89	3.6E-02
29	Gp1bb	glycoprotein Ib, beta polypeptide	-1.86	9.2E-03
30	Irx6	Iroquois related homeobox 6 (Drosophila)	-1.84	6.5E-03
31	Klf5	Kruppel-like factor 5	-1.84	2.0E-02
32	BC090627	predicted readthrough transcript (NMD candidate), 44502	-1.83	3.7E-02
33	Pram1	PML-RAR alpha-regulated adaptor molecule 1	-1.83	5.9E-03

Table B.2, Part II. Continued

	Gene Symbol	Gene	Fold Change	FDR
34	Bglap	bone gamma carboxyglutamate protein 1	-1.81	1.1E-02
35	Cby1	chibby homolog 1 (Drosophila)	-1.80	7.2E-04
36	Tmem108	transmembrane protein 108	-1.80	3.4E-02
37	Hnrnpul1	heterogeneous nuclear ribonucleoprotein U-like 1	-1.80	2.3E-03
38	Atn1	atrophin 1	-1.77	8.6E-04
39	Gm10684	predicted gene 10684	-1.77	2.8E-02
40	Prrt2	proline-rich transmembrane protein 2	-1.76	1.2E-03
41	Nat6	N-acetyltransferase 6	-1.76	4.1E-03
42	Fkbp2	FK506 binding protein 2	-1.76	2.1E-02
43	Tcf7l1	transcription factor 3	-1.75	2.1E-04
44	Otud3	OTU domain containing 3	-1.75	2.4E-03
45	Ankrd24	ankyrin repeat domain 24	-1.75	5.9E-03
46	Cnot3	CCR4-NOT transcription complex, subunit 3	-1.74	1.2E-03
47	Hspb11	heat shock protein family B (small), member 11	-1.74	6.5E-03
48	Gps2	G protein pathway suppressor 2	-1.74	1.1E-02
49	Dlx5	distal-less homeobox 5	-1.74	1.8E-03
50	Lef1	lymphoid enhancer binding factor 1	-1.74	5.0E-03
51	Slc25a23	solute carrier family 25 (mitochondrial carrier; phosphate carrier), member 23	-1.73	3.4E-04
52	Cdc42ep5	CDC42 effector protein (Rho GTPase binding) 5	-1.73	2.5E-02
53	Zfp362	zinc finger protein 362	-1.73	8.3E-04
54	Tnfrsf13b	tumor necrosis factor receptor superfamily, member 13b	-1.72	2.2E-02
55	1700026D08Rik	RIKEN cDNA 1700026D08 gene	-1.72	1.1E-02
56	Mepe	matrix extracellular phosphoglycoprotein with ASARM motif (bone)	-1.72	2.7E-03
57	Batf2	basic leucine zipper transcription factor, ATF-like 2	-1.72	2.8E-02

Table B.2, Part II. Continued

	Gene Symbol	Gene	Fold Change	FDR
58	Camsap3	calmodulin regulated spectrin-associated protein family, member 3	-1.72	5.2E-03
59	Baiap2l2	BAI1-associated protein 2-like 2	-1.72	3.2E-03
60	Rora	RAR-related orphan receptor alpha	-1.72	3.6E-02
61	Fam81a	family with sequence similarity 81, member A	-1.72	2.5E-02
62	Lyar	Ly1 antibody reactive clone	-1.71	2.1E-02
63	Zfp69	zinc finger protein 69	-1.71	2.6E-02
64	Ccdc55	coiled-coil domain containing 55	-1.70	1.1E-02
65	Amt	aminomethyltransferase	-1.70	7.2E-03
66	Cd68	CD68 antigen	-1.70	1.6E-02
67	Plagl1	pleiomorphic adenoma gene-like 1	-1.70	1.2E-04
68	Mef2d	myocyte enhancer factor 2D	-1.70	2.7E-03
69	Pax5	paired box gene 5	-1.69	4.5E-02
70	Card11	caspase recruitment domain family, member 11	-1.69	4.0E-03
71	Faim3	Fas apoptotic inhibitory molecule 3	-1.69	1.6E-02
72	Celf5	bruno-like 5, RNA binding protein (Drosophila)	-1.69	7.8E-03
73	Alyref2	Aly/REF export factor 2	-1.68	1.2E-02
74	Pacsin1	protein kinase C and casein kinase substrate in neurons 1	-1.68	1.2E-04
75	Gltscr1	glioma tumor suppressor candidate region gene 1	-1.68	2.4E-03
76	Prrt1	proline-rich transmembrane protein 1	-1.67	1.7E-02
77	Jakmip1	janus kinase and microtubule interacting protein 1	-1.67	3.7E-02
78	Shank1	SH3/ankyrin domain gene 1	-1.67	4.9E-03
79	Pin4	protein (peptidyl-prolyl cis/trans isomerase) NIMA-interacting, 4 (parvulin)	-1.66	3.3E-02
80	Cd247	CD247 antigen	-1.66	4.9E-02
81	Crocc	ciliary rootlet coiled-coil, rootletin	-1.66	4.6E-03
82	Pcgf2	polycomb group ring finger 2	-1.66	9.1E-04

Table B.2, Part II. Continued

	Gene Symbol	Gene	Fold Change	FDR
83	Sp100	nuclear antigen Sp100	-1.66	9.6E-03
84	Srp54c	signal recognition particle 54C	-1.65	3.1E-02
85	Fkbpl	FK506 binding protein-like	-1.65	2.3E-02
86	Ubxn1	UBX domain protein 1	-1.65	1.3E-02
87	Chst12	carbohydrate sulfotransferase 12	-1.65	2.2E-03
88	C1qa	complement component 1, q subcomponent, alpha polypeptide	-1.64	3.0E-03
89	Col13a1	collagen, type XIII, alpha 1	-1.64	2.1E-03
90	Clta	clathrin, light polypeptide (Lca)	-1.64	2.8E-03
91	Sap25	sin3A-binding protein, SAP25	-1.64	4.1E-02
92	S100a1	S100 calcium binding protein A1	-1.63	5.1E-03
93	Cd27	CD27 antigen	-1.63	4.7E-02
94	Dvl3	dishevelled 3, dsh homolog (Drosophila)	-1.63	1.7E-03
95	Helz	helicase with zinc finger domain	-1.63	2.6E-03
96	Fli1	Friend leukemia integration 1	-1.63	9.0E-03
97	4922501C03Rik	RIKEN cDNA 4922501C03 gene	-1.63	5.1E-03
98	Azi1	5-azacytidine induced gene 1	-1.63	7.2E-03
99	Kcnab3	potassium voltage-gated channel, shaker-related subfamily, beta member 3	-1.63	2.1E-02
100	Gatad2b	GATA zinc finger domain containing 2B	-1.62	6.9E-04
101	Zscan2	zinc finger and SCAN domain containing 2	-1.62	4.1E-02
102	Sdk2	sidekick homolog 2 (chicken)	-1.62	5.1E-03
103	Leng9	leukocyte receptor cluster (LRC) member 9	-1.61	1.1E-02
104	Mettl21b	methyltransferase like 21B	-1.61	3.1E-02
105	Safb	scaffold attachment factor B	-1.61	1.2E-02
106	Hoxa9	homeo box A9	-1.61	7.8E-03
107	Tmem191c	transmembrane protein 191C	-1.61	7.0E-03

Table B.2, Part II. Continued

	Gene Symbol	Gene	Fold Change	FDR
108	Rassf9	Ras association (RalGDS/AF-6) domain family (N-terminal) member 9	-1.61	4.7E-02
109	Mta3	metastasis associated 3	-1.61	1.1E-02
110	Gpr182	G protein-coupled receptor 182	-1.61	1.5E-02
111	Hlx	H2.0-like homeobox	-1.60	9.9E-03
112	Foxo3	forkhead box O3	-1.60	4.7E-04
113	Tmie	transmembrane inner ear	-1.60	4.1E-03
114	Zfr2	zinc finger RNA binding protein 2	-1.60	4.0E-03
115	Creb3l1	cAMP responsive element binding protein 3-like 1	-1.60	5.9E-03
116	Pqbp1	polyglutamine binding protein 1	-1.60	3.1E-03
117	Grasp	GRP1 (general receptor for phosphoinositides 1)-associated scaffold protein	-1.60	1.4E-02
118	Spen	SPEN homolog, transcriptional regulator (Drosophila)	-1.60	1.6E-03
119	Gm5918	predicted gene 5918	-1.59	3.6E-02
120	Ddrgk1	DDRGK domain containing 1	-1.59	1.3E-02
121	Gem	GTP binding protein (gene overexpressed in skeletal muscle)	-1.59	3.9E-02
122	Safb2	scaffold attachment factor B2	-1.59	2.6E-02
123	Nfix	nuclear factor I/X	-1.59	1.4E-03
124	Myl12b	myosin, light chain 12B, regulatory	-1.59	6.0E-03
125	Ccdc88c	coiled-coil domain containing 88C	-1.59	1.1E-02
126	Ybx1	Y box protein 1	-1.59	1.5E-02
127	Rassf8	Ras association (RalGDS/AF-6) domain family (N-terminal) member 8	-1.59	2.4E-02
128	Sh3bgrl3	SH3 domain binding glutamic acid-rich protein-like 3	-1.59	1.8E-02
129	Trerf1	transcriptional regulating factor 1	-1.59	1.1E-02
130	Slc8a3	solute carrier family 8 (sodium/calcium exchanger), member 3	-1.59	5.9E-04
131	Gli2	GLI-Kruppel family member GLI2	-1.59	1.1E-02
132	Pmvk	phosphomevalonate kinase	-1.59	2.9E-02

Table B.2, Part II. Continued

	Gene Symbol	Gene	Fold Change	FDR
133	Maml3	mastermind like 3 (Drosophila)	-1.59	4.3E-04
134	9930111J21Rik1	RIKEN cDNA 9930111J21 gene	-1.59	2.2E-03
135	Cic	capicua homolog (Drosophila)	-1.58	2.8E-03
136	A630007B06Rik	RIKEN cDNA A630007B06 gene	-1.58	2.0E-03
137	Bfsp1	beaded filament structural protein 1, in lens-CP94	-1.58	2.4E-02
138	Sipa1l3	signal-induced proliferation-associated 1 like 3	-1.58	7.4E-03
139	Acy3	aspartoacylase (aminoacylase) 3	-1.58	2.7E-02
140	Cep250	centrosomal protein 250	-1.58	1.1E-02
141	Taok3	TAO kinase 3	-1.58	1.4E-02
142	Setd1b	SET domain containing 1B	-1.58	2.2E-03
143	Zfhx2	zinc finger homeobox 2; similar to Zinc finger protein 409	-1.58	1.4E-02
144	Bmp7	bone morphogenetic protein 7	-1.58	9.8E-03
145	Prr12	proline rich 12	-1.57	2.0E-03
146	St14	suppression of tumorigenicity 14 (colon carcinoma)	-1.57	4.9E-02
147	Rps26	ribosomal protein S26	-1.57	1.7E-02
148	Mark4	MAP/microtubule affinity-regulating kinase 4	-1.56	1.2E-03
149	Fxyd5	FXYD domain-containing ion transport regulator 5	-1.56	2.6E-02
150	Pou2f2	POU domain, class 2, transcription factor 2	-1.56	1.4E-02
151	Ift57	intraflagellar transport 57 homolog (Chlamydomonas)	-1.56	1.4E-02
152	Zfp618	zinc fingerprotein 618	-1.56	4.4E-02
153	Cnbd2	cyclic nucleotide binding domain containing 2	-1.56	4.7E-02
154	Kank4	KN motif and ankyrin repeat domains 4	-1.56	2.1E-03
155	Hcfc1r1	host cell factor C1 regulator 1 (XPO1-dependent)	-1.56	7.4E-03
156	Ranbp1	RAN binding protein 1	-1.55	2.0E-02
157	Tspyl2	TSPY-like 2	-1.55	1.1E-02

Table B.2, Part II. Continued

	Gene Symbol	Gene	Fold Change	FDR
158	Ogfod3	2-oxoglutarate and iron-dependent oxygenase domain containing 3	-1.55	9.2E-03
159	Ebf3	early B-cell factor 3	-1.55	7.3E-03
160	Scaf4	SR-related CTD-associated factor 4	-1.55	4.9E-03
161	Ccdc88b	coiled-coil domain containing 88B	-1.55	2.0E-02
162	Mll5	myeloid/lymphoid or mixed-lineage leukemia 5	-1.55	3.1E-03
163	Foxp4	forkhead box P4	-1.55	4.9E-03
164	Ebf1	early B-cell factor 1	-1.55	1.7E-03
165	Bmp4	bone morphogenetic protein 4	-1.55	2.0E-03
166	Dtd1	D-tyrosyl-tRNA deacylase 1 homolog (S. cerevisiae)	-1.55	3.1E-02
167	Ldoc1l	leucine zipper, down-regulated in cancer 1-like	-1.55	5.9E-03
168	Mospd3	motile sperm domain containing 3	-1.54	3.9E-03
169	Treml4	triggering receptor expressed on myeloid cells-like 4	-1.54	1.5E-02
170	Lrp5	low density lipoprotein receptor-related protein 5	-1.54	1.2E-03
171	Kifc2	kinesin family member C2	-1.54	2.7E-03
172	Nucb2	nucleobindin 2	-1.54	9.1E-03
173	Atxn2	ataxin 2	-1.54	4.8E-03
174	Polr2j	polymerase (RNA) II (DNA directed) polypeptide J	-1.54	1.3E-02
175	Apobr	apolipoprotein B receptor	-1.54	1.8E-02
176	Ncoa6	nuclear receptor coactivator 6	-1.53	1.1E-03
177	Fads2	fatty acid desaturase 2	-1.53	4.0E-03
178	Pura	purine rich element binding protein A	-1.53	9.6E-03
179	Hoxa7	homeo box A7	-1.53	4.2E-03
180	Rufy4	RUN and FYVE domain containing 4	-1.53	2.8E-02
181	Praf2	PRA1 domain family 2; predicted gene 4168	-1.53	3.1E-03
182	Gripap1	GRIP1 associated protein 1	-1.53	1.1E-02

Table B.2, Part II. Continued

	Gene Symbol	Gene	Fold Change	FDR
183	2310045N01Rik	RIKEN cDNA 2310045N01 gene	-1.53	8.9E-03
184	Fip1l1	FIP1 like 1 (S. cerevisiae)	-1.53	1.1E-02
185	Prrc2a	proline-rich coiled-coil 2A	-1.53	7.2E-03
186	Rp9	retinitis pigmentosa 9 (human)	-1.53	3.6E-02
187	Tle2	transducin-like enhancer of split 2, homolog of Drosophila E(spl)	-1.53	1.7E-03
188	Map2k6	mitogen-activated protein kinase kinase 6	-1.52	2.7E-03
189	Usp53	ubiquitin specific peptidase 53	-1.52	2.7E-02
190	Brd4	bromodomain containing 4	-1.52	6.6E-03
191	Nfatc1	nuclear factor of activated T-cells, cytoplasmic, calcineurin-dependent 1	-1.52	2.1E-02
192	1700034P13Rik	RIKEN cDNA 1700034P13 gene	-1.52	4.9E-02
193	Bcl9l	B-cell CLL/lymphoma 9-like	-1.52	3.1E-03
194	Fam193a	cDNA sequence BC037112	-1.52	2.8E-03
195	2210018M11Rik	RIKEN cDNA 2210018M11 gene	-1.52	2.7E-03
196	Sugp1	SURP and G patch domain containing 1	-1.52	1.2E-02
197	Jdp2	Jun dimerization protein 2	-1.52	9.8E-03
198	Dlx3	distal-less homeobox 3	-1.52	8.4E-03
199	Ubap2l	ubiquitin associated protein 2-like	-1.52	8.9E-03
200	Dbp	D site albumin promoter binding protein	-1.52	1.1E-03
201	Hoxc6	homeo box C6	-1.52	1.9E-02
202	Ttll5	tubulin tyrosine ligase-like family, member 5	-1.52	5.8E-03
203	Ttc28	tetratricopeptide repeat domain 28	-1.52	3.1E-03
204	Shroom3	shroom family member 3	-1.52	3.8E-03
205	Calcoco1	calcium binding and coiled coil domain 1	-1.51	2.8E-03
206	Polr3gl	polymerase (RNA) III (DNA directed) polypeptide G like	-1.51	1.5E-02
207	Ncor1	nuclear receptor co-repressor 1	-1.51	3.3E-03

Table B.2, Part II. Continued

	Gene Symbol	Gene	Fold Change	FDR
208	Ankrd11	ankyrin repeat domain 11	-1.51	1.1E-02
209	Afap1l2	actin filament associated protein 1-like 2	-1.51	4.8E-03
210	Mrps5	predicted gene 13328; mitochondrial ribosomal protein S5	-1.51	3.0E-02
211	Zfp579	zinc finger protein 579	-1.51	1.6E-02
212	Evl	Ena-vasodilator stimulated phosphoprotein	-1.51	1.8E-03
213	Tmsb10	thymosin, beta 10	-1.51	2.9E-02
214	Samd1	sterile alpha motif domain containing 1	-1.51	5.2E-03
215	Hspa2	heat shock protein 2	-1.51	3.7E-03
216	Fam13c	family with sequence similarity 13, member C	-1.50	6.1E-03
217	Prpf38b	PRP38 pre-mRNA processing factor 38 (yeast) domain containing B; similar to PRP38 pre-mRNA processing factor 38 (yeast) domain containing B	-1.50	3.0E-02
218	Ncor2	nuclear receptor co-repressor 2	-1.50	1.2E-02
219	Mad1l1	mitotic arrest deficient 1-like 1	-1.50	1.5E-02
220	Serpinf1	serine (or cysteine) peptidase inhibitor, clade F, member 1	-1.50	1.6E-02

Table B.3: A complete list of genes that were differentially expressed 3 hours following a single loading session in pOC-ERαKO cortical bone in order of decreasing fold change that were: I. upregulated by mechanical loading. There were no downregulated genes. Number of genes (column A), gene symbols (column B), gene names (column C), fold change (column D), false discovery rate (FDR) (column E).

Table B.3, Part I. List of genes upregulated 3 hours after a single loading session in cortical bone of pOC-ERαKO animals

	Gene Symbol	Gene	Fold Change	FDR
1	Il6	interleukin 6	9.57	2.3E-04
2	Ptgs2	prostaglandin-endoperoxide synthase 2	6.21	3.8E-08
3	Ngf	nerve growth factor	3.74	3.0E-09
4	Ccl7	chemokine (C-C motif) ligand 7	3.51	1.0E-02
5	Medag	mesenteric estrogen dependent adipogenesis	3.32	1.1E-03
6	Dmp1	dentin matrix protein 1	3.13	1.2E-04
7	Inhba	inhibin beta-A	3.11	2.4E-07
8	Lgr6	leucine-rich repeat-containing G protein-coupled receptor 6	2.58	5.4E-05
9	Tfpi2	tissue factor pathway inhibitor 2	2.55	5.3E-05
10	Hbegf	heparin-binding EGF-like growth factor	2.32	2.8E-05
11	Notum	notum pectinacetylesterase homolog (Drosophila)	2.23	2.1E-02
12	Glis3	GLIS family zinc finger 3	2.21	1.6E-05
13	Tnfrsf11b	tumor necrosis factor receptor superfamily, member 11b (osteoprotegerin)	2.17	1.5E-02
14	Hivep3	human immunodeficiency virus type I enhancer binding protein 3	2.15	1.0E-07
15	Timp1	tissue inhibitor of metalloproteinase 1	2.01	2.3E-02
16	Srxn1	sulfiredoxin 1 homolog (S. cerevisiae)	1.99	8.3E-05
17	Fam20c	family with sequence similarity 20, member C	1.93	2.1E-03
18	Gem	GTP binding protein (gene overexpressed in skeletal muscle)	1.90	2.1E-02

Table B.3, Part I. Continued

	Gene Symbol	Gene	Fold Change	FDR
19	Adamts1	a disintegrin-like and metallopeptidase (reprolysin type) with thrombospondin type 1 motif, 1	1.74	2.0E-02
20	Socs3	suppressor of cytokine signaling 3	1.74	3.4E-05
21	Ugdh	UDP-glucose dehydrogenase	1.72	3.6E-02
22	Fgf1	fibroblast growth factor 1	1.70	1.5E-02
23	Il1rn	interleukin 1 receptor antagonist	1.69	2.0E-02
24	Heyl	hairy/enhancer-of-split related with YRPW motif-like	1.65	1.8E-06
25	Cd244	CD244 natural killer cell receptor 2B4	1.65	6.4E-03
26	Phlda1	pleckstrin homology-like domain, family A, member 1	1.64	4.0E-03
27	Bcl3	B-cell leukemia/lymphoma 3	1.63	1.7E-02
28	Uck2	uridine-cytidine kinase 2	1.63	3.9E-02
29	Gpatch4	G patch domain containing 4	1.57	3.1E-02
30	Map3k6	mitogen-activated protein kinase kinase kinase 6	1.52	4.3E-03
31	Junb	Jun-B oncogene	1.51	5.2E-03
32	Rrp12	ribosomal RNA processing 12 homolog (S. cerevisiae)	1.51	2.9E-03

Table B.4: A complete list of genes that were differentially expressed 24 hours following a single loading session in littermate control cortical bone in order of decreasing fold change that were: I. upregulated by mechanical loading and II. downregulated by mechanical loading. Number of genes (column A), gene symbols (column B), gene names (column C), fold change (column D), false discovery rate (FDR) (column E).

Table B.4, Part I. List of genes upregulated 24 hours after a single loading session in cortical bone of littermate control animals

	Gene Symbol	Gene	Fold Change	FDR
1	Ptn	pleiotrophin	2.18	1.7E-02
2	Tubb3	tubulin, beta 3; tubulin, beta 3, pseudogene 1	1.85	5.6E-03
3	Bcan	brevican	1.83	8.6E-04
4	Gsg1l	GSG1-like	1.78	1.1E-02
5	Enpp2	ectonucleotide pyrophosphatase/phosphodiesterase 2	1.74	3.1E-02
6	Smpdl3b	sphingomyelin phosphodiesterase, acid-like 3B	1.69	2.5E-02
7	Fkbp11	FK506 binding protein 11	1.63	7.5E-05
8	Hapln4	hyaluronan and proteoglycan link protein 4	1.62	3.4E-02

Table B.4, Part II. List of genes downregulated 24 hours after a single loading session in cortical bone of littermate control animals

	Gene Symbol	Gene	Fold Change	FDR
1	Adrb3	adrenergic receptor, beta 3	-3.90	6.5E-03
2	Wnt7b	wingless-related MMTV integration site 7B	-3.38	4.4E-04
3	Lamc2	laminin, gamma 2	-3.02	7.8E-03
4	Msln	mesothelin	-2.98	4.0E-05
5	Prss46	RIKEN cDNA 1700112C13 gene	-2.83	7.9E-03
6	Htra4	HtrA serine peptidase 4	-2.83	2.7E-03

Table B4, Part II. Continued

	Gene Symbol	Gene	Fold Change	FDR
7	A630023A22Rik	RIKEN cDNA A630023A22 gene	-2.82	3.1E-02
8	Lctl	lactase-like	-2.80	4.4E-04
9	F7	coagulation factor VII	-2.77	1.2E-02
10	Mt2	metallothionein 2	-2.50	4.4E-04
11	Mt1	metallothionein 1	-2.39	4.0E-05
12	Mt3	metallothionein 3	-2.38	1.0E-02
13	Nmb	neuromedin B	-2.33	1.2E-03
14	Tnfrsf9	tumor necrosis factor receptor superfamily, member 9	-2.32	8.4E-04
15	Calcr	calcitonin receptor	-2.31	9.3E-05
16	Rgs9	regulator of G-protein signaling 9	-2.27	3.7E-02
17	Pamr1	peptidase domain containing associated with muscle regeneration 1	-2.15	8.6E-04
18	Ret	ret proto-oncogene	-2.14	1.6E-02
19	Spp1	secreted phosphoprotein 1	-2.12	4.4E-04
20	Mst1r	macrophage stimulating 1 receptor (c-met-related tyrosine kinase)	-2.08	1.2E-03
21	Slc9b2	solute carrier family 9, subfamily B (NHA2, cation proton antiporter 2), member 2	-2.06	5.6E-03
22	Lif	leukemia inhibitory factor	-2.05	3.0E-04
23	Ctsk	cathepsin K	-2.04	7.7E-03
24	Galnt6	UDP-N-acetyl-alpha-D-galactosamine:polypeptide N-acetylgalactosaminyltransferase 6	-2.03	4.0E-05
25	Wisp2	WNT1 inducible signaling pathway protein 2	-2.01	5.4E-05
26	Kcnj15	potassium inwardly-rectifying channel, subfamily J, member 15	-2.00	6.0E-03
27	Dcstamp	dentrocyte expressed seven transmembrane protein	-2.00	1.9E-03
28	Gm6377	predicted gene 6377	-1.99	1.9E-02
29	Slc37a2	solute carrier family 37 (glycerol-3-phosphate transporter), member 2	-1.95	1.4E-02
30	Sfrp4	secreted frizzled-related protein 4	-1.89	4.3E-06
31	Smoc1	SPARC related modular calcium binding 1	-1.89	1.8E-05

Table B4, Part II. Continued

	Gene Symbol	Gene	Fold Change	FDR
32	Oscar	osteoclast associated receptor	-1.83	3.6E-02
33	Hyal1	hyaluronoglucosaminidase 1	-1.80	1.6E-02
34	Oit3	oncoprotein induced transcript 3	-1.78	7.7E-03
35	Tnfrsf11a	tumor necrosis factor receptor superfamily, member 11a	-1.75	5.1E-03
36	Uchl1	ubiquitin carboxy-terminal hydrolase L1	-1.70	2.4E-02
37	Snx10	sorting nexin 10	-1.70	7.9E-03
38	Tfrc	transferrin receptor	-1.69	2.3E-02
39	Rcan1	regulator of calcineurin 1	-1.69	3.9E-02
40	Fos	FBJ osteosarcoma oncogene	-1.68	1.1E-02
41	Tppp3	tubulin polymerization-promoting protein family member 3	-1.67	4.8E-02
42	Gpr137b	similar to Gpr137b protein; G protein-coupled receptor 137B	-1.65	2.5E-02
43	Fam198b	RIKEN cDNA 1110032E23 gene	-1.65	1.6E-02
44	Amz1	archaelysin family metallopeptidase 1	-1.63	7.8E-03
45	Ccr1	chemokine (C-C motif) receptor 1	-1.63	1.0E-02
46	Cyp4v3	cytochrome P450, family 4, subfamily v, polypeptide 3	-1.62	5.1E-03
47	Bcl2a1b	B-cell leukemia/lymphoma 2 related protein A1b	-1.62	6.9E-03
48	Gpr137b-ps	G protein-coupled receptor 137B, pseudogene	-1.62	1.4E-02
49	Prdm1	PR domain containing 1, with ZNF domain	-1.58	7.7E-03
50	Glb1	galactosidase, beta 1	-1.56	4.0E-02
51	Hexb	hexosaminidase B	-1.56	4.9E-02
52	Met	met proto-oncogene	-1.55	6.0E-03
53	Ank	progressive ankylosis	-1.55	5.1E-03
54	Megf10	multiple EGF-like-domains 10	-1.55	1.6E-02
55	Cd83	CD83 antigen	-1.54	8.9E-04
56	Enpp1	ectonucleotide pyrophosphatase/phosphodiesterase 1	-1.54	7.9E-03
57	Capg	capping protein (actin filament), gelsolin-like	-1.53	4.8E-02

Table B.5: A complete list of genes that were differentially expressed 24 hours following a single loading session in pOC-ERαKO cortical bone in order of decreasing fold change that were: I. upregulated by mechanical loading and II. downregulated by mechanical loading. Number of genes (column A), gene symbols (column B), gene names (column C), fold change (column D), false discovery rate (FDR) (column E).

Table B.5, Part I. List of genes upregulated 24 hours after a single loading session in cortical bone of pOC-ERαKO animals

	Gene Symbol	Gene	Fold Change	FDR
1	Rspo4	R-spondin family, member 4	137.71	3.1E-18
2	Oprd1	opioid receptor, delta 1	49.46	5.9E-05
3	Serpina1a	serine (or cysteine) peptidase inhibitor, clade A, member 1A	29.46	1.1E-02
4	Prg4	proteoglycan 4 (megakaryocyte stimulating factor, articular superficial zone protein)	5.82	4.8E-02
5	Gsg1l	GSG1-like	1.92	3.1E-03
6	Tubb3	tubulin, beta 3; tubulin, beta 3, pseudogene 1	1.62	4.9E-02

Table B.5, Part II. List of genes downregulated 24 hours after a single loading session in cortical bone of pOC-ERaKO animals

	Gene Symbol	Gene	Fold Change	FDR
1	Wisp2	WNT1 inducible signaling pathway protein 2	-2.15	9.6E-10
2	Sfrp2	secreted frizzled-related protein 2	-2.00	5.3E-02
3	Galnt6	UDP-N-acetyl-alpha-D-galactosamine:polypeptide N-acetylgalactosaminyltransferase 6	-1.68	1.1E-02
4	Cd83	CD83 antigen	-1.51	2.7E-02
5	Ccr1	chemokine (C-C motif) receptor 1	-1.51	2.7E-02

Table B.6: A complete list of genes that were differentially expressed 3 hours following a single loading session in littermate control cancellous bone in order of decreasing fold change that were: I. upregulated by mechanical loading. There were no downregulated genes. Number of genes (column A), gene symbols (column B), gene names (column C), fold change (column D), false discovery rate (FDR) (column E).

Table B.6, Part I. List of genes upregulated 3 hours after a single loading session in cancellous bone of littermate control animals

	Gene Symbol	Gene	Fold Change	FDR
1	Wnt1	wingless-related MMTV integration site 1	6.55	8.2E-12
2	Hspb7	heat shock protein family, member 7 (cardiovascular)	3.90	3.5E-02
3	Medag	mesenteric estrogen dependent adipogenesis	3.86	6.4E-04
4	Ch25h	cholesterol 25-hydroxylase	3.23	4.1E-02
5	Tnfrsf12a	tumor necrosis factor receptor superfamily, member 12a	3.14	1.7E-06
6	Baalc	brain and acute leukemia, cytoplasmic	3.11	2.0E-02
7	Ptgs2	prostaglandin-endoperoxide synthase 2	3.09	1.7E-04
8	Nt5e	5' nucleotidase, ecto	2.75	1.7E-04
9	Tnfrsf11b	tumor necrosis factor receptor superfamily, member 11b (osteoprotegerin)	2.69	2.1E-08
10	Arc	activity regulated cytoskeletal-associated protein	2.59	1.8E-02
11	Mustn1	musculoskeletal, embryonic nuclear protein 1	2.49	1.8E-02
12	Lgr6	leucine-rich repeat-containing G protein-coupled receptor 6	2.42	2.0E-02
13	Ngf	nerve growth factor	2.40	8.1E-04
14	Ncs1	neuronal calcium sensor 1	2.34	1.7E-03
15	Dmp1	dentin matrix protein 1	2.26	1.5E-02
16	Timp1	tissue inhibitor of metalloproteinase 1	2.14	1.5E-02
17	Wnt10b	wingless related MMTV integration site 10b	2.03	2.9E-03
18	Fam20c	family with sequence similarity 20, member C	1.93	7.6E-03
19	Aldh3a1	aldehyde dehydrogenase family 3, subfamily A1	1.77	4.2E-03

Table B.6, Part I. Continued

	Gene Symbol	Gene	Fold Change	FDR
20	Ugdh	UDP-glucose dehydrogenase	1.59	1.4E-02
21	Srxn1	sulfiredoxin 1 homolog (S. cerevisiae)	1.52	2.0E-02

Table B.7: A complete list of genes that were differentially expressed 3 hours following a single loading session in pOC-ERαKO cancellous bone in order of decreasing fold change that were: I. upregulated by mechanical loading and II. downregulated by mechanical loading. Number of genes (column A), gene symbols (column B), gene names (column C), fold change (column D), false discovery rate (FDR) (column E).

Table B.7, Part I. List of genes upregulated 3 hours after a single loading session in cancellous bone of pOC-ERαKO animals

	Gene Symbol	Gene	Fold Change	FDR
1	Amd1	S-adenosylmethionine decarboxylase 1	156.89	1.3E-02
2	Wnt7b	wingless-related MMTV integration site 7B	8.42	5.9E-06
3	Wnt1	wingless-related MMTV integration site 1	7.41	8.2E-06
4	Ptgs2	prostaglandin-endoperoxide synthase 2	6.85	3.7E-08
5	Fam180a	cDNA sequence BC064033	5.25	4.7E-02
6	Hspb7	heat shock protein family, member 7 (cardiovascular)	5.03	6.3E-04
7	Medag	mesenteric estrogen dependent adipogenesis	4.42	7.9E-05
8	Lgr6	leucine-rich repeat-containing G protein-coupled receptor 6	3.74	1.5E-08
9	Baalc	brain and acute leukemia, cytoplasmic	3.72	2.3E-03
10	Tnfrsf12a	tumor necrosis factor receptor superfamily, member 12a	3.66	3.1E-06
11	Mustn1	musculoskeletal, embryonic nuclear protein 1	3.53	3.2E-04
12	Dmp1	dentin matrix protein 1	3.46	1.7E-05
13	Nt5e	5' nucleotidase, ecto	3.36	2.0E-03
14	Notum	notum pectinacetylesterase homolog (Drosophila)	3.19	3.1E-05
15	Miat	myocardial infarction associated transcript (non-protein coding)	3.16	9.7E-04
16	Timp1	tissue inhibitor of metalloproteinase 1	2.89	6.4E-06
17	Tfpi2	tissue factor pathway inhibitor 2	2.87	2.5E-06
18	Ngf	nerve growth factor	2.65	2.3E-04
19	Wnt10b	wingless related MMTV integration site 10b	2.61	4.5E-04

Table B.7, Part I. Continued

	Gene Symbol	Gene	Fold Change	FDR
20	Tnfrsf11b	tumor necrosis factor receptor superfamily, member 11b (osteoprotegerin)	2.60	4.6E-04
21	Fam20c	family with sequence similarity 20, member C	2.48	4.9E-07
22	Ngef	neuronal guanine nucleotide exchange factor	2.18	8.4E-03
23	Cspg4	chondroitin sulfate proteoglycan 4	2.14	1.7E-04
24	Hivep3	human immunodeficiency virus type I enhancer binding protein 3	1.96	1.5E-05
25	Fgf1	fibroblast growth factor 1	1.89	6.3E-04
26	Ank	progressive ankylosis	1.86	3.7E-03
27	Cd276	CD276 antigen	1.81	7.3E-03
28	Gas1	growth arrest specific 1	1.81	4.6E-04
29	Ugdh	UDP-glucose dehydrogenase	1.79	1.5E-02
30	Srxn1	sulfiredoxin 1 homolog (S. cerevisiae)	1.78	3.5E-03
31	Heyl	hairy/enhancer-of-split related with YRPW motif-like	1.74	1.7E-07
32	Snai1	snail homolog 1 (Drosophila)	1.71	2.0E-03
33	Adamtsl4	ADAMTS-like 4	1.66	4.7E-02
34	Mical2	microtubule associated monoxygenase, calponin and LIM domain containing 2	1.62	2.9E-02
35	Map3k6	mitogen-activated protein kinase kinase kinase 6	1.56	2.0E-03
36	Fam129b	family with sequence similarity 129, member B	1.55	4.5E-03
37	S100a10	S100 calcium binding protein A10 (calpactin)	1.52	3.7E-02
38	Smyd5	SET and MYND domain containing 5	1.51	2.2E-02

Table B.7, Part II. List of genes downregulated 3 hours after a single loading session in cancellous bone of pOC-ERαKO animals

	Gene Symbol	Gene	Fold Change	FDR
1	Serpina3c	serine (or cysteine) peptidase inhibitor, clade A, member 3C	-2.14	3.1E-03
2	Gm4951	predicted gene 4951	-1.55	4.9E-02

Table B.8: A complete list of genes that were differentially expressed 24 hours following a single loading session in littermate control cancellous bone in order of decreasing fold change that were: I. upregulated by mechanical loading and II. downregulated by mechanical loading. Number of genes (column A), gene symbols (column B), gene names (column C), fold change (column D), false discovery rate (FDR) (column E).

Table B.8, Part I. List of genes upregulated 24 hours after a single loading session in cancellous bone of littermate control animals

	Gene Symbol	Gene	Fold Change	FDR
1	Zim1	zinc finger, imprinted 1	10.91	1.7E-02
2	Lrrn1	leucine rich repeat protein 1, neuronal	9.59	1.6E-03
3	Mfap4	microfibrillar-associated protein 4	8.16	3.2E-02
4	Trpm6	transient receptor potential cation channel, subfamily M, member 6	4.34	3.2E-02
5	Panx3	pannexin 3	2.34	1.6E-03
6	Ddit4l	DNA-damage-inducible transcript 4-like	1.58	3.2E-02

Table B.8, Part II. List of genes downregulated 24 hours after a single loading session in cancellous bone of littermate control animals

	Gene Symbol	Gene	Fold Change	FDR
1	Atp6v0e2	ATPase, H+ transporting, lysosomal V0 subunit E2	-2.22	3.2E-02
2	Fcer2a	Fc receptor, IgE, low affinity II, alpha polypeptide	-1.64	3.2E-02

Table B.9: A complete list of genes that were differentially expressed 24 hours following a single loading session in pOC-ERαKO cancellous bone in order of decreasing fold change that were: I. upregulated by mechanical loading and II. downregulated by mechanical loading. Number of genes (column A), gene symbols (column B), gene names (column C), fold change (column D), false discovery rate (FDR) (column E).

Table B.9, Part I. List of genes upregulated 24 hours after a single loading session in cancellous bone of pOC-ERαKO animals

	Gene Symbol	Gene	Fold Change	FDR
1	Rspo4	R-spondin family, member 4	537.25	3.4E-29
2	Ear12	eosinophil-associated, ribonuclease A family, member 12	292.22	1.0E-02
3	Myoz2	myozenin 2	51.42	2.3E-02
4	Oprd1	opioid receptor, delta 1	43.32	5.4E-06
5	Serpina1a	serine (or cysteine) peptidase inhibitor, clade A, member 1A	24.00	7.4E-03
6	Pax1	paired box gene 1	22.96	1.2E-02
7	Slc38a3	solute carrier family 38, member 3	17.19	1.4E-02
8	Chad	chondroadherin	16.49	5.0E-02
9	Syt8	synaptotagmin VIII	14.15	5.3E-02
10	Fxyd2	FXYD domain-containing ion transport regulator 2	14.06	2.5E-02
11	Hapln1	hyaluronan and proteoglycan link protein 1	11.54	3.7E-02
12	Ncmap	noncompact myelin associated protein	11.21	1.0E-02
13	Ihh	Indian hedgehog	11.10	3.4E-02
14	Zcchc5	zinc finger, CCHC domain containing 5	9.28	9.5E-03
15	Pcolce2	procollagen C-endopeptidase enhancer 2	8.78	2.3E-02
16	Zim1	zinc finger, imprinted 1	8.23	6.2E-03
17	Acan	aggrecan	8.15	1.0E-02
18	Prkg2	protein kinase, cGMP-dependent, type II	8.09	3.0E-02
19	Fam180a	cDNA sequence BC064033	7.71	2.5E-02

Table B.9, Part I. Continued

	Gene Symbol	Gene	Fold Change	FDR
20	Nrk	Nik related kinase	7.51	7.1E-03
21	H19	H19 fetal liver mRNA	6.95	8.5E-03
22	Plekhb1	pleckstrin homology domain containing, family B (evectins) member 1	6.91	1.2E-02
23	Tcfl5	transcription factor-like 5 (basic helix-loop-helix)	6.53	1.1E-02
24	Col4a5	collagen, type IV, alpha 5	4.98	1.2E-02
25	B230206H07Rik	RIKEN cDNA B230206H07 gene	4.85	2.2E-02
26	Tpd52l1	tumor protein D52-like 1	4.55	2.3E-02
27	Sstr2	somatostatin receptor 2	4.36	3.6E-02
28	Extl1	exostoses (multiple)-like 1	3.99	3.4E-02
29	Eps8l2	EPS8-like 2	3.89	1.1E-02
30	Crispld1	cysteine-rich secretory protein LCCL domain containing 1	3.84	2.3E-02
31	Mgp	matrix Gla protein	3.59	7.5E-03
32	Steap1	six transmembrane epithelial antigen of the prostate 1	3.53	7.4E-03
33	Scube1	signal peptide, CUB domain, EGF-like 1	3.53	1.6E-04
34	Sox8	SRY-box containing gene 8	3.50	1.1E-02
35	Panx3	pannexin 3	3.32	7.4E-03
36	Sox9	SRY-box containing gene 9	3.21	1.0E-02
37	Wscd2	WSC domain containing 2	3.05	9.7E-03
38	Gfpt2	glutamine fructose-6-phosphate transaminase 2	3.02	5.2E-02
39	Gli1	GLI-Kruppel family member GLI1	2.93	8.9E-04
40	Ppa1	pyrophosphatase (inorganic) 1	2.89	2.7E-02
41	Thbs3	thrombospondin 3	2.85	1.0E-02
42	Stc2	stanniocalcin 2	2.79	5.0E-02
43	Capn6	calpain 6	2.76	3.4E-02
44	Cpa6	carboxypeptidase A6	2.74	5.5E-03
45	Notum	notum pectinacetylesterase homolog (Drosophila)	2.72	7.4E-03

Table B.9, Part I. Continued

	Gene Symbol	Gene	Fold Change	FDR
46	Glt25d2	glycosyltransferase 25 domain containing 2	2.71	2.4E-02
47	Ptgs2	prostaglandin-endoperoxide synthase 2	2.70	4.6E-03
48	Slc38a4	solute carrier family 38, member 4	2.65	2.5E-02
49	Aldh1a3	aldehyde dehydrogenase family 1, subfamily A3	2.61	1.7E-04
50	Kif26b	kinesin family member 26B	2.56	5.0E-02
51	Arsi	arylsulfatase i	2.54	4.5E-02
52	Ntrk2	neurotrophic tyrosine kinase, receptor, type 2	2.53	6.1E-02
53	Ptch1	patched homolog 1	2.50	1.9E-03
54	Fmod	fibromodulin	2.41	1.1E-02
55	Prkcz	protein kinase C, zeta	2.40	5.2E-02
56	Kcnc3	potassium voltage gated channel, Shaw-related subfamily, member 3	2.35	1.0E-02
57	Enpp2	ectonucleotide pyrophosphatase/phosphodiesterase 2	2.32	4.1E-04
58	Ephb2	Eph receptor B2	2.24	1.7E-04
59	Cdkn1c	cyclin-dependent kinase inhibitor 1C (P57)	2.18	1.6E-03
60	Peg3	paternally expressed 3; antisense transcript gene of Peg3	2.18	2.4E-03
61	Ptn	pleiotrophin	2.18	2.3E-02
62	Miat	myocardial infarction associated transcript (non-protein coding)	2.02	2.5E-02
63	Peg3as	Peg3 opposite strand	2.02	6.1E-02
64	Fn1	fibronectin 1	1.97	1.6E-02
65	Gli2	GLI-Kruppel family member GLI2	1.95	4.6E-06
66	Car12	carbonic anyhydrase 12	1.93	1.4E-02
67	Nog	noggin	1.93	5.2E-02
68	Ntn1	netrin 1	1.93	6.9E-03
69	Papss2	3'-phosphoadenosine 5'-phosphosulfate synthase 2	1.93	2.4E-03
70	Nphp4	nephronophthisis 4 (juvenile) homolog (human)	1.87	1.1E-02
71	Zfp13	zinc finger protein 13	1.85	3.9E-02

Table B.9, Part I. Continued

	Gene Symbol	Gene	Fold Change	FDR
72	Nid2	nidogen 2	1.82	1.1E-03
73	Smpdl3b	sphingomyelin phosphodiesterase, acid-like 3B	1.79	2.7E-02
74	Cobll1	Cobl-like 1	1.79	2.7E-02
75	Shisa4	shisa homolog 4 (Xenopus laevis)	1.73	3.3E-02
76	Plagl1	pleiomorphic adenoma gene-like 1	1.73	2.6E-03
77	Col6a3	collagen, type VI, alpha 3	1.73	1.1E-02
78	Tgfb2	transforming growth factor, beta 2	1.72	5.2E-02
79	Foxc2	forkhead box C2	1.71	5.2E-02
80	Mcc	mutated in colorectal cancers	1.70	4.5E-02
81	Lrig3	leucine-rich repeats and immunoglobulin-like domains 3	1.70	2.2E-02
82	Frzb	frizzled-related protein	1.69	5.1E-02
83	Tubb3	tubulin, beta 3; tubulin, beta 3, pseudogene 1	1.67	7.4E-03
84	Ccdc80	coiled-coil domain containing 80	1.65	1.1E-02
85	Fads2	fatty acid desaturase 2	1.64	1.9E-03
86	Gsg1l	GSG1-like	1.64	2.5E-02
87	Trpv4	transient receptor potential cation channel, subfamily V, member 4	1.64	4.1E-02
88	Pcdh17	protocadherin 17	1.64	6.1E-02
89	Cspg4	chondroitin sulfate proteoglycan 4	1.59	3.5E-02
90	Snai1	snail homolog 1 (Drosophila)	1.58	5.9E-02
91	Sox12	SRY-box containing gene 12	1.57	5.3E-02
92	Adamts12	a disintegrin-like and metallopeptidase (reprolysin type) with thrombospondin type 1 motif, 12	1.56	1.7E-02
93	Lrrc16a	leucine rich repeat containing 16A	1.56	1.0E-02
94	Scd2	stearoyl-Coenzyme A desaturase 2	1.55	7.4E-03
95	A730008H23Rik	RIKEN cDNA A730008H23 gene	1.53	2.4E-02
96	Gdf10	growth differentiation factor 10	1.53	4.1E-02

Table B.9, Part II. List of genes downregulated 24 hours after a single loading session in cancellous bone of pOC-ERαKO animals

	Gene Symbol	Gene	Fold Change	FDR
1	Ear7	eosinophil-associated, ribonuclease A family, member 7	-45.51	3.3E-02
2	Klre1	killer cell lectin-like receptor family E member 1	-3.12	5.0E-02
3	Klrd1	killer cell lectin-like receptor, subfamily D, member 1	-2.64	2.3E-02
4	Gm4841	predicted gene 4841	-2.34	4.8E-02
5	Lyz1	lysozyme 1	-2.20	4.6E-02
6	Pdzd3	PDZ domain containing 3	-2.16	6.3E-02
7	Mt2	metallothionein 2	-2.15	4.8E-03
8	P2ry10	purinergic receptor P2Y, G-protein coupled 10	-2.00	2.4E-02
9	Amica1	adhesion molecule, interacts with CXADR antigen 1	-1.87	2.4E-03
10	Siglech	sialic acid binding Ig-like lectin H	-1.87	4.1E-04
11	Lpl	lipoprotein lipase; similar to Lipoprotein lipase precursor (LPL)	-1.87	1.7E-04
12	Ms4a1	membrane-spanning 4-domains, subfamily A, member 1	-1.87	1.0E-02
13	AU021092	expressed sequence AU021092	-1.81	4.1E-02
14	Il1b	interleukin 1 beta	-1.81	1.0E-02
15	Klrk1	killer cell lectin-like receptor subfamily K, member 1	-1.81	7.8E-03
16	Rspo2	R-spondin 2 homolog (Xenopus laevis)	-1.80	3.0E-02
17	Cd53	CD53 antigen	-1.78	2.3E-02
18	Slpi	secretory leukocyte peptidase inhibitor	-1.77	5.0E-02
19	Ifi27l2a	interferon, alpha-inducible protein 27 like 2A	-1.76	2.4E-03
20	Ifi47	interferon gamma inducible protein 47	-1.76	3.5E-02
21	Esm1	endothelial cell-specific molecule 1	-1.74	6.2E-03
22	Klra2	killer cell lectin-like receptor, subfamily A, member 2	-1.73	3.1E-02
23	Ccl5	chemokine (C-C motif) ligand 5	-1.71	2.4E-02
24	Serpina3f	serine (or cysteine) peptidase inhibitor, clade A, member 3F	-1.71	2.4E-02
25	Ccl6	chemokine (C-C motif) ligand 6	-1.70	1.7E-04

Table B9, Part II. Continued

	Gene Symbol	Gene	Fold Change	FDR
26	AW112010	expressed sequence AW112010	-1.69	5.1E-03
27	Ubd	ubiquitin D	-1.68	3.3E-02
28	Retnlg	resistin like gamma	-1.68	2.4E-03
29	Ddx60	DEAD (Asp-Glu-Ala-Asp) box polypeptide 60	-1.67	1.4E-02
30	H2-Ob	histocompatibility 2, O region beta locus	-1.67	1.0E-02
31	Cd209a	CD209a antigen	-1.65	1.0E-02
32	Fpr1	formyl peptide receptor 1	-1.64	1.5E-02
33	Slfn4	schlafen 4	-1.63	1.1E-02
34	Bst1	bone marrow stromal cell antigen 1	-1.62	1.1E-02
35	Ear1	eosinophil-associated, ribonuclease A family, member 1	-1.62	5.1E-02
36	Znf41-ps	ZNF41, pseudogene	-1.61	4.5E-02
37	Ccr3	chemokine (C-C motif) receptor 3	-1.60	2.5E-02
38	F630028O10Rik	RIKEN cDNA F630028O10 gene	-1.60	1.0E-02
39	Il2rb	interleukin 2 receptor, beta chain	-1.59	4.0E-02
40	Emr4	EGF-like module containing, mucin-like, hormone receptor-like sequence 4	-1.59	7.4E-03
41	Gimap3	similar to immunity-associated nucleotide 4; GTPase, IMAP family member 3	-1.58	2.7E-02
42	Trim30d	tripartite motif-containing 30D	-1.57	5.5E-02
43	Ccl9	chemokine (C-C motif) ligand 9	-1.57	1.1E-02
44	Cyp4b1	predicted gene 12839; cytochrome P450, family 4, subfamily b, polypeptide 1	-1.57	2.3E-02
45	Kmo	kynurenine 3-monooxygenase (kynurenine 3-hydroxylase)	-1.56	4.8E-02
46	Pyhin1	pyrin and HIN domain family, member 1	-1.55	1.6E-02
47	Kitl	kit ligand	-1.54	3.1E-03
48	Il1f9	interleukin 1 family, member 9	-1.52	6.1E-02
49	Slc40a1	solute carrier family 40 (iron-regulated transporter), member 1	-1.52	2.4E-02

Table B9, Part II. Continued

	Gene Symbol	Gene	Fold Change	FDR
50	Fgl2	fibrinogen-like protein 2	-1.51	2.3E-02
51	Bst2	bone marrow stromal cell antigen 2	-1.51	7.4E-03

Table B.10: A complete list of genes that were differentially expressed in naïve control cortical vs cancellous bone in order of decreasing fold change that were: I. more highly expressed in cortical bone and II. More highly expressed in cancellous bone. Number of genes (column A), gene symbols (column B), gene names (column C), fold change (column D), false discovery rate (FDR) (column E). * indicates contamination as determined by Ayturk et al.

Table B.10, Part I. List of genes more highly expressed in naïve control cortical bone

	Gene Symbol	Gene	Fold Change	FDR
1	Myh2*	myosin, heavy polypeptide 2, skeletal muscle, adult; myosin, heavy polypeptide 1, skeletal muscle, adult	1849.60	1.2E-08
2	Myot*	myotilin	482.93	4.2E-06
3	Myh1*	myosin, heavy polypeptide 2, skeletal muscle, adult; myosin, heavy polypeptide 1, skeletal muscle, adult	456.18	2.3E-07
4	Myh4*	myosin, heavy polypeptide 4, skeletal muscle	250.02	2.5E-05
5	Eef1a2*	eukaryotic translation elongation factor 1 alpha 2	165.88	9.3E-05
6	Acta1*	actin, alpha 1, skeletal muscle	130.00	3.2E-05
7	Mb*	myoglobin	125.87	2.8E-07
8	Pvalb*	parvalbumin	112.12	1.3E-04
9	Ano5*	anoctamin 5	109.16	9.3E-04
10	Ckm*	creatine kinase, muscle	97.41	2.3E-05
11	Ppp1r3a*	protein phosphatase 1, regulatory (inhibitor) subunit 3A	96.41	6.1E-04
12	Trdn*	triadin	92.65	2.5E-06
13	Myoz1*	myozenin 1	88.05	1.7E-05
14	Dhrs7c*	dehydrogenase/reductase (SDR family) member 7C	77.10	5.3E-04
15	Tnnc2*	troponin C2, fast	56.75	4.3E-05
16	Mylk2*	myosin, light polypeptide kinase 2, skeletal muscle	47.09	2.2E-04
17	Xirp2*	xin actin-binding repeat containing 2	46.79	1.1E-03
18	Ckmt2*	creatine kinase, mitochondrial 2	40.80	5.5E-06
19	Sgcg*	sarcoglycan, gamma (dystrophin-associated glycoprotein)	39.12	7.8E-04

Table B.10, Part I. Continued

	Gene Symbol	Gene	Fold Change	FDR
20	Mfap4	microfibrillar-associated protein 4	38.49	2.7E-11
21	Mybpc1*	myosin binding protein C, slow-type	35.12	4.6E-04
22	Wnt16	wingless-related MMTV integration site 16	32.60	2.2E-11
23	Lmod2*	leiomodin 2 (cardiac)	30.70	1.0E-03
24	Ostn	osteocrin	28.67	4.4E-07
25	Cilp2	cartilage intermediate layer protein 2	27.08	6.9E-12
26	Kcna7*	potassium voltage-gated channel, shaker-related subfamily, member 7	27.07	1.9E-04
27	Tnnt3*	troponin T3, skeletal, fast	26.93	8.0E-04
28	Tcap*	titin-cap	26.22	4.1E-05
29	Hbb-b2	hemoglobin, beta adult major chain; hemoglobin, beta adult minor chain	24.85	1.8E-02
30	Cilp	cartilage intermediate layer protein, nucleotide pyrophosphohydrolase	23.41	9.8E-05
31	Kcnc4*	potassium voltage gated channel, Shaw-related subfamily, member 4	20.79	4.4E-03
32	Smtnl1*	smoothelin-like 1	20.00	8.9E-04
33	A930016O22Rik*	RIKEN cDNA A930016O22 gene	19.67	8.4E-05
34	Myom2*	myomesin 2	19.58	8.0E-04
35	Actn2*	actinin alpha 2	17.37	3.7E-03
36	Itgbl1	integrin, beta-like 1	17.34	5.0E-05
37	Casq1*	calsequestrin 1	16.33	3.8E-04
38	Atp2a1*	ATPase, Ca++ transporting, cardiac muscle, fast twitch 1	16.28	3.9E-04
39	Smpx*	small muscle protein, X-linked	15.11	1.3E-02
40	Lrrn1	leucine rich repeat protein 1, neuronal	14.90	9.3E-05
41	Hfe2*	hemochromatosis type 2 (juvenile) (human homolog)	14.75	3.6E-03
42	H19*	H19 fetal liver mRNA	13.83	3.3E-07
43	Igfbp6	insulin-like growth factor binding protein 6	12.89	6.7E-08

Table B.10, Part I. Continued

	Gene Symbol	Gene	Fold Change	FDR
44	Smyd1*	SET and MYND domain containing 1	12.58	3.2E-03
45	Myl1*	myosin, light polypeptide 1	11.15	1.9E-04
46	Ampd1*	adenosine monophosphate deaminase 1 (isoform M)	10.48	4.0E-02
47	C1qtnf3	C1q and tumor necrosis factor related protein 3	10.43	1.4E-05
48	Fam180a	cDNA sequence BC064033	9.58	7.3E-07
49	Tnn	tenascin N	9.57	1.4E-06
50	Tbx4	T-box 4	9.51	1.4E-09
51	Tnni2*	troponin I, skeletal, fast 2	9.32	6.9E-04
52	Aspn	asporin	8.99	1.4E-06
53	1810041L15Rik	RIKEN cDNA 1810041L15 gene	8.93	3.0E-03
54	Fmod	fibromodulin	8.60	3.3E-12
55	Cacna1s*	calcium channel, voltage-dependent, L type, alpha 1S subunit	8.42	1.7E-03
56	Dner	delta/notch-like EGF-related receptor	8.41	3.3E-05
57	Col3a1	collagen, type III, alpha 1	8.27	4.8E-07
58	3110079O15Rik	RIKEN cDNA 3110079O15 gene	7.93	3.9E-03
59	Jsrp1*	junctional sarcoplasmic reticulum protein 1	7.72	1.5E-02
60	Col8a2	collagen, type VIII, alpha 2	7.44	8.9E-05
61	Wnt7b	wingless-related MMTV integration site 7B	7.20	2.5E-07
62	Myoz3*	myozenin 3	6.72	1.8E-02
63	Clec3a	C-type lectin domain family 3, member a	6.69	9.6E-03
64	Meox2	mesenchyme homeobox 2	6.55	1.6E-06
65	Pgm5	phosphoglucomutase 5	6.48	9.7E-06
66	Lrrc15	leucine rich repeat containing 15	6.44	7.5E-08
67	Actn3*	actinin alpha 3	6.37	1.3E-04
68	Slc38a3*	solute carrier family 38, member 3	6.32	2.1E-04
69	Ldb3*	LIM domain binding 3	6.22	2.1E-03

Table B.10, Part I. Continued

	Gene Symbol	Gene	Fold Change	FDR
70	C130021I20Rik	Riken cDNA C130021I20 gene	6.05	1.8E-07
71	Mylpf*	myosin light chain, phosphorylatable, fast skeletal muscle	6.02	5.1E-03
72	Cntfr	ciliary neurotrophic factor receptor	5.91	3.6E-05
73	Spock1	sparc/osteonectin, cwcv and kazal-like domains proteoglycan 1	5.89	1.6E-02
74	Chst8	carbohydrate (N-acetylgalactosamine 4-0) sulfotransferase 8	5.89	1.1E-05
75	Col10a1	collagen, type X, alpha 1	5.88	2.1E-02
76	3632451O06Rik	RIKEN cDNA 3632451O06 gene	5.87	5.0E-13
77	Fitm1*	fat storage-inducing transmembrane protein 1	5.82	3.3E-02
78	Scube2	similar to signal peptide, CUB domain, EGF-like 2; signal peptide, CUB domain, EGF-like 2	5.72	1.2E-07
79	Slc17a8	solute carrier family 17 (sodium-dependent inorganic phosphate cotransporter), member 8	5.70	8.0E-06
80	Klhl41	kelch-like 41	5.68	2.8E-03
81	Prrx2	paired related homeobox 2	5.61	2.6E-09
82	Thbs4	thrombospondin 4	5.48	4.7E-04
83	Nrap*	nebulin-related anchoring protein	5.39	4.4E-03
84	Megf6	multiple EGF-like-domains 6	5.26	2.5E-07
85	Nov	nephroblastoma overexpressed gene	5.19	1.4E-04
86	Plekhg4	pleckstrin homology domain containing, family G (with RhoGef domain) member 4	5.00	7.4E-08
87	Cytl1	cytokine-like 1	4.98	1.9E-02
88	Kcnj11	potassium inwardly rectifying channel, subfamily J, member 11	4.97	9.5E-03
89	Akr1c18	aldo-keto reductase family 1, member C18	4.95	5.2E-03
90	Lect1	leukocyte cell derived chemotaxin 1	4.84	4.4E-02
91	Slc6a17	solute carrier family 6 (neurotransmitter transporter), member 17	4.71	4.6E-06
92	Ttn*	titin	4.65	6.7E-03
93	Tnxb	tenascin XB	4.33	1.3E-03

Table B.10, Part I. Continued

	Gene Symbol	Gene	Fold Change	FDR
94	Neb*	nebulin	4.24	2.8E-02
95	Dpysl4	dihydropyrimidinase-like 4	4.23	1.3E-05
96	Cox7a1*	cytochrome c oxidase, subunit VIIa 1	4.18	1.1E-02
97	Des*	desmin	4.17	2.0E-03
98	Sh3bgr*	similar to putative SH3BGR protein; SH3-binding domain glutamic acid-rich protein	4.10	3.4E-02
99	Tenm3	teneurin transmembrane protein 3	4.01	5.2E-04
100	Snhg11	small nucleolar RNA host gene 11 (non-protein coding)	4.00	5.5E-05
101	Htra4	HtrA serine peptidase 4	3.96	3.3E-03
102	Sema3c	sema domain, immunoglobulin domain (Ig), short basic domain, secreted, (semaphorin) 3C	3.83	1.3E-05
103	Anxa8	annexin A8	3.80	1.2E-05
104	Col16a1	collagen, type XVI, alpha 1	3.78	3.5E-09
105	Col9a3	collagen, type IX, alpha 3	3.70	2.5E-02
106	Hspb7*	heat shock protein family, member 7 (cardiovascular)	3.67	2.2E-03
107	Adamtsl1	ADAMTS-like 1	3.65	1.5E-07
108	Mybpc2*	myosin binding protein C, fast-type	3.63	3.1E-02
109	Wnt9a	wingless-type MMTV integration site 9A	3.62	1.1E-06
110	Thbs2	thrombospondin 2	3.62	2.5E-07
111	A330021E22Rik	RIKEN cDNA A330021E22 gene	3.60	5.9E-05
112	Chad	chondroadherin	3.55	2.8E-03
113	Olfr78	olfactory receptor 78	3.54	1.9E-04
114	Galr2	galanin receptor 2	3.50	1.8E-07
115	Hhipl1	hedgehog interacting protein-like 1	3.47	3.2E-03
116	Miat	myocardial infarction associated transcript (non-protein coding)	3.46	1.2E-07
117	Postn	periostin, osteoblast specific factor	3.44	4.6E-07
118	Prtg	protogenin homolog (Gallus gallus)	3.41	2.2E-04

Table B.10, Part I. Continued

	Gene Symbol	Gene	Fold Change	FDR
119	Col9a1	collagen, type IX, alpha 1	3.40	4.4E-02
120	Ptn	pleiotrophin	3.38	3.3E-03
121	Medag	mesenteric estrogen dependent adipogenesis	3.33	2.5E-03
122	Cacng7	calcium channel, voltage-dependent, gamma subunit 7	3.31	1.5E-04
123	Tnmd	tenomodulin	3.27	4.5E-03
124	C1qtnf9	C1q and tumor necrosis factor related protein 9	3.27	1.8E-03
125	Lrrc55	leucine rich repeat containing 55	3.26	5.6E-04
126	Itm2a	integral membrane protein 2A	3.25	3.2E-13
127	Gabra3	gamma-aminobutyric acid (GABA) A receptor, subunit alpha 3	3.20	8.0E-06
128	Plat	plasminogen activator, tissue	3.18	2.8E-07
129	Epha3	Eph receptor A3	3.12	8.6E-12
130	Pcdh9	protocadherin 9	3.11	7.4E-04
131	AI593442	expressed sequence AI593442	3.08	5.9E-04
132	Peg3	paternally expressed 3; antisense transcript gene of Peg3	3.06	1.1E-06
133	Meg3	maternally expressed 3	3.05	3.3E-04
134	Hs3st5	heparan sulfate (glucosamine) 3-O-sulfotransferase 5	3.05	5.4E-05
135	Thbs3	thrombospondin 3	3.04	4.5E-06
136	Scn4b*	sodium channel, type IV, beta	3.03	4.7E-02
137	Mia	melanoma inhibitory activity	3.01	3.1E-02
138	Fam69c	RIKEN cDNA B230399E16 gene	2.98	1.1E-06
139	Matn4	matrilin 4	2.97	2.4E-08
140	Col12a1	collagen, type XII, alpha 1	2.96	1.1E-06
141	Prnd	prion protein dublet	2.95	8.2E-06
142	Fosb	FBJ osteosarcoma oncogene B	2.95	1.4E-04

Table B.10, Part I. Continued

	Gene Symbol	Gene	Fold Change	FDR
143	P4ha3	procollagen-proline, 2-oxoglutarate 4-dioxygenase (proline 4-hydroxylase), alpha polypeptide III	2.94	6.3E-06
144	Angptl2	angiopoietin-like 2	2.93	2.1E-06
145	Rab15	RAB15, member RAS oncogene family	2.93	4.2E-03
146	Susd5	sushi domain containing 5	2.92	1.2E-11
147	Emilin3	elastin microfibril interfacer 3	2.91	2.2E-03
148	Dpt	dermatopontin	2.91	1.7E-03
149	Bai2	brain-specific angiogenesis inhibitor 2	2.87	1.6E-04
150	Pnmal2	PNMA-like 2	2.87	1.4E-05
151	Prkg2	protein kinase, cGMP-dependent, type II	2.85	1.3E-02
152	Tmem200c	predicted gene 6338	2.83	2.3E-04
153	Peg3as	Peg3 opposite strand	2.82	4.6E-04
154	Rian	RNA imprinted and accumulated in nucleus	2.82	3.6E-05
155	Gucy1a2	hypothetical protein LOC100044212; guanylate cyclase 1, soluble, alpha 2	2.82	1.4E-03
156	Gpnmb	glycoprotein (transmembrane) nmb	2.82	7.3E-05
157	Sox8	SRY-box containing gene 8	2.81	1.7E-03
158	Higd1b	HIG1 domain family, member 1B	2.80	5.3E-03
159	Foxp2	forkhead box P2	2.80	7.2E-04
160	Clmn	calmin	2.80	1.1E-03
161	Piwil2	piwi-like homolog 2 (Drosophila)	2.77	1.4E-04
162	Asic3	acid-sensing (proton-gated) ion channel 3	2.76	1.7E-04
163	Pgam2*	phosphoglycerate mutase 2	2.75	2.2E-02
164	Crabp2	cellular retinoic acid binding protein II	2.75	2.8E-03
165	Dkk3	dickkopf homolog 3 (Xenopus laevis)	2.73	1.1E-09
166	Cdh13	cadherin 13	2.72	1.8E-05
167	Gpc3	glypican 3	2.70	4.5E-05

Table B.10, Part I. Continued

	Gene Symbol	Gene	Fold Change	FDR
168	Capn6	calpain 6	2.69	6.9E-12
169	Radil	Ras association and DIL domains	2.69	1.3E-03
170	Rxrg	retinoid X receptor gamma	2.67	1.1E-03
171	Msln	mesothelin	2.66	8.0E-06
172	Acan	aggrecan	2.65	1.0E-03
173	Shisa2*	shisa homolog 2 (Xenopus laevis)	2.65	6.3E-05
174	B9d1	B9 protein domain 1	2.63	1.5E-05
175	Hr	hairless	2.63	3.2E-06
176	Hrasls*	HRAS-like suppressor	2.61	3.7E-03
177	1500015O10Rik	RIKEN cDNA 1500015O10 gene	2.58	2.5E-10
178	Nox4	NADPH oxidase 4	2.58	3.5E-04
179	Comp	cartilage oligomeric matrix protein	2.54	4.9E-10
180	Sparcl1	SPARC-like 1	2.54	1.4E-06
181	Ccdc3	coiled-coil domain containing 3	2.53	1.7E-11
182	Lum	lumican	2.53	1.2E-08
183	Jph2*	junctophilin 2	2.53	6.0E-03
184	Cav3*	caveolin 3	2.53	6.9E-03
185	Islr2	immunoglobulin superfamily containing leucine-rich repeat 2	2.53	2.5E-02
186	Wnt10b	wingless related MMTV integration site 10b	2.52	1.4E-06
187	3425401B19Rik*	RIKEN cDNA 3425401B19 gene	2.50	2.8E-02
188	Gm8300	predicted gene 8300	2.50	1.4E-02
189	Angptl7	angiopoietin-like 7	2.49	3.7E-02
190	Pkia*	protein kinase inhibitor, alpha	2.49	3.4E-03
191	Hapln1	hyaluronan and proteoglycan link protein 1	2.48	2.8E-02
192	Fcrls	Fc receptor-like S, scavenger receptor	2.47	2.6E-08
193	Igsf1	immunoglobulin superfamily, member 1	2.47	1.4E-07

Table B.10, Part I. Continued

	Gene Symbol	Gene	Fold Change	FDR
194	Ambn	ameloblastin	2.47	2.0E-02
195	Hspb8*	heat shock protein 8	2.46	2.7E-02
196	Prss23	protease, serine, 23	2.46	9.4E-07
197	Spock2	sparc/osteonectin, cwcv and kazal-like domains proteoglycan 2	2.45	7.7E-03
198	Tmem255b	transmembrane protein 255B	2.44	1.1E-02
199	Dnahc7b	dynein, axonemal, heavy chain 7B; dynein, axonemal, heavy chain 7A	2.43	2.1E-02
200	Lman1l	lectin, mannose-binding 1 like	2.43	5.5E-03
201	Eno2	enolase 2, gamma neuronal	2.43	1.4E-05
202	Nbl1	neuroblastoma, suppression of tumorigenicity 1	2.42	8.6E-12
203	Lamc2	laminin, gamma 2	2.40	7.9E-05
204	Aldh1a3	aldehyde dehydrogenase family 1, subfamily A3	2.40	7.2E-03
205	Rgs11	regulator of G-protein signaling 11; similar to regulator of G-protein signaling 11	2.40	3.5E-03
206	Apod	apolipoprotein D	2.39	2.8E-02
207	Mt2	metallothionein 2	2.38	1.6E-07
208	Gm10635	predicted gene 10635	2.38	4.9E-02
209	Aebp1	AE binding protein 1	2.36	3.6E-05
210	Fam19a5	family with sequence similarity 19, member A5	2.33	2.1E-02
211	Mab21l1	mab-21-like 1 (C. elegans)	2.32	2.6E-03
212	Dok5	docking protein 5	2.32	2.3E-05
213	Serpine1	serine (or cysteine) peptidase inhibitor, clade E, member 1	2.31	1.1E-06
214	Gfpt2	glutamine fructose-6-phosphate transaminase 2	2.30	5.0E-04
215	Flnc*	filamin C, gamma	2.30	2.6E-03
216	Ssc5d	scavenger receptor cysteine rich family, 5 domains	2.29	3.7E-04
217	Rpl39l	ribosomal protein L39-like	2.28	1.1E-05
218	Ptprv	protein tyrosine phosphatase, receptor type, V	2.28	2.8E-07

Table B.10, Part I. Continued

	Gene Symbol	Gene	Fold Change	FDR
219	Sdk1	sidekick homolog 1 (chicken)	2.28	4.8E-03
220	Spp1	secreted phosphoprotein 1	2.27	1.1E-05
221	Ephb3	Eph receptor B3	2.26	5.8E-11
222	P2rx6	purinergic receptor P2X, ligand-gated ion channel, 6	2.26	7.7E-04
223	C1qtnf2	C1q and tumor necrosis factor related protein 2	2.25	5.0E-02
224	Ogdhl	oxoglutarate dehydrogenase-like	2.25	1.2E-02
225	Aspg	asparaginase homolog (S. cerevisiae)	2.24	2.6E-05
226	F3	coagulation factor III	2.23	3.0E-03
227	Gabrb3	gamma-aminobutyric acid (GABA) A receptor, subunit beta 3	2.23	1.4E-04
228	Edil3	EGF-like repeats and discoidin I-like domains 3	2.21	7.0E-09
229	Adra2b	adrenergic receptor, alpha 2b	2.20	4.6E-02
230	Ablim3	actin binding LIM protein family, member 3	2.19	2.8E-02
231	Meox1	mesenchyme homeobox 1	2.19	9.9E-03
232	Mlph	melanophilin	2.19	6.4E-04
233	Ky*	kyphoscoliosis peptidase	2.18	3.4E-02
234	Gprasp2	G protein-coupled receptor associated sorting protein 2	2.18	3.7E-02
235	Kcnmb4	potassium large conductance calcium-activated channel, subfamily M, beta member 4	2.17	1.2E-02
236	Amhr2	anti-Mullerian hormone type 2 receptor	2.17	6.8E-03
237	Begain	brain-enriched guanylate kinase-associated	2.17	1.1E-02
238	C1qtnf5	C1q and tumor necrosis factor related protein 5; membrane-type frizzled-related protein	2.17	3.5E-07
239	Lrrc17	leucine rich repeat containing 17	2.16	3.7E-08
240	D630003M21Rik	RIKEN cDNA D630003M21 gene	2.16	3.2E-03
241	Casq2	calsequestrin 2	2.16	4.4E-04
242	Ebf4	early B-cell factor 4	2.15	5.1E-03
243	Sulf1	sulfatase 1	2.14	1.0E-05

Table B.10, Part I. Continued

	Gene Symbol	Gene	Fold Change	FDR
244	Htra1	HtrA serine peptidase 1	2.14	1.4E-04
245	Wnt5b	wingless-related MMTV integration site 5B	2.14	1.4E-06
246	Lrrc8e	similar to Leucine rich repeat containing 8 family, member E; leucine rich repeat containing 8 family, member E	2.14	4.3E-02
247	Grip2	glutamate receptor interacting protein 2	2.12	6.5E-04
248	Epha4	Eph receptor A4	2.11	6.9E-04
249	Gstp2*	glutathione S-transferase, pi 2; glutathione S-transferase, pi 1; similar to glutathione S-transferase pi class A; predicted gene 3934	2.10	1.8E-03
250	Smoc2	SPARC related modular calcium binding 2	2.09	4.1E-05
251	Etv4	ets variant gene 4 (E1A enhancer binding protein, E1AF)	2.09	1.7E-02
252	Gpx3	glutathione peroxidase 3	2.09	1.9E-06
253	Hspb2*	heat shock protein 2	2.09	4.2E-05
254	Ednrb	endothelin receptor type B	2.08	1.8E-04
255	Mgp	matrix Gla protein	2.08	1.9E-05
256	Vipr2	vasoactive intestinal peptide receptor 2	2.08	4.5E-03
257	Ecm2	extracellular matrix protein 2, female organ and adipocyte specific	2.07	7.4E-07
258	Timp1	tissue inhibitor of metalloproteinase 1	2.07	5.0E-03
259	2310010J17Rik	RIKEN cDNA 2310010J17 gene	2.06	3.1E-02
260	Camk4	calcium/calmodulin-dependent protein kinase IV	2.06	2.1E-03
261	Nos2	nitric oxide synthase 2, inducible	2.04	8.1E-03
262	2310069G16Rik	RIKEN cDNA 2310069G16 gene	2.04	2.0E-02
263	Peli3	pellino 3	2.03	1.1E-02
264	4930429F24Rik*	RIKEN cDNA 4930429F24 gene	2.03	4.3E-02
265	Rnf207	ring finger protein 207	2.03	1.6E-02
266	Zfp811	zinc finger protein 811	2.02	2.1E-02
267	Col6a3	collagen, type VI, alpha 3	2.02	2.2E-04
268	Samd5	sterile alpha motif domain containing 5	2.02	4.3E-04

Table B.10, **Part I**. Continued

	Gene Symbol	Gene	Fold Change	FDR
269	Fam198a	RIKEN cDNA C730027P07 gene	2.02	2.8E-07
270	2700069I18Rik	RIKEN cDNA 2700069I18 gene	2.01	8.6E-03
271	Fgfr3	fibroblast growth factor receptor 3	2.01	3.2E-12
272	Aplp1	amyloid beta (A4) precursor-like protein 1	2.00	1.6E-04
273	Slc6a7	solute carrier family 6 (neurotransmitter transporter, L-proline), member 7	2.00	1.7E-03
274	Fam26e	family with sequence similarity 26, member E	2.00	8.7E-06
275	Cpxm2	carboxypeptidase X 2 (M14 family)	2.00	3.1E-02
276	Fzd2	frizzled homolog 2 (Drosophila)	2.00	2.8E-03

Table B.10, Part II. List of genes more highly expressed in naïve control cancellous bone

	Gene Symbol	Gene	Fold Change	FDR
1	Cbln1	cerebellin 1 precursor protein; similar to precerebellin-1	3.56	1.3E-03
2	Slco1a4	solute carrier organic anion transporter family, member 1a4	3.43	5.4E-05
3	Ly6g6c	lymphocyte antigen 6 complex, locus G6C	3.34	7.1E-04
4	Hist1h4m	histone cluster 1, H4m	3.21	2.3E-05
5	Havcr1	hepatitis A virus cellular receptor 1	3.00	3.8E-06
6	Klra18	killer cell lectin-like receptor, subfamily A, member 18	3.00	1.8E-03
7	Gpr50	G-protein-coupled receptor 50	2.48	9.0E-05
8	Adrb3	adrenergic receptor, beta 3	2.43	1.2E-02
9	Acvr1c	activin A receptor, type IC	2.41	2.5E-02
10	Pira7	paired-Ig-like receptor A7	2.40	1.0E-02
11	Efemp1	epidermal growth factor-containing fibulin-like extracellular matrix protein 1	2.39	2.4E-06

Table B.10, Part II. Continued

	Gene Symbol	Gene	Fold Change	FDR
12	Irg1	immunoresponsive gene 1	2.36	2.4E-03
13	Ptger3	prostaglandin E receptor 3 (subtype EP3)	2.32	3.3E-07
14	Clec4g	C-type lectin domain family 4, member g	2.32	5.0E-05
15	Grem1	gremlin 1	2.30	1.5E-09
16	Klk1	kallikrein 1	2.28	3.0E-05
17	F2rl2	coagulation factor II (thrombin) receptor-like 2	2.27	6.3E-10
18	Gp1ba	glycoprotein 1b, alpha polypeptide; hypothetical protein LOC100048807	2.27	9.7E-10
19	Mmrn1	multimerin 1	2.25	1.3E-13
20	Eomes	eomesodermin homolog (Xenopus laevis)	2.24	1.3E-03
21	Gm1968	predicted gene 1968	2.24	6.5E-05
22	Syt13	synaptotagmin XIII	2.23	6.6E-03
23	Ubd	ubiquitin D	2.22	7.6E-10
24	Arhgap6	Rho GTPase activating protein 6	2.22	4.0E-09
25	Akap5	A kinase (PRKA) anchor protein 5	2.22	4.2E-08
26	Clca1	chloride channel calcium activated 1	2.22	3.0E-12
27	Sycp2	synaptonemal complex protein 2	2.20	8.4E-06
28	Bicd1	bicaudal D homolog 1 (Drosophila)	2.20	8.4E-05
29	B3galt5	UDP-Gal:betaGlcNAc beta 1,3-galactosyltransferase, polypeptide 5	2.19	1.9E-02
30	Gcsam	germinal center associated, signaling and motility	2.17	2.0E-10
31	Mpl	myeloproliferative leukemia virus oncogene	2.17	3.5E-11
32	Slco1a5	solute carrier organic anion transporter family, member 1a5	2.17	4.5E-02
33	Serpina3n	serine (or cysteine) peptidase inhibitor, clade A, member 3N	2.15	1.7E-02
34	Gnaz	guanine nucleotide binding protein, alpha z subunit	2.15	6.9E-08
35	Gp1bb	glycoprotein Ib, beta polypeptide	2.15	3.1E-06
36	Ccdc150	coiled-coil domain containing 150	2.14	1.8E-04

Table B.10, Part II. Continued

	Gene Symbol	Gene	Fold Change	FDR
37	Marco	macrophage receptor with collagenous structure	2.14	1.5E-02
38	AU023871	expressed sequence AU023871	2.14	1.8E-11
39	6330409D20Rik	RIKEN cDNA 6330409D20 gene	2.14	2.5E-02
40	Rnf165	ring finger protein 165	2.13	1.3E-03
41	Slc35d3	solute carrier family 35, member D3	2.12	8.1E-09
42	Cxcl9	chemokine (C-X-C motif) ligand 9	2.12	8.2E-06
43	Mro	maestro	2.12	1.2E-02
44	E230029C05Rik	RIKEN cDNA E230029C05 gene	2.12	2.8E-02
45	Nlrp6	NLR family, pyrin domain containing 6	2.12	4.7E-05
46	Sgk2	serum/glucocorticoid regulated kinase 2	2.12	1.6E-02
47	Rspo2	R-spondin 2 homolog (Xenopus laevis)	2.10	9.6E-10
48	Btnl6	butyrophilin-like 6	2.10	1.3E-03
49	Gbx2	gastrulation brain homeobox 2	2.10	3.4E-03
50	Cxcl13	chemokine (C-X-C motif) ligand 13	2.09	5.0E-02
51	Treml1	triggering receptor expressed on myeloid cells-like 1	2.07	6.7E-11
52	Slamf1	signaling lymphocytic activation molecule family member 1	2.07	4.4E-08
53	Bex4	predicted gene 4322; brain expressed gene 4	2.07	1.8E-03
54	Chrdl1	chordin-like 1	2.07	2.8E-07
55	Tac2	tachykinin 2	2.06	3.8E-03
56	4931440F15Rik	RIKEN cDNA 4931440F15 gene	2.06	3.7E-02
57	Serpina3b	serine (or cysteine) peptidase inhibitor, clade A, member 3B	2.06	9.1E-07
58	P2ry12	purinergic receptor P2Y, G-protein coupled 12	2.06	1.0E-08
59	Serpinb2	serine (or cysteine) peptidase inhibitor, clade B, member 2	2.06	8.3E-07
60	Tubb1	tubulin, beta 1	2.06	1.0E-09
61	G6b	G6B protein	2.05	4.6E-03
62	Mc2r	melanocortin 2 receptor	2.05	1.7E-02

Table B.10, Part II. Continued

	Gene Symbol	Gene	Fold Change	FDR
63	Esm1	endothelial cell-specific molecule 1	2.04	1.1E-10
64	Alox12	arachidonate 12-lipoxygenase	2.03	8.1E-09
65	Pde3a	phosphodiesterase 3A, cGMP inhibited	2.03	1.6E-06
66	Ccr9	chemokine (C-C motif) receptor 9	2.03	2.4E-06
67	Gpm6a	glycoprotein m6a	2.02	2.8E-10
68	Clec1b	C-type lectin domain family 1, member b	2.02	1.5E-10
69	Lipg	lipase, endothelial	2.02	2.0E-08
70	Ifi205	interferon activated gene 205	2.02	2.3E-03
71	Npas4	neuronal PAS domain protein 4	2.01	1.6E-07
72	Kcnj16	potassium inwardly-rectifying channel, subfamily J, member 16	2.01	4.6E-02
73	Kcnj5	potassium inwardly-rectifying channel, subfamily J, member 5	2.01	3.9E-07
74	Csmd1	CUB and Sushi multiple domains 1	2.01	8.3E-07
75	Gp6	glycoprotein 6 (platelet)	2.00	1.3E-07
76	Nrgn	neurogranin	2.00	1.8E-07
77	D830046C22Rik	RIKEN cDNA D830046C22 gene	2.00	3.1E-05

total	353
*indicates contaminant	68
total without contaminants	285

Table B.11: A complete list of genes that were differentially expressed in littermate control animals at 3 hours in cortical vs cancellous bone at baseline in order of decreasing fold change that were: I. more highly expressed in cortical bone and II. More highly expressed in cancellous bone. Number of genes (column A), gene symbols (column B), gene names (column C), fold change (column D), false discovery rate (FDR) (column E). * indicates contamination as determined by Ayturk et al.

Table B.11, Part I. List of genes more highly expressed in control cortical bone of littermate control animals at 3 hours

	Gene Symbol	Gene	Fold Change	FDR
1	Myh4*	myosin, heavy polypeptide 4, skeletal muscle	168.63	3.2E-05
2	Ckm*	creatine kinase, muscle	110.72	4.2E-06
3	Myoc	myocilin	98.57	1.9E-04
4	Myot*	myotilin	93.59	1.4E-05
5	Myh2*	myosin, heavy polypeptide 2, skeletal muscle, adult; myosin, heavy polypeptide 1, skeletal muscle, adult	88.56	7.0E-05
6	Pvalb*	parvalbumin	84.80	9.1E-05
7	Mb*	myoglobin	83.19	5.9E-08
8	Mylk2*	myosin, light polypeptide kinase 2, skeletal muscle	78.36	2.9E-06
9	Eef1a2	eukaryotic translation elongation factor 1 alpha 2	71.88	4.3E-06
10	Acta1*	actin, alpha 1, skeletal muscle	59.29	4.9E-06
11	Xirp2*	xin actin-binding repeat containing 2	54.35	2.0E-05
12	Igfn1	immunoglobulin-like and fibronectin type III domain containing 1	52.92	1.3E-03
13	Tcap*	titin-cap	50.75	1.2E-06
14	Myh1*	myosin, heavy polypeptide 2, skeletal muscle, adult; myosin, heavy polypeptide 1, skeletal muscle, adult	48.21	6.8E-06
15	Tnnt3*	troponin T3, skeletal, fast	45.78	3.2E-06
16	Ckmt2*	creatine kinase, mitochondrial 2	43.50	2.5E-05
17	Tnnc2*	troponin C2, fast	42.17	1.7E-06
18	Mybpc1*	myosin binding protein C, slow-type	41.27	4.2E-06

Table B.11, Part I. Continued

	Gene Symbol	Gene	Fold Change	FDR
19	Ampd1*	adenosine monophosphate deaminase 1 (isoform M)	37.82	1.2E-03
20	Smpx*	small muscle protein, X-linked	33.25	8.9E-04
21	Myoz1*	myozenin 1	32.01	9.8E-05
22	Trdn*	triadin	26.02	5.9E-05
23	Myom2*	myomesin 2	24.23	9.9E-04
24	Ppp1r3a*	protein phosphatase 1, regulatory (inhibitor) subunit 3A	21.85	1.0E-02
25	Atp2a1*	ATPase, Ca++ transporting, cardiac muscle, fast twitch 1	21.12	1.4E-05
26	Wnt16	wingless-related MMTV integration site 16	20.18	5.8E-03
27	Ostn	osteocrin	19.27	1.4E-03
28	Jsrp1*	junctional sarcoplasmic reticulum protein 1	17.21	5.3E-05
29	Casq1*	calsequestrin 1	16.75	9.9E-05
30	Ucma	upper zone of growth plate and cartilage matrix associated	16.20	8.6E-04
31	Cilp	cartilage intermediate layer protein, nucleotide pyrophosphohydrolase	15.89	1.4E-03
32	Col10a1	collagen, type X, alpha 1	14.29	5.1E-04
33	Trim54*	tripartite motif-containing 54	13.15	3.9E-03
34	Foxa2	forkhead box A2	13.12	1.4E-03
35	Actc1*	actin, alpha, cardiac muscle 1; similar to alpha-actin (AA 27-375)	12.89	6.1E-03
36	1810041L15Rik	RIKEN cDNA 1810041L15 gene	12.59	1.6E-02
37	Myl1*	myosin, light polypeptide 1	12.48	9.8E-05
38	A930016O22Rik*	RIKEN cDNA A930016O22 gene	12.03	1.9E-04
39	Smyd1*	SET and MYND domain containing 1	11.84	3.1E-03
40	Krt75	keratin 75	11.76	8.5E-06
41	Lrrn1	leucine rich repeat protein 1, neuronal	11.30	6.8E-03
42	Myoz2*	myozenin 2	11.26	2.3E-03
43	Tnni2*	troponin I, skeletal, fast 2	11.21	4.3E-04

Table B.11, Part I. Continued

	Gene Symbol	Gene	Fold Change	FDR
44	Itgbl1	integrin, beta-like 1	10.91	1.8E-03
45	Hfe2*	hemochromatosis type 2 (juvenile) (human homolog)	10.68	1.6E-02
46	Mfap4	microfibrillar-associated protein 4	9.73	8.6E-03
47	Tnn	tenascin N	9.20	5.0E-08
48	Sall1	sal-like 1 (Drosophila)	9.00	4.7E-06
49	Meox2	mesenchyme homeobox 2	8.40	9.8E-09
50	H19*	H19 fetal liver mRNA	8.12	9.8E-05
51	Col9a3	collagen, type IX, alpha 3	8.05	3.1E-03
52	Myl2*	myosin, light polypeptide 2, regulatory, cardiac, slow	7.94	3.5E-03
53	Col9a1	collagen, type IX, alpha 1	7.53	5.8E-03
54	Aspn	asporin	7.47	6.2E-05
55	Actn2*	actinin alpha 2	7.45	2.0E-03
56	Mylpf*	myosin light chain, phosphorylatable, fast skeletal muscle	7.39	1.1E-03
57	Col9a2	collagen, type IX, alpha 2	7.11	2.4E-03
58	Igfbp6	insulin-like growth factor binding protein 6	7.07	3.3E-07
59	Actn3*	actinin alpha 3	6.96	1.1E-03
60	Col8a2	collagen, type VIII, alpha 2	6.93	1.0E-02
61	Spock1	sparc/osteonectin, cwcv and kazal-like domains proteoglycan 1	6.58	3.1E-03
62	Trim63*	similar to tripartite motif-containing 63; tripartite motif-containing 63	6.51	2.9E-02
63	Fgf14	fibroblast growth factor 14	6.46	9.4E-04
64	Col3a1	collagen, type III, alpha 1	6.40	1.2E-04
65	Lect1	leukocyte cell derived chemotaxin 1	6.34	1.4E-02
66	Clec3a	C-type lectin domain family 3, member a	6.28	1.6E-02
67	Cacna1s*	calcium channel, voltage-dependent, L type, alpha 1S subunit	6.23	4.1E-03
68	Cilp2	cartilage intermediate layer protein 2	6.19	1.2E-03

Table B.11, Part I. Continued

	Gene Symbol	Gene	Fold Change	FDR
69	Fgf23	similar to FGF23; fibroblast growth factor 23	6.02	1.0E-02
70	Cntfr	ciliary neurotrophic factor receptor	5.99	6.3E-07
71	Bnc2	basonuclin 2	5.92	2.3E-03
72	Ldb3*	LIM domain binding 3	5.75	2.0E-03
73	Acan	aggrecan	5.72	2.3E-03
74	Ttn*	titin	5.67	2.9E-03
75	Mfi2	antigen p97 (melanoma associated) identified by monoclonal antibodies 133.2 and 96.5	5.67	2.7E-02
76	3110079O15Rik	RIKEN cDNA 3110079O15 gene	5.60	2.7E-02
77	Slc17a8	solute carrier family 17 (sodium-dependent inorganic phosphate cotransporter), member 8	5.48	1.0E-03
78	Nrap*	nebulin-related anchoring protein	5.39	4.6E-03
79	Chad	chondroadherin	5.38	1.5E-02
80	Klhl41	kelch-like 41	5.24	4.4E-03
81	Chst8	carbohydrate (N-acetylgalactosamine 4-0) sulfotransferase 8	5.20	9.2E-06
82	Lrrc15	leucine rich repeat containing 15	5.16	8.3E-07
83	Fmod	fibromodulin	5.15	5.7E-07
84	Matn3	matrilin 3	5.06	2.6E-02
85	Mybpc2*	myosin binding protein C, fast-type	4.96	1.0E-02
86	Rpl3l*	ribosomal protein L3-like	4.92	9.3E-03
87	C1qtnf3	C1q and tumor necrosis factor related protein 3	4.79	4.7E-04
88	Trpm6	transient receptor potential cation channel, subfamily M, member 6	4.78	1.5E-04
89	Hapln1	hyaluronan and proteoglycan link protein 1	4.72	6.1E-03
90	Des*	desmin	4.64	1.2E-03
91	3632451O06Rik	RIKEN cDNA 3632451O06 gene	4.63	3.1E-07
92	Neb*	nebulin	4.42	1.4E-02
93	Thbs4	thrombospondin 4	4.38	1.2E-04

Table B.11, Part I. Continued

	Gene Symbol	Gene	Fold Change	FDR
94	Sh3bgr*	similar to putative SH3BGR protein; SH3-binding domain glutamic acid-rich protein	4.19	2.4E-02
95	Foxp2	forkhead box P2	4.19	1.0E-04
96	Tbx4	T-box 4	4.04	7.8E-04
97	Syt8	synaptotagmin VIII	3.98	1.7E-02
98	Fam180a	cDNA sequence BC064033	3.84	2.1E-03
99	Tcfl5	transcription factor-like 5 (basic helix-loop-helix)	3.81	2.0E-02
100	Nr1h4	nuclear receptor subfamily 1, group H, member 4	3.76	4.4E-03
101	Fxyd2	FXYD domain-containing ion transport regulator 2	3.74	4.4E-02
102	Dner	delta/notch-like EGF-related receptor	3.74	1.9E-02
103	Fosb	FBJ osteosarcoma oncogene B	3.70	2.7E-05
104	Cox7a1*	cytochrome c oxidase, subunit VIIa 1	3.67	8.1E-03
105	Col16a1	collagen, type XVI, alpha 1	3.60	4.6E-08
106	Slc6a17	solute carrier family 6 (neurotransmitter transporter), member 17	3.56	1.5E-04
107	Ablim3	actin binding LIM protein family, member 3	3.55	9.4E-05
108	Anxa8	annexin A8	3.55	2.6E-07
109	Prrx2	paired related homeobox 2	3.53	4.4E-04
110	Scube2	similar to signal peptide, CUB domain, EGF-like 2; signal peptide, CUB domain, EGF-like 2	3.49	2.4E-04
111	Comp	cartilage oligomeric matrix protein	3.46	1.8E-04
112	Crabp2	cellular retinoic acid binding protein II	3.45	1.9E-02
113	Spock2	sparc/osteonectin, cwcv and kazal-like domains proteoglycan 2	3.44	1.1E-05
114	Postn	periostin, osteoblast specific factor	3.44	1.7E-05
115	Htra4	HtrA serine peptidase 4	3.43	5.5E-04
116	Jph2*	junctophilin 2	3.40	8.6E-04
117	Meg3	maternally expressed 3	3.38	1.3E-06
118	Angptl2	angiopoietin-like 2	3.37	5.3E-11

Table B.11, Part I. Continued

	Gene Symbol	Gene	Fold Change	FDR
119	Miat	myocardial infarction associated transcript (non-protein coding)	3.35	4.0E-05
120	Plekhg4	pleckstrin homology domain containing, family G (with RhoGef domain) member 4	3.33	1.1E-04
121	Hspb7*	heat shock protein family, member 7 (cardiovascular)	3.33	5.4E-03
122	Hhipl1	hedgehog interacting protein-like 1	3.30	5.2E-04
123	R3hdml	R3H domain containing-like	3.30	8.1E-03
124	Thbs2	thrombospondin 2	3.26	2.6E-07
125	Tenm3	teneurin transmembrane protein 3	3.22	4.1E-05
126	Peg3	paternally expressed 3	3.20	1.7E-06
127	Tceal3	transcription elongation factor A (SII)-like 3	3.16	7.2E-05
128	Thbs3	thrombospondin 3	3.16	2.8E-08
129	Epha3	Eph receptor A3	3.09	1.3E-07
130	Ihh	Indian hedgehog	3.09	3.6E-02
131	Bai2	brain-specific angiogenesis inhibitor 2	3.08	5.4E-05
132	Prkg2	protein kinase, cGMP-dependent, type II	3.06	2.3E-02
133	Pgam2*	phosphoglycerate mutase 2	3.06	1.6E-02
134	Ptn	pleiotrophin	3.05	1.5E-04
135	Cacng7	calcium channel, voltage-dependent, gamma subunit 7	3.04	6.7E-04
136	3425401B19Rik*	RIKEN cDNA 3425401B19 gene	3.03	2.3E-03
137	Rab15	RAB15, member RAS oncogene family	2.97	4.5E-04
138	Ppp1r1a*	protein phosphatase 1, regulatory (inhibitor) subunit 1A	2.97	4.9E-03
139	Gm10635	predicted gene 10635	2.96	6.2E-03
140	Wfdc6a	WAP four-disulfide core domain 6A	2.96	2.0E-03
141	Kcns1	K+ voltage-gated channel, subfamily S, 1	2.94	6.0E-03
142	C1qtnf9	C1q and tumor necrosis factor related protein 9	2.94	8.9E-03
143	Sema3c	sema domain, immunoglobulin domain (Ig), short basic domain, secreted, (semaphorin) 3C	2.92	2.9E-04

Table B.11, Part I. Continued

	Gene Symbol	Gene	Fold Change	FDR
144	P4ha3	procollagen-proline, 2-oxoglutarate 4-dioxygenase (proline 4-hydroxylase), alpha polypeptide III	2.89	4.1E-05
145	Fez1	fasciculation and elongation protein zeta 1 (zygin I)	2.80	4.0E-03
146	Megf6	multiple EGF-like-domains 6	2.78	1.3E-04
147	Hr	hairless	2.78	4.3E-07
148	Pgm5	phosphoglucomutase 5	2.77	7.9E-03
149	Wnt9a	wingless-type MMTV integration site 9A	2.75	4.0E-03
150	Sox9	SRY-box containing gene 9	2.74	3.1E-03
151	Sema3e	sema domain, immunoglobulin domain (Ig), short basic domain, secreted, (semaphorin) 3E	2.74	4.0E-02
152	Col12a1	collagen, type XII, alpha 1	2.73	5.7E-06
153	Penk	preproenkephalin	2.71	4.1E-04
154	Bglap3	bone gamma-carboxyglutamate protein 3	2.66	1.7E-03
155	Gcnt4	predicted gene 73	2.65	2.6E-03
156	Ambn	ameloblastin	2.64	2.2E-02
157	Dpysl4	dihydropyrimidinase-like 4	2.64	6.3E-03
158	Piwil2	piwi-like homolog 2 (Drosophila)	2.62	3.2E-05
159	Arsi	arylsulfatase i	2.61	4.5E-03
160	Tnmd	tenomodulin	2.58	5.9E-03
161	Susd5	sushi domain containing 5	2.58	7.8E-07
162	Raver2	ribonucleoprotein, PTB-binding 2	2.57	1.1E-03
163	Sparcl1	SPARC-like 1	2.56	3.2E-05
164	Adamtsl1	ADAMTS-like 1	2.55	1.4E-03
165	Has2	hyaluronan synthase 2	2.54	1.6E-02
166	Wfdc1*	WAP four-disulfide core domain 1	2.53	4.9E-05
167	Aldh1a3	aldehyde dehydrogenase family 1, subfamily A3	2.48	4.5E-03
168	Asic3	acid-sensing (proton-gated) ion channel 3	2.47	6.9E-05

Table B.11, Part I. Continued

	Gene Symbol	Gene	Fold Change	FDR
169	Kcnmb4	potassium large conductance calcium-activated channel, subfamily M, beta member 4	2.47	3.5E-04
170	Timp1	tissue inhibitor of metalloproteinase 1	2.45	4.6E-05
171	Bglap	bone gamma carboxyglutamate protein 1	2.45	3.0E-05
172	Lrp2bp	Lrp2 binding protein	2.43	6.9E-03
173	Shisa2*	shisa homolog 2 (Xenopus laevis)	2.43	2.1E-02
174	Mab21l2	mab-21-like 2 (C. elegans)	2.43	2.1E-09
175	Peg3as	Peg3 opposite strand	2.42	4.4E-03
176	Mapt	microtubule-associated protein tau	2.41	3.8E-02
177	Efcc1	EF hand and coiled-coil domain containing 1	2.41	3.9E-04
178	Dpt	dermatopontin	2.40	6.4E-03
179	Oaz1	predicted gene 9786; ornithine decarboxylase antizyme 1	2.40	1.2E-02
180	Gm3893	predicted gene 3893	2.40	2.0E-05
181	Zcchc5	zinc finger, CCHC domain containing 5	2.40	2.5E-02
182	C130021I20Rik	Riken cDNA C130021I20 gene	2.39	2.3E-02
183	Dkk3	dickkopf homolog 3 (Xenopus laevis)	2.39	4.8E-04
184	Nox4	NADPH oxidase 4	2.37	3.3E-02
185	Prtg	protogenin homolog (Gallus gallus)	2.35	2.6E-02
186	Kcnab1	potassium voltage-gated channel, shaker-related subfamily, beta member 1	2.34	4.2E-02
187	Galr2	galanin receptor 2	2.33	1.5E-03
188	Sncg	synuclein, gamma	2.33	2.9E-03
189	Sytl5	synaptotagmin-like 5	2.33	4.2E-03
190	Ssc5d	scavenger receptor cysteine rich family, 5 domains	2.32	4.6E-05
191	Akr1c18	aldo-keto reductase family 1, member C18	2.32	4.5E-02
192	Tgfb2	transforming growth factor, beta 2	2.31	2.7E-05
193	Gm5124	predicted gene 5124	2.31	1.2E-03

Table B.11, Part I. Continued

	Gene Symbol	Gene	Fold Change	FDR
194	Pcdh9	protocadherin 9	2.31	1.3E-02
195	Stc2	stanniocalcin 2	2.30	1.1E-03
196	F3	coagulation factor III	2.29	4.1E-05
197	Cdh13	cadherin 13	2.29	1.3E-04
198	Arhgap22	Rho GTPase activating protein 22	2.29	1.3E-04
199	Pnmal2	PNMA-like 2	2.29	7.6E-03
200	Baalc	brain and acute leukemia, cytoplasmic	2.27	2.1E-02
201	Tnxb	tenascin XB	2.27	4.3E-02
202	Cpxm2	carboxypeptidase X 2 (M14 family)	2.27	4.4E-03
203	Aebp1	AE binding protein 1	2.26	8.3E-07
204	Itm2a	integral membrane protein 2A	2.25	2.0E-02
205	Wscd2	WSC domain containing 2	2.25	1.6E-03
206	Lrrc17	leucine rich repeat containing 17	2.25	3.2E-05
207	Car11	carbonic anhydrase 11	2.23	6.5E-03
208	Fstl4	follistatin-like 4	2.23	2.3E-02
209	Arc	activity regulated cytoskeletal-associated protein	2.22	5.0E-03
210	Tbx3	T-box 3	2.21	1.3E-04
211	Fndc1	fibronectin type III domain containing 1	2.21	2.9E-06
212	Tmeff1	transmembrane protein with EGF-like and two follistatin-like domains 1;	2.21	2.1E-02
213	Camk4	calcium/calmodulin-dependent protein kinase IV	2.20	1.6E-03
214	Emilin3	elastin microfibril interfacer 3	2.20	3.2E-02
215	LOC100504703	Mus musculus uncharacterized LOC100504703, non-coding RNA	2.20	4.0E-02
216	Lonrf2	LON peptidase N-terminal domain and ring finger 2	2.19	3.3E-03
217	Egr3	early growth response 3	2.19	2.1E-03
218	Clec2l	C-type lectin domain family, member l	2.17	8.1E-03

Table B.11, Part I. Continued

	Gene Symbol	Gene	Fold Change	FDR
219	Gabra3	gamma-aminobutyric acid (GABA) A receptor, subunit alpha 3	2.17	3.1E-02
220	Col6a5	collagen, type VI, alpha 5	2.17	1.8E-03
221	Ccdc68	coiled-coil domain containing 68	2.16	2.0E-04
222	Scube1	signal peptide, CUB domain, EGF-like 1	2.15	2.1E-04
223	Mrgprf	MAS-related GPR, member F	2.15	7.3E-03
224	2810055G20Rik	RIKEN cDNA 2810055G20 gene	2.15	1.0E-02
225	Myo16	myosin XVI	2.15	2.0E-02
226	Sost	sclerostin	2.15	4.3E-07
227	Ccdc3	coiled-coil domain containing 3	2.13	4.2E-06
228	Col6a3	collagen, type VI, alpha 3	2.13	7.2E-05
229	Nxph4	neurexophilin 4	2.12	4.9E-02
230	Gpc3	glypican 3	2.12	5.8E-04
231	Rtn4r	reticulon 4 receptor	2.12	4.3E-04
232	Htra1	HtrA serine peptidase 1	2.12	4.2E-06
233	Rgs11	regulator of G-protein signaling 11	2.10	1.4E-02
234	Prrt2	proline-rich transmembrane protein 2	2.10	7.3E-06
235	Ube2ql1	RIKEN cDNA 3110006E14 gene	2.10	2.3E-04
236	Clip3	CAP-GLY domain containing linker protein 3	2.10	6.7E-07
237	Etv4	ets variant gene 4 (E1A enhancer binding protein, E1AF)	2.09	1.7E-02
238	Dlgap3	discs, large (Drosophila) homolog-associated protein 3	2.09	3.1E-02
239	Fam131c	family with sequence similarity 131, member C	2.09	1.8E-02
240	Col6a2	collagen, type VI, alpha 2	2.08	4.3E-06
241	Wnt10b	wingless related MMTV integration site 10b	2.08	7.6E-05
242	Islr2	immunoglobulin superfamily containing leucine-rich repeat 2	2.07	4.3E-02
243	Tfcp2l1	transcription factor CP2-like 1	2.07	7.4E-03
244	Celf5	bruno-like 5, RNA binding protein (Drosophila)	2.07	9.1E-05

Table B.11, Part I. Continued

	Gene Symbol	Gene	Fold Change	FDR
245	Col2a1	collagen, type II, alpha 1	2.07	9.4E-03
246	Mab21l1	mab-21-like 1 (C. elegans)	2.05	1.1E-02
247	Fetub	fetuin beta	2.04	1.5E-03
248	Rora	RAR-related orphan receptor alpha	2.04	3.9E-03
249	Tcea3*	transcription elongation factor A (SII), 3	2.03	2.0E-03
250	Serpine1	serine (or cysteine) peptidase inhibitor, clade E, member 1	2.03	1.2E-06
251	Dnahc7b	dynein, axonemal, heavy chain 7B; dynein, axonemal, heavy chain 7A	2.02	4.0E-02
252	Fbln1	fibulin 1	2.02	1.8E-04
253	A330021E22Rik	RIKEN cDNA A330021E22 gene	2.01	4.2E-02
254	Dlx5	distal-less homeobox 5	2.00	2.5E-05
255	Shank1	SH3/ankyrin domain gene 1	2.00	4.3E-05

Table B.11, Part II. List of genes more highly expressed in control cancellous bone of littermate control animals at 3 hours

	Gene Symbol	Gene	Fold Change	FDR
1	Amd1*	S-adenosylmethionine decarboxylase 1	76.76	2.8E-03
2	Hbb-b2	hemoglobin, beta adult major chain; hemoglobin, beta adult minor chain	32.33	3.9E-02
3	Gm20594	predicted gene, 20594	10.37	5.0E-02
4	Rsc1a1	regulatory solute carrier protein, family 1, member 1; DNA-damage inducible protein 2	7.09	4.5E-02
5	Pira7	paired-Ig-like receptor A7	3.93	1.6E-02
6	Gm12505	predicted gene 12505	3.02	3.8E-02
7	Cd300c	CD300C antigen	2.89	1.1E-03
8	A730036I17Rik	RIKEN cDNA A730036I17 gene	2.75	1.1E-03
9	Adamdec1	ADAM-like, decysin 1	2.71	3.4E-03

Table B.11, Part II Continued

	Gene Symbol	Gene	Fold Change	FDR
10	Clec4g	C-type lectin domain family 4, member g	2.71	2.1E-05
11	Ly6i	lymphocyte antigen 6 complex, locus I	2.66	3.3E-03
12	Cd209d	CD209d antigen	2.61	1.7E-02
13	Gm5483	predicted gene 5483	2.58	8.1E-03
14	Dclk3	doublecortin-like kinase 3	2.57	6.2E-04
15	Cxcl5	chemokine (C-X-C motif) ligand 5	2.54	8.0E-06
16	1700027J07Rik	RIKEN cDNA 1700027J07 gene	2.49	1.0E-02
17	0610009L18Rik*	RIKEN cDNA 0610009L18 gene	2.46	4.5E-03
18	LOC100038947	signal-regulatory protein beta 1	2.44	2.5E-03
19	Gm1968	predicted gene 1968	2.39	3.5E-04
20	Glrx3	glutaredoxin 3	2.38	7.6E-03
21	Pdzd3	PDZ domain containing 3	2.38	7.0E-04
22	Lyz1	lysozyme 1	2.38	2.6E-03
23	Ubd	ubiquitin D	2.37	8.9E-04
24	Gm20939	predicted gene, 20939	2.33	4.0E-02
25	Acmsd	amino carboxymuconate semialdehyde decarboxylase	2.32	5.4E-03
26	5830428M24Rik	RIKEN cDNA 5830428M24 gene	2.28	7.6E-03
27	Slc6a3	solute carrier family 6 (neurotransmitter transporter, dopamine), member 3	2.24	2.6E-04
28	Sgk2	serum/glucocorticoid regulated kinase 2	2.24	8.4E-03
29	Efemp1	epidermal growth factor-containing fibulin-like extracellular matrix protein 1	2.24	3.2E-05
30	Fam110c	family with sequence similarity 110, member C	2.22	1.0E-02
31	Ear6	eosinophil-associated, ribonuclease A family, member 7	2.22	5.7E-08
32	Cd53	CD53 antigen	2.22	8.9E-04
33	Gad1	glutamic acid decarboxylase 1	2.20	3.1E-02
34	0610010B08Rik	RIKEN cDNA 0610010B08 gene	2.19	1.2E-02

Table B.11, Part II. Continued

	Gene Symbol	Gene	Fold Change	FDR
35	Ear1	eosinophil-associated, ribonuclease A family, member 1	2.18	2.1E-09
36	Slpi	secretory leukocyte peptidase inhibitor	2.17	1.3E-04
37	2410076I21Rik	RIKEN cDNA 2410076I21 gene	2.17	6.2E-03
38	Gm14085	predicted gene 1968	2.16	4.6E-03
39	Gm6634	predicted gene 6634	2.16	1.7E-02
40	Ccr3	chemokine (C-C motif) receptor 3	2.15	1.0E-04
41	Snrpe	small nuclear ribonucleoprotein E; predicted gene 6487	2.15	1.7E-02
42	Cd5l	CD5 antigen-like	2.14	5.1E-05
43	Ear2	eosinophil-associated, ribonuclease A family, member 2	2.14	9.8E-09
44	Xlr3b	X-linked lymphocyte-regulated 3B	2.13	2.2E-02
45	Klrd1	killer cell lectin-like receptor, subfamily D, member 1	2.12	2.0E-02
46	Cntf	Zfp91-Cntf readthrough transcript; zinc finger protein 91; ciliary neurotrophic factor	2.12	1.4E-02
47	Rfc4	replication factor C (activator 1) 4	2.11	1.0E-03
48	Cdkl1	cyclin-dependent kinase-like 1 (CDC2-related kinase)	2.11	1.3E-03
49	Ltb4r2	leukotriene B4 receptor 2	2.10	4.7E-03
50	Zpbp	zona pellucida binding protein	2.10	2.2E-02
51	Ly6g6f	lymphocyte antigen 6 complex, locus G6F	2.09	4.9E-05
52	AA467197	expressed sequence AA467197	2.08	1.1E-02
53	Kcnj9	potassium inwardly-rectifying channel, subfamily J, member 9	2.07	1.5E-02
54	Ms4a1	membrane-spanning 4-domains, subfamily A, member 1	2.06	5.1E-04
55	Snrpg	small nuclear ribonucleoprotein polypeptide G	2.06	6.1E-03
56	4931431B13Rik	RIKEN cDNA 4931431B13 gene	2.05	1.4E-02
57	Ppbp	pro-platelet basic protein	2.05	7.4E-05
58	Gm10658	predicted gene 10658	2.05	3.0E-02
59	Cenpw	centromere protein W	2.05	9.0E-03

Table B.11, Part II. Continued

	Gene Symbol	Gene	Fold Change	FDR
60	Retnlg	resistin like gamma	2.05	1.2E-05
61	Hist1h4i	histone cluster 1, H4i	2.04	8.1E-04
62	Kcna2	potassium voltage-gated channel, shaker-related subfamily, member 2	2.04	4.0E-04
63	Gm16548	predicted gene 5483	2.04	3.3E-04
64	Cldn13	claudin 13	2.03	1.5E-04
65	Rhag	Rhesus blood group-associated A glycoprotein	2.02	2.1E-05

total	320
*indicates contaminant	59
total without contaminants	261

Table B.12: A complete list of genes that were differentially expressed in littermate control animals at 24 hours in cortical vs cancellous bone at baseline in order of decreasing fold change that were: I. more highly expressed in cortical bone and II. More highly expressed in cancellous bone. Number of genes (column A), gene symbols (column B), gene names (column C), fold change (column D), false discovery rate (FDR) (column E). * indicates contamination as determined by Ayturk et al.

Table B.12, Part I. List of genes more highly expressed in control cortical bone of littermate control animals at 24 hours

	Gene Symbol	Gene	Fold Change	FDR
1	Myh4*	myosin, heavy polypeptide 4, skeletal muscle	416.27	2.3E-08
2	Pvalb*	parvalbumin	348.05	3.0E-10
3	Xirp2*	xin actin-binding repeat containing 2	330.58	3.2E-08
4	Myh2*	myosin, heavy polypeptide 2, skeletal muscle, adult	310.00	6.6E-12
5	Mb*	myoglobin	254.97	9.9E-12
6	Eef1a2*	eukaryotic translation elongation factor 1 alpha 2	250.03	3.1E-11
7	Myot*	myotilin	247.13	2.4E-10
8	Acta1*	actin, alpha 1, skeletal muscle	222.17	2.0E-13
9	Ampd1*	adenosine monophosphate deaminase 1 (isoform M)	175.50	1.8E-10
10	Ckm*	creatine kinase, muscle	166.89	2.9E-10
11	Myh1*	myosin, heavy polypeptide 1, skeletal muscle, adult	162.35	3.1E-08
12	Mylk2*	myosin, light polypeptide kinase 2, skeletal muscle	146.28	6.5E-11
13	Mybpc1*	myosin binding protein C, slow-type	141.88	3.5E-14
14	A930016O22Rik*	RIKEN cDNA A930016O22 gene	141.77	2.4E-14
15	Trdn*	triadin	132.14	6.6E-11
16	Myom2*	myomesin 2	100.69	2.9E-07
17	Smpx*	small muscle protein, X-linked	86.30	6.5E-08
18	Myoz1*	myozenin 1	84.02	3.5E-14

Table B.12, Part I. Continued

	Gene Symbol	Gene	Fold Change	FDR
19	Tnnt3*	troponin T3, skeletal, fast	83.42	2.4E-14
20	Hfe2*	hemochromatosis type 2 (juvenile) (human homolog)	78.69	4.4E-09
21	Tnnc2*	troponin C2, fast	64.64	2.3E-08
22	Clec3a	C-type lectin domain family 3, member a	53.60	8.9E-04
23	1810041L15Rik	RIKEN cDNA 1810041L15 gene	50.24	7.6E-14
24	Atp2a1*	ATPase, Ca++ transporting, cardiac muscle, fast twitch 1	43.43	9.4E-13
25	Ano5*	anoctamin 5	42.99	2.7E-06
26	Tcap*	titin-cap	41.03	1.4E-09
27	Mfap4	microfibrillar-associated protein 4	25.11	2.7E-09
28	Lrrn1	leucine rich repeat protein 1, neuronal	24.74	3.4E-11
29	Casq1*	calsequestrin 1	21.33	5.1E-08
30	Cytl1	cytokine-like 1	20.88	1.7E-03
31	Cilp2	cartilage intermediate layer protein 2	19.84	1.9E-09
32	Myoz3*	myozenin 3	19.73	2.0E-05
33	Myl1*	myosin, light polypeptide 1	18.78	3.3E-13
34	Jsrp1*	junctional sarcoplasmic reticulum protein 1	18.51	1.5E-08
35	Smyd1*	SET and MYND domain containing 1	15.71	1.0E-05
36	Ostn	osteocrin	15.31	1.3E-05
37	Tnni2*	troponin I, skeletal, fast 2	14.55	1.8E-07
38	Sall1	sal-like 1 (Drosophila)	14.43	2.3E-09
39	Actn2*	actinin alpha 2	14.17	2.0E-06
40	Itgbl1	integrin, beta-like 1	13.65	1.2E-05
41	3110079O15Rik	RIKEN cDNA 3110079O15 gene	13.52	9.4E-03
42	Actn3*	actinin alpha 3	13.49	3.5E-11
43	Mylpf*	myosin light chain, phosphorylatable, fast skeletal muscle	13.43	3.3E-09

Table B.12, Part I. Continued

	Gene Symbol	Gene	Fold Change	FDR
44	Col10a1	collagen, type X, alpha 1	13.31	1.9E-02
45	H19*	H19 fetal liver mRNA	13.22	3.3E-05
46	Igfbp6	insulin-like growth factor binding protein 6	12.28	3.9E-11
47	Zim1	zinc finger, imprinted 1	11.61	4.0E-05
48	Jph4	junctophilin 4	11.51	3.1E-08
49	Lect1	leukocyte cell derived chemotaxin 1	10.67	3.9E-03
50	Ckmt2*	creatine kinase, mitochondrial 2	10.64	3.6E-04
51	Klhl41	kelch-like 41	10.49	2.7E-08
52	Cacna1s*	calcium channel, voltage-dependent, L type, alpha 1S subunit	10.46	1.1E-06
53	Neb*	nebulin	10.46	7.5E-07
54	Mypn*	myopalladin	10.46	2.6E-03
55	Apobec2*	apolipoprotein B mRNA editing enzyme, catalytic polypeptide 2	9.68	5.5E-05
56	Cilp	cartilage intermediate layer protein, nucleotide pyrophosphohydrolase	9.39	6.4E-03
57	Ttn*	titin	9.33	2.0E-08
58	Wnt16	wingless-related MMTV integration site 16	9.31	3.4E-06
59	Cacng1*	calcium channel, voltage-dependent, gamma subunit 1	9.17	6.0E-04
60	Snhg11	small nucleolar RNA host gene 11 (non-protein coding)	9.01	3.6E-07
61	Col8a2	collagen, type VIII, alpha 2	8.46	5.8E-07
62	Mybpc2*	myosin binding protein C, fast-type	8.40	3.9E-07
63	Dner	delta/notch-like EGF-related receptor	8.39	1.8E-09
64	Rpl3l*	ribosomal protein L3-like	8.30	1.8E-04
65	Wnt7b	wingless-related MMTV integration site 7B	8.10	1.3E-11
66	Ldb3*	LIM domain binding 3	8.08	1.2E-05
67	Aspn	asporin	8.01	6.1E-08
68	Trpm6	transient receptor potential cation channel, subfamily M, member 6	7.94	3.7E-09

Table B.12, Part I. Continued

	Gene Symbol	Gene	Fold Change	FDR
69	Ucma	upper zone of growth plate and cartilage matrix associated	7.83	5.4E-03
70	Cox8b*	cytochrome c oxidase, subunit VIIIb	7.48	1.4E-05
71	Des*	desmin	7.38	1.8E-08
72	Slc38a3*	solute carrier family 38, member 3	7.14	1.1E-02
73	C1qtnf3	C1q and tumor necrosis factor related protein 3	7.07	4.3E-06
74	Spock1	sparc/osteonectin, cwcv and kazal-like domains proteoglycan 1	6.73	2.0E-06
75	Nrap*	nebulin-related anchoring protein	6.62	3.7E-05
76	Col3a1	collagen, type III, alpha 1	6.36	8.4E-07
77	Tmem215	transmembrane protein 215	6.24	2.2E-05
78	Thbs4	thrombospondin 4	6.08	1.3E-06
79	Tnn	tenascin N	6.01	1.1E-08
80	Tbx4	T-box 4	5.98	1.7E-06
81	Pgm5	phosphoglucomutase 5	5.88	4.7E-08
82	Foxp2	forkhead box P2	5.82	8.7E-12
83	Htra4	HtrA serine peptidase 4	5.80	2.0E-10
84	Sh3bgr*	SH3-binding domain glutamic acid-rich protein	5.60	1.0E-03
85	Tigd4	tigger transposable element derived 4	5.51	8.5E-03
86	Mylk4*	myosin light chain kinase family, member 4	5.47	5.3E-03
87	Plekhg4	pleckstrin homology domain containing, family G (with RhoGef domain) member 4	5.42	4.5E-09
88	Chad	chondroadherin	5.41	1.6E-02
89	Meox2	mesenchyme homeobox 2	5.39	1.1E-04
90	Nov	nephroblastoma overexpressed gene	5.38	2.4E-05
91	Fmod	fibromodulin	5.37	4.7E-09
92	Prrx2	paired related homeobox 2	5.32	3.3E-09
93	Cox7a1*	cytochrome c oxidase, subunit VIIa 1	5.00	6.2E-04

Table B.12, Part I. Continued

	Gene Symbol	Gene	Fold Change	FDR
94	Sema3c	sema domain, immunoglobulin domain (Ig), short basic domain, secreted, (semaphorin) 3C	4.98	3.0E-06
95	Hspb7*	heat shock protein family, member 7 (cardiovascular)	4.91	1.1E-06
96	Fam180a	cDNA sequence BC064033	4.85	1.9E-03
97	Matn3	matrilin 3	4.77	2.7E-02
98	Ryr1*	ryanodine receptor 1, skeletal muscle	4.74	2.0E-04
99	Scube2	signal peptide, CUB domain, EGF-like 2	4.61	8.9E-06
100	Chst8	carbohydrate (N-acetylgalactosamine 4-0) sulfotransferase 8	4.54	6.4E-05
101	Cntfr	ciliary neurotrophic factor receptor	4.50	4.9E-05
102	Lrrc15	leucine rich repeat containing 15	4.44	2.8E-10
103	Postn	periostin, osteoblast specific factor	4.37	1.2E-09
104	Miat	myocardial infarction associated transcript (non-protein coding)	4.33	9.4E-06
105	Kcnab1	potassium voltage-gated channel, shaker-related subfamily, beta member 1	4.25	1.6E-06
106	Pkia*	protein kinase inhibitor, alpha	4.24	6.1E-05
107	Pgam2*	phosphoglycerate mutase 2	4.22	3.0E-04
108	Nrk	Nik related kinase	3.97	2.0E-02
109	Megf6	multiple EGF-like-domains 6	3.92	1.5E-03
110	Slc17a8	solute carrier family 17 (sodium-dependent inorganic phosphate cotransporter), member 8	3.87	5.1E-05
111	Meg3	maternally expressed 3	3.79	1.1E-10
112	Rian	RNA imprinted and accumulated in nucleus	3.75	5.7E-08
113	C130021I20Rik	Riken cDNA C130021I20 gene	3.74	1.5E-05
114	Shisa2*	shisa homolog 2 (Xenopus laevis)	3.74	1.9E-04
115	Adamtsl1	ADAMTS-like 1	3.72	8.2E-05
116	P4ha3	procollagen-proline, 2-oxoglutarate 4-dioxygenase (proline 4-hydroxylase), alpha polypeptide III	3.67	2.9E-06

Table B.12, Part I. Continued

	Gene Symbol	Gene	Fold Change	FDR
117	Ncmap	noncompact myelin associated protein	3.64	2.1E-02
118	Col16a1	collagen, type XVI, alpha 1	3.62	7.7E-12
119	Msln	mesothelin	3.60	1.4E-08
120	A330021E22Rik	RIKEN cDNA A330021E22 gene	3.58	2.2E-04
121	Mmp12	matrix metallopeptidase 12	3.57	8.4E-03
122	Tnmd	tenomodulin	3.55	4.7E-04
123	Gcnt4	predicted gene 73	3.54	4.1E-05
124	Scn4b*	sodium channel, type IV, beta	3.50	6.6E-03
125	Fam69c	RIKEN cDNA B230399E16 gene	3.47	4.0E-07
126	C1qtnf9	C1q and tumor necrosis factor related protein 9	3.47	1.2E-02
127	Slc6a17	solute carrier family 6 (neurotransmitter transporter), member 17	3.39	2.6E-04
128	Tmod4*	tropomodulin 4	3.37	1.2E-02
129	Gabra3	gamma-aminobutyric acid (GABA) A receptor, subunit alpha 3	3.35	1.7E-06
130	Anxa8	annexin A8	3.30	7.8E-04
131	Dpysl4	dihydropyrimidinase-like 4	3.29	9.3E-06
132	Spock2	sparc/osteonectin, cwcv and kazal-like domains proteoglycan 2	3.26	6.2E-09
133	Mrgprf	MAS-related GPR, member F	3.24	3.3E-05
134	Thbs2	thrombospondin 2	3.22	6.0E-09
135	Ptn	pleiotrophin	3.20	9.9E-07
136	Zfp185	zinc finger protein 185	3.19	6.7E-03
137	Piwil2	piwi-like homolog 2 (Drosophila)	3.16	2.0E-07
138	Tenm3	teneurin transmembrane protein 3	3.15	4.5E-07
139	Medag	mesenteric estrogen dependent adipogenesis	3.13	3.3E-05
140	C1qtnf2	C1q and tumor necrosis factor related protein 2	3.12	9.5E-04
141	Crabp2	cellular retinoic acid binding protein II	3.11	1.6E-03

Table B.12, Part I. Continued

	Gene Symbol	Gene	Fold Change	FDR
142	Itm2a	integral membrane protein 2A	3.11	9.9E-12
143	Bai2	brain-specific angiogenesis inhibitor 2	3.11	1.0E-03
144	Emilin3	elastin microfibril interfacer 3	3.10	3.8E-04
145	Flnc*	filamin C, gamma	3.09	5.0E-06
146	Ablim3	actin binding LIM protein family, member 3	3.08	1.8E-04
147	Fosb	FBJ osteosarcoma oncogene B	3.05	5.3E-03
148	Mia	melanoma inhibitory activity	3.05	5.0E-02
149	Prtg	protogenin homolog (Gallus gallus)	3.03	5.0E-05
150	Aspg	asparaginase homolog (S. cerevisiae)	2.99	9.1E-06
151	Prss23	protease, serine, 23	2.97	4.3E-06
152	Peg3as	Peg3 opposite strand	2.97	2.8E-06
153	Rgs11	regulator of G-protein signaling 11	2.96	1.1E-04
154	Pnmal2	PNMA-like 2	2.96	3.4E-04
155	Rnf207	ring finger protein 207	2.95	3.7E-04
156	3632451O06Rik	RIKEN cDNA 3632451O06 gene	2.93	9.7E-07
157	Epha3	Eph receptor A3	2.92	1.5E-09
158	Col12a1	collagen, type XII, alpha 1	2.91	2.0E-08
159	B230206H07Rik	RIKEN cDNA B230206H07 gene	2.91	1.1E-03
160	Olfr78	olfactory receptor 78	2.91	1.2E-03
161	Asic3	acid-sensing (proton-gated) ion channel 3	2.90	4.6E-05
162	Jph2*	junctophilin 2	2.90	1.1E-04
163	Trim72*	tripartite motif-containing 72	2.90	2.2E-02
164	Angptl2	angiopoietin-like 2	2.89	3.8E-08
165	4930429F24Rik*	RIKEN cDNA 4930429F24 gene	2.88	9.1E-03
166	Sparcl1	SPARC-like 1	2.88	5.4E-08

Table B.12, Part I. Continued

	Gene Symbol	Gene	Fold Change	FDR
167	Slmo1	slowmo homolog 1 (Drosophila)	2.88	6.8E-03
168	Susd5	sushi domain containing 5	2.87	1.1E-04
169	Gng8	guanine nucleotide binding protein (G protein), gamma 8	2.86	2.3E-03
170	Obscn*	obscurin, cytoskeletal calmodulin and titin-interacting RhoGEF	2.85	1.1E-02
171	Plat	plasminogen activator, tissue	2.81	6.1E-09
172	Lrrc17	leucine rich repeat containing 17	2.81	4.5E-09
173	Wnt10b	wingless related MMTV integration site 10b	2.78	1.6E-09
174	Alpk3*	alpha-kinase 3	2.78	5.3E-03
175	Gm10635	predicted gene 10635	2.77	1.6E-03
176	Ogdhl	oxoglutarate dehydrogenase-like	2.77	1.0E-02
177	Kcp	kielin/chordin-like protein	2.70	1.0E-03
178	Ngfr	nerve growth factor receptor (TNFR superfamily, member 16)	2.70	3.1E-04
179	Ccl12	chemokine (C-C motif) ligand 12	2.67	8.3E-03
180	Wnt9a	wingless-type MMTV integration site 9A	2.65	6.8E-06
181	Thbs3	thrombospondin 3	2.64	3.1E-05
182	Wnt2b	wingless related MMTV integration site 2b	2.64	4.2E-08
183	1500015O10Rik	RIKEN cDNA 1500015O10 gene	2.62	2.5E-08
184	F3	coagulation factor III	2.60	4.5E-06
185	Edil3	EGF-like repeats and discoidin I-like domains 3	2.60	1.0E-06
186	Prnd	prion protein dublet	2.60	2.2E-06
187	Ptprv	protein tyrosine phosphatase, receptor type, V	2.59	1.1E-07
188	Galr2	galanin receptor 2	2.59	2.0E-06
189	Peg3	paternally expressed 3	2.54	2.3E-05
190	Txlnb*	taxilin beta	2.51	4.7E-02
191	Camk4	calcium/calmodulin-dependent protein kinase IV	2.49	2.9E-06

Table B.12, Part I. Continued

	Gene Symbol	Gene	Fold Change	FDR
192	Rab15	RAB15, member RAS oncogene family	2.49	6.7E-03
193	Eif3j1	eukaryotic translation initiation factor 3, subunit J1	2.46	4.3E-02
194	Best1	bestrophin 1; hypothetical protein LOC100046789	2.44	1.6E-04
195	Lrrc55	leucine rich repeat containing 55	2.44	3.8E-02
196	Aldh1a3	aldehyde dehydrogenase family 1, subfamily A3	2.44	2.2E-02
197	Dkk3	dickkopf homolog 3 (Xenopus laevis)	2.41	2.5E-09
198	Epha4	Eph receptor A4	2.41	6.2E-06
199	Hspb8*	heat shock protein 8	2.40	5.8E-03
200	Ccdc3	coiled-coil domain containing 3	2.40	1.7E-08
201	Comp	cartilage oligomeric matrix protein	2.39	2.4E-02
202	Gpnmb	glycoprotein (transmembrane) nmb	2.39	2.7E-07
203	Tnxb	tenascin XB	2.38	1.0E-02
204	Rbp7	retinol binding protein 7, cellular	2.37	1.2E-02
205	Sulf1	sulfatase 1	2.37	3.3E-13
206	Mall	mal, T-cell differentiation protein-like	2.35	3.4E-03
207	Igsf1	immunoglobulin superfamily, member 1	2.35	1.7E-05
208	Rarres1	retinoic acid receptor responder (tazarotene induced) 1	2.34	2.8E-04
209	Dnahc1	dynein, axonemal, heavy chain 1	2.34	6.2E-06
210	Col6a3	collagen, type VI, alpha 3	2.32	5.2E-07
211	Dpt	dermatopontin	2.32	4.9E-03
212	Snap91	synaptosomal-associated protein 91	2.32	3.9E-02
213	Fcrls	Fc receptor-like S, scavenger receptor	2.32	9.7E-06
214	Sost	sclerostin	2.32	2.4E-04
215	Slc6a7	solute carrier family 6 (neurotransmitter transporter, L-proline), member 7	2.30	3.8E-06
216	Gabrb3	gamma-aminobutyric acid (GABA) A receptor, subunit beta 3	2.30	1.3E-04

Table B.12, Part I. Continued

	Gene Symbol	Gene	Fold Change	FDR
217	Spp1	secreted phosphoprotein 1	2.28	2.4E-06
218	Hr	hairless	2.28	6.9E-06
219	Capn6	calpain 6	2.27	1.5E-02
220	Meox1	mesenchyme homeobox 1	2.27	8.1E-05
221	Rtn2*	reticulon 2 (Z-band associated protein)	2.26	2.9E-02
222	A730090H04Rik	RIKEN cDNA A730090H04 gene	2.26	1.5E-03
223	Lgi3	leucine-rich repeat LGI family, member 3	2.25	3.3E-03
224	Asphd2	aspartate beta-hydroxylase domain containing 2	2.25	3.4E-04
225	Etv4	ets variant gene 4 (E1A enhancer binding protein, E1AF)	2.25	1.7E-03
226	Radil	Ras association and DIL domains	2.25	4.5E-02
227	Nptxr	neuronal pentraxin receptor	2.24	4.6E-02
228	Pamr1	peptidase domain containing associated with muscle regeneration 1	2.24	1.4E-05
229	Chd5	chromodomain helicase DNA binding protein 5	2.22	1.2E-02
230	Col6a5	collagen, type VI, alpha 5	2.22	3.3E-06
231	AI593442	expressed sequence AI593442	2.22	1.2E-02
232	Gpr115	G protein-coupled receptor 115	2.22	4.5E-02
233	Htra1	HtrA serine peptidase 1	2.22	1.7E-06
234	Tgfb2	transforming growth factor, beta 2	2.21	3.7E-04
235	Cacng7	calcium channel, voltage-dependent, gamma subunit 7	2.21	4.0E-02
236	Mlph	melanophilin	2.21	1.3E-04
237	Eps8l2	EPS8-like 2	2.19	3.9E-03
238	Pygm*	muscle glycogen phosphorylase	2.18	4.4E-03
239	Tppp3	tubulin polymerization-promoting protein family member 3	2.17	6.7E-06
240	Islr2	immunoglobulin superfamily containing leucine-rich repeat 2	2.17	4.7E-02
241	Kcne4	potassium voltage-gated channel, Isk-related subfamily, gene 4	2.16	7.9E-04

Table B.12, Part I. Continued

	Gene Symbol	Gene	Fold Change	FDR
242	Mt2	metallothionein 2	2.16	5.4E-04
243	Srl*	sarcalumenin	2.15	2.8E-03
244	Sox5	SRY-box containing gene 5	2.15	1.2E-02
245	Mgp	matrix Gla protein	2.15	6.1E-05
246	Fbln1	fibulin 1	2.14	3.3E-08
247	Clmn	calmin	2.14	8.6E-03
248	Cdh13	cadherin 13	2.14	1.4E-03
249	Cmya5*	cardiomyopathy associated 5	2.14	1.4E-03
250	Tub	cDNA sequence BC049265; tubby candidate gene	2.14	3.1E-06
251	Gprasp2	G protein-coupled receptor associated sorting protein 2	2.13	1.8E-02
252	1700007J10Rik	RIKEN cDNA 1700007J10 gene	2.13	3.1E-02
253	Eno3*	enolase 3, beta muscle	2.12	4.2E-03
254	Matn2	matrilin 2	2.12	4.0E-06
255	Mmp13	matrix metallopeptidase 13	2.12	3.6E-03
256	Lum	lumican	2.10	3.9E-05
257	Serpind1	serine (or cysteine) peptidase inhibitor, clade D, member 1	2.10	2.1E-02
258	Mustn1	musculoskeletal, embryonic nuclear protein 1	2.10	6.4E-05
259	Arntl2	aryl hydrocarbon receptor nuclear translocator-like 2;	2.10	3.9E-02
260	Ulk4	unc-51-like kinase 4 (C. elegans)	2.09	3.2E-02
261	Abhd3	abhydrolase domain containing 3	2.09	6.0E-03
262	Eno2	enolase 2, gamma neuronal	2.08	5.7E-05
263	Higd1b	HIG1 domain family, member 1B	2.07	3.6E-02
264	Ssc5d	scavenger receptor cysteine rich family, 5 domains	2.07	2.1E-02
265	Rpl39l	ribosomal protein L39-like	2.07	1.7E-03
266	Enpp1	ectonucleotide pyrophosphatase/phosphodiesterase 1	2.07	7.2E-10

Table B.12, Part I. Continued

	Gene Symbol	Gene	Fold Change	FDR
267	Ecm2	extracellular matrix protein 2, female organ and adipocyte specific	2.06	1.3E-05
268	Lamc2	laminin, gamma 2	2.06	3.7E-02
269	Nox4	NADPH oxidase 4	2.05	1.6E-02
270	Tmod2	tropomodulin 2	2.05	4.1E-03
271	C1qtnf5	C1q and tumor necrosis factor related protein 5; membrane-type frizzled-related protein	2.05	2.9E-07
272	Ogn	osteoglycin	2.04	2.4E-04
273	Gpx3	glutathione peroxidase 3	2.03	7.3E-06
274	Cav1	caveolin 1, caveolae protein	2.03	1.0E-07
275	Tnfaip6	tumor necrosis factor alpha induced protein 6	2.02	5.4E-03
276	Megf10	multiple EGF-like-domains 10	2.02	3.8E-08
277	Asap3	ArfGAP with SH3 domain, ankyrin repeat and PH domain 3	2.02	6.2E-06
278	Cys1	cystin 1	2.01	4.3E-03
279	Arhgap44	Rho GTPase activating protein 44	2.01	6.5E-03
280	Dnahc7b	dynein, axonemal, heavy chain 7B	2.00	4.2E-02

Table B.12, Part II. List of genes more highly expressed in control cancellous bone of littermate control animals at 24 hours

	Gene Symbol	Gene	Fold Change	FDR
1	Ear12	eosinophil-associated, ribonuclease A family, member 12	439.55	4.2E-03
2	Cbln1	cerebellin 1 precursor protein	5.14	1.3E-06
3	Ly6g6c	lymphocyte antigen 6 complex, locus G6C	3.54	3.7E-03
4	Hist1h4m	histone cluster 1, H4m	2.79	7.0E-04

Table B.12, Part II. Continued

	Gene Symbol	Gene	Fold Change	FDR
5	Btnl6	butyrophilin-like 6	2.65	1.4E-03
6	Serpinb2	serine (or cysteine) peptidase inhibitor, clade B, member 2	2.61	6.6E-11
7	Ubd	ubiquitin D	2.55	2.0E-10
8	AU023871	expressed sequence AU023871	2.50	2.6E-13
9	Gp1ba	glycoprotein 1b, alpha polypeptide; hypothetical protein LOC100048807	2.48	3.2E-12
10	Alox12	arachidonate 12-lipoxygenase	2.48	5.3E-13
11	Treml1	triggering receptor expressed on myeloid cells-like 1	2.45	5.2E-14
12	Gpr50	G-protein-coupled receptor 50	2.42	2.9E-03
13	Tubb1	tubulin, beta 1	2.42	1.4E-14
14	Marco	macrophage receptor with collagenous structure	2.42	1.4E-02
15	Cxcl5	similar to LPS-induced CXC chemokine; chemokine (C-X-C motif) ligand 5	2.40	1.7E-03
16	Slamf1	signaling lymphocytic activation molecule family member 1	2.38	4.9E-10
17	Ccdc37	coiled-coil domain containing 37	2.37	1.3E-02
18	Gp6	glycoprotein 6 (platelet)	2.36	4.0E-12
19	Lipg	lipase, endothelial	2.35	2.4E-14
20	Spatc1	spermatogenesis and centriole associated 1	2.35	8.3E-03
21	Mpl	myeloproliferative leukemia virus oncogene	2.35	1.1E-12
22	Efemp1	epidermal growth factor-containing fibulin-like extracellular matrix protein 1	2.35	2.0E-08
23	Nrgn	neurogranin	2.34	1.1E-12
24	Ccdc92	coiled-coil domain containing 92	2.33	1.9E-08
25	Syt13	synaptotagmin XIII	2.33	8.5E-03
26	Clca1	chloride channel calcium activated 1	2.32	9.0E-13
27	Gnaz	guanine nucleotide binding protein, alpha z subunit	2.32	7.7E-13
28	Ccdc150	coiled-coil domain containing 150	2.31	4.9E-06

Table B.12, Part II. Continued

	Gene Symbol	Gene	Fold Change	FDR
29	Clec1b	C-type lectin domain family 1, member b	2.29	1.7E-10
30	Cd5l	CD5 antigen-like	2.29	2.3E-07
31	Slc6a4	solute carrier family 6 (neurotransmitter transporter, serotonin), member 4	2.27	1.9E-07
32	Gp5	glycoprotein 5 (platelet)	2.27	4.9E-10
33	Nlrp6	NLR family, pyrin domain containing 6	2.26	9.9E-05
34	Npas4	neuronal PAS domain protein 4	2.25	2.6E-07
35	Ly6g6f	lymphocyte antigen 6 complex, locus G6F	2.24	7.0E-04
36	Ppbp	pro-platelet basic protein	2.24	1.0E-06
37	Clec4g	C-type lectin domain family 4, member g	2.22	4.2E-04
38	Hmga2-ps1	high mobility group AT-hook 2, pseudogene 1	2.21	1.8E-10
39	Gramd1c	GRAM domain containing 1C	2.20	3.1E-05
40	Aldob	aldolase B, fructose-bisphosphate	2.20	3.4E-05
41	Lypd6	LY6/PLAUR domain containing 6	2.19	4.5E-02
42	Gp1bb	glycoprotein Ib, beta polypeptide	2.18	1.2E-07
43	Sec14l5*	SEC14-like 5 (S. cerevisiae)	2.17	1.0E-04
44	Gpm6a	glycoprotein m6a	2.17	4.9E-07
45	Tesc	tescalcin	2.16	1.7E-06
46	Itga2b	integrin alpha 2b	2.16	2.3E-08
47	Ufsp1	UFM1-specific peptidase 1	2.14	1.0E-07
48	Kcna2	potassium voltage-gated channel, shaker-related subfamily, member 2	2.14	2.9E-07
49	F2rl2	coagulation factor II (thrombin) receptor-like 2	2.14	4.5E-11
50	Cd226*	CD226 antigen	2.13	1.9E-04
51	Tnfsf14	tumor necrosis factor (ligand) superfamily, member 14	2.13	2.4E-14
52	Spic	Spi-C transcription factor (Spi-1/PU.1 related)	2.13	2.9E-09

Table B.12, Part II. Continued

	Gene Symbol	Gene	Fold Change	FDR
53	Gcsam	germinal center associated, signaling and motility	2.12	7.6E-08
54	Mfsd2b	predicted gene 1964	2.12	2.4E-10
55	Gad1	glutamic acid decarboxylase 1	2.12	1.1E-02
56	Cass4	Cas scaffolding protein family member 4	2.12	1.5E-07
57	Mmrn1	multimerin 1	2.12	4.4E-13
58	Reep2	receptor accessory protein 2	2.11	6.9E-08
59	2010204K13Rik	RIKEN cDNA 2010204K13 gene	2.10	2.1E-02
60	Hoxb8	homeo box B8	2.10	3.4E-03
61	Slc24a5	solute carrier family 24, member 5	2.09	1.0E-07
62	Grap2*	GRB2-related adaptor protein 2	2.09	1.5E-10
63	Itgad	integrin, alpha D	2.09	1.9E-06
64	Fcna	ficolin A	2.09	2.5E-10
65	Stab2	similar to FEX2; stabilin 2	2.08	2.4E-14
66	Slc35d3	solute carrier family 35, member D3	2.07	4.6E-07
67	Treml4	triggering receptor expressed on myeloid cells-like 4	2.07	1.9E-07
68	Slc6a3	solute carrier family 6 (neurotransmitter transporter, dopamine), member 3	2.06	4.4E-04
69	Cited4	Cbp/p300-interacting transactivator, with Glu/Asp-rich carboxy-terminal domain, 4	2.06	3.8E-04
70	Ptger3	prostaglandin E receptor 3 (subtype EP3)	2.05	4.7E-04
71	Ccdc67	coiled-coil domain containing 67	2.05	3.5E-02
72	Rbpms2	predicted gene 3470; RNA binding protein with multiple splicing 2	2.05	4.7E-09
73	Esm1	endothelial cell-specific molecule 1	2.05	2.4E-14
74	Gbx2	gastrulation brain homeobox 2	2.05	4.9E-03
75	Cdh1	cadherin 1	2.04	2.6E-03
76	BC016579	cDNA sequence, BC016579	2.04	3.0E-02

Table B.12, Part II. Continued

	Gene Symbol	Gene	Fold Change	FDR
77	Fmo2	flavin containing monooxygenase 2	2.03	1.3E-07
78	Kcna3	potassium voltage-gated channel, shaker-related subfamily, member 3	2.03	1.5E-04
79	Pls1	plastin 1 (I-isoform)	2.03	4.4E-05
80	Bin2	bridging integrator 2	2.03	2.9E-11
81	Guca1b	guanylate cyclase activator 1B	2.03	2.4E-02
82	P2rx1	purinergic receptor P2X, ligand-gated ion channel, 1	2.03	6.6E-05
83	Grem1	gremlin 1	2.03	1.2E-09
84	Ache*	acetylcholinesterase	2.02	1.5E-08
85	Akap5	A kinase (PRKA) anchor protein 5	2.01	2.1E-04
86	Hal	histidine ammonia lyase	2.01	2.2E-02
87	Serpina3f	serine (or cysteine) peptidase inhibitor, clade A, member 3F	2.00	3.9E-05
88	Vwf	Von Willebrand factor homolog	2.00	1.1E-09
89	Kcnj9	potassium inwardly-rectifying channel, subfamily J, member 9	2.00	6.0E-03

total	369
*indicates contaminant	75
total without contaminants	294

Table B.13: A complete list of genes that were differentially expressed in pOC-ERαKO animals at 3 hours in cortical vs cancellous bone at baseline in order of decreasing fold change that were: I. More highly expressed in cortical bone and II. More highly expressed in cancellous bone. Number of genes (column A), gene symbols (column B), gene names (column C), fold change (column D), false discovery rate (FDR) (column E). * indicates contamination as determined by Ayturk et al.

Table B.13, Part I. List of genes more highly expressed in control cortical bone of pOC-ERαKO animals at 3 hours

	Gene Symbol	Gene	Fold Change	FDR
1	Xirp2*	xin actin-binding repeat containing 2	2016.93	2.3E-11
2	Myh1*	myosin, heavy polypeptide 2, skeletal muscle, adult; myosin, heavy polypeptide 1, skeletal muscle, adult	1950.34	3.4E-17
3	Myh4*	myosin, heavy polypeptide 4, skeletal muscle	957.03	2.3E-06
4	Myh2*	myosin, heavy polypeptide 2, skeletal muscle, adult; myosin, heavy polypeptide 1, skeletal muscle, adult	540.45	2.7E-09
5	Trim54*	tripartite motif-containing 54	425.80	4.4E-10
6	Smpx*	small muscle protein, X-linked	420.56	8.9E-10
7	Myot*	myotilin	347.39	1.0E-09
8	Ppp1r3a*	protein phosphatase 1, regulatory (inhibitor) subunit 3A	338.57	9.8E-08
9	Sgcg*	sarcoglycan, gamma (dystrophin-associated glycoprotein)	296.14	1.2E-08
10	Smtnl1*	smoothelin-like 1	293.08	2.8E-08
11	Eef1a2*	eukaryotic translation elongation factor 1 alpha 2	278.59	4.7E-09
12	Dhrs7c*	dehydrogenase/reductase (SDR family) member 7C	277.31	1.0E-07
13	Mylk2*	myosin, light polypeptide kinase 2, skeletal muscle	257.82	7.5E-16
14	Ankrd1	ankyrin repeat domain 1 (cardiac muscle)	253.96	1.0E-08
15	Acta1*	actin, alpha 1, skeletal muscle	248.33	8.9E-08
16	Mybpc1*	myosin binding protein C, slow-type	226.90	1.4E-09

Table B.13, Part I. Continued

	Gene Symbol	Gene	Fold Change	FDR
17	Pvalb*	parvalbumin	223.09	8.2E-07
18	Klhl40	kelch-like 40	208.31	1.6E-08
19	Trdn*	triadin	206.14	2.0E-11
20	Mb*	myoglobin	198.04	2.1E-09
21	Myom2*	myomesin 2	169.25	1.2E-09
22	Tnnt3*	troponin T3, skeletal, fast	153.94	8.9E-10
23	Ampd1*	adenosine monophosphate deaminase 1 (isoform M)	138.98	5.3E-08
24	Ckm*	creatine kinase, muscle	125.67	9.8E-07
25	Tcap*	titin-cap	122.05	2.1E-09
26	Myoz3*	myozenin 3	116.10	1.0E-07
27	Myoc	myocilin	108.53	2.2E-06
28	Cilp	cartilage intermediate layer protein, nucleotide pyrophosphohydrolase	105.27	3.3E-06
29	Tnnc2*	troponin C2, fast	97.68	1.2E-06
30	Sypl2*	synaptophysin-like 2	78.78	3.1E-08
31	Myoz1*	myozenin 1	78.42	9.2E-05
32	A930016O22Rik*	RIKEN cDNA A930016O22 gene	76.07	1.6E-08
33	Igfn1	immunoglobulin-like and fibronectin type III domain containing 1	72.72	1.7E-05
34	Hfe2*	hemochromatosis type 2 (juvenile) (human homolog)	71.06	1.6E-08
35	Abra*	actin-binding Rho activating protein	68.31	3.3E-08
36	Ano5*	anoctamin 5	63.14	5.4E-07
37	Atp2a1*	ATPase, Ca++ transporting, cardiac muscle, fast twitch 1	55.51	5.9E-06
38	Klhl31*	kelch-like 31 (Drosophila)	46.09	3.6E-05
39	Smyd1*	SET and MYND domain containing 1	42.61	6.7E-05
40	Casq1*	calsequestrin 1	39.54	2.0E-05
41	Lmod2*	leiomodin 2 (cardiac)	37.21	2.9E-07

Table B.13, Part I. Continued

	Gene Symbol	Gene	Fold Change	FDR
42	Ostn	osteocrin	35.26	2.0E-07
43	Trim63*	similar to tripartite motif-containing 63; tripartite motif-containing 63	33.44	1.4E-06
44	Myl1*	myosin, light polypeptide 1	29.98	2.7E-07
45	Tnni2*	troponin I, skeletal, fast 2	29.94	6.8E-05
46	Cacna1s*	calcium channel, voltage-dependent, L type, alpha 1S subunit	29.87	2.2E-07
47	Kcnc4*	potassium voltage gated channel, Shaw-related subfamily, member 4	26.72	3.8E-03
48	Thbs4	thrombospondin 4	24.56	1.9E-13
49	Kcna7*	potassium voltage-gated channel, shaker-related subfamily, member 7	23.77	7.2E-07
50	Cilp2	cartilage intermediate layer protein 2	23.54	5.7E-08
51	Actn3*	actinin alpha 3	22.40	1.2E-04
52	Mylpf*	myosin light chain, phosphorylatable, fast skeletal muscle	22.29	3.0E-05
53	Xirp1*	xin actin-binding repeat containing 1	21.94	7.7E-04
54	Jsrp1*	junctional sarcoplasmic reticulum protein 1	18.76	9.2E-05
55	Ldb3*	LIM domain binding 3	17.68	3.2E-04
56	Mybpc2*	myosin binding protein C, fast-type	17.45	3.5E-04
57	Apobec2*	apolipoprotein B mRNA editing enzyme, catalytic polypeptide 2; similar to APOBEC-2 protein	17.25	1.9E-04
58	Ttn*	titin	16.41	8.9E-05
59	Actn2*	actinin alpha 2	16.12	8.9E-05
60	Mypn*	myopalladin	15.79	1.5E-02
61	Mfap4	microfibrillar-associated protein 4	15.65	2.5E-03
62	Kcnj11	potassium inwardly rectifying channel, subfamily J, member 11	15.33	3.2E-05
63	Lrrn1	leucine rich repeat protein 1, neuronal	14.85	2.4E-04
64	Fitm1*	fat storage-inducing transmembrane protein 1	14.56	7.0E-04
65	Nrap*	nebulin-related anchoring protein	14.53	2.8E-04
66	Ckmt2*	creatine kinase, mitochondrial 2	14.22	1.4E-03

Table B.13, Part I. Continued

	Gene Symbol	Gene	Fold Change	FDR
67	Lmod3*	leiomodin 3 (fetal)	13.29	2.2E-04
68	Cacng1*	calcium channel, voltage-dependent, gamma subunit 1	11.62	3.9E-03
69	Igfbp6	insulin-like growth factor binding protein 6	11.47	2.1E-09
70	Des*	desmin	10.90	3.4E-04
71	Sh3bgr*	similar to putative SH3BGR protein; SH3-binding domain glutamic acid-rich protein	10.68	6.1E-04
72	Neb*	nebulin	10.52	1.1E-03
73	Angptl7	angiopoietin-like 7	10.41	1.7E-05
74	Rpl3l*	ribosomal protein L3-like	10.33	2.0E-03
75	Mylk4*	myosin light chain kinase family, member 4	10.18	3.6E-03
76	Murc*	muscle-related coiled-coil protein	9.93	6.3E-03
77	Wnt16	wingless-related MMTV integration site 16	9.85	1.9E-03
78	Itgbl1	integrin, beta-like 1	9.72	3.4E-03
79	Klhl41	kelch-like 41	9.70	1.5E-04
80	Fgf14	fibroblast growth factor 14	9.54	1.7E-05
81	C1qtnf3	C1q and tumor necrosis factor related protein 3	9.47	2.7E-03
82	Cox8b*	cytochrome c oxidase, subunit VIIIb	9.22	4.2E-03
83	Synpo2l*	synaptopodin 2-like	9.05	1.9E-03
84	H19*	H19 fetal liver mRNA	8.96	2.6E-04
85	Asb14*	ankyrin repeat and SOCS box-containing 14	8.84	1.5E-03
86	Aspn	asporin	8.82	4.5E-06
87	Tigd4	tigger transposable element derived 4	8.78	1.4E-03
88	Tbx4	T-box 4	8.15	1.0E-09
89	Atp1a2*	ATPase, Na+/K+ transporting, alpha 2 polypeptide	7.71	5.0E-03
90	1810041L15Rik	RIKEN cDNA 1810041L15 gene	7.70	7.5E-03
91	Pdlim3*	PDZ and LIM domain 3	7.64	2.3E-03

Table B.13, Part I. Continued

	Gene Symbol	Gene	Fold Change	FDR
92	Lrrc15	leucine rich repeat containing 15	7.44	2.1E-07
93	Meox2	mesenchyme homeobox 2	7.28	1.0E-07
94	Slc17a8	solute carrier family 17 (sodium-dependent inorganic phosphate cotransporter), member 8	7.25	1.5E-02
95	Dusp13*	dual specificity phosphatase 13	7.13	1.7E-02
96	Fam180a	cDNA sequence BC064033	7.10	1.9E-04
97	Myh14	myosin, heavy polypeptide 14	6.80	4.2E-02
98	Cntfr	ciliary neurotrophic factor receptor	6.68	2.7E-04
99	Tnn	tenascin N	6.57	2.1E-06
100	Pgam2*	phosphoglycerate mutase 2	6.43	4.4E-03
101	Tmod4*	tropomodulin 4	6.38	1.0E-03
102	Ryr1*	ryanodine receptor 1, skeletal muscle	6.37	1.8E-02
103	Cox7a1*	cytochrome c oxidase, subunit VIIa 1	6.30	7.2E-03
104	Sall1	sal-like 1 (Drosophila)	6.20	3.0E-04
105	Hspb7*	heat shock protein family, member 7 (cardiovascular)	6.06	4.9E-06
106	Sema3c	sema domain, immunoglobulin domain (Ig), short basic domain, secreted, (semaphorin) 3C	5.72	6.5E-05
107	Scube2	similar to signal peptide, CUB domain, EGF-like 2; signal peptide, CUB domain, EGF-like 2	5.50	2.1E-05
108	Col3a1	collagen, type III, alpha 1	5.48	3.5E-04
109	Clcn1*	chloride channel 1	5.38	4.2E-02
110	Islr2	immunoglobulin superfamily containing leucine-rich repeat 2	5.36	1.2E-03
111	Fmod	fibromodulin	5.11	5.6E-06
112	Wnt7b	wingless-related MMTV integration site 7B	5.02	2.9E-04
113	Angptl1	angiopoietin-like 1	4.78	2.3E-03
114	Fndc1	fibronectin type III domain containing 1; similar to fibronectin type III domain containing 1	4.76	1.1E-06

Table B.13, Part I. Continued

	Gene Symbol	Gene	Fold Change	FDR
115	Obscn*	obscurin, cytoskeletal calmodulin and titin-interacting RhoGEF	4.76	4.9E-03
116	Tnxb	tenascin XB	4.74	1.8E-02
117	Col8a2	collagen, type VIII, alpha 2	4.59	2.1E-02
118	Pgm5	phosphoglucomutase 5	4.58	1.7E-04
119	Jph2*	junctophilin 2	4.48	2.0E-02
120	Scn4b*	sodium channel, type IV, beta	4.46	4.0E-02
121	Postn	periostin, osteoblast specific factor	4.35	4.8E-05
122	Nov	nephroblastoma overexpressed gene	4.29	1.3E-02
123	Duoxa1	dual oxidase maturation factor 1	4.29	5.9E-04
124	Txlnb*	taxilin beta	4.28	8.6E-03
125	Bnc2	basonuclin 2	4.15	2.4E-03
126	Miat	myocardial infarction associated transcript (non-protein coding)	3.98	1.0E-06
127	Angptl2	angiopoietin-like 2	3.97	8.9E-10
128	Flnc*	filamin C, gamma	3.97	4.9E-05
129	Trpm6	transient receptor potential cation channel, subfamily M, member 6	3.89	1.2E-03
130	P4ha3	procollagen-proline, 2-oxoglutarate 4-dioxygenase (proline 4-hydroxylase), alpha polypeptide III	3.84	1.5E-03
131	Prrx2	paired related homeobox 2	3.79	1.6E-03
132	Plekhg4	pleckstrin homology domain containing, family G (with RhoGef domain) member 4	3.76	1.1E-04
133	Snhg11	small nucleolar RNA host gene 11 (non-protein coding)	3.74	5.8E-03
134	Srl*	sarcalumenin	3.68	1.7E-03
135	C130021I20Rik	Riken cDNA C130021I20 gene	3.68	4.9E-03
136	Rtn2*	reticulon 2 (Z-band associated protein)	3.68	1.3E-02
137	Pkia*	protein kinase inhibitor, alpha	3.61	1.7E-02
138	Htra4	HtrA serine peptidase 4	3.59	2.7E-02

Table B.13, Part I. Continued

	Gene Symbol	Gene	Fold Change	FDR
139	C1qtnf9	C1q and tumor necrosis factor related protein 9	3.59	7.9E-03
140	Pygm*	muscle glycogen phosphorylase	3.57	1.9E-02
141	Apod	apolipoprotein D	3.54	1.5E-03
142	Thbs2	thrombospondin 2	3.53	4.3E-06
143	3425401B19Rik*	RIKEN cDNA 3425401B19 gene	3.51	1.9E-02
144	Col16a1	collagen, type XVI, alpha 1	3.49	1.1E-07
145	Nox4	NADPH oxidase 4	3.49	7.9E-05
146	Ablim3	actin binding LIM protein family, member 3	3.48	4.2E-04
147	Tenm3	teneurin transmembrane protein 3	3.39	2.6E-04
148	Chst8	carbohydrate (N-acetylgalactosamine 4-0) sulfotransferase 8	3.38	4.0E-03
149	Zfp185	zinc finger protein 185	3.33	1.9E-02
150	Fgf23	similar to FGF23; fibroblast growth factor 23	3.31	3.0E-02
151	Ptn	pleiotrophin	3.29	2.5E-03
152	Ankrd23*	ankyrin repeat domain 23	3.28	1.6E-02
153	Col12a1	collagen, type XII, alpha 1	3.28	5.3E-06
154	Penk	preproenkephalin	3.26	3.5E-02
155	Gabra3	gamma-aminobutyric acid (GABA) A receptor, subunit alpha 3	3.23	1.9E-02
156	Dkk3	dickkopf homolog 3 (Xenopus laevis)	3.19	3.5E-04
157	Shisa2*	shisa homolog 2 (Xenopus laevis)	3.13	3.9E-02
158	Eno3*	enolase 3, beta muscle	3.13	2.3E-02
159	Meg3	maternally expressed 3	3.12	1.9E-07
160	Lrrc17	leucine rich repeat containing 17	3.08	1.4E-06
161	Hhipl1	hedgehog interacting protein-like 1	3.05	1.1E-02
162	Kcnab1	potassium voltage-gated channel, shaker-related subfamily, beta member 1	3.05	2.2E-04
163	3632451O06Rik	RIKEN cDNA 3632451O06 gene	3.02	6.9E-03

Table B.13, Part I. Continued

	Gene Symbol	Gene	Fold Change	FDR
164	Anxa8	annexin A8	3.02	4.3E-04
165	Ppp1r3c*	protein phosphatase 1, regulatory (inhibitor) subunit 3C	3.00	2.7E-02
166	Rian	RNA imprinted and accumulated in nucleus	2.97	3.0E-04
167	Gpnmb	glycoprotein (transmembrane) nmb	2.97	1.8E-05
168	Cmya5*	cardiomyopathy associated 5	2.97	1.0E-02
169	Itm2a	integral membrane protein 2A	2.93	3.7E-04
170	Foxp2	forkhead box P2	2.90	1.1E-02
171	Tppp3	tubulin polymerization-promoting protein family member 3	2.90	2.4E-04
172	Spock2	sparc/osteonectin, cwcv and kazal-like domains proteoglycan 2	2.88	2.6E-04
173	Gpc3	glypican 3	2.87	2.1E-05
174	Spock1	sparc/osteonectin, cwcv and kazal-like domains proteoglycan 1	2.84	3.6E-02
175	Myo16	myosin XVI	2.83	1.4E-03
176	Hspb8*	heat shock protein 8	2.76	3.5E-02
177	Tmem38a*	transmembrane protein 38A	2.76	4.4E-02
178	Thbs3	thrombospondin 3	2.76	4.7E-03
179	Epha3	Eph receptor A3	2.74	2.5E-06
180	Cacng7	calcium channel, voltage-dependent, gamma subunit 7	2.71	1.0E-03
181	Rgs11	regulator of G-protein signaling 11; similar to regulator of G-protein signaling 11	2.70	1.9E-02
182	Dnahc1	dynein, axonemal, heavy chain 1	2.63	6.7E-04
183	Camk4	calcium/calmodulin-dependent protein kinase IV	2.61	1.5E-03
184	Medag	mesenteric estrogen dependent adipogenesis	2.61	1.1E-02
185	Rab15	RAB15, member RAS oncogene family	2.59	2.6E-03
186	Best1	bestrophin 1; hypothetical protein LOC100046789	2.59	7.0E-03
187	Art5*	ADP-ribosyltransferase 5	2.58	3.8E-03
188	Glrb	glycine receptor, beta subunit	2.57	9.6E-03

Table B.13, Part I. Continued

	Gene Symbol	Gene	Fold Change	FDR
189	Prtg	protogenin homolog (Gallus gallus)	2.57	4.8E-03
190	Tceal3	transcription elongation factor A (SII)-like 3	2.56	4.4E-04
191	Ccdc3	coiled-coil domain containing 3	2.55	8.1E-12
192	Higd1b	HIG1 domain family, member 1B	2.54	3.8E-02
193	Glt8d2	glycosyltransferase 8 domain containing 2	2.53	1.7E-04
194	Tnmd	tenomodulin	2.52	8.2E-03
195	C1qtnf2	C1q and tumor necrosis factor related protein 2	2.51	4.3E-02
196	Sparcl1	SPARC-like 1	2.48	3.2E-06
197	Slc6a17	solute carrier family 6 (neurotransmitter transporter), member 17	2.47	9.7E-03
198	Mustn1	musculoskeletal, embryonic nuclear protein 1	2.45	5.5E-03
199	Tgfb2	transforming growth factor, beta 2	2.45	1.0E-03
200	Dpysl4	dihydropyrimidinase-like 4	2.44	1.7E-02
201	Clmn	calmin	2.44	4.5E-02
202	Ccdc141	RIKEN cDNA 2610301F02 gene	2.44	2.9E-03
203	Matn2	matrilin 2	2.43	6.6E-05
204	Msln	mesothelin	2.42	1.5E-04
205	Piwil2	piwi-like homolog 2 (Drosophila)	2.41	1.9E-03
206	Aebp1	AE binding protein 1	2.41	4.7E-06
207	Cdh13	cadherin 13	2.40	3.3E-05
208	Col6a3	collagen, type VI, alpha 3	2.39	2.9E-05
209	Arhgap22	Rho GTPase activating protein 22	2.38	2.2E-02
210	Peg3	paternally expressed 3; antisense transcript gene of Peg3	2.35	2.1E-02
211	Adamtsl1	ADAMTS-like 1	2.34	2.8E-02
212	Asic3	acid-sensing (proton-gated) ion channel 3	2.34	2.6E-04
213	Scn2b	sodium channel, voltage-gated, type II, beta	2.32	1.8E-03

Table B.13, Part I. Continued

	Gene Symbol	Gene	Fold Change	FDR
214	Radil	Ras association and DIL domains	2.31	1.1E-02
215	Galr2	galanin receptor 2	2.31	5.5E-03
216	Cys1	cystin 1	2.31	1.9E-02
217	Lum	lumican	2.29	3.0E-02
218	Plat	plasminogen activator, tissue	2.29	4.3E-02
219	Sost	sclerostin	2.29	4.3E-02
220	Wnt10b	wingless related MMTV integration site 10b	2.29	5.4E-04
221	Tmeff1	transmembrane protein with EGF-like and two follistatin-like domains 1	2.29	3.1E-02
222	Cobl	cordon-bleu	2.28	4.3E-02
223	Baalc	brain and acute leukemia, cytoplasmic	2.28	3.9E-02
224	Ecm2	extracellular matrix protein 2, female organ and adipocyte specific	2.27	1.4E-06
225	Slc6a7	solute carrier family 6 (neurotransmitter transporter, L-proline), member 7	2.27	1.0E-04
226	Mall	mal, T-cell differentiation protein-like	2.24	4.2E-02
227	Usp13*	ubiquitin specific peptidase 13 (isopeptidase T-3)	2.24	1.5E-02
228	Rnf207	ring finger protein 207	2.24	3.1E-02
229	Hr	hairless	2.24	1.3E-02
230	Hrc*	histidine rich calcium binding protein	2.24	2.8E-02
231	Adamts17	a disintegrin-like and metallopeptidase (reprolysin type) with thrombospondin type 1 motif, 17	2.24	1.4E-04
232	Pamr1	peptidase domain containing associated with muscle regeneration 1	2.22	8.0E-06
233	Sulf1	sulfatase 1	2.21	3.2E-07
234	Peg3as	Peg3 opposite strand	2.21	2.1E-02
235	Prnd	prion protein dublet	2.20	2.3E-03
236	Serpine1	serine (or cysteine) peptidase inhibitor, clade E, member 1	2.19	8.2E-04
237	Cyb5r2	cytochrome b5 reductase 2	2.19	1.7E-02
238	Edil3	EGF-like repeats and discoidin I-like domains 3	2.18	5.7E-06

Table B.13, Part I. Continued

	Gene Symbol	Gene	Fold Change	FDR
239	Adcy1	adenylate cyclase 1	2.17	1.6E-03
240	Nbl1	neuroblastoma, suppression of tumorigenicity 1	2.17	3.0E-02
241	Dnahc7b	dynein, axonemal, heavy chain 7B	2.17	2.5E-02
242	D630003M21Rik	RIKEN cDNA D630003M21 gene	2.16	1.2E-02
243	Ssc5d	scavenger receptor cysteine rich family, 5 domains	2.16	1.3E-05
244	Htra1	HtrA serine peptidase 1	2.15	2.2E-05
245	Mn1	meningioma 1	2.14	3.2E-02
246	Gabrb3	gamma-aminobutyric acid (GABA) A receptor, subunit beta 3	2.13	1.7E-02
247	P2rx6	purinergic receptor P2X, ligand-gated ion channel, 6	2.12	4.4E-02
248	Gpx3	glutathione peroxidase 3	2.10	6.8E-05
249	Magix	MAGI family member, X-linked	2.10	1.6E-02
250	Pdgfrl	platelet-derived growth factor receptor-like	2.09	1.4E-02
251	Jph1*	junctophilin 1	2.09	4.0E-02
252	Epha4	Eph receptor A4	2.08	1.3E-04
253	Hmcn1	hemicentin 1	2.08	8.3E-03
254	Meox1	mesenchyme homeobox 1	2.08	6.6E-03
255	Wfdc1*	WAP four-disulfide core domain 1	2.07	3.4E-02
256	Lama2	laminin, alpha 2	2.06	1.3E-02
257	Efcc1	EF hand and coiled-coil domain containing 1	2.06	1.3E-02
258	Ankrd29	ankyrin repeat domain 29	2.03	4.7E-03
259	Npy	neuropeptide Y	2.03	2.9E-03
260	Ube2ql1	RIKEN cDNA 3110006E14 gene	2.03	1.1E-03
261	Timp1	tissue inhibitor of metalloproteinase 1	2.03	1.9E-03
262	Smoc2	SPARC related modular calcium binding 2	2.03	1.7E-02
263	Rassf9	Ras association (RalGDS/AF-6) domain family (N-terminal) member 9	2.03	5.0E-03

Table B.13, Part I. Continued

	Gene Symbol	Gene	Fold Change	FDR
264	Lonrf2	LON peptidase N-terminal domain and ring finger 2	2.02	2.0E-02
265	Ptprv	protein tyrosine phosphatase, receptor type, V	2.01	7.5E-06

Table B.13, Part II. List of genes more highly expressed in control cancellous bone of pOC-ERαKO animals at 3 hours

	Gene Symbol	Gene	Fold Change	FDR
1	Ly6g6c	lymphocyte antigen 6 complex, locus G6C	3.42	6.0E-03
2	Clec4g	C-type lectin domain family 4, member g	3.40	1.1E-04
3	G6b	G6B protein	3.11	3.9E-04
4	Ccdc150	coiled-coil domain containing 150	2.82	3.0E-06
5	Kcnj5	potassium inwardly-rectifying channel, subfamily J, member 5	2.81	2.4E-06
6	Slamf1	signaling lymphocytic activation molecule family member 1	2.73	1.0E-09
7	Reep2	receptor accessory protein 2	2.72	2.2E-05
8	Gp6	glycoprotein 6 (platelet)	2.69	1.4E-06
9	Serpinb2	serine (or cysteine) peptidase inhibitor, clade B, member 2	2.69	2.1E-07
10	AU023871	expressed sequence AU023871	2.69	2.3E-06
11	Gp1ba	glycoprotein 1b, alpha polypeptide	2.65	8.2E-06
12	Akap5	A kinase (PRKA) anchor protein 5	2.63	1.2E-03
13	Cd226*	CD226 antigen	2.60	1.1E-07
14	Lypd6	LY6/PLAUR domain containing 6	2.60	1.8E-02
15	Gm13710	predicted gene 13710	2.60	3.4E-02
16	Ppbp	pro-platelet basic protein	2.56	9.2E-07
17	F2rl2	coagulation factor II (thrombin) receptor-like 2	2.54	1.8E-06

Table B.13, Part II. Continued

	Gene Symbol	Gene	Fold Change	FDR
18	Gp5	glycoprotein 5 (platelet)	2.52	2.8E-05
19	Mmrn1	multimerin 1	2.49	4.9E-06
20	Slc16a9	solute carrier family 16 (monocarboxylic acid transporters), member 9	2.48	1.7E-06
21	Clec1b	C-type lectin domain family 1, member b	2.48	4.9E-07
22	Cxcl5	chemokine (C-X-C motif) ligand 5	2.47	2.8E-04
23	Ly6g6f	lymphocyte antigen 6 complex, locus G6F	2.47	6.5E-05
24	Gcsam	germinal center associated, signaling and motility	2.47	1.5E-05
25	Tubb1	tubulin, beta 1	2.46	2.5E-06
26	Ptprn	protein tyrosine phosphatase, receptor type, N	2.45	4.6E-03
27	Mpl	myeloproliferative leukemia virus oncogene	2.45	1.9E-05
28	Gm1968	predicted gene 1968	2.44	3.3E-04
29	Nlrp6	NLR family, pyrin domain containing 6	2.43	6.7E-03
30	Treml1	triggering receptor expressed on myeloid cells-like 1	2.43	1.1E-05
31	Alox12	arachidonate 12-lipoxygenase	2.43	8.6E-06
32	Gnaz	guanine nucleotide binding protein, alpha z subunit	2.41	6.7E-04
33	Dclk3	doublecortin-like kinase 3	2.41	3.4E-02
34	Slc14a1	solute carrier family 14 (urea transporter), member 1	2.41	3.8E-05
35	Elovl7	ELOVL family member 7, elongation of long chain fatty acids (yeast)	2.40	7.2E-05
36	Tnfsf15	tumor necrosis factor (ligand) superfamily, member 15	2.40	3.4E-02
37	Itga2b	integrin alpha 2b	2.40	1.3E-04
38	Clca1	chloride channel calcium activated 1	2.39	2.3E-06
39	Pf4	platelet factor 4	2.37	2.5E-05
40	Pls1	plastin 1 (I-isoform)	2.37	4.1E-05
41	Igfbp2	insulin-like growth factor binding protein 2	2.36	2.2E-04
42	Ache*	acetylcholinesterase	2.36	6.5E-05

Table B.13, Part II. Continued

	Gene Symbol	Gene	Fold Change	FDR
43	Slc6a4	solute carrier family 6 (neurotransmitter transporter, serotonin), member 4	2.36	1.3E-06
44	Pkd1l3	polycystic kidney disease 1 like 3	2.35	2.5E-03
45	E230029C05Rik	RIKEN cDNA E230029C05 gene	2.34	3.7E-02
46	Aldob	aldolase B, fructose-bisphosphate	2.32	1.4E-02
47	Ltb4r2	leukotriene B4 receptor 2	2.32	4.1E-02
48	Kng2	kininogen 2	2.32	1.4E-06
49	Mrvi1	MRV integration site 1	2.31	4.4E-05
50	Ufsp1	UFM1-specific peptidase 1	2.30	3.2E-05
51	Gramd1c	GRAM domain containing 1C	2.30	8.0E-06
52	Gp9*	glycoprotein 9 (platelet)	2.30	2.3E-04
53	Gp1bb	glycoprotein Ib, beta polypeptide	2.29	2.6E-04
54	C530008M17Rik	RIKEN cDNA C530008M17 gene	2.28	3.5E-05
55	Mfsd2b	predicted gene 1964	2.28	4.5E-05
56	Nrgn	neurogranin	2.28	2.2E-05
57	Slc6a20a	solute carrier family 6 (neurotransmitter transporter), member 20A	2.27	1.7E-02
58	Rbpms2	RNA binding protein with multiple splicing 2	2.27	5.6E-06
59	Ppp1r14a	protein phosphatase 1, regulatory (inhibitor) subunit 14A	2.27	4.6E-02
60	Il1a	interleukin 1 alpha	2.27	3.1E-06
61	P2rx1	purinergic receptor P2X, ligand-gated ion channel, 1	2.26	2.2E-05
62	Rgs18	regulator of G-protein signaling 18	2.26	3.7E-07
63	Slc24a5	solute carrier family 24, member 5	2.25	2.2E-04
64	Dok2	docking protein 2	2.25	1.4E-06
65	Tesc	tescalcin; similar to Tescalcin	2.25	3.6E-03
66	Plek	pleckstrin	2.23	4.9E-06
67	Vwf	Von Willebrand factor homolog	2.23	9.5E-04

Table B.13, Part II. Continued

	Gene Symbol	Gene	Fold Change	FDR
68	Slc35d3	solute carrier family 35, member D3	2.21	1.0E-03
69	Kng1	kininogen 1	2.21	1.8E-06
70	Selp	selectin, platelet	2.20	7.6E-06
71	Hist1h1d	histone cluster 1, H1d	2.19	2.3E-02
72	Slc6a3	solute carrier family 6 (neurotransmitter transporter, dopamine), member 3	2.18	1.8E-03
73	Ubd	ubiquitin D	2.18	1.8E-04
74	C6	complement component 6	2.17	4.0E-04
75	Ptger3	prostaglandin E receptor 3 (subtype EP3)	2.17	2.7E-04
76	Lipg	lipase, endothelial	2.16	2.0E-04
77	Serpina3b	serine (or cysteine) peptidase inhibitor, clade A, member 3B	2.16	1.2E-02
78	Cd5l	CD5 antigen-like	2.16	7.1E-04
79	F5	coagulation factor V	2.16	4.5E-05
80	Robo3	roundabout homolog 3 (Drosophila)	2.15	1.6E-03
81	Trpc6	transient receptor potential cation channel, subfamily C, member 6	2.15	1.4E-05
82	D830046C22Rik	RIKEN cDNA D830046C22 gene	2.15	2.4E-03
83	Kcna2	potassium voltage-gated channel, shaker-related subfamily, member 2	2.15	5.1E-05
84	AI504432	expressed sequence AI504432	2.14	1.4E-07
85	Angpt1	angiopoietin 1	2.14	4.9E-06
86	Prkar2b	protein kinase, cAMP dependent regulatory, type II beta	2.13	6.2E-06
87	Grem1	gremlin 1	2.13	2.0E-03
88	Cass4	Cas scaffolding protein family member 4	2.12	9.9E-05
89	Dhcr24	24-dehydrocholesterol reductase	2.12	1.5E-04
90	Pde3a	phosphodiesterase 3A, cGMP inhibited	2.11	9.9E-05
91	Cited4	Cbp/p300-interacting transactivator, with Glu/Asp-rich carboxy-terminal domain, 4	2.11	7.2E-03
92	Arhgap6	Rho GTPase activating protein 6	2.09	6.7E-04

Table B.13, Part II. Continued

	Gene Symbol	Gene	Fold Change	FDR
93	Fcna	ficolin A	2.09	1.8E-04
94	Hist1h4m	histone cluster 1, H4m	2.09	4.0E-02
95	Chrdl1	chordin-like 1	2.09	2.5E-06
96	Sdpr	serum deprivation response	2.08	1.2E-05
97	Npas4	neuronal PAS domain protein 4	2.08	6.3E-04
98	Esm1	endothelial cell-specific molecule 1	2.07	6.3E-05
99	Kcnj9	potassium inwardly-rectifying channel, subfamily J, member 9	2.07	3.5E-02
100	Susd2	sushi domain containing 2	2.07	1.7E-04
101	Gpm6a	glycoprotein m6a	2.06	4.2E-04
102	Tmem40	transmembrane protein 40	2.06	6.1E-05
103	Fmo2	flavin containing monooxygenase 2	2.06	7.2E-05
104	Gm16548	predicted gene 16548	2.05	5.4E-03
105	Scimp	SLP adaptor and CSK interacting membrane protein	2.04	2.4E-02
106	Sec14l5*	SEC14-like 5 (S. cerevisiae)	2.04	6.2E-03
107	Gfi1b	growth factor independent 1B	2.04	1.0E-03
108	Serpinb10	serine (or cysteine) peptidase inhibitor, clade B (ovalbumin), member 10	2.03	6.0E-04
109	Tmem178	transmembrane protein 178	2.02	1.9E-03
110	I830077J02Rik	RIKEN cDNA I830077J02 gene	2.02	3.5E-04
111	Darc	Duffy blood group, chemokine receptor	2.02	7.6E-04
112	F2rl3	coagulation factor II (thrombin) receptor-like 3	2.02	4.9E-03
113	Slc30a10	solute carrier family 30, member 10	2.01	2.9E-02
114	Lat	linker for activation of T cells	2.01	2.4E-03
115	Gata1	GATA binding protein 1	2.01	7.9E-04
116	Ubash3b	ubiquitin associated and SH3 domain containing, B	2.00	2.7E-06

Table B.13, Part II. Continued

total	381
*indicates contaminant	102
total without contaminants	279

Table B.14 A complete list of genes that were differentially expressed in pOC-ERαKO animals at 24 hours in cortical vs cancellous bone at baseline in order of decreasing fold change that were: I. more highly expressed in cortical bone and II. more highly expressed in cancellous bone. Number of genes (column A), gene symbols (column B), gene names (column C), fold change (column D), false discovery rate (FDR) (column E). * indicates contamination as determined by Ayturk et al.

Table B.14, Part I List of genes more highly expressed in control cortical bone of pOC-ERαKO animals at 24 hours

	Gene Symbol	Gene	Fold Change	FDR
1	Myh4*	myosin, heavy polypeptide 4, skeletal muscle	609.91	8.2E-04
2	Myoz2*	myozenin 2	506.34	2.7E-07
3	Ear12	eosinophil-associated, ribonuclease A family, member 3; eosinophil-associated, ribonuclease A family, member 12; eosinophil-associated, ribonuclease A family, member 2	454.02	6.1E-04
4	Ppp1r3a*	protein phosphatase 1, regulatory (inhibitor) subunit 3A	323.01	1.2E-07
5	Vgll2	vestigial like 2 homolog (Drosophila)	301.32	4.0E-06
6	Myh1*	myosin, heavy polypeptide 2, skeletal muscle, adult; myosin, heavy polypeptide 1, skeletal muscle, adult	250.40	3.5E-07
7	Smtnl1*	smoothelin-like 1	204.21	7.1E-08
8	Trim63*	similar to tripartite motif-containing 63; tripartite motif-containing 63	179.43	9.5E-06
9	Ckm*	creatine kinase, muscle	178.74	1.1E-05
10	Abra*	actin-binding Rho activating protein	175.19	4.7E-06
11	Mylk2*	myosin, light polypeptide kinase 2, skeletal muscle	149.17	3.5E-08
12	Myh2*	myosin, heavy polypeptide 2, skeletal muscle, adult; myosin, heavy polypeptide 1, skeletal muscle, adult	145.69	2.6E-05
13	Eef1a2*	eukaryotic translation elongation factor 1 alpha 2	137.37	4.7E-07
14	Myot*	myotilin	132.89	1.6E-08
15	Myom2*	myomesin 2	129.01	3.1E-06
16	Dhrs7c*	dehydrogenase/reductase (SDR family) member 7C	127.38	1.0E-06

Table B.14, Part I Continued

	Gene Symbol	Gene	Fold Change	FDR
17	Ampd1*	adenosine monophosphate deaminase 1 (isoform M)	122.12	3.1E-06
18	Acta1*	actin, alpha 1, skeletal muscle	113.98	3.2E-05
19	Ano5*	anoctamin 5	107.33	7.2E-06
20	Xirp2*	xin actin-binding repeat containing 2	99.81	9.8E-04
21	Tcap*	titin-cap	97.57	2.0E-10
22	Atp2a1*	ATPase, Ca++ transporting, cardiac muscle, fast twitch 1	94.56	4.1E-07
23	Mb*	myoglobin	93.55	1.2E-05
24	Smyd1*	SET and MYND domain containing 1	90.83	7.1E-08
25	Tnnt3*	troponin T3, skeletal, fast	90.17	2.2E-06
26	Trdn*	triadin	88.29	1.2E-07
27	Tnnc2*	troponin C2, fast	87.00	4.1E-07
28	Klhl40	kelch-like 40	86.38	3.6E-04
29	Pvalb*	parvalbumin	84.22	3.1E-04
30	Sypl2*	synaptophysin-like 2	78.39	3.0E-06
31	Lmod2*	leiomodin 2 (cardiac)	72.98	1.1E-06
32	Ckmt2*	creatine kinase, mitochondrial 2	68.20	3.5E-08
33	Nctc1*	non-coding transcript 1	67.93	1.8E-04
34	Asb15*	ankyrin repeat and SOCS box-containing 15	65.71	2.0E-04
35	Hhatl*	hedgehog acyltransferase-like	64.21	3.2E-05
36	Hfe2*	hemochromatosis type 2 (juvenile) (human homolog)	63.03	3.4E-06
37	Casq1*	calsequestrin 1	63.01	1.1E-06
38	Mybpc1*	myosin binding protein C, slow-type	62.95	1.0E-05
39	Klhl31*	kelch-like 31 (Drosophila)	56.14	1.1E-04
40	Smpx*	small muscle protein, X-linked	53.91	3.1E-06
41	Trim54*	tripartite motif-containing 54	46.54	3.2E-05

Table B.14, Part I Continued

	Gene Symbol	Gene	Fold Change	FDR
42	Cilp	cartilage intermediate layer protein, nucleotide pyrophosphohydrolase	46.46	2.5E-02
43	Actn2*	actinin alpha 2	46.18	6.1E-07
44	Myoz1*	myozenin 1	46.12	3.0E-06
45	A930016O22Rik*	RIKEN cDNA A930016O22 gene	44.46	7.8E-07
46	Yipf7*	Yip1 domain family, member 7	43.96	1.0E-04
47	Murc*	muscle-related coiled-coil protein	41.22	4.9E-06
48	Cacna1s*	calcium channel, voltage-dependent, L type, alpha 1S subunit	40.24	1.2E-07
49	2310002L09Rik*	RIKEN cDNA 2310002L09 gene	39.18	4.4E-04
50	Jsrp1*	junctional sarcoplasmic reticulum protein 1	38.79	1.0E-05
51	Kcnc4*	potassium voltage gated channel, Shaw-related subfamily, member 4	38.58	3.4E-05
52	Tnni2*	troponin I, skeletal, fast 2	37.61	4.0E-05
53	Mylpf*	myosin light chain, phosphorylatable, fast skeletal muscle	36.56	7.8E-07
54	Mybpc2*	myosin binding protein C, fast-type	35.43	1.4E-04
55	Nrap*	nebulin-related anchoring protein	34.37	6.6E-08
56	Ankrd1	ankyrin repeat domain 1 (cardiac muscle)	33.68	8.3E-04
57	Clcn1*	chloride channel 1	32.74	1.4E-04
58	Neb*	nebulin	32.51	1.6E-06
59	Myl1*	myosin, light polypeptide 1	32.15	4.8E-06
60	Ldb3*	LIM domain binding 3	32.09	1.0E-06
61	Rpl3l*	ribosomal protein L3-like	31.66	2.9E-07
62	Ttn*	titin	31.13	8.6E-07
63	Igfn1	immunoglobulin-like and fibronectin type III domain containing 1	30.65	8.6E-04
64	Actn3*	actinin alpha 3	29.95	1.1E-06
65	Kcna7*	potassium voltage-gated channel, shaker-related subfamily, member 7	26.17	1.3E-04
66	Sgcg*	sarcoglycan, gamma (dystrophin-associated glycoprotein)	24.56	4.4E-04

Table B.14, Part I Continued

	Gene Symbol	Gene	Fold Change	FDR
67	H19*	H19 fetal liver mRNA	22.91	1.1E-07
68	Fitm1*	fat storage-inducing transmembrane protein 1	22.78	2.2E-04
69	Dusp13*	dual specificity phosphatase 13	21.12	2.4E-04
70	Ryr1*	ryanodine receptor 1, skeletal muscle	20.65	9.9E-06
71	Myoz3*	myozenin 3	20.59	3.6E-03
72	Adamts8	a disintegrin-like and metallopeptidase (reprolysin type) with thrombospondin type 1 motif, 8	19.08	4.9E-06
73	Myoc	myocilin	19.03	1.2E-02
74	Mylk4*	myosin light chain kinase family, member 4	18.95	2.1E-04
75	Mypn*	myopalladin	18.86	1.3E-03
76	Mybph	myosin binding protein H	18.85	3.6E-02
77	Des*	desmin	18.28	1.4E-06
78	Klhl41	kelch-like 41	18.21	6.2E-04
79	Fbxo40*	F-box protein 40	17.69	3.6E-03
80	Thbs4	thrombospondin 4	17.29	3.7E-04
81	Sh3bgr*	similar to putative SH3BGR protein; SH3-binding domain glutamic acid-rich protein	16.37	4.3E-05
82	Apobec2*	apolipoprotein B mRNA editing enzyme, catalytic polypeptide 2; similar to APOBEC-2 protein	15.44	3.5E-04
83	Xirp1*	xin actin-binding repeat containing 1	14.87	1.4E-03
84	Asb11*	ankyrin repeat and SOCS box-containing 11	14.72	4.5E-03
85	Lmod3*	leiomodin 3 (fetal)	14.29	1.9E-04
86	Cox8b*	cytochrome c oxidase, subunit VIIIb	13.89	9.6E-04
87	Synpo2l*	synaptopodin 2-like	13.44	1.4E-03
88	Pgam2*	phosphoglycerate mutase 2	13.34	1.7E-04
89	Cacng1*	calcium channel, voltage-dependent, gamma subunit 1	13.17	1.1E-03
90	Atp1a2*	ATPase, Na+/K+ transporting, alpha 2 polypeptide	12.48	5.0E-05

Table B.14, Part I Continued

	Gene Symbol	Gene	Fold Change	FDR
91	Scn4b*	sodium channel, type IV, beta	11.95	4.5E-04
92	Tigd4	tigger transposable element derived 4	11.27	1.1E-03
93	Asb5*	ankyrin repeat and SOCs box-containing 5	11.09	2.3E-02
94	Ppp1r14c*	protein phosphatase 1, regulatory (inhibitor) subunit 14c	10.65	1.2E-03
95	Slc38a3*	solute carrier family 38, member 3	10.28	1.3E-02
96	Sel1l3*	RIKEN cDNA 2310045A20 gene	10.18	1.0E-03
97	Pdlim3*	PDZ and LIM domain 3	10.03	1.1E-03
98	Txlnb*	taxilin beta	10.00	1.1E-04
99	Prkag3*	protein kinase, AMP-activated, gamma 3 non-catatlytic subunit	9.89	7.7E-03
100	Kcnj11	potassium inwardly rectifying channel, subfamily J, member 11	9.70	3.0E-02
101	Ostn	osteocrin	9.56	1.6E-04
102	Cox7a1*	cytochrome c oxidase, subunit VIIa 1	9.51	3.6E-04
103	Hspb7*	heat shock protein family, member 7 (cardiovascular)	9.50	1.6E-05
104	Myl2*	myosin, light polypeptide 2, regulatory, cardiac, slow	9.06	2.1E-02
105	Obscn*	obscurin, cytoskeletal calmodulin and titin-interacting RhoGEF	9.00	2.0E-04
106	Alpk3*	alpha-kinase 3	8.81	4.8E-04
107	Myo18b*	myosin XVIIIb	8.74	2.6E-04
108	Tmod4*	tropomodulin 4	8.50	1.8E-03
109	Cilp2	cartilage intermediate layer protein 2	8.00	1.8E-03
110	Trim72*	tripartite motif-containing 72	7.95	8.2E-03
111	Mfap4	microfibrillar-associated protein 4	7.91	7.0E-03
112	C1qtnf9	C1q and tumor necrosis factor related protein 9	7.67	1.0E-05
113	Hspb6*	heat shock protein, alpha-crystallin-related, B6	7.57	6.2E-04
114	Nos1	nitric oxide synthase 1, neuronal	7.49	5.4E-02
115	Chad	chondroadherin	7.34	5.7E-02

Table B.14, Part I Continued

	Gene Symbol	Gene	Fold Change	FDR
116	Ankrd23*	ankyrin repeat domain 23	7.32	5.5E-04
117	Itgb1bp2*	integrin beta 1 binding protein 2	7.26	2.3E-02
118	Fndc5*	fibronectin type III domain containing 5	7.25	4.9E-03
119	Igfbp6	insulin-like growth factor binding protein 6	7.22	1.6E-04
120	Rtn2*	reticulon 2 (Z-band associated protein)	6.98	1.1E-03
121	Lrrn1	leucine rich repeat protein 1, neuronal	6.96	1.9E-02
122	Cox6a2*	cytochrome c oxidase, subunit VI a, polypeptide 2	6.30	7.8E-03
123	Fam180a	cDNA sequence BC064033	5.85	2.7E-02
124	Plekhb1	pleckstrin homology domain containing, family B (evectins) member 1	5.79	7.8E-03
125	Pygm*	muscle glycogen phosphorylase	5.73	1.7E-03
126	Flnc*	filamin C, gamma	5.72	2.1E-04
127	Wnt16	wingless-related MMTV integration site 16	5.68	5.3E-03
128	Cmya5*	cardiomyopathy associated 5	5.58	7.3E-04
129	Pkia*	protein kinase inhibitor, alpha	5.32	9.8E-04
130	Phkg1*	phosphorylase kinase gamma 1	5.29	9.5E-03
131	Tbx4	T-box 4	5.27	7.6E-06
132	Meox2	mesenchyme homeobox 2	5.25	7.6E-05
133	Dusp26	dual specificity phosphatase 26 (putative)	5.22	2.1E-02
134	Apod	apolipoprotein D	5.19	3.9E-04
135	Itgbl1	integrin, beta-like 1	5.15	2.1E-03
136	Sh3rf2	SH3 domain containing ring finger 2	5.09	3.0E-02
137	Hspb8*	heat shock protein 8	5.05	3.1E-04
138	Aspn	asporin	4.96	9.6E-05
139	Scn4a*	sodium channel, voltage-gated, type IV, alpha	4.92	1.6E-02
140	3425401B19Rik*	RIKEN cDNA 3425401B19 gene	4.88	3.8E-03

Table B.14, Part I Continued

	Gene Symbol	Gene	Fold Change	FDR
141	Pgm5	phosphoglucomutase 5	4.82	8.3E-05
142	Mcpt4	mast cell protease 3; mast cell protease 4	4.76	4.6E-02
143	Cntfr	ciliary neurotrophic factor receptor	4.75	1.7E-02
144	Rbm24*	RNA binding motif protein 24	4.66	2.2E-02
145	Ndrg2*	N-myc downstream regulated gene 2	4.55	3.2E-03
146	Eno3*	enolase 3, beta muscle	4.53	4.2E-03
147	Tpm2*	tropomyosin 2, beta	4.52	8.6E-04
148	Chst8	carbohydrate (N-acetylgalactosamine 4-0) sulfotransferase 8	4.40	2.3E-03
149	Me3	malic enzyme 3, NADP(+)-dependent, mitochondrial	4.37	1.7E-02
150	Srl*	sarcalumenin	4.33	2.7E-03
151	Serinc2	serine incorporator 2; hypothetical protein LOC100044221	4.22	2.0E-02
152	Tnn	tenascin N	4.16	1.1E-07
153	Wnk2	WNK lysine deficient protein kinase 2	4.16	2.7E-02
154	Ablim3	actin binding LIM protein family, member 3	4.12	1.1E-03
155	Tmem38a*	transmembrane protein 38A	4.10	8.6E-03
156	Myl3*	myosin, light polypeptide 3	4.03	4.5E-02
157	Jph2*	junctophilin 2	4.01	1.2E-03
158	Sall1	sal-like 1 (Drosophila)	4.01	5.1E-03
159	Fndc1	fibronectin type III domain containing 1; similar to fibronectin type III domain containing 1	3.98	3.4E-05
160	Lrrc15	leucine rich repeat containing 15	3.91	6.7E-07
161	Jph4	junctophilin 4	3.88	3.9E-02
162	Tpd52l1	tumor protein D52-like 1	3.85	1.9E-02
163	Fmod	fibromodulin	3.81	4.7E-07
164	Csrp3	cysteine and glycine-rich protein 3	3.73	2.7E-02
165	Synpo2*	synaptopodin 2	3.64	3.2E-02

Table B.14, Part I Continued

	Gene Symbol	Gene	Fold Change	FDR
166	Mapt	microtubule-associated protein tau	3.61	3.3E-02
167	Duox1	dual oxidase 1	3.59	8.0E-03
168	Ky*	kyphoscoliosis peptidase	3.48	5.8E-02
169	Sema3c	sema domain, immunoglobulin domain (Ig), short basic domain, secreted, (semaphorin) 3C	3.46	3.5E-02
170	Crabp2	cellular retinoic acid binding protein II	3.45	4.1E-03
171	Tpsb2	tryptase beta 2	3.41	4.9E-02
172	Col3a1	collagen, type III, alpha 1	3.39	1.7E-03
173	Penk	preproenkephalin	3.36	1.5E-02
174	Cers1	ceramide synthase 1	3.36	3.2E-02
175	Mrgprf	MAS-related GPR, member F	3.24	1.3E-02
176	C1qtnf2	C1q and tumor necrosis factor related protein 2	3.24	1.3E-02
177	Megf6	multiple EGF-like-domains 6	3.23	8.0E-03
178	Hspa1a	heat shock protein 1B; heat shock protein 1A; heat shock protein 1-like	3.21	1.2E-02
179	Nexn*	nexilin	3.20	1.8E-02
180	Rab15	RAB15, member RAS oncogene family	3.15	3.5E-04
181	Prrx2	paired related homeobox 2	3.10	1.3E-02
182	Ppp1r3c*	protein phosphatase 1, regulatory (inhibitor) subunit 3C	3.09	2.9E-02
183	Acta2	actin, alpha 2, smooth muscle, aorta	3.09	1.2E-03
184	Pm20d2	peptidase M20 domain containing 2	2.98	2.4E-02
185	P4ha3	procollagen-proline, 2-oxoglutarate 4-dioxygenase (proline 4-hydroxylase), alpha polypeptide III	2.96	5.9E-03
186	Angptl2	angiopoietin-like 2	2.94	3.7E-05
187	Ssc5d	scavenger receptor cysteine rich family, 5 domains	2.94	2.9E-05
188	Angptl7	angiopoietin-like 7	2.88	4.3E-02
189	Duoxa1	dual oxidase maturation factor 1	2.87	1.9E-02

Table B.14, Part I Continued

	Gene Symbol	Gene	Fold Change	FDR
190	Meg3	maternally expressed 3	2.81	2.3E-04
191	Sparcl1	SPARC-like 1	2.80	4.5E-12
192	Mustn1	musculoskeletal, embryonic nuclear protein 1	2.79	3.8E-02
193	Kcns1	K+ voltage-gated channel, subfamily S, 1	2.77	1.8E-02
194	Cacng7	calcium channel, voltage-dependent, gamma subunit 7	2.76	2.3E-03
195	Zfp185	zinc finger protein 185	2.70	3.1E-02
196	Pfkm*	phosphofructokinase, muscle	2.68	2.4E-02
197	Cdh13	cadherin 13	2.67	2.4E-06
198	Miat	myocardial infarction associated transcript (non-protein coding)	2.65	3.4E-05
199	Aebp1	AE binding protein 1	2.64	7.1E-08
200	Postn	periostin, osteoblast specific factor	2.60	1.6E-03
201	Tgfb2	transforming growth factor, beta 2	2.59	6.9E-07
202	Thbs2	thrombospondin 2	2.56	1.5E-04
203	Plekhg4	pleckstrin homology domain containing, family G (with RhoGef domain) member 4	2.56	8.2E-03
204	Sncg	synuclein, gamma	2.56	5.8E-02
205	Aldh1a3	aldehyde dehydrogenase family 1, subfamily A3	2.55	2.2E-05
206	Tenm3	teneurin transmembrane protein 3	2.55	2.2E-05
207	Anxa8	annexin A8	2.54	3.8E-02
208	Cav3*	caveolin 3	2.53	3.1E-02
209	Myo16	myosin XVI	2.52	2.6E-02
210	Usp13*	ubiquitin specific peptidase 13 (isopeptidase T-3)	2.49	1.4E-02
211	Spock2	sparc/osteonectin, cwcv and kazal-like domains proteoglycan 2	2.48	7.4E-03
212	Sox8	SRY-box containing gene 8	2.47	4.8E-02
213	Nptxr	chromobox homolog 6; neuronal pentraxin receptor; Cbx6-Nptxr readthrough transcripts	2.46	3.6E-02

Table B.14, Part I Continued

	Gene Symbol	Gene	Fold Change	FDR
214	Ptn	pleiotrophin	2.45	6.1E-04
215	Thbs3	thrombospondin 3	2.43	8.2E-03
216	Bai2	brain-specific angiogenesis inhibitor 2	2.43	5.9E-03
217	Efhd1	EF hand domain containing 1	2.42	4.8E-02
218	Mmp12	matrix metallopeptidase 12	2.42	4.4E-02
219	Col16a1	collagen, type XVI, alpha 1	2.41	1.7E-04
220	Nox4	NADPH oxidase 4	2.40	1.1E-02
221	Spock1	sparc/osteonectin, cwcv and kazal-like domains proteoglycan 1	2.39	4.7E-02
222	Gpnmb	glycoprotein (transmembrane) nmb	2.37	7.0E-04
223	Tagln	transgelin	2.34	6.6E-03
224	Ptgs2	prostaglandin-endoperoxide synthase 2	2.33	4.4E-03
225	Col12a1	collagen, type XII, alpha 1	2.32	2.0E-05
226	Scube1	signal peptide, CUB domain, EGF-like 1	2.27	9.4E-03
227	Jph1*	junctophilin 1	2.26	4.9E-02
228	Npy	neuropeptide Y	2.25	3.4E-03
229	Gng8	guanine nucleotide binding protein (G protein), gamma 8	2.24	5.5E-02
230	Morn4	MORN repeat containing 4	2.23	2.8E-02
231	Tbx3	T-box 3	2.20	2.1E-03
232	Gpc3	glypican 3	2.19	1.1E-04
233	Slc6a17	solute carrier family 6 (neurotransmitter transporter), member 17	2.19	4.7E-02
234	Sema6c	sema domain, transmembrane domain (TM), and cytoplasmic domain, (semaphorin) 6C	2.16	4.6E-02
235	Prnd	prion protein dublet	2.13	2.0E-02
236	Hr	hairless	2.13	1.1E-03
237	3632451O06Rik	RIKEN cDNA 3632451O06 gene	2.13	2.0E-02
238	Fabp3*	fatty acid binding protein 3, muscle and heart	2.11	3.1E-02

Table B.14, Part I Continued

	Gene Symbol	Gene	Fold Change	FDR
239	Pacsin3*	protein kinase C and casein kinase substrate in neurons 3	2.10	2.6E-02
240	Edn1	endothelin 1	2.10	4.8E-02
241	Tppp3	tubulin polymerization-promoting protein family member 3	2.09	2.4E-02
242	Fzd2	frizzled homolog 2 (Drosophila)	2.06	1.9E-02
243	Hapln3	hyaluronan and proteoglycan link protein 3	2.06	3.3E-02
244	Nog	noggin	2.05	6.7E-03
245	Apln	apelin	2.05	4.9E-03
246	Asphd2	aspartate beta-hydroxylase domain containing 2	2.05	2.0E-02
247	Meox1	mesenchyme homeobox 1	2.05	1.9E-02
248	Gli1	GLI-Kruppel family member GLI1	2.03	2.0E-02
249	Map6	microtubule-associated protein 6	2.03	4.2E-02
250	Scx	scleraxis	2.01	8.0E-03
251	Cd248	CD248 antigen, endosialin	2.01	2.8E-03
252	Htra1	HtrA serine peptidase 1	2.00	9.7E-06

Table B14, Part II. List of genes more highly expressed in control cancellous bone of pOC-ERαKO animals at 24 hours

	Gene Symbol	Gene	Fold Change	FDR
1	Ear7	eosinophil-associated, ribonuclease A family, member 7	460.22	1.4E-04
2	Cbln1	cerebellin 1 precursor protein	3.37	3.6E-02
3	Klre1	killer cell lectin-like receptor family E member 1	3.23	1.1E-02
4	4930431P03Rik	RIKEN cDNA 4930431P03 gene	2.67	2.0E-02
5	Pdia2	protein disulfide isomerase associated 2	2.62	3.9E-03
6	Nlrp6	NLR family, pyrin domain containing 6	2.58	2.5E-03

Table B14, Part II. Continued

	Gene Symbol	Gene	Fold Change	FDR
7	G6b	G6B protein	2.54	3.9E-03
8	Ltb4r2	leukotriene B4 receptor 2	2.43	4.6E-02
9	BC016579	cDNA sequence, BC016579	2.39	1.1E-02
10	Fcer1a	Fc receptor, IgE, high affinity I, alpha polypeptide	2.37	4.6E-02
11	Pf4	platelet factor 4	2.36	1.1E-08
12	Ubd	ubiquitin D	2.35	1.5E-06
13	Pdzd3	PDZ domain containing 3	2.31	8.2E-03
14	Aldob	aldolase B, fructose-bisphosphate	2.26	4.5E-04
15	Gp9	glycoprotein 9 (platelet)	2.22	4.0E-10
16	0610039K10Rik	RIKEN cDNA 0610039K10 gene	2.22	3.3E-02
17	Efemp1*	epidermal growth factor-containing fibulin-like extracellular matrix protein 1	2.18	4.2E-03
18	Esm1	endothelial cell-specific molecule 1	2.18	5.5E-07
19	Slc35d3	solute carrier family 35, member D3	2.17	8.6E-05
20	Gpr174	G protein-coupled receptor 174	2.17	2.8E-03
21	Clec4g	C-type lectin domain family 4, member g	2.16	2.9E-02
22	Gm5483	predicted gene 5483	2.16	3.6E-02
23	Ly6g6f	lymphocyte antigen 6 complex, locus G6F	2.15	5.5E-07
24	Cd226	CD226 antigen	2.15	1.1E-06
25	Smim5	small integral membrane protein 5	2.14	1.2E-03
26	Ifi47*	interferon gamma inducible protein 47	2.14	1.4E-04
27	Cd5l	CD5 antigen-like	2.14	2.7E-05
28	5033406O09Rik	RIKEN cDNA 5033406O09 gene	2.13	1.1E-02
29	Chrdl1	chordin-like 1	2.12	2.7E-08
30	Serpinb2	serine (or cysteine) peptidase inhibitor, clade B, member 2	2.10	2.4E-03
31	Serpina3f	serine (or cysteine) peptidase inhibitor, clade A, member 3F	2.08	4.3E-05

Table B14, Part II. Continued

	Gene Symbol	Gene	Fold Change	FDR
32	Cxcl5	similar to LPS-induced CXC chemokine; chemokine (C-X-C motif) ligand 5	2.08	1.1E-02
33	Rgs18	regulator of G-protein signaling 18	2.08	1.1E-06
34	Gm16548	predicted gene 16548	2.08	1.1E-04
35	Slamf1	signaling lymphocytic activation molecule family member 1	2.07	1.4E-06
36	Ppbp	pro-platelet basic protein	2.06	3.4E-05
37	D830046C22Rik	RIKEN cDNA D830046C22 gene	2.06	4.2E-03
38	Tacstd2	tumor-associated calcium signal transducer 2	2.06	4.0E-02
39	Kcnj5	potassium inwardly-rectifying channel, subfamily J, member 5	2.05	1.4E-07
40	Slc6a4	solute carrier family 6 (neurotransmitter transporter, serotonin), member 4	2.05	4.7E-07
41	Tesc	tescalcin; similar to Tescalcin	2.05	3.4E-05
42	Slc30a10	solute carrier family 30, member 10	2.03	1.9E-02
43	P2rx1	purinergic receptor P2X, ligand-gated ion channel, 1	2.03	1.5E-06
44	Kng2	kininogen 2	2.03	3.3E-05
45	Slc6a3	solute carrier family 6 (neurotransmitter transporter, dopamine), member 3	2.03	8.4E-03
46	Gp5	glycoprotein 5 (platelet)	2.01	2.8E-09
47	F2rl3	coagulation factor II (thrombin) receptor-like 3	2.01	1.1E-04
48	Gp6	glycoprotein 6 (platelet)	2.01	4.1E-07
49	Kcna3	potassium voltage-gated channel, shaker-related subfamily, member 3	2.00	8.2E-03

total	301
*indicates contaminant	129
total without contaminants	172